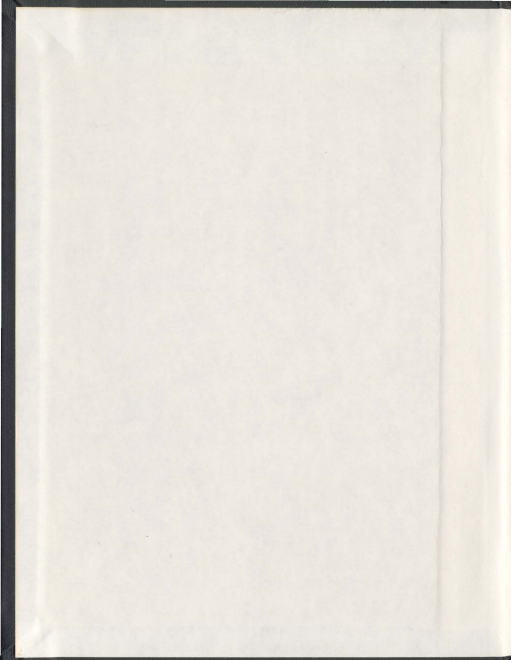


NEW BIODEGRADABLE ELASTOMERS FOR DRUG
AND THERAPEUTIC PROTEIN DELIVERY

MOHAMED ABDEL FATTAH SHAKER MAHMOUD



001311



Memorial University of Newfoundland

New Biodegradable Elastomers for Drug and Therapeutic Protein Delivery

By

Mohamed Abdel Fattah Shaker Mahmoud

A thesis submitted to the School of graduate studies in partial fulfillment of the requirements for the degree of *Doctor of Philosophy*.

In

Pharmaceutical Sciences

School of Pharmacy

Supervisory Committee:

Dr. Mohsen Daneshtalab

Dr. Husam Younes

Dr. Lili Wang

Dr. Yuming Zhao

Winter 2011

DEDICATION

This thesis is dedicated to my country, EGYPT, which has never failed to provide me with financial support, and helping me during the time I spent to pursue my graduate studies. It is also dedicated to my father, who taught me that to earn knowledge needs effort and consistency. It is also dedicated to my mother, who taught me that even the largest task can be accomplished if it is done one step at a time.

This thesis would be incomplete without the support given by my wife to whom this thesis is dedicated. Her ever-lasting support kept my spirits up when the muses failed me. I strongly believe that without her continuous encouragement, the huge task of performing research and writing this thesis was impossible.

ABSTRACT

Over the past few years, and with the tremendous advances in recombinant protein technology, cytokines and other therapeutic proteins have emerged as a promising and effective strategy in immunotherapy of cancer. As such, much of the current research has focused on many aspects of developing new drug delivery systems which are capable of targeting and controlling the release of cytokines for the treatment of cancer. Most of those efforts however were directed towards the systemic administration of cytokines which is often limited by side effects and the necessity to administer these therapeutic proteins in a clinical setting. There are several reasons for the attractiveness of the regional delivery approach of cytokines in cancer therapy. It is generally recognized that loco-regional delivery localizes the cytokines actions and activities into the vicinity of tumors, reducing the dose required, providing uniform delivery and can result in an improved therapeutic outcome with much less side effects or toxicity. Different strategies have been utilized to deliver interleukin 2 (IL-2) to the tumor site including gene therapy and polymeric drug delivery systems. Some of the polymeric delivery systems investigated to date include liposomes, hydrogels and biodegradable microspheres made from polylacticacid, polyglycolicacid and their copolymers. An extensive evaluation of the different delivery approaches utilized for IL-2 has been reviewed in chapter 1. These delivery strategies have inherent problem in maintaining the required therapeutic activity over time and/or in preserving their content of the loaded IL-2 and /or maintaining its stability during their formulation techniques.

The main objective of our studies was to formulate a new biodegradable polymeric drug delivery system capable of providing a constant and sustained IL-2 delivery rate. The new polymeric system will be designed in a manner in which the IL-2 protein particles could be easily dispersed, into this

synthesized polymeric system, in a protein friendly formulation condition. This shall provide an environment to maintain IL-2 stability and activity while within the delivery device and prior to it being released. On the other hand the release, which is undergone by utilizing the osmotic driven release mechanism, shall facilitate complete release of the protein before the device eventually degrades and becomes bioabsorbable. In addition, the use of a slowly hydrolysable copolymer would reduce or eliminate the production of an acidic environment within the device until the vast majority of the loaded protein is released, before any significant reduction in the mechanical properties of the biomaterial occurs due to its hydrolysis.

These new polymeric biomaterials are based on the poly(diols-tricarballoylate) (PDT) photocrosslinked elastomers. The synthesis was carried out by the polycondensation reaction of tricarballoylic acid and alkylene diols, followed by acrylation and visible light photo-curing under ambient temperature and solventless conditions, which is described in chapter 3. Chapter 4 describes the *in vitro* evaluation of the osmotic-driven release mechanism by a release study using the papaverine hydrochloride, as a model for a water soluble drug. The examinations of *in vitro* cytotoxicity, *in vivo* biocompatibility and biodegradability were also conducted to assess the elastomers' biological performance after long term contact with lung epithelial cell line and soft subcutaneous tissue of Sprague-Dawley rats, the details of which is described in chapter 5. Eventually, different IL-2 loaded devices have been formed by homogenous distribution of the co-lyophilized IL-2 and stabilizing/osmotic excipient particles throughout the acrylated prepolymer which is then photocrosslinked. These experiments are described in chapter 6. The *in vitro* IL-2 release studies in phosphate buffer saline of pH 7.4 were undertaken to demonstrate the proposed osmotic mechanism and to determine the time frame for the release. The activity of the released IL-2 was also examined *in vitro*

using C57BL/6 mouse cytotoxic T lymphocyte. Chapter 7 is devoted to "General Discussions and Conclusions."

Overall, the results have shown that the prepared elastomers were rubbery and their mechanical properties can be controlled through manipulations of the chain length of the diol used and the degree of polymer acrylation. As well, the papaverine hydrochloride release rate, from 10% v/v loaded cylinder-shaped matrices, was found to be dependent on the degree of macromer acrylation. Decreasing the degree of acrylation of the prepolymers resulted in reduction in the crosslinking density of the formed elastomeric matrices. Furthermore, it was found that co-formulating papaverine hydrochloride with trehalose increases the release rate without altering the linear nature of the drug release kinetics. The results also have demonstrated that these elastomers, with different degrees of acrylation, showed promising non cytotoxicity results with Mv1Lu cells and received reasonably consistent results between the two common cell viability assays (MTT and ^3H -thymidine incorporation). The *in vivo* implantation results showed that no macroscopic signs of inflammation or adverse tissue reactions were observed at implant retrieval sites. We have shown *in vivo* justification to confirm the potential of these elastomers as soft-tissue friendly materials as well as the candidacy of these elastomers as biodegradable biomaterials for long term application. We have also demonstrated that elastomer selection can be tailored to achieve the desired implantation period and release rates. Promising results regarding osmotic-driven controlled IL-2 release have been demonstrated via typical zero-order release kinetics. The increase in the device's surface area and the incorporation of trehalose in the loaded lyophilized mixture increased the IL-2 release rate. As well, it was shown that the decrease in the degree of prepolymer acrylation of the prepared devices increased the IL-2 release rate. Cell based bioactivity

assay for IL-2 over a release period of 28 days showed that the released IL-2 retained more than 94% of its initial activity.

ACKNOWLEDGEMENTS

First of all, I owe my deepest gratitude to my country EGYPT for providing me with the scholarship to do my PhD.

My heartily thanks to my supervisors Drs. Husam Younes and Mohsen Daneshtalab for their support and guidance from the initial to the final steps of development of this thesis, and to Drs. Lili Wang and Yuming Zhao for serving as my committee members and providing me with advice and helpful consultation. The research work of the thesis has been financially supported by a grant from Natural Sciences and Engineering Research Council of Canada (NSERC). This thesis would not have been possible without the collaboration and encouragement of Drs. Jules Doré, Noriko Daneshtalab, Patricia Wadeen and Mowafa Hamodata.

I am also very appreciative of the time and patience put forth by Dr. Linda Hensamen the director of the School of Pharmacy at Memorial University. I offer my regards and blessings to all of my colleagues who supported me in any respect during the completion of the project. I am also thankful to all the faculty and staff of the School of Pharmacy and the School of Graduate Studies that helped me along the way, in particular the positive thoughts of Ms. Denise Burke, Ms. Heather Bugler, Ms. Sharon Tucker and Ms. Jennifer Deon.

Last but not least, many thanks to my family for supporting me throughout this long journey. I could not have done this without the steadfast prayers and well wishes from my parents and my wife. The positive thoughts from my sister Ms. Wessam Shaker and my brothers Drs. Ahmad Shaker and Mahmoud Shaker kept me afloat and provided me with the inspiration to continue this work.

TABLE OF CONTENTS

DEDICATION	ii
ABSTRACT	iii
ACKNOWLEDGEMENTS	vii
TABLE OF CONTENTS	viii
LIST OF TABLES	xiii
LIST OF FIGURES	xv
LIST OF ABBREVIATIONS	xxi
 CHAPTER 1: Interleukin-2: Evaluation of Routes of Administration and Current Delivery Systems in Cancer Therapy	 1
1.1. BACKGROUND	3
1.2. MECHANISMS OF ACTION	7
1.3. PHYSICAL PROPERTIES AND STRUCTURE	10
1.4. PHARMACOKINETICS	13
1.5. LOCO-REGIONAL VERSUS SYSTEMIC DELIVERY	16
1.6. SUSTAINED (CONTINUOUS) VERSUS INTERMITTENT RELEASE	23
1.7. DELIVERY SYSTEMS AND DOSAGE FORMS: ADVANTAGES AND LIMITATIONS	25
1.8. CONCLUSIONS	46
1.9. REFERENCES	47
 CHAPTER 2: Photocrosslinked Polymers: New Emerging Biomaterials for Controlled Drug Delivery and Other Biomedical Application	 65
2.5.1. Scaffold and tissue fabrication	80
2.5.2. Cell encapsulation	81
2.6. PHOTOPOLYMERIZATION IN THERAPEUTIC DELIVERY	82
2.6.1. Photopolymerized Hydrogels	84
2.6.2. Photopolymerizable Elastomers	91

2.7.	CONCLUSIONS	95
2.8.	REFERENCES	95
CHAPTER 3: Synthesis, Characterization and Cytocompatibility of Poly(diols-tricarballoylate) Visible Light Photocrosslinked Biodegradable Elastomer		104
3.1.	INTRODUCTION	106
3.2.	EXPERIMENTAL	109
3.2.1.	Materials	109
3.2.2.	Synthesis of Poly(diols-tricarballoylate) Prepolymers	109
3.2.3.	Acrylation of Prepolymer	110
3.2.4.	Photocuring of the Acrylated Prepolymers	112
3.2.5.	Chemical and Thermal Characterization	112
3.2.6.	Mechanical Properties and Sol Content Measurements	114
3.2.7.	<i>In vitro</i> Degradation	115
3.2.8.	<i>In vitro</i> Cytocompatibility and Cell Proliferation	115
3.3.	RESULTS AND DISCUSSION	116
3.3.1.	Chemical and Thermal Characterization	117
3.3.2.	Mechanical Properties and Sol Content Measurements	125
3.3.3.	<i>In vitro</i> Degradation	128
3.3.3.1.	<i>Influence of chain length on in vitro degradation</i>	128
3.3.3.2.	<i>Degradation behavior</i>	129
3.3.3.3.	<i>Changes in the mechanical properties during in vitro degradation</i>	132
3.3.4.	<i>In vitro</i> Cytocompatibility with Fibroblast Cell	136
3.4.	CONCLUSIONS	138
3.5.	REFERENCES	139
CHAPTER 4: Osmotic-Driven Release of Papaverine Hydrochloride from Novel Biodegradable Poly(decane-co-tricarballoylate) Elastomeric Matrices		144
4.1.	INTRODUCTION	146
4.2.	EXPERIMENTAL	150
4.2.1.	Materials	150

4.2.2.	Synthesis and Characterization of Acrylated Poly(decane-co-tricarballoylate) Prepolymer	150
4.2.3.	Elastomeric Matrices Preparation and Characterization Fabrication of PH loaded	152
4.2.4.	Elastomeric Cylinders	153
4.2.5.	Osmotic Activity Measurements	153
4.2.6.	<i>In vitro</i> Release Studies	154
4.2.7.	<i>In vitro</i> Degradation Study	154
4.2.8.	Scanning Electron Microscopy	155
4.3.	RESULTS AND DISCUSSION	155
4.3.1.	Elastomer Preparation and Characterization	156
4.3.2.	<i>In vitro</i> Release and Degradation Studies	160
4.3.2.1.	<i>Impact of polymer degradation on drug release</i>	165
4.3.2.2.	<i>Impact of the osmolality of the release media</i>	167
4.3.2.3.	<i>Effect of degree of prepolymer acrylation</i>	168
4.3.2.4.	<i>Effect of osmotic excipient</i>	171
4.3.3.	Scanning electron microscopy	174
4.4.	CONCLUSIONS	174
4.5.	REFERENCES	176
CHAPTER 5: Biocompatibility and Biodegradability of Implantable Drug Delivery Matrices Based on Novel Poly(decane-co-tricarballoylate) Photocured Elastomers		179
5.1.	INTRODUCTION	181
5.2.	EXPERIMENTAL	183
5.2.1.	Materials	183
5.2.2.	Preparation of Prepolymers and Elastomers	184
5.2.3.	<i>In vitro</i> Cytotoxicity and Proliferation Assays	186
5.2.3.1.	<i>Preparation of degradation aliquots</i>	186
5.2.3.2.	<i>Cell culture</i>	187

5.2.3.3.	<i>The MTT3-(4,5-dimethylthiazol-2-yl)-2,5-diphenyltetrazolium bromide assay</i>	187
5.2.3.4.	<i>³H-Thymidine incorporation assay for DNA synthesis</i>	188
5.2.4.	<i>In vivo Biocompatibility and Degradation Studies</i>	189
5.2.4.1.	<i>Animal preparation and subcutaneous implantation</i>	189
5.2.4.2.	<i>Implant retrieval and histological preparations</i>	192
5.2.4.3.	<i>Macroscopic and histological evaluation</i>	192
5.2.4.4.	<i>Physical characterization of excised cylinders</i>	193
5.2.4.5.	<i>In vitro degradation</i>	195
5.2.5.	<i>Statistical Analysis</i>	195
5.3.	RESULTS	195
5.3.1.	<i>In vitro Cytotoxicity</i>	195
5.3.1.1.	<i>MTT assay</i>	197
5.3.1.2.	<i>³H-Thymidine incorporation assay</i>	197
5.3.2.	<i>In vivo Biocompatibility</i>	200
5.3.2.1.	<i>Biological responses and histology</i>	200
5.3.5.	<i>In vitro and In vivo Degradation</i>	206
5.4.	DISCUSSION	211
5.6.	CONCLUSIONS	216
5.7.	REFERENCES	216
CHAPTER 6:	Sustained Interleukin-2 Delivery from Photocrosslinked Biodegradable Poly(decane-co-tricarballoylate) Elastomer	220
6.1.	INTRODUCTION	222
6.2.	EXPERIMENTAL	226
6.2.1.	Materials	226
6.2.2.	Synthesis and Characterization of Acrylated Poly(decane-co-tricarballoylate) Prepolymer	228
6.2.3.	Elastomeric Matrices Preparation and Characterization	228
6.2.4.	Preparation of IL-2 Loaded Elastomeric Delivery Systems	229
6.2.5.	Effect of Formulation Conditions on the IL-2 Bioactivity	230

6.2.6.	<i>In vitro</i> Release Studies	230
6.2.7.	Cell Line Culture and IL-2 Bioactivity Assay	232
6.2.8.	Scanning Electron Microscopy	233
6.2.9.	Statistics Analysis	233
6.3.	RESULTS AND DISCUSSION	234
6.3.1.	Elastomer Preparation and Characterization	235
6.3.2.	<i>In vitro</i> Release Studies	238
6.3.2.1.	<i>Effect of degree of prepolymer acrylation</i>	239
6.3.2.2.	<i>Effect of the device shape on the release</i>	243
6.3.2.3.	<i>Effect of loading percentage</i>	246
6.3.2.4.	<i>Effect of BSA/TH mass ratio on IL-2 release</i>	248
6.3.2.5.	<i>Impact of elastomer degradation on IL-2 release</i>	250
6.3.3.	Bioactivity of the Released IL-2	254
6.3.4	Scanning Electron Microscopy	256
6.4.	CONCLUSIONS	257
6.5.	REFERENCES	258
CHAPTER 7: General Discussion and Conclusions		263
	REFERENCES	273

LIST OF TABLES

Table	Title	page
1.1	Therapeutic effects of free IL-2 on human cancer patients	5
1.2	Summary of representative pre-clinical animal studies demonstrating the efficacy and toxicity of using different routes of administration and dosing schedules of IL-2.	20
1.3	Summary of representative clinical studies demonstrating the efficacy and toxicity of using different routes of administration and dosing schedules of IL-2	21
1.4	Summary of the polymeric controlled/sustained release delivery systems used for IL-2.	30
2.1	Examples of different photoinitiators with their reported application	71
2.2	Selected examples of synthetic degradable polymers and their biomedical applications.	76
3.1	Results of GPC and end group analysis of poly(diols-tricarballoylate) prepolymers.	118
3.2	Thermal properties of poly(diols-tricarballoylate) prepolymers, acrylated prepolymer and elastomers.	124
3.3	Mechanical properties and sol content of poly(diols-tricarballoylate) elastomers.	127
3.4	The linear regression coefficients values for PDT elastomers during <i>in vitro</i> degradation in PBS (pH 7.4).	135
4.1	Mechanical properties and sol content of poly(decane-co-tricarballoylate) elastomers.	159
4.2	Osmotic activity of saturated solutions of papaverine hydrochloride, trehalose and used release media.	161
5.1	Mechanical properties and sol content of PDET prepared elastomers.	196
5.2	Tissue reactions to PDET implanted samples of different degrees of acrylation and PLGA sutures.	202

5.3	Zero-order kinetic parameters and linear regression coefficients of the changes in the mechanical data for PDET elastomers during <i>in vitro</i> and <i>in vivo</i> degradation studies.	209
6.1	Mechanical properties and sol content of poly(decane-co-tricarallylate) elastomers.	236
6.2	The regression values of IL-2 released from PDET micro-cylinders and disks shape specimens, with different degrees of acrylation (DA).	244

LIST OF FIGURES

Figure	Title	page
1.1	A proposed mechanism of action of IL-2.	9
1.2	Human IL-2 crystalline structure	12
2.1	Schematic representation of the photo-initiated polymerization.	69
3.1	Schematic illustration of the synthesis, acrylation and photocuring of poly(diols-tricarballlylate).	111
3.2	FTIR analysis of POT, A: before acrylation, B: after acrylation and C: after photocuring.	120
3.3	¹ H NMR spectrum of (a) poly(octane-tricarballlylate) prepolymer, (b) acrylated poly(octane-tricarballlylate) prepolymer.	121
3.4	Differential Scanning Calorimetry thermograms of poly(diols-tricarballlylate) (A) prepolymers, (B) acrylated prepolymers and (C) elastomers.	123
3.5	(a) stress-strain curves of poly(diols-tricarballlylate) elastomers. (b) POT elastomer shows 100% recovery after being stretched to break.	126
3.6	Degradation results of poly(diols-tricarballlylate) elastomers in PBS at 37 °C. (a) percentage weight loss versus time. (b) percentage water absorption versus time. Error bars represent the standard deviation of the mean of measurements from three samples.	130
3.7	Images of the PDDT elastomers during <i>in vivo</i> degradation after: (a) 0, (b) 1, (c) 4, and (d) 12 weeks.	131
3.8	Change in tensile properties of the elastomers during degradation in PBS at 37°C. (a) Young's modulus, (b) ultimate stress and (c) ultimate strain, lines are fitted curves to equation (1) and (2). Error bars represent the standard deviation of the mean of measurements from three samples.	133
3.9	Phase contrast images of human fibroblasts cells with POT elastomeric films and polystyrene plate control after 24 hr of culturing.	137
3.10	Human fibroblasts cell density after 24 hr incubation with different weight of different PDT elastomeric films, relative to control polystyrene plat.	137

- 4.1 Schematic representation of osmotic swelling, rupture and release mechanism. (A) Water vapor diffuses to the inside of the elastomer. (B) The water dissolves the solid drug and exert osmotic pressure on the inside (C) The pressure causes micro-cracks in the elastomer and the drug content is then released upon polymer relaxation. (D) The process occurs in a serial fashion towards the center of the cylinder as each cross-sectional layer of compartments rupture. 148
- 4.2 Schematic illustration of the synthesis, acrylation and photocuring of poly(decane-tricarballoylate). (A) The step-reaction polymerization of tricarballoylic acid and decane diol was catalyzed by stannous 2-ethylhexanoate. The acrylation was carried out using acryloyl chloride in the presence of triethylamine. To photo-crosslink, acrylated prepolymer was mixed with camphorquinone (the photoinitiator) and crosslinked under visible light (40mW/cm²). (B) Schematic representation of the method of preparing PH loaded elastomeric cylindrical monoliths. 151
- 4.3 NMR spectra of PDET. (A) ¹H-NMR of PDET prepolymer before acrylation (B) ¹H-NMR of PDET prepolymer after acrylation. (C) Solid-state ¹³C-NMR spectrum of PDET100 elastomer. 157
- 4.4 Stress-strain curves of PDET elastomers of different degrees of acrylation. 158
- 4.5 Cumulative percent of PH released from PDET₁₀₀ elastomers in different release media. Error bars represent the standard deviation of the mean of measurements from four samples. 163
- 4.6 Release of amaranth trisodium dye from PDET₁₀₀ elastomeric cylinders and the change in the cylinders geometry in PBS release medium. (A) A representative image of amaranth trisodium loaded elastomeric cylinders before the start of the release study. (B) A representative image of amaranth trisodium loaded cylinders after 3 months of the start of the release study. (C) A representative image of a blank elastomeric cylinder before the start of the degradation study. (D) The image of the same cylinder at the conclusion of the release study. 164
- 4.7 Percentage water absorption versus time of PDET elastomeric cylinders of different degrees of acrylation in PBS at 37°C. Error bars represent the standard deviation of the mean of measurements from three samples. 166
- 4.8 Linear regression of release data of PH from PDET₁₀₀ elastomeric cylinders in different release media. Error bars represent the standard deviation of the mean of measurements from four samples. 169
- 4.9 Cumulative percent of PH released in phosphate saline buffer from PDET

cylinders with different degrees of acrylation (DA). Error bars represent the standard deviation of the mean from four measurements. Where error bars are not shown when the standard deviation is smaller than the symbol.	170
4.10 Effect of incorporating different weight ratios of trehalose to papaverine hydrochloride on the osmotic-driven release rate from PDET ₁₀₀ elastomeric cylinders. Error bars represent the standard deviation of the mean from four measurements. Where error bars are not shown when the standard deviation is smaller than the symbol.	173
4.11 Scanning electron microscopy photographs of PH/TH (weight ratio 1:2) loaded PDET ₁₀₀ cylinders. (A) Surface image before the start of the release study. (B) Surface image after the conclusion of the release study. (C) Cross-sectional view of the cylinder at the conclusion of the release study.	175
5.1 A schematic illustration of the synthesis, acrylation and photocuring of poly(diols-tricarballylate) elastomers. The step growth polymerization of tricarballic acid and alkylene diol was catalyzed by stannous-2-ethylhexanoate. The acrylation was carried out using acryloyl chloride in the presence of triethylamine. To photocrosslink, the acrylated prepolymer was mixed with the photoinitiator, camphorquinone and triethanolamine and crosslinked under visible light.	185
5.2 A diagrammatic illustration of the implantation sites for the specimens in each rate.	191
5.3 The effect of PDET elastomers of different degrees of acrylation on the Mv1Lu epithelial cell viability estimated by MTT assay after 1, 7, 14 and 28 days of elastomer degradation. Results are expressed as the percentage of viable cells compared with phosphate buffer saline (PBS) treated controls (mean \pm SD, $n = 6$). The significance of the results was determined by comparison with control value using 2-way ANOVA; * $p < 0.05$.	198
5.4 The effect of PDET elastomers of different degrees of acrylation on Mv1Lu epithelial cells proliferation and DNA synthesis using ³ H-thymidine incorporation assay after 1, 7, 14 and 28 days of elastomer degradation in comparison to control. Results are expressed as the percentage of ³ H-thymidine incorporation relative to that of PBS-treated controls (mean \pm SD, $n = 6$). Transforming growth factor β (2ng/ml) was used as a positive control (+ve control) and sterile saline treated wells served as a negative control (-ve control). The significance of the results was determined by comparison with control value using 2-way ANOVA; * $P < 0.05$.	199
5.5 Elastomer implants as dissected along with soft tissue and skin around them. Images (A) and (B) show representative PDET ₁₀₀ implants at 4 and 12 weeks	

- respectively. Images (C) and (D) show representative PDET₅₀ implants at 4 and 12 weeks respectively. No necrosis, granulomas, or sign of dystrophic soft tissue calcification can be seen around any of the implants. 201
- 5.6 Representative histological images of the tissue surrounding cylindrical PDET elastomeric implants and PLGA sutures (control) showing macrophages (black arrows) and fibrin layer (white arrows) at the implantation site. PDET₁₀₀ implants after (A) 2 weeks at 4x magnification (B) 2 weeks at 20 x magnification and (C) 12 weeks at 20x magnification. PDET₅₀ implants after (D) 2 weeks at 4x magnification (E) 2 weeks at 20 x magnification and (F) 12 weeks at 20x magnification. PLGA implants after (G) 2 weeks at 4x magnification (H) 2 weeks at 20 x magnification and (I) 12 weeks at 20x magnification. 203
- 5.7 Degradation studies of PDET elastomers of different degrees of acrylation. (A) *In vitro* and *in vivo* percentage weight loss versus time. (B) *In vitro* and *in vivo* percentage water absorption versus time. Each point represents mean \pm SD ($n = 3$). 207
- 5.8 Changes in mechanical properties of PDET₁₀₀ and PDET₅₀ elastomers during *in vivo* and *in vitro* degradation. (A) Young's modulus at time t , E_t (B) Ultimate tensile stress at time t , σ_t (C) Ultimate tensile strain at time t , ϵ_t . Lines on the figures are fitted curves to zero-order degradation kinetics equation. Each point represents mean \pm SD ($n = 3$). Kinetics parameters and linear regression coefficients are reported in table 5.2. 208
- 6.1 Schematic representation of osmotic swelling, rupture and release mechanism A) water diffusion through the elastomer reach to the first layer of encapsulated drug particles. B) the imbibed water dissolves the solid drug at solid polymer interface, creating a saturated solution surrounding elastomer, causes it to swell and exert pressure on the inside wall. C) the pressure causes micro-cracks to form in the elastomer and the dissolved protein/excipients content is then released. The process is repeated with the subsequent layer of particle which leads to interconnected network formation. D) the osmotic release from a cylinder shape elastomer. 225
- 6.2 Schematic illustration of the synthesis, acrylation and photocuring of poly(decane-tricarballoylate). The step-reaction polymerization of tricarballoylic acid and decane diol was catalyzed by stannous 2-ethylhexanoate. The acrylation was done by reacting with acryloyl chloride in the presence of triethylamine. To photocrosslink, acrylated prepolymer was mixed with the photoinitiator, poured into a sealed glass mold and crosslinked under visible light (40mW/cm²). 227
- 6.3 Stress-strain curves of different PDET elastomeric micro-cylinders. 237

- 6.4 Cumulative percent of IL-2 released in phosphate saline buffer from PDET micro-cylinders (A) disks (B) shape specimens, with different degrees of acrylation (DA). Each point represents the mean of triplicate experiments, and the error bars represent one standard deviation about the mean. Error bars are not shown when the standard deviation is smaller than the symbol. 241
- 6.5 Cumulative percent of IL-2 released from PDET elastomers with different degree of acrylation (DA) and different device shape. Each point represents the mean of triplicate experiments. The error bars represent the standard deviation about the mean. Error bars are not shown when the standard deviation is smaller than the symbol. 245
- 6.6 Release data of IL-2 from different loaded percentage PDET micro-cylinders with 50% degree of acrylation, (A) represent the percentage released and (B) represent the cumulative amount of IL-2 release. Each point represents the mean of triplicate experiments. The error bars represent standard deviation about the mean. Error bars are not shown when the standard deviation is smaller than the symbol. 247
- 6.7 (A) and (B) are cumulative percent of IL-2 released from PDET micro-cylinders with 100% and 50% degree of acrylation, respectively, in existence of different molar ratio of bovine serum albumin (BSA) and trehalose (TH). (C) The release kinetic of TH (triangles), BSA(circles) and IL-2 (squares) from PDET micro-cylinders with 100% degree of acrylation. The solid symbols are for 50% degree of acrylation, the hollow symbols are for 100% degree of acrylation and the lines correspond to the IL-2 release. Each point represents the mean of triplicate experiments, and the error bars represent one standard deviation about the mean. Where error bars are not shown when the standard deviation is smaller than the symbol. 249
- 6.8 Percentage water absorption and weight remain versus time of PDET elastomeric micro-cylinders of different degrees of acrylation (DA) in PBS at 37°C. Error bars represent the standard deviation of the mean of measurements from three samples. 252
- 6.9 A, B and C are scanning electron photomicrographs of blank PDET₁₀₀ microcylinders after the end of 12 week degradation. D, E and F are scanning electron photomicrographs of IL-2 loaded (with BSA:TH ratio 1:4). PDET₁₀₀ microcylinders after the end of 60 days release study. A and D are microcylinders images at 20X magnification. B and E are surface images at 2000X magnification. C and F Cross-sectional view of the microcylinders at 2000X magnification. 253
- 6.10 Bioactivity profiles of IL-2 released from PDET with Different, (A) shape of releasing device (B) degree of acrylation (c) loading % (D) different weight ratio of BSA and TH. Each point represents the mean of triplicate experiments. The error bars represent the standard deviation about the mean. 255

LIST OF ABBREVIATIONS

ACRL	acryloyl chloride
APDT	acrylated poly(diols-tricarballlylate)
AT	amaranth trisodium
AUC	area under the curve
BSA	bovine serum albumin
CR	complete regression
CTLL-2	cytotoxic T lymphocyte
CQ	camphorquinone
CDC13	chloroform- <i>d</i>
¹³ C-NMR	carbon 13 nuclear magnetic resonance
DA	degree of acrylation
DE	double emulsion
DLLA	d,l-lactide
DMAP	4-dimethyl aminopyridine
DMEM	dulbecco's modified eagle medium
DMPA	2, 2-dimethoxy-2-phenyl acetophenone
DSC	differential scanning calorimeter
DW	distilled water
E	young's modulus
EBD	electron backscatter diffraction
EDMAB	ethyl 4-N,N-dimethylamino-benzoate
EDX	energy dispersive X-ray
ELISA	enzyme-linked immunosorbant assay
ϵ	ultimate tensile strain
ϵ -CL	ϵ -caprolactone
FDA	food and drug administration/agency
FT- IR	fourier transform infrared
GPC	gel permeation chromatography

HA	hyaluronic acid
HEMA	2-hydroxyethylmethacrylate
HGF	hepatocyte growth factor
hIL-2	human interleukin-2
HIV	human immunodeficiency virus
¹ H-NMR	proton nuclear magnetic resonance
HyPG	hyperbranched polyglycerol
IFN- γ	interferon- γ
IL-2	interleukin-2
ITX	isopropyl thioxanthone
JAK 3	janus kinase 3
LAK	lymphokine-activated killer
MAPK	mitogen-activated protein kinase
MCT	mercury cadmium telluride
MHC	major histocompatibility complex
M_n	number average molecular weight
MRT	mean residence time
MTT	3-(4,5-dimethylthiazol-2-yl)-2,5-diphenyltetrazolium bromide
M_w	weight average molecular weight
NK	natural killer
NSAIDs	non steroidal antiinflammatory drugs
Pa	pascal
PBS	phosphate buffer saline
PD	progressive disease
PDDT	poly(dodecane diol-co-tricarballoylate)
PDET	poly(decane diol-co-tricarballoylate)
PDT	poly(diols-tricarballoylate)
PEG	polyethyleneglycol
PH	papaverine hydrochloride

PHT	poly(hexane diol-co-tricarballoylate)
PI3K	phosphatidyl inositol 3-kinase
PLG	poly(lactide-co-glycolide)
PLGA	poly(lactic acid-co-glycolic acid)
POT	poly(octane diol-co-tricarballoylate)
PR	partial regression
PTK	protein tyrosine kinases
PVA	polyvinylalcohol
R	universal gas constant
rhIL-2	recombinant human interleukin-2
RI	differential refractometer
rmIL-2	recombinant murine interleukin 2
RSA	rat serum albumin
ρ_x	crosslinking density
SD	stable disease
SEM	scanning electron microscope
SE	single emulsion
STAT 5	signal transducers and activators of transcription 5
σ^u	ultimate tensile stress
$t_{1/2}$	half-life
TEA	triethylamine
TH	trehalose
THF	tetrahydrofuran
TMC	trimethylene carbonate
UV	ultra-violet
VEGF	vascular endothelial growth factor
V_i	initial volume of distribution
V_{ss}	steady state volume of distribution

CHAPTER 1

Interleukin-2: Evaluation of Routes of Administration and Current Delivery Systems in Cancer Therapy

The content of this chapter was published in the *Journal of Pharmaceutical Sciences* 98, 7, 2268-2298

(2009)

Mohamed A. Shaker and Husam M. Younes

ABSTRACT

Despite the fact that different administration routes and delivery systems have been used for interleukin-2 (IL-2) delivery, little has been reported regarding the most efficient strategies used to deliver IL-2 in a non-toxic, efficient, stable and safe manner. Systemic IL-2 administration has always been associated with rapid clearance and severe toxicity as a result of its narrow therapeutic index. Loco-regional IL-2 delivery however, is used to localize IL-2 actions and activities into the vicinity of tumors and can result in an improved therapeutic outcome with much less side effects or toxicity. The purpose of this chapter is to report on the different properties and aspects of IL-2, including its mechanism of action, physicochemical properties, and structure which have an impact on the activity, stability and formulation of IL-2 dosage forms and delivery systems. In addition, advantages and limitations of the currently available techniques and strategies to deliver IL-2 will also be covered.

1.1. BACKGROUND

Interleukin-2 (IL-2) is a cytokine messenger protein which activates parts of the immune system. It is one of the members of the interleukins family that was discovered in early 1976.¹ Although members of this family are structurally similar, IL-2 demonstrated an extraordinary unique contribution to the concept of immunotherapy as a whole and to cancer therapy in particular. IL-2 is particularly important as it regulates both inflammatory and immune responses by stimulating the growth of blood cells in the immune system.² Many studies established IL-2 as the lymphocytotropic cytokine responsible for signaling helper T-lymphocyte (CD4+ T-cell) proliferations.^{2,3} It was in 1983 that the immunotherapeutic potential of IL-2 alone, without any adoptive transfer of cytotoxic T-cells, was introduced in the treatment of cancer.⁴

In comparison with other cytokines, IL-2 has been found to be more effective against many types of tumors when it is administered alone.⁵ In addition to being an essential factor for the growth of T-cells, IL-2 also enhances various T-cells and natural killer (NK) cell functions. IL-2 activates lymphokine-activated killer (LAK) cells which have the ability to destroy tumor cells and improve the recovery of immune function in certain immunodeficiency cases. Furthermore, IL-2 is considered to be the most important cytokine in the generation of memory T-cells, which are able to undergo secondary expansion upon their second encounter to an antigen.⁶ Although IL-2 and interferon- α 2b in the early-1990s were both approved by the United States Food and Drug Agency (FDA) for treatment of cancer^{5,7}, IL-2 proved to have more applications in the treatment of both hematological malignancies and immunogenic tumors. In fact, IL-2 would offer an alternative approach to the traditional adoptive immunotherapy by its use to stimulate lymphocytes to proliferate *in vitro* which will help the patient in avoiding the exposure to human antigens.⁸

Therapeutically, IL-2 has been reported to have applications in the treatment of a number of different types of cancer diseases. These include but are not restricted to metastatic melanoma,⁹ kidney carcinoma,¹⁰ lymphoma,¹¹ hepatocellular carcinoma,¹² colorectal carcinoma,¹³ head and neck carcinoma,¹⁴ bladder carcinoma,¹⁵ nasopharyngeal carcinoma,¹⁶ mesothelioma,¹⁷ gastrointestinal cancer,¹⁸ ovarian carcinoma,¹⁹ lung cancer,²⁰ malignant pleural effusions,²¹ and basal cell carcinoma.²² Table 1.1 summarizes some of clinical trials conducted to investigate the aforementioned applications of IL-2.

Also, IL-2 was found to be effective in experimental mice with surgical minimal residual tumor disease after cancer resection surgery,^{23,24} or the use of chemotherapy.^{25,26} It was reported that short-term preoperative IL-2 immunotherapy abolishes postoperative immunodeficiency and can induce immunological control of the growth of minimal residual disease.²⁷ It can also inhibit the growth of tumor residue and metastases in mice after chemotherapy with cyclophosphamide,²⁵ ifosfamide²⁶ and imiquinod.²⁸

It was not until 1987 that IL-2 was first approved by the FDA to be used alone or in combination with LAK cells as an anticancer agent. This FDA approval was mainly for treatment of advanced melanoma, advanced kidney cancer and as an adjuvant for vaccines.⁵ Recombinant forms of IL-2 are now sold with different brand names such as Proleukin®, Teceleukin®, Ontak®, Aldesleukin® and Interking®. Proleukin® injection was the first IL-2 therapy approved by the FDA for patients with metastatic melanoma in 1998.⁹ Currently, and due to the fact that deficiency of functional IL-2 plays a pivotal role in the pathogenesis of many chronic viral infections, IL-2 is under clinical trials for the treatment of human immunodeficiency virus (HIV) and hepatitis C viral infections.^{29,30}

Table 1.1 Therapeutic effects of free IL-2 on human cancer patients.

Tumor Type	Study Type	# of Patients	Route of Admin.	Doses and Dosing scheme	Response* (antitumor effect)	Ref.
Melanoma	Phase II trial	23	Intralesional injection	0.6–6 Million IU 2–3 times weekly for 1–12 weeks. Dose depended on lesion size	<ul style="list-style-type: none"> • 15 patients with CR • 5 patients with PR • 3 patients with PD 	Radny et al. ⁹
Renal Carcinoma	Phase I trial	23	a) iv continuous 24-hour infusion, b) iv single daily 15-minute bolus injection, or c) a combination of a and b	1.0 or 3.0 X 10 ⁶ U/m ² /day	<ul style="list-style-type: none"> • above 50% reduction of total tumor in 3 patients • 11 patients had CR by day 56 • 9 patients were with SD at day 56 but subsequently progressed. 	Sosman et al. ¹⁰
Lymphomas	Phase II trial	61	Intravenous infusion	20 X 10 ⁶ IU/m ² /d was used for induction, consisting of three courses of 5, 4, and 3 days on weeks 1, 3, and 5, respectively, for a total dose of 240 X 10 ⁶ IU/m ²	<ul style="list-style-type: none"> • 5 patients with CR • 6 patients with PR • 12 patients with SD • 6 patients with PD 	Gisselbrecht et al. ¹¹
Hepatic carcinoma	Phase I trial	5	Intratumoral	1.05 x 10 ⁶ –3.6 x 10 ⁶ U per patient once weekly over 2–4 weeks	<ul style="list-style-type: none"> • 1 patient with PR • 3 patients with SD • 1 patient with PD 	Shirai et al. ¹²
Colorectal carcinoma	Phase I trial	24	Intravenous infusion	18 x 10 ⁶ U/m ² per 24 h for 5 days, followed by three injections of 5-fluorouracil (600 mg/m ²) and folinic acid (25mg/m ²) at weekly intervals	<ul style="list-style-type: none"> • 2 patients with CR • 5 patients with PR • 7 patients with SD • 10 patients with PD 	Simpson et al. ¹³
Head & neck carcinomas	Phase II trial	10	Perilymphatic	daily injections of 200 units of IL-2 over 10 days	<ul style="list-style-type: none"> • 3 patients with CR • 3 patients with PR 	Cortesina et al. ¹⁴
Bladder carcinoma	Phase I trial	9	Intravesical infusion	3x10 ⁶ IU/day (3 patients), 9x10 ⁶ IU/day (3 patients) and 27x10 ⁶ IU/day (3 patients)	<ul style="list-style-type: none"> • 9 patients with CR 	Ferlazzo et al. ¹⁵
Naso-pharyngeal carcinomas	Phase I trial	10	Transnasal	3x10 ⁶ U on 5 days in weeks 2, 4, and 6 of the 7-weeks following 7,000 cGy radiotherapy	<ul style="list-style-type: none"> • After 5 years, 63% of the IL-2 treated patients were disease-free versus 8% of the control patients 	Jacobs et al. ¹⁶
Mesothelioma	Phase II trial	22	Intrapleural	21 x10 ⁶ IU/m ² /day for 5 days.	<ul style="list-style-type: none"> • 1 patient with CR • 11 patients with PR • 3 patients with SD 	Astoul et al. ¹⁷

Tumor Type	Study Type	# of Patients	Route of Admin.	Doses and Dosing scheme	Response* (antitumor effect)	Reference
Gastro-intestinal Cancer	Phase I trial	16	Intratumoral	1.5-9 MIU	• 6 patients with PR • 10 patients with PD	Krastev et al. ¹⁸
Ovarian Carcinoma	Phase I trial	17	Intraperitoneal	6x10 ⁴ , 6x10 ⁵ , 6x10 ⁶ and 3x10 ⁷ IU/m ² /day by two different infusion schedules.	• 6 patient with CR • 3 patients with PR • 8 patients with PD	Taylor et al. ¹⁹
Lung Cancer & Malignant pleural effusions.	Phase II trial	11	Intrapleural	1000 units/day for 14 to 28 days through a trocar catheter 3 to 4 days after tumor resection	• 9 patient with CR	Yasumoto et al. ²⁰
Lung Cancer & Malignant pleural effusion	Phase I trial	21	Intrapleural	9 x 10 ⁶ IU of rIL-2 on the first and second day of each week for 3 weeks.	• 7 patient with CR • 6 patients with PR • 8 patients with PD	Masotti et al. ²¹
Basal cell carcinoma	Phase I trial	12	Perilesional	3000 to 1,200, 000 IU of PEG-IL-2 in one to four weekly	• 8 patient with CR • 3 patients with PR • 1 patients with SD	Kaplan et al. ²²

* CR: complete regression, PR: partial regression, SD: stable disease, PD: progressive disease

Although IL-2 has been extensively investigated and approved for the use in the treatment of a broad range of diseases, it still possesses many limitations and properties that restrict its full clinical use. Systemic IL-2 therapy, which is the main route of administration, is reported to be complicated by life-threatening toxicities some of which are similar to those seen with other cytokines. Flu-like malaise, low blood pressure, fevers, nausea, vomiting, diarrhea, chills, swelling, weight gain, confusion, skin rashes, and changes in blood chemistry are commonly seen in patients receiving systemic IL-2 injections.³¹ In addition to the above side effects, reversible hepatic dysfunction characterized by hyperbilirubinaemia and "vascular leakage syndrome" which is an increase in the vascular permeability and a decrease in vascular resistance, are considered two of the major complications resulting from the systemic IL-2 therapy which may result in hypotension and increase in the body weight of up to ten percent due to extra vascular fluid accumulation.^{31,32}

— —

With the purpose of finding solutions to the aforementioned complications and limitations that accompanied IL-2 systemic administration, many researchers investigated alternate modes and strategies for delivering this cytokine with the goal of achieving less toxicity and optimal clinical outcome. In this chapter, emphasis will be placed on the different means of optimizing the anticancer therapy of IL-2 by utilizing an understanding of its immunological action, structure, pharmacokinetics, and relating all of this knowledge to the different strategies used in delivering this cytokine to its site of action.

1.2. MECHANISMS OF ACTION

Although most of the issues relating to how IL-2 exerts its effect are fairly clear, the exact cellular mechanism of action of IL-2 is still not yet fully understood. Several theories were proposed on

explaining the cellular mechanism of IL-2,^{7,33,34} however, the most acceptable theory today states that IL-2 is taken by activated CD4+ T-cells which express IL-2 specific receptors.³⁵ Those receptors are reported to be composed of three subunits: IL-2 receptor alpha (IL-2R α), beta (IL-2R β), and gamma (IL-2R γ). The low-affinity alpha chain (CD25) is a unique and specific marker for the IL-2 receptor, whereas the medium-affinity beta chain (CD122) is common to both the IL-2 and IL-15 receptors, but the high-affinity gamma chain (p64-CD132) is common to all cytokine receptors.³⁶ The binding of IL-2 with IL-2R, beta and gamma chains in specific, is responsible for signal transduction through activation of several signaling molecules such as Janus Kinase 3 (JAK 3),³⁷ protein tyrosine kinases (PTK),³⁸ signal transducers and activators of transcription 5 (STAT 5) protein,³⁹ the mitogen-activated protein kinase (MAPK)³³ and phosphatidyl inositol 3-kinase (PI3K) pathways.⁴⁰

The generated signals from the subsequent interaction of IL-2 with its receptors then result in alteration in cell behavior that was seen through five event signals: stimulation of tumor specific activated cytotoxic T-cells growth;⁴¹ generation and differentiation of LAK cell activity and augmentation of NK cell mediated cytotoxicity of tumor cell;⁴¹ activation of the endothelium and up-regulation of adhesion molecules on T-cells, which results in enhanced migration of T-cells to the tumor; enhancement of major histocompatibility complex (MHC) expression on tumor cells and antigen-presenting cells; and proliferation of immunoglobulin in B-cells and cytotoxic macrophages.⁴² Figure 1.1 shows a representation of the proposed mechanism of action of IL-2.

All of the signals transmitted by IL-2 provide the rationale for using this cytokine for the treatment of cancer. The mitogenic effect of IL-2 on T-cells, LAK and NK cells can provide the organ of tumor-

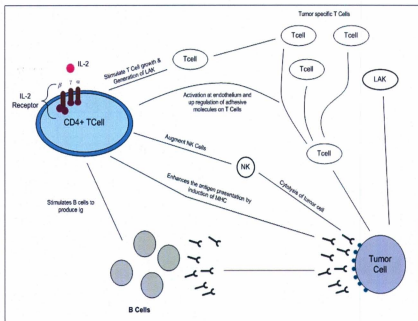


Figure 1.1 A proposed mechanism of action of IL-2.

bearing individuals with an expanded pool of effector cells and the cytotoxic effect which is directed against malignant, but not normal cells in the body.⁴¹

1.3. PHYSICAL PROPERTIES AND STRUCTURE

The structure and the physicochemical properties of IL-2 are important aspects in understanding the function, activity and in designing the optimal therapeutic strategies and delivery systems for this cytokine. IL-2 is a member of a four-helical bundle family of proteins. It has a structure similar to that of human growth hormone and has been reported to have an isoelectric point (pI) of 7.9. It is susceptible to deamidation of the asparagine amino acid, at position 88 of its amino acid sequence, upon its storage in aqueous solutions (pH 5.0 at 25 °C) for periods exceeding two months. This deamidation occurs in a much accelerated fashion at 40 °C compared to 25 °C but reported not to occur at temperatures below 5 °C.⁴³ The biologic activity of IL-2 is sensitive to acidic conditions as it forms a compact denatured state at pH of 2.1 or lower with subsequent loss of activity.^{44,45} Furthermore, it is heat sensitive and undergoes irreversible thermal denaturation and aggregation in solution at temperature exceeding 44 °C.⁴⁴⁻⁴⁶

Natural human IL-2 (hIL-2) is an amphipathic 15.5 kDa globular glycosylated protein with a various degree of glycosylation, as estimated from gel filtration. It is glycosylated at position 3 by the amino acid threonine.⁴⁷ Its primary structure is represented by 133 amino acids, which shows no significant homologies in the primary structure with other cytokines.^{48,49} Recombinant human IL-2 (rhIL-2), which is produced by recombinant protein technology, maintains the native amino acid sequence and biological activity of hIL-2 but, as with many recombinant proteins, possesses some differences in its glycosylation. It is recognized that, in contrast to the naturally occurring hIL-2, rhIL-2 lacks partially, or completely, the carbohydrate moieties attached to its structure.⁵⁰ To improve the pharmacokinetic

properties and the half-life of rhIL-2, modification of this cytokine with various carbohydrate moieties (glycosylation) was studied. As with many proteins, both degree of glycosylation and the glycan moiety used in its glycosylation have tremendous impact on the biological activity, hepatic metabolism, and renal elimination of this cytokine.⁵²

The IL-2 molecule contains one intramolecular disulphide bridge, as determined by a combination of peptide mapping and protein sequencing, linking between cysteine amino acids at positions 58 and 105. Both of these cysteine residues and the presence of the critical disulphide bond are important for maintaining the stability of the tertiary structure of IL-2 which is essential for the biological activity of IL-2.^{52,53} The carbohydrate moiety present in the structure of IL-2 molecules, added after translation of the IL-2 gene, has no effect on its bioactivity, but has an increase in hydrodynamic size sufficient to increase its systemic duration of action.⁵⁴ This carbohydrate moiety represents the molecular heterogeneity of natural IL-2, and it can be speculated that this moiety has some functions during the intra-cellular transport of IL-2 molecules.⁵⁴ The similarities in the structural and functional properties suggest that IL-2 derived from humans, rats, mice and apes are analogous to each other and have similar bioactivity. The only difference between human and murine IL-2 is a unique repeating of 12 consecutive glutamine residues at N-terminal of mature murine IL-2.⁵⁵

The X-ray crystallographic analysis of the three dimensional structure of IL-2 molecules showed it to be composed of a compact bundle of four antiparallel α -helices with short hairpin loops between helices and without any spatial correspondence between sequential helices (see Figure 1.2 for reference).⁵⁵ This suggests that one portion of these molecules forms a structural scaffold, which underlies the receptor binding-facets of the molecules.⁵⁶ The receptor contact sites have been localized with the N-terminal and C-terminal portion of IL-2 molecules.⁵⁵

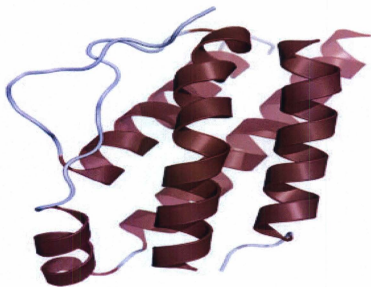


Figure 1.2. Human IL-2 crystalline structure (reproduced from Ref. 55).

1.4. PHARMACOKINETICS

The rate and extent at which the maximum IL-2 concentration is reached in the bloodstream depends mainly on its physicochemical properties (molecular weight, size, and degree of glycosylation), the dosage form design, and its route of administration. As it is the case with all the other acid-sensitive protein drugs, IL-2 faces many stability and physiological challenges when given orally. This explains the reason for it being mainly given by alternative routes of administration. For most patients, the primary route of administration of IL-2 is subcutaneous (sc) injections under the skin.⁵⁷ Intravenous (iv) injections, on the other hand, whether given as a bolus or in infusion form,⁵⁷ are more commonly used for patients under close clinical monitoring as this is considered an intensive patient treatment that is usually given in intensive care units. Other less traditional delivery routes used to administer IL-2 include: intrapleural,⁵⁸ intrathecal,⁵⁹ intraventricular,⁶⁰ intravesicular,¹⁵ intrasplenic (is),⁶² intralesional⁶³ intracranial,⁶⁴ intrahepatic⁷ and by inhalation.⁶⁵ Depending on the route of administration used, different concentrations at the tumor site were usually obtained with the highest being always achieved after localized injections of IL-2, which also proved to result in complete tumor eradication.⁶⁶⁻

68

Following iv administration, the pharmacokinetic profile of rhIL-2 is characterized by high plasma concentrations that decline in a bi-modal exponential form. The initial elimination phase of IL-2, which is mainly due to extracellular-distribution and renal elimination was reported to have a plasma half-life ($t_{1/2}$) of 7-14 minutes.^{57,66} The second phase of elimination, which is attributed solely to excretion via the kidneys, is slower and was estimated to have a terminal plasma $t_{1/2}$ of 85 minutes.⁶⁶ It is well established that more than 80% of the amount of IL-2, which is cleared from the circulation and presented to the

kidney, is metabolized to amino acids in the cells lining the proximal convoluted tubules.⁶⁹ The initial volume of distribution (V_i) of rhIL-2 in mice following iv bolus injection of 500 $\mu\text{g/kg}$ was reported to be 39 ml/kg while its steady state volume of distribution (V_{ss}) is 87 ml/kg with an area under the curve (AUC) of 1.51h/ $\mu\text{g/ml}$ and a clearance rate of 330 ml/h/kg.⁷⁰ Similarly, continuous six-hour iv or ip infusion of IL-2 resulted in detectable steady state serum levels after two hours followed by a rapid drop in the plasma level when the drug infusion stopped.⁶⁶ With respect to im injections of IL-2, it was reported that such administration routes resulted in plasma levels that are typically 10 to 100 times lower than those obtained following iv injections but with a more extended effect. On the other hand, when IL-2 was administered subcutaneously, it was detectable in the plasma within fifteen minutes and achieved a half-life of 2.4 hours and a 100 % bioavailability relative to iv dosing.⁶⁹ It was also demonstrated that the presence of soluble IL-2 receptor decreases the AUC of IL-2 in patients with metastatic renal cell carcinoma.⁷¹ Therefore, the sc route of administration was looked at being more preferred over iv injections since sc injections form depots in the subcutaneous tissues and result in sustained released IL-2 concentrations which are sufficient to bind to more than half of the high-affinity IL-2Rs that are expressed by antigen activated T- and NK cells.⁷⁰

Another parameter that might have an impact on the pharmacokinetics of IL-2 administration by the systemic route is the plasma level of soluble IL-2Rs preceding the treatment. Clinical studies showed that soluble IL-2Rs in tumor-bearing patients is 3- 8 folds higher than in normal individuals (1315 U /ml in which each 3U is equivalent to 1 pg of purified protein).⁷² The α chain is thought to be released from the cell membrane of activated T cells by proteolytic cleavage. The presence of the soluble IL-2R α is therefore thought to reflect the state of T cell activation in this patient's population.⁷³ As such, the failure to saturate all the soluble plasma IL-2Rs could be the reason for variations in the bioavailability

of IL-2. Although there are no studies that report on the effect of these soluble receptors on the distribution and other pharmacokinetics parameters of IL-2, the high affinity of IL-2 to the soluble IL-2Rs will decrease the amount of IL-2 which reaches the interstitial fluid in the relevant tissue site.^{72,74}

During systemic administration of rhIL-2 in humans, elevated soluble IL-2 receptor levels have been found.⁷⁵ The soluble IL-2Rs differs from its membrane-bound counterpart with respect to size, binding capacity and ligand specificity. The soluble form of the human IL-2 receptor is a glycosylated protein with a molecular weight between 35 and 50 kDa.⁷⁶ It binds to IL-2 with low affinity (K_d : 10 nmol/L) which is comparable with the affinity to the membrane bound α -chain of the IL-2 receptor.² The α -chain is expressed on activated T cells which combines with the β - and γ -chains to constitute a high-affinity IL-2R with a 1000-fold higher affinity to IL-2 than presented by the soluble IL-2Rs.⁷⁷⁻⁸⁰ It has been hypothesized that the competition between the membrane-bound and the soluble receptor for IL-2 causes inhibition of IL-2 dependent mechanisms. So far, no data are available on the exact influence of sIL-2R on IL-2 pharmacokinetics.

The preceding discussion illustrates that systemic administration of IL-2 results in unequal and unpredictable distribution and rapid clearance from the body. As such, smaller amounts will reach the tumor cells. In addition, the presence of the endogenous soluble IL-2Rs adversely affects the amount of IL-2 that is free and penetrates the tissues and the organs.⁷¹ Also, to obtain IL-2 in concentrations high enough to saturate those high-affinity soluble receptors, at least 20 mg of IL-2 must be administered,⁷² as the total extra-cellular space in a normal adult is approximately 14 liters. This relative large dose is enough to evoke all the IL-2 systemic side effects.

1.5. LOCO-REGIONAL VERSUS SYSTEMIC DELIVERY

Although systemic injections (iv, im, and ip) are reported to be the most commonly used routes for delivering IL-2 when used in cancer immunotherapy,^{31,62} the intratumoral and loco-regional administration strategies of this cytokine have been reported to be more successful and demonstrate much effectiveness against a broad range of cancers, specifically those associated with solid tumors.⁸² This mode of IL-2 administration provides many advantages over systemic administration. First, local IL-2 administration more often involves the use of lower doses, which results in the absence of the major side effects and toxicities that usually accompany the use of systemic administration.⁶⁷ Second, localized tumors that are resistant to chemotherapy and irradiation, such as tumors located in the head and neck regions, brain tumors, breast tumors and urinary bladder carcinomas, can be efficiently eradicated by loco-regional IL-2 immunotherapy.^{83,84} Similarly, tumors which are often localized close to body surfaces and are not amenable to surgery or conventional therapy, such as malignant melanoma, could be successfully treated with local IL-2 administration.⁸⁵ Third, loco-regional delivery of IL-2 simulates its normal physiological paracrine release pattern and results in less unequal and unpredictable distribution of IL-2 throughout the body tissues and fluids that are usually common in systemic injections. In this manner, side effects and toxicity will decrease tremendously.^{86,87} It is well known that systemically injected IL-2 creates a response that follows the endocrine release pattern of cytokines which usually occurs in response to immune stimulation in which the cytokine diffuses out of the microenvironment to the blood stream where it becomes highly diluted and rapidly eliminated from the body.⁶⁶ Furthermore, dose tolerability following systemic administration of high doses of IL-2 therapy is a well reported phenomenon where the response rate of IL-2 may decrease down to 10% less than that of the most frequently applied doses.^{88,89} This has typically resulted in a subsequent gradual increase of IL-

2 dosing regimen during the maintenance therapy, with a significant increase in the systemic toxicity. Fourth, although the regional and intratumoral IL-2 administrations will result in limited diffusion of the IL-2 into the blood stream, nevertheless, the immune cells (T and NK cells) after being stimulated locally (in the microenvironment) by IL-2 would diffuse through the extracellular fluids to neighboring cells in the surrounding region and also travel in the circulation, producing defensive mechanisms against other tumors without the need for the cytokine itself to circulate.⁹⁰ Additionally, it was also found that the systemic delivery of IL-2 to patients with malignant tumors in the central nervous system, such as tumor in the spinal cord, the cerebrum, the cerebellum, and the brain stem, was not effective as IL-2 was unable to cross the blood brain barrier.⁹⁶ Finally, local delivery sustains the immune effect and prolongs the half-life of the injected IL-2 in the area of the growing tumor as well as in the circulation.⁹¹

The effect of local IL-2 therapy was reported to be through the induction of local massive edema in the vicinity of the tumor cells. This edema is due to the induced vascular leakage and causes extensive tumor necrosis owing to the accompanied interstitial pressure that causes collapse of capillaries and difficulties of nutrients and oxygen reaching tumor cells.⁹² In addition, local IL-2 induces angiogenesis in the normal connective tissue around the tumor, allowing infiltration of leukocytes (mainly macrophages). The infiltrating macrophages will form granulomatous lesions at the site of the tumor and will ultimately resolve the tumor.⁹³

Various studies have been aimed at investigating the effectiveness and safety of loco-regional delivery of IL-2 and other similar cytokines. One of the first studies on the therapeutic efficacy and safety of local administration of IL-2 in cancer therapy was reported in 1983. *Bubenik et al.*, showed that peritumoral IL-2 injections could inhibit the growth of the experimentally induced fibrosarcoma tumors in preclinical B10 male mice models.⁴ In this study, groups of 3-month-old mice received doses of 5 x

10^4 MC11 tumor cells sc at day 0 and were then given either repeated injections of IL-2-containing supernatants from rat spleen cultures or control preparations in 0.5 ml amounts of medium at days 1, 3, 5, 7, 9, 11, 13, 15, 17, and 19. The injections were given subcutaneously around the site of the tumor inoculum. Treatment of tumor-bearing mice with IL-2 preparations differing in the concentration of IL-2 revealed that IL-2 concentrations higher than 1 U/ml were necessary to produce a significant tumor-inhibitory effect. It was also concluded that the tumor-inhibitory effects were dependent on the concentration of IL-2 and the repeated injections of the supernatants. This study represented one of the first few preclinical attempts in the therapeutic utilization of local IL-2 alone, without being accompanied by the adoptive transfer of cytotoxic T-cells in the treatment of cancer. Further evidence for the efficacy of local IL-2 administration has been provided by the positive results of the preliminary clinical trials that were conducted using local administration of IL-2.

Pizza *et al.*, found that repeated intratumoral injections of 1969-4046 U of bovine IL-2 over 7-54 days lead to almost complete regression of the urinary bladder carcinoma.⁸⁹ They concluded that the dose-dependent antitumor immunological effects were mediated by IL-2 activity alone and not dependent on the level of foreign bovine protein contained in the preparation. Also, it was concluded that in none of the patients treated were any early or late adverse clinical side effects observed. In another study, Yasumoto *et al.*, carried out an investigation on the effect of intrapleural administration of rhIL-2 in 11 patients suffering from malignant pleurisy due to solid tumors in their lungs.²⁰ The 6 patients who were subjected to surgical resection of the primary tumor were given IL-2. Clinically, malignant cells in the pleural effusion disappeared in 9 of 11 patients 4 to 10 days after the start of the treatment. Recent studies conducted by Caporale *et al.*, on rats also demonstrated the efficacy of loco-regional IL-2 therapy in colon carcinoma.⁹⁴ Furthermore, promising results were reported with many other studies that investigated the advantages of loco-regional IL-2 over its systemic administration

including but not restricted to intra/peri-lesional local injection,^{91,95} intra-cavity infusion,⁹⁶ intra-vesicle administration⁹⁷ and inhalation,⁶⁵ all of which suggest that local IL-2 therapy is more effective in raising an antitumor action against transplanted tumor, as well as spontaneous tumor of various origin and immunogenicity, than any systemic applications.⁹⁸ Tables 1.2 and 1.3 list more details regarding pre-clinical and clinical studies conducted in that regard including those discussed above.

In addition to the above, local IL-2 therapy was always superior to the systemic treatment in all the studies in which a direct comparison was made between systemic and local treatment.⁹⁵⁻⁹⁷ Also, it was reported that in some cases, local IL-2 was even more effective in treating distant tumors than systemic administration of the cytokine.^{95,99,100} Jacobs *et al.*, recently concluded that local IL-2 is more effective than systemic application in patients with nasopharyngeal carcinoma.¹⁶ The researchers combined standard irradiation therapy with local IL-2 therapy. During the 5 years of the study, the results revealed that 63 % of the patients showed a disease free survival; whereas no response was observed with *chi et al.*, who applied single modality systemic IL-2 therapy.¹⁰¹

It can be concluded from the above discussion that local IL-2 administration restores paracrine pattern of release of IL-2 upon lymphocytes stimulation rather than simulating its endocrine release pattern under immune stress or stimuli. As well, the regional mode of administration of IL-2 and the limited diffusion of this paracrine IL-2 to blood stream would minimize the exposure of many other cell and organs that do not need to be switched to the immunostimulated state. In this manner, side effects and toxicity would be decreased. It has also been observed that lymphatic cells and other cytokine activated by IL-2 locally would travel in the circulation, producing defensive mechanisms, without the

Table 1.2. Summary of representative pre-clinical animal studies demonstrating the efficacy and toxicity of using different routes of administration and dosing schedules of IL-2.

Route of Administration		Dose & Dosing Schedule	Tumor Type	Response	Toxicities Observed	Ref.
Systemic	intra peritoneal	4.8×10^4 IU every day for 5 days	erythro-leukaemia	complete remission in 50% of the treated mice	No toxicity data reported	Thompson et al. ⁷⁰
		1.0×10^5 IU three times a day for 5 days	sarcoma	regression of hepatic metastases in 66-95% of the treated murine model	sever acute toxicity: weight gain, ascites and pleural effusions	Lafrèniere et al. ¹⁹¹
		$1.5 - 3.0 \times 10^5$ IU three times a day for 5 days	sarcoma and melanoma	regression of transplanted tumors and pulmonary metastases in 66-95% of the treated murine model	No toxicity data reported	Rosenberg et al. ¹⁹²
Local	subcutaneous	4 weeks infusion of 424 and 286 IU/kg/day	prostatic adeno-carcinoma	decrease tumor growth	no significant toxicity	Henriksson et al. ¹⁹⁴
	intratumoral	single injection of 2.5×10^6 IU	colon cancer	significant responses in all treated rats	no discomfort in any animal	Caporale et al. ⁹⁴
	peritumoral	single injection of 4.5×10^6 IU	colon carcinoma	delay in tumor growth, but no cure was obtained	No toxicity data reported	Kusnierczyk et al. ¹⁹³
		four time injection of 4.5×10^6 IU	colon carcinoma	60% of the treated mice cured	No toxicity data reported	Kusnierczyk et al. ¹⁹³
		multiple injection of 2×10^5 IU twice a week for 2 consecutive weeks	bovine ocular squamous-cell carcinoma	67% of the treated cows cured	no noticeable side effect reported	Den Otter et al. ⁴¹
		$0.2 - 2 \times 10^6$ IU/day for 10 days.	ocular squamous cell carcinomas	50 -69 % of tumours treated	mild side effects: edema and swelling in the tumors	Stewart et al. ¹⁸⁸
		2.5×10^6 IU as single dose	mammary carcinomas	increase the survival in all treated animal	No toxicity data reported	Moiseeva et al. ¹⁹⁰

Table 1.3. Summary of representative clinical studies demonstrating the efficacy and toxicity of using different routes of administration and dosing schedules of IL-2.

	Route of Administration	Dose & Dosing schedule	Tumor Type	Response	Toxicities observed	Ref.
Systemic	intermittent bolus injection	72×10^3 IU/kg every 8 hours for 5 days repeated after 7 to 10 days.	metastatic renal cell carcinoma	7% complete response and 8% partial response	acute toxicity: severe malaise and infections	Yang et al. ⁹¹
		720×10^3 IU/kg every 8 hours for 5 days repeated after 7 to 10 days.	metastatic renal cell carcinoma	3% complete response and 17% partial response	severe toxicity: grade III or IV thrombocytopenia, malaise, and hypotension	Yang et al. ⁹¹
		1×10^6 IU/kg every 8 hr for 5 days.	metastatic renal cell carcinoma	2% complete response, 10% had partial responses, and 2% had a minor response.	acute toxicities: hypotension, weight gain, oliguria, and elevation of bilirubin and creatinine levels	Rosenberg et al. ⁹¹
	intermittent intravenous infusion	6 and 7.2×10^3 IU/kg for 15 minute every 8 hours for up to 14 consecutive doses as clinically tolerated	metastatic renal cell carcinoma	14% of the patient responded (5% complete responses and 9% partial responses).	severe acute toxicities: hypotension, arrhythmia oliguria, and elevation of bilirubin and creatinine levels	Fyfe et al. ⁹²
	intrapleural effusions	$1-2.8 \times 10^6$ IU/day up to 10 days	lung carcinoma	cancer cells disappeared in 82% of the patients	minimum adverse effect: fever, increase of pleural effusion, and eosinophilia	Yasumoto et al. ⁹³
Local	intraperitoneal	$1.5-9 \times 10^6$ IU/day	abdominal cancer	37.5% of the treated patient improved	negligible adverse effect: fever and local skin rash	Krastev et al. ⁹⁴
	inhalation	$18-36 \times 10^6$ IU/day	pulmonary or mediastinal metastases	16% responded; 49% disease stabilized and 35% disease progressed.	mild local toxicity and consisted mainly of cough.	Gooding et al. ⁹⁵
	intracranial	single injection of $0.8-5.4 \times 10^3$ IU	malignant gliomas	26% of the patient responded (13% complete responses and 13% partial responses).	no marked side effects, except for slight fever and chill.	Yoshida et al. ⁹⁶
	intratumoral	3×10^6 IU/day for 5 consecutive days.	papillary bladder carcinoma	80% of the treated patient cured	no toxic effect	Den Otter et al. ⁹⁷
	intra- and	$6-12 \times 10^6$ IU	multiple	complete remission	no systemic side	Pföhler et

peri-lesional	every 8 hr over 12 weeks	cutaneous metastases of malignant melanoma	achieved	effects were reported	al. ⁸¹
intra-lesional	0.6-6x 10 ⁶ IU 2-3 times weekly, over 1-57 weeks, depending on lesion size.	skin and soft-tissue melanoma	85% complete response and 6% partial response were achieved.	inflammatory reaction at the site of injection with local swelling and erythema	Radny et al. ⁹
intrapleural	9 x 10 ⁶ IU intrapleural twice/week, for 4 weeks, 3 x 10 ⁶ IU IL-2 were subcutaneously administered thrice weekly for up to 6 months, in non-progressing patients.	malignant pleural mesothelioma	increase survival of all patients, 32% with disease stabilization, 3% complete regression and 19% partial regression.	mild to moderate toxicity, mainly a flu-like syndrome	Castagneto et al. ¹⁸⁹

need for the IL-2 itself to circulate.⁹⁹ In other words, the beneficial effect of IL-2 administration is consistently maximized by localized delivery. Consequently, it can be concluded that the recent results suggest that the regional administration might provide the best strategy for IL-2 immunotherapy of tumors.

1.6. SUSTAINED (CONTINUOUS) VERSUS INTERMITTENT RELEASE

In view of the discussion above, the following questions come to mind: What is the maximum concentration required in the local microenvironment? Do we need an intermittent or continuous release of IL-2? Although several recent studies described the application of IL-2 and the superiority of its regional delivery over its systemic administration in the treatment of different tumors,^{101,102} little has been reported regarding the most efficient and least toxic mode of delivering this cytokine to its site of action. It has been established in almost all reported cases that a single IL-2 injection, in whatever manner local or systemic, is not sufficient for completing the tumor eradication and there is a requirement for frequent repeated injections of IL-2.¹⁰³ The already approved IL-2 cancer therapy protocol requires a dosing schedule of intravenous administration every eight hours for five days, followed by another five-day course after day nine.¹⁰⁴ In the same manner, the standard local immunotherapy with IL-2 includes local injections for five consecutive days. This intermittent mode of administration during treatment is characterized by relatively high frequency of dosing, which requires a healthcare professional and may be inconvenient to the patient. In addition, most of the tumor localization strategies prevent repeated injections for technical and ethical reasons.⁶⁷ In the mean time, a simpler alternative continuous delivery strategy offers a better approach to maintaining the therapeutic tissue level, avoiding the imperfections of recurrent administration methodology. Obviously, it will be a great step forward if patients can be treated with only a single injection of a slow delivery system, in

which IL-2 is gradually released during certain consecutive days, for maintaining a long-lasting therapeutic level at the site of the growing tumor.¹⁰⁵ The important issue that should be addressed in the intermittent mode of administration is that the T-cells are exposed to a throb or wave of the delivered IL-2, which is characterized by a time and concentration dependent decline in the action.¹⁰⁶

This mode of IL-2 delivery was the focus of research conducted by *Otter* and his coworkers.¹³ This research group explored the consequent outcome of massive intermittent peritumoral IL-2 injection on transplanted murine colon carcinoma. Although after four IL-2 injections more than 45% of the mice were cured, it was perceived that there was a possibility of tumor re-growth while the IL-2 level declined. In another study, *Da Pozzo et al.*, examined the toxicity and the immunologic effects of localized prolonged infusions of low dose rIL-2 in dogs.¹⁰⁷ The results demonstrated that continuous regional infusion with relatively low doses of IL-2 was able to stimulate peripheral blood LAK cells effect. This study not only proved that continuous localized administration is a safe method of IL-2 delivery with the absence of major side effects, but also confirmed its higher ability to selectively increase the number and activity of NK cells when compared to the intermittent mode. Additionally, a study was done by *Naito et al.*, to examine the difference between intermittent and continuous delivery of IL-2 into tumor bearing mice.¹⁰⁶ In this study, they compared the antitumor effect of continuous infusion (iv, ip and is) versus a single daily dose of the same injection route. The results manifested that for all routes of administration, continuous infusion prolonged host survival, and was vastly superior in antitumor efficacy than bolus doses. They also reported that uninterrupted IL-2 concentration at the tumor site had augmented the CD8+ T-cell induction.¹⁰⁶ Many other studies aimed at studying the advantages of sustained release of IL-2 including the use of minimum osmotic pumps,¹⁰⁸ liposomal formulations¹⁰⁹ and polymer based release systems have been conducted.¹¹⁰ All these studies concluded

that the continuous delivery represented the method of choice as it enhances IL-2 efficiency in immunotherapy against the tumor by increasing the mean residence time (MRT) of the IL-2 and decreases the number of injections.

Based on the discussion just presented, it can be concluded that maintaining localized IL-2 dose at a low and continuous level in the tumor vicinity is important, as it results in avoiding side effects which accompany intermittent high IL-2 dosing regimen, preventing the cytokine level at the tumor site from fluctuation, augmenting the antitumor immuno-stimulatory performance of this cytokine and increasing the patient compliance.

1.7. DELIVERY SYSTEMS AND DOSAGE FORMS: ADVANTAGES AND LIMITATIONS

Since its discovery in 1976, different delivery systems and strategies have been explored to formulate and deliver IL-2 while at the same time trying to achieve two major goals. The first is to deliver and target IL-2 specifically and safely to its site of action to maximize its therapeutic efficacy while minimizing its toxicity. The other is to overcome stability issues during the preparation of dosage forms containing this cytokine, and to help in maintaining its stability during storage of the dosage form and after administration to the body. Work in this area is ongoing.

With respect to IL-2, which is acid sensitive and which possesses other stability problems, early studies focused mainly on achieving a localized and/or sustained/controlled release to help in increasing the therapeutic outcome, in extending its half-life in plasma and in decreasing the amount to which other non-tumor or non-infected tissues are exposed upon administering this potent cytokine. Currently,

studies concerning how efficient the methods and strategies used to formulate IL-2 to achieve the two mentioned goals are running in parallel with efforts to use it in the treatment of different neoplastic and viral diseases.

As with other protein therapeutics, administering IL-2 by the oral route has been a challenge and an elusive target since its discovery. The major barriers in developing oral formulations for IL-2 include but are not restricted to poor intrinsic permeability, luminal and cellular enzymatic degradation, rapid clearance, and chemical and conformational instabilities.¹¹¹

In spite of the obstacles described above, many researchers attempted to investigate the use of the oral route for IL-2 delivery. For example, *Koren and Fleischmann* studied the myelosuppressive effect of IL-2 orally administered to mice.¹¹² They demonstrated that oral administration of IL-2 was shown to exert systemic effects by suppressing both the peripheral white blood cell counts and the bone marrow in a dose-dependent manner. Those observations suggested that the induction of systemic effects by orally administered cytokines may be a general phenomenon. Moreover, *Toth et al.*, reported a double blind study in which they evaluated the effect of orally administered IL-2 on the hematological variables in feline leukemia-positive cats.¹¹³ Their results revealed that oral administration of 400 IU of rIL-2 decreased the mean corpuscular hemoglobin concentration after 7 days in cats which returned to the control level by 14 days. Other researchers have also demonstrated that IL-2 delivered to the oral cavity can transfer signals through the mucus membranes and as such induced systemic responses.¹¹⁴

In spite of the above encouraging results, conventional approaches to address those barriers facing IL-2 oral delivery, which have been workable with traditional, small, organic drug molecules, have not

readily fully translated into effective IL-2 formulations yet As such, the development of a clinically effective and approved oral formulation of IL-2 is still something to be materialized. Currently, the research conducted to overcome the obstacles for the absorption of IL-2 from the gastrointestinal tract includes the co-administration of enzyme inhibitors and/or absorption enhancers, the encapsulation in liposomes, micro-emulsions, the use of biodegradable mucoadhesive nanoparticles, and the modification of the cytokine structure through the attachment of chemical moieties.¹¹⁵

Among the other systems which are extensively investigated for delivering IL-2 are inhalers. Administering IL-2 via pulmonary inhalation is currently receiving enormous attention due to its applications in both regional and systemic IL-2 delivery in cancer therapy. Potential advantages of this delivery route for protein-containing drugs like IL-2 include a greater extent of absorption due to an absorptive surface area of approximately 140 m² and high volume of blood (5000 ml/min in the human lung) flowing through the lungs which result in high IL-2 bioavailability.¹¹⁶ Lack of some form of peptidase/protease activity when compared with the gastrointestinal tract and lack of first-pass hepatic metabolism of absorbed compounds adds to the potential benefits of protein drug administration via pulmonary inhalation.

A local immunotherapy using high-dose IL-2 inhalation therapy was clinically scheduled by *Huland et al.*, to 116 patients with metastatic renal cell carcinoma. The results obtained throughout the duration of six years of inhalatory IL-2 therapy concluded that progressive pulmonary metastases responded dramatically in the 15 % of patients for a median of 15.5 months and were stabilized in 55% of patients for a median of 6.6 months.⁶⁵ Many other studies also reported the therapeutic potential and the advantages of inhalatory delivery of IL-2.¹¹⁷⁻¹²⁰

Based on the encouraging results obtained to date and the rapid advances being made in IL-2 inhalation therapy, it can be anticipated that additional formulation approaches such as the different aspects of aerosol technology might be developed to this delivery technique in the near future. By applying aerosol technique, we could achieve more uniform distribution with greater extent of penetration into the peripheral or the alveolar region of the lung. Although pulmonary delivery is very attractive because of the large absorption area and avoidance of first-pass metabolism in the liver, goals such as device effectiveness, ease of use, and low cost, as well as dosage reproducibility, sustained drug release, rapid tissue uptake, optimal targeting, and reduced side effects, are still rather elusive. Also, the relative inefficiency and volume limitations of inhalation delivery currently limit this approach to molecules of relatively high potency like IL-2. Nevertheless, in light of the fast growing drug-delivery market, the pharmaceutical industry and medical device companies seek technical solutions to these problems to meet the demands of investors, stock holders, healthcare providers, and patients.

In general, the delivery systems developed for IL-2 were divided into two main categories. The first category aimed at increasing IL-2 therapeutic outcome through extending its half-life. This category includes but is not restricted to gene therapy,^{122,123} liposomes,^{124,125} polymeric microspheres,^{126,64} thermo responsive synthetic polymers,¹²⁷ hydrogels,¹²⁸ and biodegradable elastomeric devices.¹³² It is important to state here that the above used references are only representative citations for research work conducted on those IL-2 delivery systems and do not constitute a comprehensive list of all the work done in that area. In the following section, the advantages and limitations of each of these formulation strategies and delivery systems will be examined individually. Table 1.4 lists more details regarding some of these controlled/sustained delivery systems.

Several approaches have been investigated to increase IL-2 plasma half-life by decreasing its body clearance. One of those successful approaches is to increase the molecular weight of IL-2 by binding it with PEG derivatives like monomethoxy polyethyleneglycol in a process named PEGylation.¹³⁰ The addition of PEG molecule to IL-2 resulted in an increase in the hydrodynamic radius of IL-2 molecule, which in turn decreased its glomerular filtration rate and reduced the renal clearance up to 130 fold in comparison to the free non-PEGylated IL-2 molecule.¹³¹ As well, the covalent attachment of PEG to IL-2 proved to improve its water solubility, thermal and physical stability and protected it against enzymatic degradations. On the negative side, although this approach succeeded in increasing the half life of IL-2 in the blood stream, the addition of this hydrophilic moiety to IL-2 resulted in a significant decrease in IL-2 lipophilicity which leads to a decrease in its absorption via the lymphatic system and subsequent reduction in its lymphatic concentration. In addition, IL-2 activity was found to be heavily influenced in a harmful way by the degree and the site of its PEGylation.¹³² In conclusion, the use of PEGylation technology to IL-2 allows the dosing interval to increase, resulting in improved patient convenience and enhances quality of life. However, it might decrease the clinical effectiveness of IL-2 for the aforementioned reasons and could increase the level of undesirable side effects of IL-2 which is related to the high and prolonged plasma concentration.¹³⁰ Another approach to prolong IL-2 *in vivo* half-life, in order to extend its therapeutic efficiency, was the genetic fusion of IL-2 molecule with human serum albumin. An example of using this albumin fusion technology is "Albuleukin[®]" which is a long-acting form of IL-2 approved for cancer. Albuleukin[®] has the advantageous pharmacokinetics properties of albumin and it can distribute between vascular and extravascular tissue of the body.⁶⁹ The pharmacological and pharmacokinetic profiles of Albuleukin[®] following a single iv injection to mice

Table 1.4. Summary of the polymeric controlled/sustained release delivery systems used for IL-2.

Delivery System	Administration. route	Polymer/ ingredients	Main <i>in vitro</i> release mechanism	Initial release phase (% & duration)	Duration of <i>in vitro</i> release	Bioactivity of IL-2 released	<i>In vivo</i> therapeutic efficacy	Reference
Liposomes	intravenous	dimyristoyl phosphatidylcholine	degradation	40-60% in the first 2 hours	24 hours	not reported	not reported	Nivelle et al. ¹⁵⁰
	subcutaneous injection	dimyristoyl phosphatidylcholine	degradation	not reported	not reported	not reported	improved immune responses and tumor protection.	Johnston et al. ¹²⁴
Hydrogels	intraperitoneal implantation	methacrylated and hydroxyl ethyl methacrylated Dextran	diffusion	20- 80% depending on water content and hydrogel composition	5-10 days	50-80% of the released IL-2 was biactive	more effective than free IL-2 injections	De Groot et al. ¹⁵²
	subcutaneous injection	DL-lactide, glycolide and polyethyleneglycol	temperature sensitive diffusion	18-25% released within the first day	20	57-90% of the released IL-2 was biactive	37- 49.5% tumor inhibition in rats	Qiao et al. ¹⁵⁵
	intratumoral injection	polyethyleneglycol co-poly lactide	diffusion	5% within the first 24 hours	6 days	not reported	more effective than free IL-2 injections	Hiemstra et al. ¹²⁸
Polymeric microspheres	intramuscular	Poly(lactide)	diffusion and degradation	25% burst within the first 1-3 days of the release period	30 days	40%	not conducted	Sharma et al. ¹⁶⁰
	intramuscular	Poly(lactide-co-glycolide)	diffusion and degradation	10-15% burst in the initial 36 hours	30 days	80%	not conducted	Thomas et al. ¹⁵⁹
	intracranial and intrahepatic	gelatin and chondroitin sulphate	diffusion and degradation	no <i>in vitro</i> release study was reported	14 days	50-75% of the released IL-2 was biactive	more effective in protecting the animal model	Hanes et al. ¹⁶⁶

	injections						than genetically secreted IL-2	
	intracranial implantation	gelatin and chondroitin sulphate	diffusion and degradation	80% within the first 7 days	52 days	not reported	improved the animal survival rate	Rhines et al. ⁶⁴
	not reported	dipalmitoylphosphatidylcholine and Eudragit E 100	diffusion and degradation	80% was released during the first 2 days	30 days	25-80% of the released was biactive	no <i>in vivo</i> therapeutic efficacy was conducted	Thomas et al. ¹³⁹
	not reported	chitosan	diffusion and degradation	35% released within the first 3 days	200 days	not reported	the paper did not report the <i>in vivo</i> therapeutic efficacy	Ozbas-Turan et al. ¹⁶²
Thermo responsive polymers (ReGel®)	subcutaneous injection	poly(lactide-co-glycolide)-block-polyethyleneglycol	temperature sensitive diffusion	25% was released during the first 1hr	3-4 days	bioactivity of the released IL-2 maintained	superior in the reducing tumor growth and animal model survival than free IL-2	Samkowski et al. ¹¹⁹
Polymeric nanoparticles (Medusa II®)	subcutaneous injection	poly-L-glutamate grafted with alpha-tocopherol	diffusion.	not reported	3-5 days	bioactivity study of the release IL-2 did not reported	superior than free IL-2	Li et al. ¹⁸⁴
Elastomer	peritumoral implantation	poly(caprolactone-co-D,L lactide)	diffusion + osmotic pressure driven release	80% released within the first 7 days	40 days	80% of the released IL-2 was biactive	no <i>in vivo</i> therapeutic efficacy was conducted	Gu et al. ¹²⁹

was reported to have a longer plasma half-life than free IL-2 with activity exerted over a longer period of time.⁶⁹ This continuous immuno-stimulation supports the antitumor effect of IL-2 and requires less administrated doses for successful therapy.^{61,67} Similarly, IL-2 was fused with another human pro-apoptotic protein with the name 'Bax'. This fused protein complex, "IL-2-Bax", provided more effective elimination of the tumor and improved survival rate while less frequent administration than regular IL-2 therapy was needed.¹¹⁰

Denileukin diftitox (Ontak®), was the first IL-2 fusion protein to be approved by the FDA for therapeutic use.¹³³ It is a recombinant protein composed of the amino acid sequences for diphtheria toxin followed by the sequences for IL-2. Ontak® represents an example of a fused protein that targets cells bearing high affinity IL-2 receptors internalized via receptor-mediated endocytosis in an acidified vesicle. It is proteolytically cleaved within the endosome liberating the enzymatically active portion of the diphtheria toxin. This diphtheria toxin fragment is released into the cytosol inhibiting the protein synthesis and leading to malignant cell death.

In spite of the advantages seen from the above protein fusion technologies, however, immunogenicity and formation of antibodies is one of the major reported problems that were faced when the used protein was obtained from biologically contaminated sources. In addition, the antitumor action of this form of IL-2 was only limited to highly perfused organs (liver, spleen, and lymph nodes) where it was highly localized.¹³⁴

The use of IL-2 gene therapy has been extensively explored to obtain a sustained local IL-2 concentration to minimize its systemic toxicity, while retaining its immunobiological efficacy. The transfection of IL-2 gene into tumor cells, both *in vitro* and *in vivo*, had shown to produce a specific immune response with reported tumor reduction. There are several molecular approaches for introducing IL-2 gene directly into the tumor to allow local productions of cytokines. These included the use of tumor cells that have been genetically altered *in vitro* to secrete IL-2,^{135,136} the use of adenovirus vectors expressing IL-2,^{137,138} the use of plasmid DNA/lipid complexes for the *in vivo* direct delivery of IL-2 cDNA into tumors^{139,140} and by using non-viral vectors like polymers and liposomes.¹⁴¹ The possible utility of the approach has been demonstrated in many clinical trials. In one study,¹⁴² a total of 21 patients received 10^7 - 10^9 plaque forming units of intratumoral injections of a retroviral vector containing IL-2 gene. Treatment was well tolerated with only minor adverse effects; however, only very low levels of IL-2 mRNA were detected in tumor biopsy samples taken from patients.

Gene therapy has potential; however, there are some unresolved issues and problems surrounding it. First, it is reported that viral vectors could elicit immune reactions and acute toxicities resulting from the infusion of the foreign materials; humoral immune responses against the gene products; and cellular immune responses against the transduced cells.^{143,144} Besides, some of the integrating viral vectors still have a potential risk of insertional mutagenesis. Also, it cannot be overlooked that two cases of death have been previously reported in human gene therapy using adenoviral and retroviral vectors.¹⁴⁴ Second, as noted in the aforementioned example, *in vivo* transfection rates, particularly for tumor cells, are low. This low transfection rate necessitates harvesting cells such as tumor infiltrating lymphocytes or tumor cells and treating them to express increased cytokines.¹⁴⁵ The cell population is then established *in vitro* and returned to the patient. Tumor cells are irradiated before being returned to the patient, to prevent

reintroduction of replication competent tumor cells.¹³⁵ This process is labour intensive, and difficult to achieve. Most human tumors are difficult to establish as *in vitro* cell lines, and extensive subcloning and *in vitro* replication might alter the original antigenic composition of the primary tumor.¹⁰⁸ Moreover, it may take several months to transduce a tumor cell. Such patient-individualized therapy is therefore very cost intensive. Finally, this approach is fraught with ethical issues.

Liposomal formulations have been extensively used by researchers for formulating IL-2 loaded sustained-release delivery systems. As non-toxic and biodegradable carriers, liposomes can incorporate IL-2 in its lipid bilayer. In many of these studies, IL-2 has been found to be efficiently incorporated when formulated by using negatively charged liposomes.¹⁴⁶⁻¹⁵⁰ The results from those studies show that IL-2 consistently adsorbs onto the surface of liposomes, due to electrostatic interaction between the positively charged IL-2 and the negatively charged liposomal components, and not in the aqueous interior. As such, the encapsulation efficiency of IL-2 within the liposomal structure was always low and was found to be influenced by the density of negatively charged lipid in the liposomes. Specifically, it ranged from 25% for liposomes composed of egg phosphatidylcholine and 20% egg phosphatidylglycerol or cholesteryl hemisuccinate to 80% for liposomes composed of egg phosphatidylcholine only.¹⁴⁹ In one study conducted by *Kopenhagen et al.*,¹⁴⁹ although it was concluded that no differences in the protein structure were observed using the circular dichroism scans of free rIL-2 and rIL-2 adsorbed to the liposome preparation, the *in vitro* activity assays demonstrated that rIL-2 liposomes possessed only 47% activity when compared to free rIL-2.¹⁴⁶ Furthermore, the release period of IL-2 from liposomal formulations were always short. For example, in a study conducted by *Neville et al.*,¹⁵⁰ it was demonstrated that up to 60% of the total loaded rIL-2 was released as a burst within the first two hours while all the rIL-2 was released from the liposomal preparations by

24 hr. This behavior has been noted with other proteins, such as interferon-gamma,¹⁵¹ in which 75% of the initially loaded cytokine was released within the first 8 hours.

Liposomes have the distinct advantage of easy administration by injection. However, they also have distinct disadvantages. As a result of short term stability, they produce relatively short drug release durations necessitating additional painful injections, and release rates are neither sustained nor controllable. Thus, they do not appear to be optimal for sustained, local delivery.

Hydrogels have also been used as carriers for localized and sustained release of IL-2 using polymers from both natural and synthetic sources.^{105,152-154} For example, *De Groot et al.*, developed IL-2-containing macroscopic cylinder-shaped non-biodegradable methacrylated dextran hydrogels by redox initiated polymerization reaction using potassium peroxy-disulfate.¹⁵² The *in vitro* release studies showed that within the first 2 days, almost 30% of the encapsulated IL-2 was released with a total of 40% released in the first 5 days. This 5-day release profile revealed that this hydrogel might be able to mimic the current treatment protocol with free IL-2 for 5 consecutive days. Additionally, two months following the intraperitoneal injection implantation of cylinders of this hydrogel (loaded with 5×10^6 IU IL-2) in experimental mice model with lymphosarcoma showed that 87.5 % of the treated mice (7 of the 8 mice) survived longer time than the control tumor mice and 62% cure rate (5 of 8 mice) was achieved.¹⁵²

Hiemstra et al., developed a PEG-(poly L-lactide) and PEG-(poly D-lactide) hydrogels in which the rhIL-2 was loaded by mixing it with aqueous solutions of these copolymers.¹⁰¹ The release of IL-2 from this colloidal gel was constant and sustained, and the therapeutic effect in the treatment of lymphoma was retarded up to 2 weeks in comparison with free rhIL-2. The zero order release kinetics and

effectiveness of the released IL-2 indicated that PEG-lactate hydrogels was a promising platform for sustained delivery of IL-2. A more recent study was conducted by Qiao and coworkers to demonstrate the feasibility of long term sustained-release of IL-2 from injectable thermosensitive hydrogels synthesized by bulk copolymerization of DL-lactide, glycolide and PEG1500 (see Table 1.4 for details).¹⁵⁵

As seen from the aforementioned examples, the advantages of hydrogels as delivery vehicles are that they are as soft as body tissue, and thus are considered to be very biocompatible and can be designed to be biodegradable.^{105,128,152} However, they possess few limitations. First, for most protein drugs, hydrogels possess drug stability issues with storage because of the presence of a large degree of water in the device; second, hydrogels made from natural materials like collagen and gelatin are frequently immunogenic^{156,157} and are more difficult to manipulate or process than synthetic polymers; Finally, hydrogels made from natural materials like dextran are typically characterized by weakness in their mechanical properties, batch-to-batch variations and the release rate was not controlled.

On the other hand, although hydrogels made from synthetic polymers can be reproducibly and reliably manufactured, their chemical modifications can be easily made to tailor their properties and mechanical strengths to a specific application, and their sterilization is often easier. They possess few limitations. First, many of those prepared hydrogels are either not biodegradable or possess very low biodegradability and so a surgical removal step would be required; Second, as seen in the aforementioned examples in the above discussion, the constant release achieved was always short with high percentage of release achieved in the first few hours or days; Third, in chemically crosslinked hydrogels formulation, crosslinking agents are needed, which most often are toxic and may damage the

incorporated proteins and peptides. On the other side, physically crosslinked hydrogels depending on hydrophilic interaction¹⁵⁵ may also lead to denaturation of the loaded cytokine.

Polymeric microspheres/nanospheres have also been developed which are designed to deliver constant amounts of encapsulated IL-2 in a controlled and/or sustained manner. Such formulations provide one of the most promising localized delivery systems for cytokines to tumors. The microspheres/nanospheres are reported to be typically made from a biodegradable polymeric material like polylactide-co-glycolide (PLG),^{158,159} polylacticacid (PLA),^{160,161} chitosan,¹⁶² alginate/chitosan,¹⁶³ dextran,^{164,165} and gelatin/chondroitin-6-sulfate.^{64,166}

Microspheres made from PLG and PLA in which IL-2 is loaded as discrete solid particles typically release the drug in three phases: an initial burst; diffusion controlled release; and erosion controlled release. The initial burst is due to protein particles adsorbed onto the microsphere surface, while the diffusion controlled release is a result of dissolved protein diffusing through the water-filled pores and channels within the microspheres.^{167,168} To obtain a constant release rate from PLG or PLA microspheres, the diffusion phase must overlap with the erosion release phase such that new pores or channels are created. Polymeric microspheres have the advantages of not only providing a constant release, but of being easily injected to the target site, providing a long term release duration, consisting of proven biocompatible materials, having a reasonable shelf-life and degrading to completely bioresorbable compounds. They thus appear to be a very promising formulation.

The main problem with PLG and PLA microspheres is maintenance of protein stability. The activity of a protein molecule is determined by its conformation in solution. Proteins are susceptible to

aggregation, denaturation and adsorption at interfaces, deamidation, isomerization, cleavage, oxidation, thiol disulfide exchange, and β elimination in aqueous solutions. The major factors affecting these changes are mechanical forces such as shear, the presence of surfactants, buffers, ionic strength, the presence of oxidizers such as ions, radicals and peroxide, light, pH and temperature. Thus, protein denaturation and aggregation may result in a loss of potency and the conformation changes in the protein molecule may make the protein immunogenic.¹⁶⁹

As it is the case with protein drugs, IL-2 possesses a number of stability problems. Firstly, IL-2 is susceptible to loss of activity under acidic conditions due to the disruption of the cysteine bond integrity, which is the key to IL-2 activity as a result of protonation. Loss of cysteine bonding has been correlated to activity loss of at least 50%.^{53,170} Furthermore, at low pH, unfolding takes place for IL-2 resulting in the formation of compact denaturated hydrophobic clusters that facilitate the aggregation of protein.⁴⁶ Various means of stabilizing proteins in solution have been determined. These include the addition of compounds such as polyols, inorganic salts, and amino acids.¹⁷¹

The problems of using the PLG microsphere formulation involve both acidic protein degradation, and denaturation at an organic solvent-water interface. The bulk erosion characteristics of this polymeric system can allow water infiltration and swelling in the matrix prior to release. This will result in the accumulation of the carboxylic acid based monomers and oligomers (lactic acid and glycolic acid) in the core of the PLG microspheres which has been found to decrease the pH in the pores and channels of the device to as low as 1.5.¹⁷² As explained above, at this pH, IL-2 is certain to lose the majority of its activity. In addition, IL-2-loaded microspheres are typically prepared using a water-in oil-in water (w/o/w) emulsification procedure in which the protein is dissolved in the aqueous phase. This

preparation procedure has also been found to result in protein denaturation due to the contact of the protein with the polymer solvent at the solvent-water interface.^{159,173}

There are few reports in which IL-2 has been incorporated in PLG and PLA microspheres and its activity after release studied.¹⁵⁸⁻¹⁶¹ Sharma *et al.*¹⁶⁰ used phase inversion encapsulation to load IL-2 into PLA. They demonstrated that PLA nanospheres are able to release IL-2 for 30 days with 25% released between days 1-3. They also reported that the bioactivity of day 1 rIL-2 released samples (post-release activity) was only 40%. In a similar approach, Egilmez *et al.*, also loaded rIL-2 into PLA nanospheres.¹⁶¹ They demonstrated an encapsulation efficiency of 71% and release of 22% within the first 3 days. The total rIL-2 release process lasted for 7 days and the composite bioactivity of all rIL-2 released was approximately 50%.

Thomas *et al.*,¹⁵⁹ reported the use of double emulsion (DE) and single emulsion (SE) methods to prepare PLG (50/50) based microspheres. Both microsphere systems demonstrated sustained release behavior over a period of almost 30 days. The SE prepared particles showed a 10-15% burst in the initial 36 hours followed by a slower linear release rate that lasted through day five. Subsequently, there was a phase of induction followed by another period of release. The DE prepared spheres exhibited a similar overall time course of release, although the magnitude was larger in terms of the percentage of total content released. Both SE and DE prepared microspheres demonstrated reduction in activity over the delivery period. The bioactivity of IL-2 released from microspheres prepared by DE was around 80% for the first 5 days, and then rapidly dropped to less than 40% by day 10. On the other hand, the bioactivity of IL-2 released from microspheres prepared by SE was around 85% for the first 4 days, and then rapidly dropped to less than 50% by day 7. Thus maintaining the stability of IL-2 within PLG

microspheres is still a problem. This stability problem may be overcome by changing the design of the microspheres surface geometry to permit the complete release of IL-2 via diffusion before significant degradation takes place. One possibility of doing so is through the use of microporous microspheres wherein the cytokine is loaded completely into the pore and not surrounded by polymer. IL-2 release would then proceed via diffusion through the tortuous channels, which may proceed at a faster rate than polymer degradation.¹⁷⁴ A study to demonstrate this concept was conducted by *Hora et al.*,¹⁵⁸ They reported that PLG microspheres only delivers very limited amounts of the encapsulated PEG-IL-2 daily. However when IL-2 was co-encapsulated with human serum albumin in the same polymer, an initial burst of 8-10% was observed with an increase in release rate of IL-2 to about 2-3% per day in a bioactive form continuously over a 20- to 30-day period. This was mainly attributed to the porous structure formed upon using human serum albumin with PLG.

Alternatively, a different release mechanism could be employed. It has been demonstrated that a constant drug release rate is achievable from a rubbery polymer matrix in which the drug is distributed as discrete particles. Due to osmotic water penetration, ruptures occur in the polymer and dissolved drug solution is forced out of the device.^{175,176} Accomplishing this type of release mechanism with microspheres using novel elastomeric materials is currently under investigation.¹⁷⁷

In an attempt to avoid the harsh effect on IL-2's stability and bioactivity caused by using organic solvents in the preparation of IL-2 microspheres, other aqueous-based polymers and preparation methods were introduced. IL-2 loaded dextran^{164,165} and gelatin-chondroitin-6-sulphate based microspheres^{64,166} are typical examples of such microsphere formulations.

The use and tissue reaction of subcutaneous injections of IL-2 loaded dextran microspheres was investigated in rats by Cadee *et al.*,¹⁶⁴ In their study, microspheres based on methacrylated dextran (non-degradable), dextran derivatized with lactate-hydroxyethyl methacrylate, or derivatized with hydroxyethyl methacrylate (degradable) were prepared. The tissue reaction over a period of 6 weeks of the injected dextran microspheres was compared to similar injections of PLG microspheres. They showed that both dextran-based microspheres were well tolerated and are suitable candidates for IL-2 slow release systems.

Dextran-based microspheres are promising; however, they possess few limitations which make PLG microspheres a more favorable system. First, the use of non-degradable dextrans like methacrylated dextran microspheres requires a second visit to the site of injection for the removal of the depleted microspheres. Second, although this study shows that both non-degradable and degradable dextran-based microspheres are well tolerated after subcutaneous injection in rats, PLG microspheres were overall less cytotoxic and showed lower numbers of infiltrating granulocytes compared to both degradable and non-degradable dextran based microspheres.^{164,165}

Other promising aqueous-based microsphere formulations that do not necessitate the use of organic solvents in their preparation are the gelatin-chondroitin-6-sulphate based microspheres. These microsphere formulations were investigated for the purpose of intratumoral and sustained delivery of IL-2 for experimental brain and liver tumors and for treatment of experimental malignant glioma in mice and rats.^{64,166} The results demonstrated the ability of those carriers to stimulate long acting antitumor immunity that provided an avenue for their use as a method of treating a variety of cancers. In one study, Rhines *et al.*,⁶⁴ investigated the encapsulation, release kinetics, and the bioactivity of IL-2 from

gelatin-chondroitin-6-sulphate based microspheres. The study revealed that the encapsulation efficiency was approximately 88.5%. The release profile was characterized with a rapid release rate (almost 80%) within the first 7 days followed by a much slower release over a total period of approximately 52 days.⁶⁴ The *in vitro* bioassay studies conducted by the same team in a previous study using the same formulation approach demonstrated that IL-2 retained only a total of approximately 50% of its original bioactivity over a total release period of 2 weeks.¹⁶⁶

Gelatin-chondroitin-6-sulphate based microspheres have potential. However, gelatin based preparations face the same challenges and limitations discussed under hydrogels-forming preparations. In addition, there are other specific issues that should be addressed. First, as seen from the aforementioned examples, one disadvantage of gelatin microspheres is that drug release rates are usually very rapid; therefore, these microspheres may not be useful if a controlled and constant slow release rate is required in the diffusion phase of the release period.¹⁷⁸ Second, gelatin as a material possesses poor mechanical properties which is one of the reasons for the initial rapid release rate.¹⁷⁹ Third, glutaraldehyde which is a crosslinking agent that has been thoroughly examined for its use in gelatin-based systems and found to significantly improve the mechanical and thermal properties of gelatin hydrogels is cytotoxic, and biodegradation of glutaraldehyde cross-linked materials *in vivo* has the potential to release cytotoxic agents.¹⁸⁰ Since gelatin is more readily degraded than fibrillar collagen, release of glutaraldehyde and its reaction products would be more likely from hydrogels than from glutaraldehyde cross-linked collagen-based preparations. As such, glutaraldehyde crosslinking still remains as a potential problem in clinical application of gelatin although quenching strategies have been developed to reduce that effect. Finally, although coacervation methods for preparing protein loaded microspheres are simpler to perform than suspension crosslinking methods and the particles are less

toxic, a disadvantage is that the particles are not particularly stable and aggregate easily to form larger microspheres. It has been difficult, to date, to use coacervation methods to prepare protein nanospheres around 200 nm or less for potential use as injectable preparations.¹⁸¹

Chitosan microspheres have also been investigated to deliver constant amounts of encapsulated IL-2 in a controlled and/or sustained manner. In a study conducted by *Ozbas-Turan et al.*,¹⁶² IL-2 loading of chitosan microspheres was made by using two different methods; rIL-2 was either added to the sodium sulfate solution during the preparation, or it was adsorbed onto the surface of empty microspheres. In this study different parameters such as amount and addition method of protein, concentration of chitosan, volume of sodium sulfate solution, and incorporation or not of the glutaraldehyde were investigated. In addition, encapsulation efficiency, release kinetics, and the bioactivity of IL-2 were also reported. In general, rIL-2 encapsulation efficiency in these microspheres was high (75–98%). The release profiles were biphasic, characterized by an initial protein burst followed by slow protein release which continued for 200 days. The study showed that adsorption of rIL-2 onto the empty chitosan microspheres caused a remarkable delay on the release of the protein. In a previous study,¹⁸¹ chitosan/alginate polyelectrolyte complexes which were prepared by inducing the gelation of sodium alginate solution with calcium chloride were also used to prepare porous microspheres. The pores formed in the microspheres result as a consequence of the lyophilization process since during crosslinking, the polysaccharide swell in a continuous liquid phase, which is removed during lyophilization. More than 95% of IL-2 was loaded into the alginate/chitosan microspheres and the *in vitro* release of IL-2 in phosphate buffer saline occurred in 5 days with almost 75% released in the first 3 days. The investigators concluded that almost 100% of the active IL-2 was recovered in the release medium but without specifying the methodology used to access the activity of IL-2.

Chitosan is a polymer with outstanding properties for drug delivery: it is biodegradable, biocompatible, bioadhesive and has permeation enhancing properties. It has also been reported that it has a biostimulating activity on the immune system.¹⁸² However, one major disadvantage of chitosan is its limited solubility in water. Chitosan requires dilute acidic solutions for dissolution. The low pH of chitosan solution tends to denature most proteins including IL-2. As for alginates, one of their major disadvantages is their uncontrollable *in vivo* degradation behavior due to their weak mechanical properties which make them not suitable for controlled release delivery systems when a burst free and initial slow release is needed.¹⁸³ This was evident in the aforementioned example in which all IL-2 loaded in the chitosan/alginate microspheres was released within 5 days at a very high rate.

Further, the polymer based strategy that is currently available to produce injectable polymeric controlled release systems, is the incorporation of IL-2 into synthetic polymeric formula followed by direct injection into the tumor site. There are two popular strategies developed for this technique. One is composed of mixing IL-2 with sterile aqueous solution of polylactide-co-glycolide and PEG tri-block polymer (ReGel®) and subsequently injecting the mixture locally into the tumor site.¹²⁷ Upon entering the tissue and in response to body temperature (above 30 ° C) the blend quickly transforms into a biodegradable gel depot. Samlowski *et al.*, examined the release profile of IL-2 from this polymeric depot.¹²⁷ The preparation resulted in a release pattern that was sustained for up to 96 hours with initial burst release.¹²⁷ The *in vivo* results of this technique were also examined by the same research group. They demonstrated that peritumoral injection of ReGel/IL-2 induced a significant regression in tumor growth and improved survival of the treated animals. This drug delivery technique possesses a lot of advantages including: easy fabrication and preparation; avoidance of the use of organic solvents or

surfactants; biocompatibility with the body tissue and achievement of high loading capacity. While at the same time, and in the manner like PLG polymer, this tri-block polymer breaks down by bulk hydrolysis and liberates acidic monomers that causes a drop in the pH inside this gel before complete release of the protein, resulting in a compromise in the stability and bioactivity of the loaded protein.¹⁸⁴ The other strategy involves the use of Medusa II[®] nanospheres for delivery of IL-2. The Medusa II consists of α -tocopherols (hydrophobic moiety) which are grafted to the L-glutamate unit to thermodynamically undergo self-assembly into hydrophobic nanodomains in a water medium, which result in the aggregation of the hydrophilic L-glutamate chains, forming a colloidal suspension of the nanoparticles.

The release from these nanoparticles is based on displacement of IL-2 by endogenous proteins present in physiological fluids and the reversible interaction with the polymer.¹⁸⁵ A pharmacokinetic study was carried out to compare the sc injections of Medusa II- based IL-2 with rhIL-2 (Proleukin[®]) on different animal models.¹⁸⁵ This study revealed that the release from this formulation extended one or two days over the rhIL-2, with decrease in the relative bioavailability. Additionally, a clinical trial conducted on renal carcinoma patients confirmed the presence of IL-2 in the blood of the patients who received a sc injection of Medusa II- based IL-2 but not with those who received free rhIL-2.¹⁸⁶ Although Medusa II is a protein-friendly delivery technique in maintaining the IL-2 stability, the detection of IL-2 in the serum following release of IL-2 from this system may contribute more to the systemic side effects of IL-2 in patients. Furthermore, this technique is new and there are still the undetermined effects of the delivery vehicle and long term storage on the stability of proteins and peptides.

Other delivery systems used in localized cancer immunotherapy are the biodegradable elastomeric matrices which utilizes the osmotic pressure-driven delivery approach. Biodegradable elastomeric devices loaded with interferon- γ , vascular endothelial growth factor and IL-2 have been investigated and reported lately for their suitability as controlled release drug delivery systems.^{129,186,176} These polymeric devices were prepared by UV photocrosslinking of an acrylated star-poly(ϵ -caprolactone-co-D,L-lactide) macromer. The controlled release mechanism was achieved by distributing the protein as lyophilized particles within the matrix and relied on the osmotic activity of the enclosed excipients to compel the protein out of the matrix. In this study, the release rate was constant and the release pattern was nearly zero-order with minimal burst effect.^{186,176} Unlike PLG microspheres, osmotic-driven mechanism of IL-2 releases most of the drug before significant polymer degradation becomes the predominant controller of the drug release process. Having said that, there is still a number of issues which have an impact on the stability profile of loaded proteins that should be addressed in this strategy. Mainly, the use of organic solvents during the device preparation may change the protein conformation. In addition, the use of ultra-violet radiation during the photocuring of this elastomer was reported to denature proteins and consequently destroys their biological activity.¹⁸⁷ To date, there are no preclinical or clinical study on the *in vivo* therapeutic efficacy of this new delivery system. Such investigations and studies are required to examine its ability to fit in the IL-2 delivery systems pipeline. Table 1.4 lists and summarizes some of the most commonly investigated polymeric controlled delivery systems for IL-2.

1.8. CONCLUSIONS

The following conclusions can be drawn from this review. First, continuous and loco-regional delivery of IL-2 in the vicinity of the tumor site is a desirable mode of delivery as it closely reflects the cytokine natural release pattern and results in a more effective treatment with fewer side effects. Second,

long-acting formulations such as PEGylation and protein fusion techniques, prolongs IL-2 action but do not adapt with IL-2 localization concept. Third, of the examined localized IL-2 sustained release strategies, biodegradable polymeric vehicles would be able to circumvent the problems associated with short-term stability of liposomes and other similar delivery systems. However, controlling the microclimate pH of the delivery system and avoiding the use of organic solvents in the preparation and drug loading steps are among the biggest challenges that are faced to stabilize IL-2 in any biodegradable polymeric carrier. Finally, an area of future investigation, is the use of solventless drug loading and more protein friendly crosslinking techniques to overcome the limitations associated with the preparation and use of UV photocrosslinked star-poly(ϵ -caprolactone co D,L-lactide) elastomers which utilizes osmotic-driven delivery mechanism. Encouraging results regarding stability of peptidomimetic drugs have been achieved now with the use of novel biodegradable elastomers utilizing solventless drug loading methods and less destructive visible light crosslinking techniques. However, the stability and bioactivity of therapeutic proteins like IL-2 and Endostatins from these novel elastomers has yet to be investigated.

1.9. REFERENCES

- 1- Morgan DA, Ruscetti FW, Gallo R. 1976. Selective in vitro growth of T lymphocytes from normal human bone marrows. *Science* 193:1007-1008.
- 2- Smith KA. 1988. Interleukin-2: inception, impact, and implications. *Science* 240:1169-1176.
- 3- Smith KA. 1990. Cytokines in the nineties. *Eur Cytokine Netw* 1:7-13.
- 4- Bubenik J, Perlmann P, Indrova M, Simova J, Jandlova T, Neuwirt J. 1983. Growth inhibition of an MC-induced mouse sarcoma by TCGF (IL 2)-containing preparations. Preliminary report. *Cancer Immunol Immunother* 14:205-206.
- 5- Culliton BJ. 1992. FDA panel backs interleukin-2. *Nature* 355:287.

- 6- Bachmann MF, Wolint P, Walton S, Schwarz K, Oxenius A. 2007. Differential role of IL-2R signaling for CD8+ T cell responses in acute and chronic viral infections. *Eur J Immunol* 37:1502-1512.
- 7- Chiarion-Sileni V, Bianco PD, Romanini A, Guida M, Paccagnella A, Palma MD, Naglieri E, Ridolfi R, Silvestri B, Michiara M, Salvo GL. 2006. Tolerability of intensified intravenous interferon alfa-2b versus the ECOG 1684 schedule as adjuvant therapy for stage III melanoma: a randomized phase III italian melanoma inter-group trial. *BMC Cancer* 6:44-53.
- 8- Rosenberg SA, Spiess P, Lafreniere R. 1986. A new approach to the adoptive immunotherapy of cancer with tumor-infiltrating lymphocytes. *Science* 233:1318-1321.
- 9- Radny P, Caroli UM, Bauer J, Paul T, Schlegel C, Eigentler TK, Weide B, Schwartz M, Garbe C. 2003. Phase II trial of Intralesional therapy with interleukin-2 in soft tissue melanoma metastases. *Br J Cancer* 89:1620-1626.
- 10- Sosman JA, Kohler PC, and Hank J, Moore KH, Bechhofer R, Storer B, Sondel PM. 1988. Repetitive weekly cycles of recombinant human interleukin- 2: Responses of renal carcinoma with acceptable toxicity. *J Natl Cancer Inst* 80:60-63.
- 11- Gisselbrecht C, Maraninchi D, Pico JL, Milpied N, Coiffier B, Divine M, Tiberghien P, Body A, Tilly H, Boulat O, Brandely M. 1994. Interleukin-2 treatment in lymphoma: A phase II multicenter study. *Blood* 83:2081-2085.
- 12- Shirai M, Watanabe S, Nishioka M. 1990. Antitumour effect of intratumoral injection of human recombinant interleukin-2 in patients with hepatocellular carcinoma: a preliminary report. *Eur J Cancer* 26:1045-1048.
- 13- Cortesina G, De-Stefani A, Giovarelli M, Barioglio MG, Cavallo GP, Jemma C, and Forni G. 1988. Treatment of recurrent squamous cell carcinoma of the head and neck with low doses of interleukin-2 injected perilymphatically. *Cancer* 12: 2482-5.
- 14- Simpson WG, Heys SD, Whiting PH, Eremin O, Broom I. 1995. Acute phase proteins and recombinant interleukin-2 therapy: prediction of response and survival in patients with colorectal cancer. *Clin Exp Immunol* 99: 143-147.
- 15- Ferlazzo G, Magno C, Lupo G, Rizzo M, Iemmo R, Semino C, and Melioli G. 1995. A phase I study of intravesical continuous perfusion of recombinant interleukin-2 in patients with superficial bladder cancer. *Am J Clin Oncol* 18:100-104.

- 16- Jacobs JLL, Hordijk GJ, Jürgenliemk-Schulz IM, Terhaard CHJ, Koten JW, Battermann JJ, Den Otter W. 2005. Treatment of stage III-IV nasopharyngeal carcinomas by external beam irradiation and local low doses of IL-2. *Cancer Immunol Immunother* 54:792-798.
- 17- Astoul P, Picat-Joossen D, Viallat JR, Boutin C. 1998. Intrapleural administration of interleukin-2 for the treatment of patients with malignant pleural mesothelioma: a Phase II study. *Cancer* 83:2099-2104.
- 18- Krastev Z, Koltchakov C, Tomova R, Deredjian S, Alexiev A, Popov D, Tomov B, Koten JW, Jacobs J, Den Otter W. 2005. Locoregional IL-2 low dose application for gastrointestinal tumors. *World J Gastroenterol* 11:5525-5529.
- 19- Taylor DD, Edwards RP, Case CR, Gercel-Taylor C. 2004. Modulation of CD3-zeta as a marker of clinical response to IL-2 therapy in ovarian cancer patients. *Gynecol Oncol* 94:54-60.
- 20- Yasumoto K, Mivazaki K, Nagashima A, Ishida T, Kuda T, Yano T, Sugimachi K, Nomoto K. 1987. Induction of lymphokine-activated killer cells by intrapleural instillations of recombinant interleukin-2 in patients with malignant pleurisy due to lung cancer. *Cancer Res* 47:2184-2187.
- 21- Masotti A, Fumagalli L, Morandini GC. 1997. Intrapleural administration of recombinant interleukin-2 in non-small cell lung cancer with neoplastic pleural effusion. *Monaldi Arch Chest Dis* 52:225-228.
- 22- Kaplan B, Moy RL. 2000. Effect of perilesional injections of PEG-interleukin-2 on basal cell carcinoma. *Dermatol Surg* 26:1037-1040.
- 23- Bubenik J, Mikyskova R, Vonka V, Mendoza L, Simova J, Smahel M, Indrova M. 2003. Interleukin-2 and dendritic cells as adjuvants for surgical therapy of tumours associated with human papillomavirus type 16. *Vaccine* 21 891-896.
- 24- Mikyskova R, Indrova M, Simova J, Jandlova T, Bieblova J, Jinoch P, Bubenik J, Vonka V. 2004. Treatment of minimal residual disease after surgery or chemotherapy in mice carrying HPV16-associated tumours: Cytokine and gene therapy with IL-2 and GM-CSF. *Int J Oncol* 24:161-167.
- 25- Bubenik J, Simova J, Bubenikova D, Zeuthen J, Indrova M. 1995. Interleukin-2 gene therapy of residual EL-4 leukaemia potentiates the effect of cyclophosphamide pretreatment. *J Cancer Res Clin Oncol* 121:39-43.
- 26- Indrova M, Bubenik J, Mikyskova R, Mendoza L, Simova J, Bieblova J, Jandlova T, Jinoch P, Smahel M, Vonka V, Pajtasz-Piasecka E. 2003. Chemoimmunotherapy in mice carrying HPV16-

- associated, MHC class I+ and class I- tumours: Effects of CBM-4A potentiated with IL-2, IL-12, GM-CSF and genetically modified tumour vaccines. *Int J Oncol* 22:691-695.
- 27- Brivio F, Fumagalli L, Chiarelli M, Denova M, Bertolini A, Cetta M, Nespoli A. 2007. Immunotherapy in radical surgery of colorectal carcinoma. *Chir Ital* 59:635-640.
 - 28- Green DS, Bodman-Smith MD, Dalgleish AG, and Fischer MD. 2007. Phase I/II study of topical imiquimod and intralesional interleukin-2 in the treatment of accessible metastases in malignant melanoma. *Br J Dermatol* 156:337-345.
 - 29- Durier C, Capitant C, Lascaux AS, Goujard C, Oksenhendler E, Poizot-Martin I, Viard JP, Weiss L, Netzer E, Delfraissy JF, Aboulker JP, Levy Y. 2007. Long-term effects of intermittent interleukin-2 therapy in chronic HIV-infected patients (ANRS 048-079 Trials). *AIDS* 21:1887-1897.
 - 30- Golden-Mason L, Castelblanco N, O'Farrelly C, Rosen HR. 2007. Phenotypic and functional changes of cytotoxic CD56pos natural T cells determine outcome of acute hepatitis C virus infection. *J Virol* 81:9292-9298.
 - 31- Rosenberg SA, Lotze MT, Muul LM, Chang AE, Avis FP, Leitman S, Linehan WM, Robertson CN, Lee RE, Rubin JT. 1987. A progress report on the treatment of 157 patients with advanced cancer using lymphokine-activated killer cells and interleukin-2 or high-dose interleukin-2 alone. *N Engl J Med* 316:889-897.
 - 32- Lotze MT, Matory YL, Rayner AA, Ettinghausen SE, Vetto JT, Seipp CA, Rosenberg SA. 1986. Clinical effects and toxicity of interleukin-2 in patients with cancer. *Cancer* 58:2764-2772.
 - 33- Waldmann TA. 2006. The biology of interleukin-2 and interleukin-15: implications for cancer therapy and vaccine design. *Nat Rev Immunol* 6:595-601.
 - 34- Malek TR. 2007. The biology of interleukin-2. *Annu Rev Immunol* 26:453-479.
 - 35- Smith KA. 1984. Interleukin 2. *Annu Rev Immunol* 2:319-333.
 - 36- Bazan JZ, Mckay DB. 1992. Unraveling the structure of IL-2. *Science* 257:410-413.
 - 37- Zhu MH, Berry JA, Russell SM, Leonard WJ. 1998. Delineation of the regions of interleukin-2 (IL-2) receptor beta chain important for association of Jak1 and Jak3. Jak1-independent functional recruitment of Jak3 to IL-2Rbeta. *J Biol Chem* 273:10719-10725.
 - 38- Takeshita T, Arita T, Higuchi M, Asao H, Endo K, Kuroda H, Tanaka N, Murata K, Ishii N, Sugamura K. 1997. STAM, signal transducing adaptor molecule, is associated with Janus kinases and involved in signaling for cell growth and c-myc induction. *Immunity* 6:449-457.

- 39- Rodig SJ, Meraz MA, White JM, Lampe PA, Riley JK, Arthur CD, King KL, Sheehan KC, Yin L, Pennica D, Johnson EM Jr, Schreiber RD. 1998. Disruption of the Jak1 gene demonstrates obligatory and nonredundant roles of the Jaks in cytokine-induced biologic responses. *Cell* 93:373-383.
- 40- Ward SG, Cantrell DA. 2001. Phosphoinositide 3-kinases in T lymphocyte activation. *Curr Opin Immunol* 13:332-338.
- 41- Bachmann M F, Oxenius A. 2007. Interleukin 2: from immunostimulation to immunoregulation and back again. *EMBO Rep* 8:1142-1148.
- 42- Janssen RA, Mulder NH, The TH, de Leij L. 1994. The immunological effects of interleukin-2 *in vivo*. *Cancer Immunol Immunother* 39:207-216.
- 43- Sasaoki K, Hiroshima T, Kusumoto S, Nishi K. 1992. Deamidation at asparagine-88 in recombinant human interleukin 2. *Chem Pharm Bull (Tokyo)* 40:976-980.
- 44- Pao-Li W, Thomas PJ. 1993. Thermal-induced denaturation of two model proteins: effect of poloxamer 407 on solution stability. *Int J Pharm* 96:41-49.
- 45- Wang W, Antonsen K, Wang YJ, Wang DQ. 2008. pH dependent effect of glycosylation on protein stability. *Eur J Pharm Sci* 33:120-127.
- 46- Gounji P. 1999. PhD Thesis: The effect of pH and temperature on the conformational stability of recombinant human interleukin-2. University of Connecticut, USA.
- 47- Korner LJ, Dettmer R, Kopp J, Gaestel M, Malz W. 1986. Simple Preparative Two-Step Purification of Interleukin-2 from Culture Medium of Lectin-Stimulated Normal Human Lymphocytes. *J Immunol Meth* 87:185-191.
- 48- Welte K, Wang CY, Mertelsmann R, Venuta S, Feldman SP, Moore MA. 1982. Purification of human interleukin 2 to apparent homogeneity and its molecular heterogeneity. *J Exp Med* 156:454-464.
- 49- Wang A, Lu SD, Mark DF. 1984. Site-specific mutagenesis of the human interleukin-2 gene: structure-function analysis of the cysteine residues. *Science* 224:1431-1433.
- 50- Maria CD, Brigitte TH. 2003. Native and recombinant interleukin-2, two functionally distinct molecules. *Mole Immunol* 40:279-286.
- 51- Cumming DA. 1991 Glycosylation of recombinant protein therapeutics: control and functional implications. *Glycobiology* 1:115-130.

- 52- Robb RJ, Kutny RM, Panico M, Morris HR, and Chowdhry V. 1984. Amino acid sequence and post-translational modification of human interleukin 2. *Proc Natl Acad Sci USA* 81:6486-6490.
- 53- Liang SM, Thatcher DR, Liang CM, Allet B. 1986. Studies of Structure-Activity Relationships of Human Interleukin-2. *J Biol Chem* 261:334-337.
- 54- Kashima N, Nishi-Takaoka C, Fujita T, Taki S, Yamada G, Hamuro J, Taniguchi T. 1985. Unique structure of murine interleukin-2 as deduced from cloned cDNAs. *Nature* 313:402-404.
- 55- Arkin MR, Randal M, Delano WL, Hyde J, Luong TN, Oslob JD, Raphael DR, Taylor L, Wang J, McDowell RS, Wells JA, Braisted AC. 2003. Binding of small molecules to an adaptive protein-protein interface. *Proc Natl Acad Sci USA* 100:1603-1608.
- 56- Brandhuber BJ, Boone T, Kenney WC, McKay DB. 1987. Three-dimensional structure of interleukin-2. *Science* 238:1707-1709.
- 57- Lotze MT, Frana LW, Sharrow SO, Robb RJ, Rosenberg SA. 1985. *In vivo* administration of purified human interleukin 2. I. Half-life and immunologic effects of the Jurkat cell line-derived interleukin 2. *J Immunol* 134:157-166.
- 58- Goey SH, Eggermont AM, Punt CJ, Slingerland R, Gratama JW, Oosterom R, Oskam R, Bolhuis RL, Stoter G. 1995. Intrapleural administration of interleukin 2 in pleural mesothelioma: a phase I-II study. *Br J Cancer* 72:1283-1288.
- 59- Fathallah-Shaykh HM, Zimmerman C, Morgan H, Rushing E, Schold SCJr, Unwin DH. 1996. Response of primary leptomeningeal melanoma to intrathecal recombinant interleukin-2. A case report *Cancer* 77:1544-1550.
- 60- Meyers CA, Yung WK. 1993. Delayed neurotoxicity of intraventricular interleukin-2: a case report. *J Neurooncol* 15:265-267.
- 61- Den Otter W, Hill FW, Klein WR, Koten JW, Steerenberg PA, De Mulder PH, Rhode C, Stewart R, Faber JA, Ruitenberg EJ. 1995. Therapy of bovine ocular squamous-cell carcinoma with local doses of interleukin-2: 67% complete regressions after 20 months of follow-up. *Cancer Immunol Immunother* 41:10-14.
- 62- Thatcher N, Dazzi H, Johnson RJ, Russell S, Ghosh AK, Moore M, Chadwick G, Craig RD. 1989. Recombinant interleukin-2 (rIL-2) given intrasplenically and intravenously for advanced malignant melanoma. A phase I and II study. *Br J Cancer* 60:770-774.

- 63- Suda T, Hashizume H, Aoshima Y, Yokomura K, Sato J, Inui N, Nakamura Y, Fujisawa T, Enomoto N, Chida K. 2007. Management of interleukin-2 induced severe bronchoconstriction. *Eur Respir J* 29:612-613.
- 64- Rhines LD, Sampath P, Di-Meco F, Lawson HC, Tyler BM, Hanes J, Olivi A, Brem H. 2003. Local immunotherapy with interleukin-2 delivered from biodegradable polymer microspheres combined with interstitial chemotherapy: a novel treatment for experimental malignant glioma. *Neurosurgery* 52:872-879.
- 65- Huland E, Heinzer H, Mir TS, Huland H. 1997. Inhaled interleukin-2 therapy in pulmonary metastatic renal cell carcinoma: six years of experience. *Cancer J Sci Am* 3:S98-105.
- 66- Konrad MW, Hemstreet G, Hersh EM, Mansell PW, Mertelsmann R, Kolitz JE, E. Bradley C. 1990. Pharmacokinetics of recombinant interleukin 2 in humans. *Cancer Res* 50:2009-2017.
- 67- Dillman RO. 1994. The clinical experience with interleukin-2 in cancer therapy. *Cancer Biother* 9:183-209.
- 68- Mekhail T, Wood L, Bukowski R. 2000. Interleukin-2 in cancer therapy: uses and optimum management of adverse effects. *BioDrugs* 14:299-318.
- 69- Melder RJ, Osborn BL, Riccobene T, Kanakaraj P, Wei P, Chen G, Stolow D, Halpern WG, Migone TS, Wang Q, Grzegorzewski KJ, Gallant G. 2005. Pharmacokinetics and in vitro and *in vivo* anti-tumor response of an interleukin-2-human serum albumin fusion protein in mice. *Cancer Immunol Immunother* 54:535-547.
- 70- Thompson JA, Lee DJ, Cox WW, Lindgren CG, Collins C, Neraas KA, Dennin RA, Fefer A. 1987. Recombinant interleukin 2 toxicity, pharmacokinetics, and immunomodulatory effects in a phase I trial. *Cancer Res* 47:4202-4207.
- 71- Kirchner GL, Franke A, Buer J, Beil W, Probst-Kepper M, Wittke F, Overmann K, Lassmann S, Hoffmann R, Kirchner H, Ganser A, Atzpodi J. 1998. Pharmacokinetics of recombinant human interleukin-2 in advanced renal cell carcinoma patients following subcutaneous application. *Br J Clin Pharmacol* 46:5-10.
- 72- Gooding R, Riches P, Dadian G, Moore J, Gore M. 1995. Increased soluble interleukin-2 receptor concentration in plasma predicts a decreased cellular response to IL-2. *Br J Cancer* 72:452-455.
- 73- Rubin LA, Nelson DL. 1990. The soluble interleukin-2 receptor: biology, function, and clinical application. *Ann. Intern. Med.* 113: 619-627.

- 74- Lissoni P, Barni S, Tisi E, Rovelli F, Pittalis S, Rescaldani R, Vigore L, Biondi A, Ardizzioia A, Tancini G. 1993. *In vivo* biological results of the association between interleukin-2 and interleukin-3 in the immunotherapy of cancer. *Eur J Cancer* 29A: 1127-1132.
- 75- Voss SD, Hank JA, Nobis CA, Fisch P, Sosman JA, Sondel PM. 1989. Serum levels of low affinity interleukin-2 receptor molecule (TAC) during IL-2 therapy reflect systemic lymphoid mass activation. *Cancer Immunol Immunother* 29:261-269.
- 76- Rubin LA, Kurmann CC, Fritz ME, Biddison WE, Boutin B, Yarchoan R, Nelson DL. 1985. Soluble interleukin-2 receptors are released from activated human lymphoid cells *in vitro*. *J Immunol* 135:3172-3177.
- 77- Lassalle P, Sergeant M, Delneste Y, Gosset P, Wallaert B, Zandecki M. 1992. Levels of soluble IL-2 receptor in plasma from asthmatics. Correlations with blood eosinophilia, lung function, and corticosteroid therapy. *Clin Exp Immunol* 87:266-271.
- 78- Hänninen EL, Körfer A, Hadam M, Schneekloth C, Dallmann I, Menzel T, Kirchner H, Poliwooda H, Atzpodien J. 1991. Biological monitoring of low-dose interleukin-2 in humans: soluble interleukin. 2 receptors, cytokines, and cell surface phenotypes. *Cancer Res* 50:6312-6316.
- 79- Waldmann T. 1993. The IL-2/IL-2-receptor system: a target for rational immune intervention. *Immunol Today* 14:264-270.
- 80- Noguchi M, Yoshiaki N, Russel SM, Ziegler SF, Tsang M, Cao X, Leonard WJ. 1993. Interleukin-2 receptor gamma-chain: a functional component of the interleukin-7 receptor. *Science* 262:1877-1880.
- 81- Pfohler C, Steinhäuser S, Wagner A, Ugurel S, and Tilgen W. 2004. Complete remission of cutaneous satellite and in-transit metastases. After intralesional therapy with interleukin-2 in 2 patients with malignant melanoma. *Hautarzt* 55:171-175.
- 82- Buback J, Indrova M. 1987. Cancer immunotherapy using local interleukin 2 administration. *Immunol Lett* 16:305-309.
- 83- Ewend MG, Thompson RC, Anderson R, Sills AK, Staveley-O'Carroll K, Tyler BM, Hanes J, Brat D, Thomas M, Jaffee EM, Pardoll DM, Brem H. 2000. Intracranial paracrine interleukin-2 therapy stimulates prolonged antitumor immunity that extends outside the central nervous system. *J Immunother* 23:438-448.

- 84- Bubenik J. 1990. Local and regional immunotherapy of cancer with interleukin 2. *J Cancer Res Clin Oncol* 116:1-7.
- 85- Bubenik J. 2004. Interleukin-2 therapy of cancer. *Folia Biol (Praha)* 50:120-130.
- 86- Donohue JH, Rosenberg SA. 1983. The fate of interleukin-2 after *in vivo* administration. *J Immunol* 130:2203-2208.
- 87- Fyfe G, Fisher RI, Rosenberg SA, Sznol M, Parkinson DR, Louie AC. 1995. Results of treatment of 255 patients with metastatic renal cell carcinoma who received high-dose recombinant interleukin-2 therapy. *J Clin Oncol* 13:688-696.
- 88- Rosenberg SA, Lotze MT, Muul LM, Leitman S, Chang AE, Ettinghausen SE, Matory YL, Skibber JM, Shiloni E, Vetto JT. 1985. Observations on the systemic administration of autologous lymphokine-activated killer cells and recombinant interleukin-2 to patients with metastatic cancer. *N Engl J Med* 313:1485-1492.
- 89- Pizza G, Severini G, Menniti D, De Vinci C, Corrado F. 1984. Tumour regression after intralesional injection of interleukin 2 (IL-2) in bladder cancer. Preliminary report. *Int J Cancer* 34:359-367.
- 90- Carpagnano GE, Spanevello A, Curci C, Salerno F, Palladino GP, Resta O, Di Gioia G, Carpagnano F, Foschino Barbaro MP. 2007. IL-2, TNF-alpha, leptin: local versus systemic concentrations in NSCLC patients. *Oncol Res* 16:375-381.
- 91- Yang JC, Topalian SL, Parkinson D, Schwartzentruber DJ, Weber JS, Ettinghausen SE, White DE, Steinberg SM, Cole DJ, Kim HI. 1994. Randomized comparison of high-dose and low-dose intravenous interleukin-2 for the therapy of metastatic renal cell carcinoma: an interim report. *J Clin Oncol* 12:1572-1576.
- 92- Jacobs JJ, Sponden D, Den Otter W. 2005. Local interleukin 2 therapy is most effective against cancer when injected intratumorally. *Cancer Immunol Immunother* 54:647-654.
- 93- Baselmans AH, Koten JW, Battermann JJ, Van Dijk JE, Den Otter W. 2002. The mechanism of regression of solid SL2 lymphosarcoma after local IL-2 therapy. *Cancer Immunol Immunother* 51:492-498.
- 94- Caporale A, Brescia A, Galati G, Castelli M, Saputo S, Terrenato I, Cucina A, Liverani A, Gasparrini M, Ciardi A, Scarpini M, Cosenza UM. 2007. Locoregional IL-2 therapy in the treatment of colon cancer. Cell-induced lesions of a murine model. *Anticancer Res* 27:985-989.

- 95- Kudo-Saito C, Garnett CT, Wansley EK, Schlom J, Hodge JW. 2007. Intratumoral delivery of vector mediated IL-2 in combination with vaccine results in enhanced T cell avidity and anti-tumor activity. *Cancer Immunol Immunother* 56:1897-1910.
- 96- Hayes RL, Koslow M, Hiesiger EM, Hymes KB, Hochster HS, Moore EJ, Pierz DM, Chen DK, Budzilovich GN, Ransohoff J. 1995. Improved long term survival after intracavitary interleukin-2 and lymphokine-activated killer cells for adults with recurrent malignant glioma. *Cancer* 76:840-852.
- 97- Den Otter W, Dobrowolski Z, Bugajski A, Papla B, Van Der Meijden AP, Koten JW, Boon TA, Siedlar M, Zembala M. 1998. Intravesical interleukin-2 in T1 papillary bladder carcinoma: regression of marker lesion in 8 of 10 patients. *J Urol* 159:1183-1186.
- 98- Dubinett SM, Patrone L, Tobias J, Cochran AJ, Wen DR, McBride WH. 1993. Intratumoral interleukin-2 immunotherapy: activation of tumor-infiltrating and splenic lymphocytes *in vivo*. *Cancer Immunol Immunother* 36:156-162.
- 99- Vaage J. 1991. Peri-tumor interleukin-2 causes systemic therapeutic effect via interferon-gamma induction. *Int J Cancer* 49:598-600.
- 100- Sone S, Ogura T. 1994. Local interleukin-2 therapy for cancer, and its effector induction mechanisms. *Oncology* 51:170-176.
- 101- Chi KH, Myers JN, Chow KC, Chan WK, Tsang YW, Chao Y, Yen SH, Lotze MT. 2001. Phase II trial of systemic recombinant interleukin-2 in the treatment of refractory nasopharyngeal carcinoma. *Oncology* 60:110-115.
- 102- Den Otter W, Jacobs JJ, Battermann JJ, Hordijk GJ, Krastev Z, Moiseeva EV, Stewart RJ, Ziekman PG, Koten JW. Local therapy of cancer with free IL-2. *Cancer Immunol Immunother* 57:931-950.
- 103- Bubenik J, Indrova M, Perlmann P, Berzins K, Mach O, Kraml J, Toulcova A. 1985. Tumour inhibitory effects of TCGF/IL-2-containing preparations. *Cancer Immunol Immunother* 19:57-61.
- 104- West WH, Tauer KW, Yannelli JR, Marshall GD, Orr DW, Thurman GB, Oldham RK. 1987. Constant-infusion recombinant interleukin-2 in adoptive immunotherapy of advanced cancer. *N Engl J Med* 316:898-905.

- 105- Bos GW, Jacobs JJ, Koten JW, Van Tomme S, Veldhuis T, van Nostrum CF, Den Otter W, Hennink WE. 2004. *In situ* crosslinked biodegradable hydrogels loaded with IL-2 are effective tools for local IL-2 therapy. *Eur J Pharm Sci* 21:561-567.
- 106- Naito K, Pellis NR, Kahan BD. 1988. Effect of continuous administration of interleukin 2 on active specific chemimmunotherapy with extracted tumor-specific transplantation antigen and cyclophosphamide. *Cancer Res* 48:101-108.
- 107- Da Pozzo LF, Hough KL, Holder WD Jr. 1992. Toxicity and immunologic effects of continuous infusion of recombinant human interleukin-2 administered by selective hepatic perfusion in dogs. *Surgery* 111:326-334.
- 108- Nishimura T, Uchiyama Y, Yagi H, Hashimoto Y. 1986. Administration of slowly released recombinant interleukin 2. Augmentation of the efficacy of adoptive immunotherapy with lymphokine-activated killer (LAK) cells. *J Immunol Methods* 91:21-27.
- 109- Kanaoka E, Takahashi K, Yoshikawa T, Jizomoto H, Nishihara Y, Uchida N, Maekawa R, Hirano K. 2002. A significant enhancement of therapeutic effect against hepatic metastases of M5076 in mice by a liposomal interleukin-2 (mixture). *J Control Release* 82:183-187.
- 110- Aqeilan R, Kedar R, Ben-Yehudah A, and Lorberboum-Galski H. 2003. Mechanism of action of interleukin-2 (IL-2)-Bax, an apoptosis-inducing chimaeric protein targeted against cells expressing the IL-2 receptor. *Biochem J* 370:129-140.
- 111- Lee HJ. 2002. Protein drug oral delivery: The Recent Progress. *Arch Pharm Res* 25:572-584.
- 112- Koren S, Fleischmann WR Jr. 1994. Modulation of peripheral leukocyte counts and bone marrow function in mice by oral administration of interleukin-2. *J Interferon Res* 14:343-347.
- 113- Toth T, Cummins J, Moore D. 1994. Effects of very-low-dose oral cytokine treatment on hematological values in feline leukemia- positive cells. *J Interferon Res* 14: S187.
- 114- Georgiades JA, Fleischmann WR Jr. 1996. Oral application of cytokines. *Biotherapy* 8:205-212.
- 115- Semalty A, Semalty M, Singh R, Saraf SK, Saraf S. 2007. Properties and formulation of oral drug delivery systems of protein and peptides. *Indian J Pharm Sci* 69:741-747.
- 116- Hollinger MA. 1985. Respiratory pharmacology and toxicology (saunders monographs in pharmacology and therapeutics), pp. 1-20.
- 117- Enk AH, Nashan D, Rubben A, Knop J. 2000. High dose inhalation interleukin-2 therapy for lung metastases in patients with malignant melanoma. *Cancer* 88:2042-2046.

- 118- Merimsky O, Gez E, Weitzen R, Nehushtan H, Rubinov R, Hayat H, Peretz T, Ben-Shahar M, Biran H, Katsenelson R, Mermershtein V, Loven D, Karminsky N, Neumann A, Matcejevsky D, Inbar M. 2004. Targeting pulmonary metastases of renal cell carcinoma by inhalation of interleukin-2. *Ann Oncol* 15:610-612.
- 119- Esteban-Gonzalez E, Carballido J, Navas V, Torregrosa Z, Munoz A, Mon MA. 2007. Retrospective review in patients with pulmonary metastases of renal cell carcinoma receiving inhaled recombinant interleukin-2. *Anticancer Drugs* 18:291-296.
- 120- Skubitz KM, Anderson PM. 2000. Inhalational interleukin-2 liposomes for pulmonary metastases: a phase I clinical trial. *Anticancer Drugs* 11:555-563.
- 121- Greenwald RB, Yang K, Zhao H, Conover CD, Lee S, Filpula D. 2003. Controlled release of proteins from their poly(ethylene glycol) conjugates: drug delivery systems employing 1,6-elimination. *Bioconj Chem* 14:395-403.
- 122- Abdel-Wahab Z, Li WP, Osanto S, Darrow TL, Hessling J, Vervaert CE, Burrascano M, Barber J, Seigler H. F. 1994. Transduction of human melanoma cells with interleukin-2 gene reduces tumorigenicity and enhances host antitumor immunity: a nude mouse model. *Cell Immunol* 159:26-39.
- 123- Hoffman DM, Figlin RA. 2000. Intratumoral interleukin 2 for renal-cell carcinoma by direct gene transfer of a plasmid DNA/DMRIE/DOPE lipid complex. *World J Urol* 18:152-156.
- 124- Johnston D, Reynolds SR, Bystryk JC. 2006. Interleukin-2/liposomes potentiate immune responses to a soluble protein cancer vaccine in mice. *Cancer Immunol Immunother* 55:412-419.
- 125- Kanaoka E, Takahashi K, Yoshikawa T, Jizomoto H, Nishihara Y, Hirano K. 2003. Continuous release of interleukin-2 from liposomal IL-2 (mixture of interleukin-2 and liposomes) after subcutaneous administration to mice. *Drug Dev Ind Pharm* 29:1149-1153.
- 126- Hsu W, Lesniak MS, Tyler B, Brem H. 2005. Local delivery of interleukin-2 and adriamycin is synergistic in the treatment of experimental malignant glioma. *J Neurooncol* 74:135-140.
- 127- Samlowski WE, McGregor JR, Jurek M, Baudys M, Zentner GM, Fowers KD. 2006. ReGel polymer-based delivery of interleukin-2 as a cancer treatment. *J Immunother* 29:524-535.
- 128- Hiemstra C, Zhong Z, Van Tomme, Sr, van Steenberg MJ, Jacobs JJ, Den Otter W, Hennink WE, Feijen J. 2007. *In vitro* and *in vivo* protein delivery from *in situ* forming poly(ethylene glycol)-poly(lactide) hydrogels. *J Control Release* 119:320-327.

- 129- Gu F, Neufeld R, Amsden B. 2007. Sustained release of bioactive therapeutic proteins from a biodegradable elastomeric device. *J Control Release* 117:80-89.
- 130- Knauf MJ, Bell DP, Hirtzer P, Luo ZP, Young JD, Katre NV. 1988. Relationship of effective molecular size to systemic clearance in rats of recombinant interleukin-2 chemically modified with water-soluble polymers. *J Biol Chem* 263:15064-15070.
- 131- Harris JM, Martin NE, Modi M. 2001. Pegylation: a novel process for modifying pharmacokinetics. *Clin Pharmacokinet* 40:539-551.
- 132- Fontana A, Spolaore B, Mero A, Veronese F.M. 2008. Site-specific modification and PEGylation of pharmaceutical proteins mediated by transglutaminase. *Adv Drug Deliv Rev* 60:13-28.
- 133- Turturro F. 2007. Denileukin difitox: a biotherapeutic paradigm shift in the treatment of lymphoid-derived disorders. *Expert Rev Anticancer Ther* 7:11-17.
- 134- Yao Z, Dai W, Perry J, Brechbiel MW, Sung C. 2004. Effect of albumin fusion on the biodistribution of interleukin-2. *Cancer Immunol Immunother* 53:404-410.
- 135- Sobol RE, Royston I, Fakhrai H, Shawler DL, Carson C, Dorigo O, Gjerset R, Gold DP, Koziol J, Mercola D. 1995. Injection of colon carcinoma patients with autologous irradiated tumor cells and fibroblasts genetically modified to secrete interleukin-2 (IL-2): a phase I study. *Hum Gene Ther* 6:195-204.
- 136- Cao X, Chen C, Zhang W, Tao Q, Yu Y, Ye T. 1996. Enhanced efficacy of combination of IL-2 gene and IL-6 gene-transfected tumor cells in the treatment of established metastatic tumors. *Gene Ther* 3:421-426.
- 137- Vieweg J, Boczkowski D, Roberson KM, Edwards DW, Philip M, Philip R, Rudoll T, Smith C, Robertson C, Gilboa E. 1995. Efficient gene transfer with adeno-associated virus-based plasmids complexed to cationic liposomes for gene therapy of human prostate cancer. *Cancer Res* 55:2366-2372.
- 138- Toloza EM, Hunt K, Swisher S, McBride W, Lau R, Pang S, Rhoades K, Drake T, Belldegrun A, Glaspy J, Economou JS. 1996. *In vivo* cancer gene therapy with a recombinant interleukin-2 adenovirus vector. *Cancer Gene Ther* 3:11-17.
- 139- Parker SE, Khatibi S, Margalith M, Anderson D, Yankauckas M, Gromkowski SH, Latimer T, Lew D, Marquet M, Manthorpe M, Hobart P, Hersh E, Stopeck AT, Norman J. 1996. Plasmid DNA gene therapy: studies with the human interleukin-2 gene in tumor cells *in vitro* and in the murine B16 melanoma model *in vivo*. *Cancer Gene Ther* 3:175-185.

- 140- Saffran DC, Horton HM, Yankauckas MA, Anderson D, Barnhart KM, Abai AM, Hobart P, Manthorpe M, Norman JA, Parker SE. 1998. Immunotherapy of established tumors in mice by intratumoral injection of interleukin-2 plasmid DNA: induction of CD8+ T-cell immunity. *Cancer Gene Ther* 5:321-330.
- 141- Kupfer J. 1997. DNA delivery vectors for somatic cell gene therapy. In Park E, editor. *Controlled drug delivery: challenges and strategies*, Washington DC: American Chemical Society. p 27-48.
- 142- Griscelli F, Opolon P, Saulnier P, Mami-Chouaib F, Gautier E, Echchakir H, Angevin E, Le Chevalier T, Bataille V, Squiban P, Tursz T, Escudier B. 2003. Recombinant adenovirus shedding after intratumoral gene transfer in lung cancer patients, *Gene Ther* 10:386-395.
- 143- Lehrman S. 1999. Virus treatment questioned after gene therapy death. *Nature* 401:517-518.
- 144- Hacein-Bey-Abina S, Von Kalle C, Schmidt M, Le Deist F, Wulffraat N, McIntyre E, Radford I, Villeval J L, Fraser CC, Cavazzana-Calvo M, Fischer A. 2003. A serious adverse event after successful gene therapy for X-linked severe combined immunodeficiency. *N Engl J Med* 348:255-256.
- 145- Zhao Z, Leong KW. 1996. Controlled delivery of antigens and adjuvants in vaccine development. *J Pharm Sci* 85:1261-1270.
- 146- Bergers JJ, Otter WD, Dullens HFJ, Kerkvliet CTM, Crommelin DJA. 1993. Interleukin-2-containing liposomes: interaction of interleukin-2 with liposomal bilayers and preliminary studies on application in cancer vaccines. *Pharm Res* 10:1715-1721.
- 147- Kulkarni SS, Kasi LP, Tucker SL, Pizzini RP. 1987. *In vivo* augmentation of mitogen response by liposome-encapsulated interleukin-2 in mice. *Ann N Y Acad Sci* 507:344 - 347.
- 148- Kanaoka E, Takahashi K, Yoshikawa T, Jizomoto H, Nishihara Y, Hirano K. 2001. A novel and simple type of liposome carrier for recombinant interleukin-2. *J pharm pharmacol* 53:295-302.
- 149- Koppenhagen FJ, Visser AJW, Herron JN, Storm G, Crommelin DJA. 1998. Interaction of recombinant interleukin-2 with liposomal bilayers. *J Pharm Sci* 87:707-714.
- 150- Neville ME, Boni LT, Pflug LE, Popescu MC, Robb RJ. 2000. Biopharmaceutics of liposomal interleukin 2, oncolipin. *Cytokine* 12:1691-1701.
- 151- van Slooten ML, Storm G, Zoephel A, Kupcu Z, Boerman O, Crommelin DJA, Wagner E, Kircheis R. 2000. Liposomes containing interferon-gamma as adjuvant in tumor cell vaccines. *Pharm Res* 17: 42-48.

- 152- De Groot CJ, Cadee JA, Koten JW, Hennink WE, Den Otter W. 2002. Therapeutic efficacy of IL-2-loaded hydrogels in a mouse tumor model. *Int J Cancer* 98:134-140.
- 153- Cadee JA, De Groot CJ, Jiskoot W, Den Otter W, Hennink WE. 2002. Release of recombinant human interleukin-2 from dextran-based hydrogels. *J Control Release* 78:1-13.
- 154- Fujiwara T, Sakagami K, Matsuoka J, Shiozaki S, Fujioka K, Takada Y, Uchida S, Onoda T, Orita K. 1991. Augmentation of antitumor effect on syngeneic murine solid tumors by an interleukin 2 slow delivery system, the IL-2 mini-pellet *Biotherapy* 3:203-209.
- 155- Qiao M, Chen D, Hao T, Zhao X, Hu H, Ma X. 2008. Injectable thermosensitive PLGA-PEG-PLGA triblock copolymers-based hydrogels as carriers for interleukin-2. *Pharmazie* 63:27-30.
- 156- Lynn AK, Yannas IV, Bonfield W. 2004. Antigenicity and immunogenicity of collagen. *J Biomed Mater Res B Appl Biomater* 71:343-354.
- 157- Kumagai T, Kamada M, Igarashi C, Yuri K, Furukawa H, Nagata N, Saito A, Okui T, Yano S. 2002 . Gelatin-specific cellular immune responses persist for more than 3 years after priming with gelatin containing DTaP vaccine. *Clin Exp Allergy* 32:1510-1514.
- 158- Hora MS, Rana RK, Nunberg JH, Tice TR, Gilley RM, Hudson ME. 1990. Controlled release of interleukin-2 from biodegradable microspheres. *Biotechnology (N.Y.)* 8:755-758.
- 159- Thomas TT, Kohane DS, Wang A, Langer R. 2004. Microparticulate formulations for the controlled release of interleukin-2. *J Pharm Sci* 93:1100-1109.
- 160- Sharma A, Harper CM, Hammer L, Nair RE, Mathiowitz E, Egilmez NK. 2004. Characterization of cytokine encapsulated controlled-release microsphere adjuvants. *Cancer Biother Radiol* 19:764-769.
- 161- Egilmez NK , Jong YS , Iwanuma Y , Jacob JS , Santos CA , Chen FA, Mathiowitz E, Bankert RB. 1998. Cytokine immunotherapy of cancer with controlled release biodegradable microspheres in a human tumor xenograft/SCID mouse model. *Cancer Immunol Immunother* 46:21-24.
- 162- Ozbas-Turan S, Akbuga J, Aral C. 2002. Controlled release of interleukin-2 from chitosan microspheres. *J Pharm Sci* 91:1245-1251.
- 163- Liu LS, Lius SQ, Ng SY, Froix M, Ohno T, Heller J. 1997. Controlled release of interleukin-2 for tumour immunotherapy using alginate/chitosan porous microspheres. *J Control Rel* 43:65-74.

- 164- Cadee JA, Brouwer LA, Den Otter W, Hennink WE, Van Luyn MJA. 2001. A comparative biocompatibility study of microspheres based on cross-linked dextran or poly(lactic-co-glycolic) acid after subcutaneous injection in rats. *J Biomed Mater Res* 56:600-609.
- 165- Koten JW, Van Luyn MJA, Cadee JA, Brouwer L, Hennink WE, Bijleveld C, Den Otter W. 2003. IL-2 loaded dextran microspheres with attractive histocompatibility properties for local IL-2 cancer therapy. *Cytokine* 24:57-66.
- 166- Hanes J, Sills A, Zhao Z, Suh KW, Tyler B, DiMeco F, Brat DJ, Choti MA, Leong KW, Pardoll DM, Brem H. 2001. Controlled local delivery of interleukin-2 by biodegradable polymers protects animals from experimental brain tumors and liver tumors. *Pharm Res* 18:899-906.
- 167- Spenlehauer G, Vert M, Benoit JP, Chabot F, Veillard M. 1988. Biodegradable cisplatin microspheres prepared by the solvent evaporation method: morphology and release characteristics. *J Control Rel* 7: 217-229.
- 168- Mehta RC, Thanoo BC, Deluca PP. 1996. Peptide containing microspheres from low molecular weight and hydrophilic poly(d,l-lactide-co-glycolide). *J Control Rel* 41: 249-257.
- 169- Lee VHL. 1991. Changing needs in drug delivery in the era of peptide and protein drugs. In Lee VHL, editor. *Peptide and protein drug delivery*. New York: Marcel Dekker. p 1-56.
- 170- Cohen FE, Kosen PA, Kuntz ID, Epstein LB, Ciardelli TL, Smith KA. 1986. Structure-activity studies of interleukin-2. *Science* 234:349-352.
- 171- Qeswein JQ, Shire SJ. 1991. Physical biochemistry of protein drugs. In Lee VHL, editor. *Peptide and protein drug delivery*. New York: Marcel Dekker. p 167-202.
- 172- Fu K, Pack DW, Laverdiere A, Son S, Langer R. 1998. Visualization of pH in degrading polymer microspheres. *Proceed Int'l Symp Control Rel Bioact Mater* 25: 150-151.
- 173- Hora MS, Rana RK, Nunberg JH, Tice TR, Gilley RM. 1990. Release of human serum albumin from poly(lactide-co-glycolide) microspheres. *Pharm Res* 7: 1190-1194.
- 174- Atkins TW, Peacock SJ. 1996. The incorporation and release of bovine serum albumin from poly(beta-hydroxybutyrate-hydroxyvalerate) microspheres. *J Biomater Sci Polym Ed* 7:1065-1073.
- 175- Michaels AS, Guilod MS. 1979. Osmotic bursting drug delivery device. US patent no. 4177256.
- 176- Younes HM. 2002. PhD Thesis: New biodegradable elastomers for interferon- γ delivery. University of Alberta, Canada.

- 177- Shaker MA, Younes HM. 2008. Synthesis and Characterization of Poly(diols-tricarballoylate) Photocrosslinked Biodegradable Elastomers. *Am J Pharm Ed.* 72: 118.
- 178- Tsung M, Burgess DJ. 1997. Preparation and characterization of heparin/gelatin microspheres. *J Pharm Sci.* 5:603-607.
- 179- Bigi A, Cojazzi G, Panzavolta S., Rubini K., Roveri N. 2001 Mechanical and thermal properties of gelatin films at different degrees of glutaraldehyde crosslinking. *Biomaterials* 22:763-768.
- 180- Speer DP, Chvapil M, Eskelson CD, Ulreich J. 1980. Biological effects of residual glutaraldehyde in glutaraldehyde-tanned collagen biomaterials. *J Biomed Mater Res* 14:753-764.
- 181- Coombes GA, Lin W, O'Hagen DT, Davis SS. 1999. Preparation of protein microspheres, films and coatings. US Patent no. 6007791.
- 182- Paul W, Sharma CP. 2000. Chitosan: A drug carrier for the 21st century: A review. *STP Pharma Sci* 10:5-22.
- 183- Eiselt P, Yeh J, Latvala RK, Shea LD, Mooney DJ. 2000. Porous carriers for biomedical applications based on alginate hydrogels. *Biomaterials* 21:1921-1927.
- 184- Li L, Schwendeman SP. 2005. Mapping neutral microclimate pH in PLGA microspheres. *J Control Rel* 101:163-173.
- 185- Chan YP, Meyrueix R, Kravtsoff R, Nicolas F, Lundstrom K. 2007. Review on Medusa: a polymer-based sustained release technology for protein and peptide drugs. *Expert Opin Drug Deliv* 4:441-451.
- 186- Gu F, Younes HM, El-Kadi AO, Neufeld RJ, Amsden BG. 2005. Sustained interferon-gamma delivery from a photocrosslinked biodegradable elastomer. *J Control Rel* 102:607-617.
- 187- Glenn FV, Rex MT. 1995. UVA radiation-induced oxidative damage to lipids and proteins *in vitro* and in human skin fibroblasts is dependent on iron and singlet oxygen. *Free Radic Biol Med* 18:721-730.
- 188- Stewart RJ, Hill FW, Masztalerz A, Jacobs JJ, Koten J W, and Den Otter W. 2006. Treatment of ocular squamous cell carcinomas in cattle with interleukin-2. *VetRec.* 159:668-672.
- 189- Castagneto B, Zai S, Mutti L, Lazzaro A, Ridolfi R, Piccolini E, Ardizzoni A, Fumagalli L, Valsuani G, and Botta M. 2001 . Palliative and therapeutic activity of IL-2 immunotherapy in unresectable malignant pleural mesothelioma with pleural effusion: Results of a phase II study on 31 consecutive patients. *Lung Cancer* 31:303-310.

- 190- Moiseeva EV, Merkulova IB, Bijleveld C, Koten JW, Miroshnikov AI, and Den Otter W. 2003. Therapeutic effect of a single peritumoral dose of IL-2 on transplanted murine breast cancer. *Cancer Immunol.Immunother.* 52:487-496.
- 191- Lafreniere R and Rosenberg SA. 1985. Successful immunotherapy of murine experimental hepatic metastases with lymphokine-activated killer cells and recombinant interleukin 2. *Cancer Res.* 45:3735-3741.
- 192- Rosenberg SA, Mule JJ, Spiess PJ, Reichert CM, and Schwarz SL. 1985. Regression of established pulmonary metastases and subcutaneous tumor mediated by the systemic administration of high-dose recombinant interleukin 2. *J Exp Med* 161:1169-1188.
- 193- Kusnierczyk H, Pajtasz-Piasecka E, Koten JW, Bijleveld C, Krawczyk K, Den Otter W. 2004. Further development of local IL-2 therapy of cancer: multiple versus single IL-2 treatment of transplanted murine colon carcinoma. *Cancer Immunol Immunother* 53:445-452.
- 194- Henriksson R, Widmark A, Bergh A, Damber JE. 1992. Interleukin-2-induced growth inhibition of prostatic adenocarcinoma (Dunning R3327) in rats. *Urol Res* 20:189-191.
- 195- Yoshida S, Tanaka R, Takai N, and Ono K. 1988. Local administration of autologous lymphokine-activated killer cells and recombinant interleukin 2 to patients with malignant brain tumors. *Cancer Res* 48:5011-5016.

CHAPTER 2

Photocrosslinked Polymers: New Emerging Biomaterials for Controlled Drug Delivery and Other Biomedical Applications

The content of this chapter is to be submitted to the *Journal of Therapeutic Delivery*

Mohamed A. Shaker and Husam M. Younes.

ABSTRACT

Photopolymerization has been widely used in several biomedical applications including therapeutic delivery, tissue engineering and cell encapsulation as it combines the properties of both the photopolymerizable precursors and the photocrosslinked networks. Nowadays, photopolymerization technology has expanded to show promising applications and uses in protein and gene delivery as well as other drug delivery designs and technologies. The present chapter aims to provide an in-depth review on the latest advances in the utilization of photopolymerization technology in the drug delivery field with discussions on the properties and the compatibility of the photocrosslinked biomaterials used. The discussion will mainly emphasize on the potential use of photopolymerization in targeted, controlled, and sustained drug delivery systems.

2.1. BACKGROUND

The history of photopolymerization, which is an irreversible light-induced polymerization reaction, can be traced back to the ancient Egyptians who used this technique in mummification. The mummified were wrapped in cloths which were soaked in lavender oil. The oil was then dried and photopolymerized into a protective polymer upon exposure to sunlight.¹ Since then, the use of photopolymerization technology has significantly expanded into many biomedical applications. This is because photopolymerization is able to provide a rapid conversion of liquid prepolymers to gels or solid crosslinked polymers resulting in polymer networks. Not surprisingly, the research in this field has attracted great attention for its tremendous uses and applications in the engineering of soft tissue and in drug delivery systems as well.²⁻⁷

A significant number of current controlled drug delivery strategies are based on the design and fabrication of synthesized biodegradable photopolymerizable vehicles. Compared to other materials, polymers have occupied a central status in the fabrication of implantable systems as they can meet several criteria such as biocompatibility and reproducibility, furthermore, a polymeric matrix can be slowly degraded allowing for the controlled release of pharmaceutical agents from a medical device.²⁻⁴ This chapter is aimed at covering the recent developments from a biomedical and drug delivery applications point of view, covering the photopolymerization techniques.

Photopolymerization is a flexible polymerization process and enjoys several advantages over the conventional (thermal and solution) polymerization techniques. Firstly, the spatial and temporal control can be easily achieved during the photopolymerization process through controlling the exposure area and the time of light incidence, hence precise control of polymerization can be achieved. Secondly, photopolymerization can take place very rapidly at room temperature, in a matter of few seconds to

minutes. Thirdly, the process can be conducted at a temperature and pH that resemble the physiological ranges during fabrication which can allow easy and rapid production of complex matrix devices.^{2,3,7} In addition to the above, photopolymerizable formulations can be typically solvent free hence minimizing volatile organic omissions. Also, the biomaterials can be created in situ in a minimally invasive manner. In situ fabrication of polymers is attractive for a variety of biomedical applications as it can allow one to form complex shapes that adhere and conform to tissue structures. It is not surprising then that the utilization of photo-polymerized polymer networks has been suggested in drug delivery system and other biomedical application.^{2,3,8}

2.2. PHOTINITIATORS AND PHOTOPOLYMERIZATION

In general, there are two main steps in photopolymerization namely, photoinitiation and polymerization, as illustrated in Figure 2.1. Photoinitiation utilizes photoinitiators which are molecules responsible for initiating the reaction of polymerization by producing reactive species upon light absorption.^{2,3} Frequently used sources of electromagnetic radiation comprise electron beam radiation, ultraviolet (UV) light and γ -radiation. Increasing use is being made of deep UV light (< 200 nm), visible light, near infrared radiation and microwaves.

There are two types of photoinitiators: cationic and radical. Cationic photoinitiators act upon molecules containing epoxies or molecules which undergo polycondensation reactions. This type of photoinitiator is not compatible with biological systems since its reactivity is inhibited by water and hence will not be dealt with further in this chapter. Radical photoinitiators on the other hand are water-compatible and act on molecules containing an acrylate or styrene group. The range of wavelengths used is typically near UV (300-400nm).

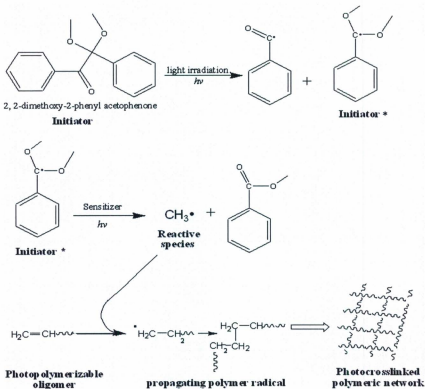


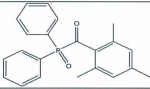
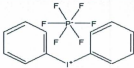
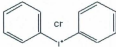

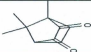
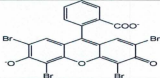
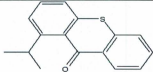
Figure 2.1. Schematic representation of the photoinitiated polymerization

When the system is exposed to appropriate light, the photo-sensitizers, which can be regarded as photo-catalysts, absorb the energy and transfer it to the photoinitiators and/or act with photoinitiators, which then cause the photoinitiator to break into primary reactive species, usually free radicals. Reactive species then generate the polymerization in subsequent steps. Some photopolymerization system can be irradiated without using photoinitiators such as inulin-methacrylic anhydride which can be photocrosslinked by long time UV irradiation.⁹

Over the last decade, various photoinitiators have been explored for photopolymerization (Table 2.1). Since photoinitiators are reactive molecules, that may even in trace amounts cause damage to human tissues, only those photoinitiators with stringent characteristics and criteria can be utilized for drug delivery and other biomedical applications.^{2,10,11} First, photoinitiators should be completely stable and when dissolved in reactive monomers should not initiate spontaneous polymerization. Second, when irradiated, photoinitiators should undergo photolysis with high quantum efficiency and without liberation of by-products that inhibit polymerization or degrade the quality of the final product. Third, photoinitiators should have as low toxicity as possible, both locally and systemically. Fourth, photoinitiators should be biocompatible with cells or molecules entrapped with the forming polymers, and also with cells and tissues in the vicinity of implantation or injection site. Finally, the synthesis of the prospective photoinitiators should be reasonably straightforward and inexpensive. Apart from the above criteria, the final choice of initiators is frequently based upon similarly reported systems in the literature or prior experience.¹²

Table 2.1. Examples of different photoinitiators with their structures.

Class	photoinitiators	Structure
Ketone	Irgacure 2959 (2-hydroxy-1-[4-(hydroxyethoxy)phenyl]-2-methyl-1-propanone)	
	Irgacure 184 (1-hydroxycyclohexyl-1-phenyl ketone)	
	Irgacure 369 (2-Benzyl-2-(dimethylamino)-4'-morpholinobutyrophenone)	
	4-Benzoylbenzyl-trimethylammonium chloride	
	Irgacure 907(2-Methyl-1[4-(methylthio)phenyl]-2-morpholinopropan-1-one)	
Acetophenone derivative	Irgacure 6512 (2, 2-dimethoxy-2-phenyl acetophenone) [DMPA]	
Phosphine oxide	Irgacure 819 bis(2,4,6-trimethylbenzoyl)phenylphosphine oxide (BAPO)	

	Lucirin diphenyl(2,4,6-trimethylbenzoyl)phosphine oxide TPO	
Iodonium salt	diphenyl iodonium hexafluorophosphate	
	diphenyl chloride	
Camphor compounds	Camphor (1,7,7-Trimethylbicyclo[2.2.1]heptan-2-one)	
	Camphorquinone (1R,4S-1,7,7-trimethyl norbornane-2,3-dione)	
Eosin Y	Eosin Y (disodium 2-(2,4,5,7-tetrabromo-6-oxido-3-oxo-xanthen-9-yl) benzoate)	
Visible light photosensitizer	Isopropyl thioxanthone	

According to their mechanism of action, radical photoinitiators are divided into two general classes. The first (type I) undergoes a uni-molecular bond cleavage upon irradiation to yield free radicals. The majority of these types include aromatic carbonyl compounds containing suitable groups which facilitate direct photo-fragmentation.¹³ Whereas, the second (type II) are subjected to bimolecular reaction, where the excited photoinitiator interacts with photo-sensitizer to generate free radicals. The polymerization pathways of this type II are two: hydrogen abstraction and photo induced electron transfer, followed by fragmentation.¹³

Photoinitiators have also been categorized according to the type of light used to induce photoinitiation process into Ultraviolet (UV), visible and laser photoinitiators.¹⁴ The only difference between them is the difference in light energy absorption capability at the appropriate wavelength. The UV photoinitiators in turn include various classes and over the last decade, most of them have been reported to be used for drug delivery purposes. One of the most important groups of UV photoinitiators used in biomedical applications includes ketones as functional groups. The reactive radicals in this group can be formed through a photo-cleavage of a bond to the carbonyl group. Different kinds of ketones photoinitiators with different reactive side chains are reported such as α -hydroxy ketone, α -amino ketone, and amino aryl ketone, such as Irgacure 2959 (2-hydroxy-1-[4-(hydroxyl ethoxy) phenyl]-2-methyl-1-propanone),^{10,14-16} Irgacure 184 (1-hydroxycyclohexyl-1-phenyl ketone)¹⁷ is the most commonly used ketone photoinitiators in tissue engineering. Also, it has been investigated for the purpose of crosslinking pH-sensitive glycol polymers for oral drug delivery systems.¹⁸ An acetophenone derivative 4-Benzoylbenzyl-trimethylammonium chloride is another group of UV photoinitiators used in drug delivery. The 2, 2-dimethoxy-2-phenyl acetophenone (DMPA) is one example of an acetophenone that has been significantly used as a photoinitiator for photopolymerization of PEG to form hydrogels for use in biomaterial

studies.^{3,19-21} Irgacure 6512 (2-dimethoxy-2-phenyl acetophenone), was also used to form hydrogels from PEG derivatives in several other studies.^{2,21,22} Also, phosphine oxides such as monoacylphosphine (Lucirin TPO), bisacylphosphine (Irgacure 819) as well as iodonium salt such as diphenyl iodonium hexafluorophosphate have been used in biomedical studies.

Photoinitiators having absorption capabilities in the visible light energy range are based on dyes, quinines, diketones, and heterocyclic chemical structures. Camphor compounds such as camphorquinone (CQ), camphor and amine compounds such as triethylamine and triethanolamine^{2,23,24} and compounds such as isopropyl thioxanthone (ITX) and ethyl 4-N,N-dimethylamino-benzoate (EDMAB)^{2,23,25} have also found use as photoinitiators for tissue engineering, drug delivery and cell encapsulation. In addition, eosin Y have a broad use such as interfacial photopolymerization of PEG diacrylate²⁶⁻²⁸ and photocrosslinked pluronic hydrogel for plasmid DNA release.²⁶ Also, metallocene compounds such as Irgacure 784 have been used in drug delivery.

The main differences between UV and visible light cured materials are in the use of a photoinitiator that absorbs the appropriate wavelength of light energy. UV photoinitiators of both classes are available. However, visible light photoinitiators belong almost exclusively to the second class of photoinitiators. Visible light contains about five percent UV light.

2.3. PHOTOCROSSLINKABLE POLYMERS

Various polymers have been explored for photopolymerization as drug delivery matrices, from which the drug can be gradually released. The development of novel drug delivery system is a very active part of biomedical industry due to obvious therapeutic and economic advantages in the method of drug administration. Considering the application, biodegradable biomaterials are most commonly

used.²⁹ Almost all the photopolymerizable biomaterials commonly have a photopolymerizable moiety in their backbone, located at one or both ends of the molecules. Acrylate or methacrylate moieties are the most commonly used moieties; they can be covalently crosslinked with the excitation of radical generating photoinitiators. The use of photocrosslinkable biodegradable polymers for the fabrication of biomedical applications offers two major advantages. First, the elimination of a surgery step to remove the implanted prosthesis after the healing of the tissues. Second, the possibility of triggering and guiding the tissue regeneration via degradation of the material. A list of selected examples of biodegradable polymers and their biomedical applications are illustrated in Table 2.2.

Polyethyleneglycol is widely explored for biomedical applications due to its excellent biocompatibility and degradability. Several derivatives have been explored including acrylate or methacrylate derivatives, poly(propylenefumarate-co-ethyleneglycol)³⁰ and PEG fumarate.³¹ PEG diamethacrylates and PEG urethane-dimethacrylates are also studied and showed good biocompatibility, they have been successfully used, both *in vivo* and *in vitro*, by several groups as scaffold materials.³² PEG-diacrylamide is also an interesting new derivative for *in vivo* photopolymerization. Although acrylamide is very toxic, PEG-acrylamide should not be toxic due to its high molecular weight and hydrophilicity, which will restrict access of the polymer to the cell's interior. Additionally, it undergoes rapid free-radical polymerization and is easily attached with peptides via a conjugate addition reaction.⁸

Polyvinylalcohol (PVA) has been shown to be protein non-adhesive, thus PVA offers the potential for cell selectivity through incorporation of bioactive moieties. The number of cross-linkable groups on the PVA chain can be widely varied, permitting greater manipulation of hydrogel mechanical properties. Additionally, the pendant hydroxyl groups on PVA provide many more available sites for the

Table 2.2. Selected examples of synthetic photocrosslinkable biodegradable polymers and their biomedical applications.

Polymers	Photocrosslinked Moiety	Application	Reference
Polyethyleneglycol	methacrylate	cartilage tissue engineering	Lin-Gibson et al. ³²
Pluronic	acrylate	controlled DNA release	Chun et al. ²⁶
Polyvinylalcohol	methacrylate	scaffolds material	West et al. ⁴
Polyesterpolyol	acrylate	tissue sealants	Nivasu et al. ⁵⁸
Inulin- succinic anhydride	methacrylate	pH-responsive drug delivery	Tripodo et al. ³⁶
polyanhydrides	methacrylate	orthopedic application	Burkoth et al. ⁵⁴
poly(acrylic acid)	methacrylate	mucoadhesive drug delivery system	Serra et al. ⁸⁰
PEG-diacrylamide	diacrylamide	reendothelialization promoting materials	Elbert et al. ²⁷
Poly(ϵ -caprolactone-co-D,L-Lactide)	acrylate	reendothelialization promoting materials	Younes et al. ⁸⁴
Hyaluronic acid	methacrylate	cell encapsulation	Bae et al. ⁵⁷
Dextran and polyaspartamide	glycidyl methacrylate	pH-responsive drug delivery	Pitarresi et al. ³⁸
polyphosphoester	acrylate	injectable scaffolds	Qiang et al. ¹⁵
Fumurate-based unsaturated poly(ester amide) and poly(ethylene glycol)	diacrylate	local anticancer drug delivery	Kai et al. ⁸³

attachment of bioactive molecules.⁴ Furthermore, PVA hydrogels have been studied as great candidate of protein-releasing matrices.³³ Jennifer *et al.*, investigated the use of photoactive PVA derivatives that form crosslinked hydrogels in the presence of cells and tissues functionalized with the cell-adhesive peptide RGDS (Arg-Gly-Asp-Ser) and are found to support the attachment and spreading of fibroblasts in a dose-dependent manner.⁴ Pluronic polymers are block copolymers of polyethyleneoxide and polypropylene oxide exhibit such a thermal gelling property. Photocrosslinked pluronic hydrogels have been used as delivery systems for several proteins and genes including IL-2, urease,³⁴ rat intestinal natrituretic factor.^{33,35} Poly(2-hydroxyethylmethacrylate) (poly(HEMA)) was also used as a drug carrier due to its ability to release entrapped drug in aqueous medium as well as its good compatibility.⁷ Hyperbranched polyglycerol (HyPG)yl methacrylate, which was derivatized with glycidyl methacrylate also showed great potential for drug delivery and for tissue engineering purposes.²²

Naturally occurring biodegradable polymers such as dextran, inulin,³⁶ collagens,^{37,38} hyaluronic acid,³⁷ and polyphosphester,¹⁵ whose degradability in the body is well known, have been also broadly explored for photopolymerization use. Among the natural materials for photopolymerization, polysaccharides represent good candidates to prepare bioerodible hydrogels used for drug delivery systems. Polysaccharides are readily available and can be degraded by hydrolysis, or enzymatically degraded in certain cases. Besides their compatibility and biodegradability, they possess hydroxyl-functional groups that can be used for the chemical modifications leading to crosslinking and the formation of hydrogels, these hydroxyl groups can also be used for the covalent attachment of drugs or other therapies to the hydrogel backbone.^{36,38} Several groups have demonstrated the release of drugs from polysaccharides matrices. Dextran is another natural polysaccharide that finds wide use in the pharmaceutical field.^{39,40} Photocrosslinked dextran derivative containing methacrylate moieties

represents a simple and reproducible procedure to obtain networks able to swell in aqueous medium.

2.4. BIOCOMPATIBILITY OF PHOTOCROSSLINKED POLYMERS

Any biomaterial intended for final conversion to a biomedical device or drug carrier must undergo rigorous processing and characterization as well as comprehensive safety testing. A biocompatible material must demonstrate appropriate interaction with the host in specific application and implant site and biocompatibility reflects the interaction that may be influenced by a number of factors related to the material, such as surface topography, charge, and chemistry. Similarly, biocompatibility is also influenced by properties of the host tissue, including local pH, blood transport rate, and presence of lipid and tissue type. Absorbable materials may be shaped into very diverse device forms, thus the ensuing discussion on toxicity and biocompatibility will be focused on the chemical as well as physical influence of the bulk material or device and its degraded product on the host tissue.⁴¹ Moreover, factors such as the energy of the polymerizing light, the heat and the radical species produced during the polymerization, the degree of monomer conversion and the toxicity of photoinitiators / monomers can influence cytotoxicity of the photopolymerizable biomaterials. However, it was found that these parameters may be controlled by changing the type of photoinitiator and light intensity.² It is well known that *in vitro* cytotoxicity testing evaluates lyses, growth inhibition and other impact on cells by medical devices.⁴² However, the current testing guidelines set for the assessment of cytotoxicity are not suitable for hydrogels, because it is difficult to place hydrogel in contact with cells and then remove the material without causing damage to the cells. Consequently, separate methodologies have to be used for testing the hydrogel in the presence of cells. Transwell inserts, which contain the hydrogel and polymeric solutions, were developed as an outstanding technique for an indirect contact testing.³⁷

It is also important to consider cell interactions here since the most of materials discussed are commonly used for *in vivo* purposes. These biomaterials must be tested by the use of cell viability test. There is either direct or indirect method to test cell viability. For direct test, as the name suggests, cells are placed in direct contact with the materials and for indirect testing samples are extracted in the medium used to culture the cells and the extract is then placed in prepared cell culture.³⁷ In addition to cell viability tests, the ability of photoinitiated materials to promote or inhibit cell adhesion has been investigated. For examples, the hydrophilic polymers such as PEG can inhibit cell adhesion whereas hydrophobic copolymers such as polystyrene promote cell adhesion.^{7,43} Moreover, attaching bioactive molecules to those biodegradable photopolymers, such as cell adhesive peptides, can change the cellular behavior. In brief, when biological molecules are conjugated with the biomaterial, the cells will respond only to the incorporated ligand, substantially unaffected by spuriously adsorbed proteins.²⁷ Hubbell *et al.*, studied the application of a novel hydrogel prepared by PEG diacrylate derivatives. They modified the hydrogel by binding it with Arg-Gly-Asp (RGD-containing peptide). The results revealed that the modifications promoted fibroblast spreading.^{27,44} Also, Hern *et al.*, showed that PEG can also be functionalized with bioactive peptide molecules to promote cell adhesion.⁴⁵ In addition, poly(lactide-co-llysine)⁴⁶ and PVA⁴ polymers had been modified with RGD peptide to enhance cell attachment and to support the spreading of fibroblasts in a dose dependent manner.

2.5. PHOTOPOLYMERIZATION IN TISSUE ENGINEERING

Photopolymerization has been used in a wide range of biomedical applications and is still considered an attractive approach for a variety of further biomedical investigations. A variety of biomedical applications have been used in medicine such as scaffold and tissue fabrication,⁴⁷ blood vessel

adhesives,⁴⁴ adhesion prevention barriers,²⁷ fabrication of biomaterial used as joint replacement,⁴⁸ teeth restoration,^{49,50} and in cell encapsulation for tissue replacement strategies.⁵¹ In this part of the review, some of the main utilization of photopolymerization in the biomedical and drug delivery field are discussed in detail.

2.5.1. Scaffold and tissue fabrication

The field of tissue engineering has witnessed new trends with advances in photopolymerization technologies. As *in vitro* models of living tissue, these techniques may be useful in developing therapies for replacing lost tissue function. Replacing physiological functions lost in damaged organ can be obtained by combining of cells and tissues to form a three-dimensional structured tissue. Researchers have been able to fabricate tissue engineering scaffolds with complex three-dimensional architectures, using stereolithography and photolithography methods as well as polymer chemistry. Stereolithography is a three-dimensional photopolymerization technique that uses an ultraviolet laser beam to photocrosslink the photopolymerizable polymer. Laser beam is directed into a layer of liquid polymer, causing cross-linking to the exposed area and after covering with a new layer of polymer the process is repeated. Cooke *et al.*, demonstrated the application of stereolithography for the production of biodegradable three-dimensional structure tissue.⁴⁷ On the other hand photolithography method is potentially used for the production of both single and multilayer biomaterials. The feasibility of using photolithography process to build and control the fabrication of polymer scaffolds has successfully been demonstrated, and a photolithographic method of patterning dried 2-hydroxyethyl methacrylate, which is later rehydrated before cell seeding, is also reported.⁵² Also, Jeffrey *et al.*, developed a simple yet rapid method of creating various shaped patterned surfaces using photocrosslinkable chitosan. They reported

the prepared chitosan patterned surfaces (cardiac fibroblasts, cardiomyocytes and osteoblasts) to be stable for up to 18 days.⁵³

An alternative method for hepatocyte transplantation is the implantation of tissue engineered hepatocyte spheroids (hepatocytes on biodegradable polymer). Spheroids have a liver-like morphology and preserved specific metabolic function and may serve as an *in vivo* substitute for lost liver function. *Valerie et al.*, have fabricated a hepatic tissue by using a multilayer photopatterning platform. They have used a photopolymerizable PEG hydrogel which is able to support hepatocyte survival and liver-specific function. Specifically, they incorporated adhesive peptides able to ligate integrin on these adhesion-dependent cells.⁵¹

Anseth et al., investigated a new class of methacrylate anhydride monomers such as methacrylated sebacic acid, methacrylated 1,3-bis(p-carboxyphenoxy) propane and methacrylated 1,6-bis(p-carboxyphenoxy) hexane for orthopedic applications⁵⁴ They successfully used such monomers in a tibia bone defect and preliminary histological evaluation showed good adhesion of the polymer to the cortical bone and medullar cavity. Furthermore, to secure metallic orthopedic implants, bone cements based on methyl methacrylate have been used to form rigid polymers.⁵⁶

2.5.2. Cell encapsulation

In cell encapsulation, transplanted cells are protected from immune rejection by artificial semi-permeable membrane; such encapsulation can be achieved using biodegradable polymer. The photopolymerized polymer should potentially allow allo- or xeno-transplantation without the use of

immunosuppressive. Several photo-polymeric encapsulation systems have been developed^{52,56} or are currently being tested in clinical trials.⁵⁷

Diabetes is one of the most significant areas of current research for encapsulation of cells, specifically the islet cells of the pancreas that produces insulin. *Cruise et al.*,⁵⁶ investigated a method of xeno-protection toward a bio-artificial endocrine pancreas. They illustrated the importance of interfacial photopolymerization to form polyethylene glycol (PEG) membranes for encapsulating islets of langerhans. The results from this study illustrated *in vitro* and *in vivo* function of the photo-encapsulated porcine islets and the capability of this membrane to prevent immune rejection in a discordant xenograft model. Moreover using static glucose stimulation and perfusion assays the encapsulated islets were shown to be glucose responsive.⁵² Additionally, *Elisseff et al.*, have suggested that the feasibility of photopolymerizing system provides an efficient method to encapsulate cells. They described the encapsulation of bovine and ovine chondrocytes in a poly (ethylene oxide)-dimethacrylate and poly (ethylene glycol) semi-interpenetrating network using a photopolymerization process.⁵⁶

A new concept for cell encapsulation was proposed by *Bae et al.*, who developed photopolymerizable beads with methacrylated hyaluronic acid and N-vinyl pyrrolidone. They directly injected viable cells into the beads by using microinjection technique. The results indicated that the cells could proliferate well within these beads and beads could be potentially used as injectable cell delivery vehicles for regenerating tissue defects.⁵⁷

2.6. PHOTOPOLYMERIZATION IN THERAPEUTIC DRUG DELIVERY

Targeted delivery of drug molecules to organs or special sites is one of the most challenging research

areas in the pharmaceutical sciences. By developing photocrosslinked delivery systems such as hydrogels, elastomers, and nanoparticles a new frontier is opened for improving drug delivery.⁶²⁻⁷⁰ Drug release can be controlled through spatial and temporal control of the photopolymerizable matrix to achieve sustained delivery. This can be achieved when a photopolymerizable polymer is combined with a drug in such a way that the active agent is released from the material in a predesigned manner to yield more effective therapies; while eliminating the potential for both under and overdosing. Usually a drug dissolved or dispersed uniformly throughout the photocrosslinked devices so that the release from such matrix systems is governed mainly by the diffusion process. The uniformly dispersed drug exhibits release rates that continuously diminish with time as a result of the increasing diffusion resistance and decreasing area due to geometry limitations. On the other hand, the release of the active agent may be designed to be constant over a long period by utilizing the osmotic-driven release mechanism using osmotic excipient, or it may be triggered by the environment or other external events. Hence, methods of using geometry factors and the surface erosion-controlled⁶⁰ and swelling-controlled mechanisms have been utilized for constant rate drug release.⁶¹

Moreover, photopolymerized biomaterials are also opening up new opportunities in implantable drug delivery systems in a minimally invasive manner. This is often preferable to the use of an injectable drug. *In situ* polymerizable polyesterpolyol were prepared with succinic acid and polyethyleneglycol of different molecular weights by Tammishetti's research group, as well as examining the *in vitro* release of entrapped sulfamethoxazole from this cross linked matrices.⁵⁸ the results of this release studies suggested that they can also be used for controlled delivery of antibiotics over a short period of time. Meanwhile, Langer *et al.*, hypothesized that light may cause a photopolymerization through the penetration of skin. They chose to inject polyethyleneoxide as a model polymer hydrogel system to test

the penetration of UV and visible light through the skin. Successfully, they obtained the polymers through photopolymerization. This result came up with "trans-dermal photopolymerization" that can be applied to both minimally invasive implantation and drug delivery.⁸ Additionally, photopolymerizable drug derivatives can be used for achieving sustained release drugs to improve the efficiency of drug therapies. This approach was illustrated when *Lawson et al.*, synthesized a photopolymerizable PEG-acrylate derivative of vancomycin, which could be covalently attached to a titanium implant alloy to form a bactericidal surface which prevented infections in the setting of orthopedic hardware.⁵⁹ This technique allows a loading dose several thousand times larger than that achieved with photopolymerizable polymer coupling approaches and holds promise for the treatment of orthopedic infections.

2.6.1 Photopolymerized Hydrogels

Photopolymerized hydrogels are a three-dimensional network of hydrophilic polymers held together by association bonds such as covalent bonds and weaker cohesive forces such as hydrogen, ionic bonds, and intermolecular hydrophobic associations. They have gained popularity as controlled release carriers for drugs and proteins due to their high water content, good biocompatibility, and consistency similar to soft-tissue. Moreover, they have high permeability to oxygen, nutrients and other water soluble metabolites.^{3,42} Although, their use in prolonged and controlled drug delivery has been widely investigated, there is still need for the development of hydrogels using feasible methods still exists.³⁸ Degradation of the photopolymerized hydrogel matrix not only allows a customized release of entrapped molecules but also evades the removal of the device from body.^{38,39}

There are two general methods for loading drugs into photocrosslinked hydrogel. One method requires the monomer to be mixed with drug, initiator and cross-linker and is photopolymerized to entrap the drug within the matrix. In the other method, a preformed photopolymerized hydrogel is allowed to swell to equilibrium in a suitable drug solution.⁴⁰ Drug diffuses from the photopolymerized hydrogel when it is placed in an environment causing it to swell and increases the mesh size. It is also important to ensure that the polymeric system is not over-crosslinked as the drug will not be able to diffuse out of the system. At the same time, the drug must be investigated to ensure that it can withstand the polymerization and will not react with the monomers in the system. *Peppas et al.*, developed a kinetic experiment to study the effect of solute on the polymerization process, and found that the presence of a solute results in a more heterogeneous material, a delay in the gel point and in greater microgel regions. Additionally, their study also revealed that presence of a low molecular weight solute increased the rate of polymerization.⁵⁶

Some photopolymerized hydrogels can be prepared at physiological pH and room temperature in the presence of a nontoxic photoinitiator upon exposure to UV light. The rapid photopolymerization process allows cells to be seeded homogeneously with the hydrogel with minimal exposure to UV light under biologically compatible conditions. Furthermore, gelation can be controlled both temporally and spatially by altering prepolymer concentration, photoinitiator concentration and exposure to UV light.⁴ Photocrosslinked polyanhydrides have highly predictable drug release profiles that depend on the polymer-erosion rate and implant geometry in many biomaterial applications where drug release would be beneficial.^{10,71,72} Amphiphilic block copolymers can be used as stimuli-sensitive synthetic hydrogels that shows a reversible sol gel transition behavior at a certain temperature range. These Hydrogels, such as pluronic hydrogels, were paid more attention for their unique properties including thermo-

sensitivity.⁷⁵⁻⁷⁷

Photopolymerized hydrogels are attractive for use in localized drug delivery as they can be crosslinked *in situ* and thus adhere and conform to the targeted tissue.³ Due to an enormous number of drugs and proteins used for various types of therapies, the applications of photopolymerizable hydrogels are countless. These applications include sustained DNA delivery,^{78,79} controlled release of cytokines,⁷³ mucoadhesive delivery systems,⁸⁰ and live vaccine ballistic delivery.⁸¹ For example, photocrosslinked pluronic hydrogels have been used for a sustained delivery of therapeutic genes for wound healing and tissue generation.⁷⁸ Similarly, *Park et al.*, successfully synthesized photocrosslinked hyaluronic acid (HA)/pluronic hydrogels for sustained release of proteins. When DNA was loaded in the hydrogel for sustained delivery, various release profiles were attained by varying UV irradiation time and modified HA amounts. This shows that the pluronic hydrogel can be utilized as a potential candidate material for *in vivo* sustained gene delivery after fine-tuning various formulation parameters.⁷⁹

The main objective of using photopolymerizable hydrogels is the control of drug release, which has been studied extensively. Theopylline,³⁸ gentamicin⁸² and live vaccine⁸¹ were released in a well-defined release pattern from different photopolymerized hydrogels. Also, photopolymerized hydrogel was used for the delivery of highly potent, but relatively toxic, anticancer drugs without inducing side effects. This was revealed when *Kai et al.*, synthesized paclitaxel loaded biodegradable hydrogels by the photopolymerization of two precursors: a fumurate-based unsaturated poly(ester amide) and PEG diacrylate. Sustained paclitaxel was released over a two-month period without an initial burst release from these hydrogels.⁸³ Furthermore, *Dimitrios et al.*, prepared doxorubicin encapsulated polymeric hydrogel nanoparticles by photopolymerization of PEG and poloxamer 407, in which the drug was

released in a sustained manner, with a minor burst, over a period of one week.⁸² Site specific delivery of drugs is another example of photopolymerized hydrogel applications. This was shown when *Peppas et al.*, modified poly(acrylic acid) with PEG onto their back bone chains to developed novel acrylic-based hydrogel used as a mucoadhesive delivery systems.⁸⁰

The aforementioned applications of hydrogels usually involve a single layer in which the drug is uniformly dispersed. However, it is difficult to obtain a single layer that possesses all the properties required for a specific application.⁹ Some applications may require the matrix to possess a diverse range of properties such as pH sensitivity, high water absorption, and constant drug release. Although sometimes these properties can be attained with a single material, it is difficult to obtain multiple properties in a single layer that can satisfy the intended application of the material or device. Thus, the capability to construct multiple layers of varied composition in a single membrane or device would increase the range of applications of these systems. Hydrogel multilayers may provide more precise properties when a single material cannot meet the requirements for the application. For example, *Anesth et al.*, investigated the use of photopolymerization of multi-laminated poly(HEMA) to create layered matrix devices with nonuniform concentration profiles with the goal of controlled drug release. They state that the polymerization conditions are sufficiently mild to be carried out in the presence of biological materials.⁹

Many approaches, as well, have been explored to improve the efficiency of gene delivery by using the photocrosslinked hydrogels as non viral vectors.^{66,67} One area of research is focused on identifying photocrosslinked polymer matrices to deliver DNA to cells *in vivo*, where they have been shown to increase DNA resistance to degradation by nucleases,¹⁰ increase plasmid DNA uptake compared to

bolus delivery methods,^{10,26} and provide controlled dosing. In addition, sustained DNA release can prolong foreign gene expression,^{26,66} thereby reducing the need for repeated dosing, which is a significant advantage for long-term gene therapy.¹⁰

Several types of polymer matrices have been explored for DNA delivery, with biodegradable hydrogel systems being the most common. The first example of this was demonstrated in the design of a photopolymer platform that enables simultaneous encapsulation of plasmid DNA by *Anseth et al.* They first protected the DNA from the effects of photoinitiating conditions (ultraviolet light and photoinitiator radicals) and then plasmid DNA was photoencapsulated and the quantity and quality of the released DNA was assessed. The results showed that encapsulated plasmid DNA was released in active forms (supercoiled and relaxed plasmids) with an overall 60% recovery. Therefore, this photopolymerization platform allowed for the creation of engineered tissues with enhanced control of cell behavior through the spatially and temporally controlled release of plasmid DNA.¹⁰ In another work carried out by the same research group, photopolymerized PEG-based macromolecules with various degradation rates to control the DNA release profiles were prepared. These photocrosslinked hydrogels were designed in a manner to release DNA for periods of 6-100 days with either nearly linear or delayed burst release profiles while maintaining biological activity.⁶⁶

Controlled DNA release was also achieved by loading plasmid DNA in a photopolymerizable diacrylated pluronic (water soluble tri-block copolymers of polyethyleneoxide-b-polypropyleneoxide-b-polyethyleneoxide) in the presence and absence of vinyl group-modified HA. Various release profiles were attained by varying UV irradiation time and modifying the ratio of hyaluronic acid. The released DNA was not chemically affected during the release period and substantially maintained the functional gene expression activities.²⁶ In addition, *Wieland et al.*, investigated the photocrosslinking of acrylated

PEG-hyaluronic acid as a controlled release vehicle for gene therapy vectors. The release from these hydrogels was dependent on the physical properties for both the hydrogel and the vector. The polymer content and relative composition of HA and PEG influenced the transport of the vector through the hydrogel by modulating the swelling ratio, water content, and degradation rate. The release study also revealed that the majority of the release occurring during the initial 2 days and the cumulative release increased with decreasing PEG or increasing HA content. Therefore, these studies demonstrated the dependence of non-viral vector release on the physical properties of the hydrogel and the vector, suggesting vector and hydrogel designs for maximizing localized delivery of non-viral vectors.⁶⁷ However, with PEG-hyaluronic acid delivery vehicles, DNA encapsulation efficiencies are low which can be improved by introducing amphiphilic molecules. More important, though, is the DNA damage that has been observed as result of degradation. Degrading PEG-hyaluronic acid produces acidic degradation products that accumulate and are thought to damage encapsulated DNA. Researchers are investigating more porous structures to reduce accumulation of degradation products in the implant interior, thereby mitigating damage to pH sensitive molecules like DNA.

Some applications may require the matrix to possess a diverse range of properties such as pH sensitivity, high water absorption, and constant drug release. The swelling or shrinking of stimuli-responsive photopolymerized material in response to small changes in pH or temperature can be used to control drug release. For example, the development of a glucose sensitive insulin releasing system for diabetes therapy was developed by using a pH responsive polymer. The polymer can be mixed and compressed with glucose oxidase, bovine serum albumin, and insulin. When the photopolymerized matrix was exposed to glucose, it was oxidized to form gluconic acid. As the hydration state was changed by a decrease in the pH, then insulin was released.⁴² On the other hand, a maleic and/or succinic anhydride derivative of insulin are suitable candidates to avoid the release of ibuprofen (the

model drug) in the gastric region, due to their low swelling and a great resistance in simulated gastric fluid (pH = 0.1). These crosslinked polymers showed very little release of ibuprofen in simulated gastric fluid and a great release in simulated intestinal fluid. This pH sensitive photopolymerized insulin derivative was approved to be a suitable candidate for non steroidal antiinflammatory drugs (NSAIDs) or other drugs with a potential irritating effect on the gastric mucosa, susceptible of acidic degradation or with a specific activity in the intestine.³⁶ Also, *Peppas et al.*, synthesized a novel pH responsive polymer containing grafted PEG chains by photopolymerization as oral protein delivery carriers. In acidic media (pH = 2.2), insulin release from the hydrogel was very slow. However, as the pH of the medium shifted to 6.5, a rapid release of biologically active insulin took place as a strong indication of their potential as a matrix for an oral formulation of insulin and as a model to avoid the release of drugs in the gastric region.⁶⁸

Temperature sensitive vehicles were synthesized by photopolymerization of vinyl group modified hyaluronic acid (HA).¹⁶ The synthesized HA/ pluronic gradually collapsed with increasing temperature over the range of 5–40 °C, suggesting that the pluronic component formed self-associating micelles in the hydrogel structure, revealing that the protein stability events such as aggregation and non specific release rate could be controlled by modulating the adsorption. Poly(N-isopropylacrylamide) based polymers are explored as a topic of various smart biomaterials since it undergoes a reversible temperature-sensitive phase transition in aqueous solutions at approximately 32 °C. *Nguyen et al.*, have investigated composite hydrogels with temperature-sensitive properties using photocrosslinking. Their novel composite materials are composed of nanoparticles made of poly(N-isopropylacrylamide). The *in vitro* bovine serum albumin (BSA) release studies from these hydrogels demonstrated that these nanoparticles were embedded inside the PEG polymeric matrix and the composite material was able to

release BSA in response to changes in temperature. These nanoparticle hydrogel networks have advantages in applications of controlled drug delivery systems because of their temperature sensitivity and their ability of *in situ* photopolymerization.^{16,69}

2.6.2. Photopolymerizable Elastomers

Over the past 15 years, the literature on biomedical applications for elastomers has grown considerably and reports have appeared regularly. Elastomers owned for its broad uses in biomedical applications: The exhibition of mechanical properties as soft as body tissues make them attractive for the implantation in the highly challenged non static part of the body. Their elasticity can be utilized along with osmotic pressure to generate linear release profiles for water soluble compounds in drug delivery.^{62,64} Several types of biodegradable elastomeric matrices have been explored for drug delivery.^{62,64} The rationale behind these elastomers is the use of non-toxic, readily available and inexpensive monomers. In addition, the availability of various molecular weights of similar monomers provides flexibility to tune the mechanical and degradation characteristics of the resulting elastomers. Lifetimes of such biodegradable material could be successfully adjusted by varying the molecular weight of the polymer, degree of crystallinity and crosslinking density.⁶²

The photopolymerizable elastomers exemplify an ideal carrier for prolonged delivery of thermosensitive drugs. Thermosensitive drugs such as protein and peptides are to be incorporated into the device as solid particles which require the polymer to cure near ambient temperature. The photocrosslinked biodegradable elastomers can undergo free radical polymerization upon exposure to UV or visible light at room temperatures and process rapidly.⁸⁵ There are many photocurable

monomers/oligomers that can be photocrosslinked to form elastomers such as methacrylated star-poly(ϵ -caprolactone-co-D,L-lactide),⁸⁸ poly(ϵ -caprolactone-co-trimethylene carbonate),⁸⁹ poly(ϵ -caprolactone) by end-functionalization with maleic or itaconic anhydride,⁹⁰ poly(ϵ -caprolactone) chain extended with 4,4(adipoyldioxy) dicinnamic acid.⁹¹

Most of the therapeutic proteins require long term and site localized delivery, although, most of them are administered via multiple injection regimens. In addition, the self storage stability and low patient compliance have also hampered their translation to clinic.⁶²⁻⁶⁴ As a result, an extensive amount of research has gone into the development of photocrosslinked elastomers as a more effective means of administering protein drugs. This was demonstrated when a photocrosslinked biodegradable elastomer, star poly(ϵ -caprolactone-co-d,l-lactide) was designed in an attempt to deliver bioactive cytokines such as interferon- γ (IFN- γ), interleukin 2 (IL-2), and vascular endothelial growth factor (VEGF). *Younes et al.*, chose ϵ -caprolactone and D,L-lactide as monomers, which have good compatibilities and a star polymer architecture in their elastomer since the physical properties of the final network can be easily altered on the basis of the number of arms in the star copolymer (e.g., crosslinking density).⁸⁶ Moreover, a comparison of elastomers prepared from linear versus star (3-isocyanatopropyl) triethoxysilane terminated polylactide demonstrated that better mechanical properties were achieved with the star-poly lactide.⁸⁷ This result was attributed to the higher crosslinking density achievable using a star prepolymer architecture. Depending on the osmotic pressure release mechanism IFN- γ was released from the optimum formulation at a constant rate of 23 ng/day over three weeks.⁶² A cell-based assay showed that over 83% of released IFN- γ was bioactive. Also, a constant release rate for IL-2 and VEGF was achieved as the mechanical properties maintained during the release period.⁶² However, the bioactivity profile for VEGF show a marked drop after the first week of release as a result of hydrolytic

degradation and acidic monomer accumulation inside the elastomers ($\text{pH} < 5$). Furthermore, it was demonstrated that bovine serum albumin and trehalose co-lyophilized with the cytokine were released at the same rate as the protein drug. Thus, this delivery formulation may be clinically useful for sustained, local delivery of acid resistant proteins. However, there are still a number of issues which may have an impact on the stability profile of loaded proteins that should be addressed in this strategy. For example, the use of organic solvents during the device preparation may change the protein conformation. Also, the use of ultraviolet radiation during the photocuring of this elastomer was reported to denature proteins and consequently destroys their biological activity.⁶² To date, there are no *in vivo* preclinical or clinical studies on the therapeutic efficacy of this new delivery system.

Beside that, another elastomer was developed by Chapanian *et al.*, to provide the delivery of vascular endothelial growth factor (VEGF_{165}) and hepatocyte growth factor (HGF) by preparing a dual-layered cylinder, in which VEGF_{165} was in the outer layer and HGF in the inner layer.⁹² This elastomer is based on trimethylene carbonate (TMC) since it degrades without producing potentially harmful acidic degradation products, and its mechanical properties can be tailored by copolymerizing with d,l-lactide (DLLA) and ϵ -caprolactone ($\epsilon\text{-CL}$) and by controlling the crosslinking density. VEGF_{165} and HGF were lyophilized separately or together with trehalose, rat serum albumin (RSA) and NaCl and their bioactivities after released were assessed *in vitro*. They revealed that TMC based elastomer combined with an osmotic mechanism to release acid sensitive growth factors in bioactive form, alone or in combination, controlled rates and sequences. The prepared cylinders were able to provide a sustained release of highly bioactive VEGF_{165} and HGF for more than 10 days. When released in combination from the same device, VEGF_{165} and HGF were released at similar rates. A constant release of VEGF alone was first obtained, followed by overlapping and constant release of the two growth

factors after a period of 4 days. Having said that, the use of organic solvents and ultra violet radiation during the photocuring are issues that should be addressed, since they have an impact on the stability profile of loaded proteins. Also, more *in vivo* investigations and studies are still required to examine its ability to fit in the protein delivery system pipeline.

Shaker et al., have demonstrated the ability to rapidly form elastomeric structures from acrylated poly(diols-tricarballoylate) (PDT) using visible light crosslinking in the presence of camphorquinone (CQ) as a biocompatible photoinitiator and under solvent-free conditions.⁹³ The tricarballoylic acid and the alkylene diol were selected as building blocks for the construction of the new elastomers since tricarballoylic acid is abundantly present in food products and possesses structural similarity to several biological active compounds such as citric acid and amino acid.⁹³ On the other hand, aliphatic diols are reported to be biocompatible intermediate compounds used in the synthesis of polymeric systems including, polyester elastomers, coatings, adhesives, and polymeric plasticizers. Diols as well, add many high performance characteristics to the final structure of the elastomer such as hydrolytic stability, increased flexibility, improved adhesion, and surface hardness. The avoidance of UV photocrosslinking drawbacks, the solvent-free preparation process, and the controllable drug delivery,⁹⁴ as well as biocompatibility properties⁹⁵ of these biodegradable polymers make them excellent candidates for use in thermosensitive therapeutic protein and peptide delivery. A release study for loaded IL-2 elastomer utilizing the osmotic driven release mechanism done by the same research group. The results show this elastomer was able to control the IL-2 release over a period of 28 days and the increase in the elastomeric device's surface area and the incorporation of trehalose in the loaded lyophilized mix increased the IL-2 release rate. As well, the results showed that the decrease in the degree of prepolymer acrylation of the prepared elastomeric devices increased the IL-2 release rate. Also the data showed that

the released IL-2 retained more than 94% of its initial activity. More details regarding the release and bioactivity results of loaded protein with this elastomer is described in chapter 6.

2.7. CONCLUSIONS

Photopolymerization technology is the reaction of monomers or oligomers to form a linear or crosslinked polymer structure by light induced initiation. It is a very promising multidisciplinary technology that could be used to produce polymeric networks for biomedical applications. Well defined photoinitiated polymers such as hydrogels and elastomers can be formed with varying polymer formulations in three dimensional patterns and they can also be designed to degrade via hydrolytic or enzymatic processes. Furthermore, they can also be modified with biofunctional moieties within their structure to manipulate cell behavior since have been widely explored for and become more attractive for future research. For drug delivery applications, some "smart" photopolymerizable biomaterials have generally been synthesized through modification of some molecules which are sensitive to circumstance parameters such as temperature and pH. These can become potential candidates for controlled drug release.

2.8. REFERENCES

- 1- Benson GG, Hemingway SR, Leach FN. 1978. Composition of the wrappings of an ancient Egyptian mummy [proceedings]. *J Pharm Pharmacol* 30:78.
- 2- Biancamaria B. 2006. Photopolymerization of biomaterials: issues and potentialities in drug delivery, tissue engineering, and cell encapsulation applications. *J Chem Technol Biotechnol* 81:491-499.
- 3- Nguyen KT, West JL. 2002. Photopolymerizable hydrogels for tissue engineering applications. *Biomaterials* 23: 4307-4314.

- 4- Schmedlen RH, Masters KS, West JL. 2002. Photocrosslinkable polyvinyl alcohol hydrogels that can be modified with cell adhesion peptides for use in tissue engineering. *Biomaterials* 23: 4325-32.
- 5- Raymond B, Symour CE, Carraher Jr. 1993. *Polymer Chemistry* p158-170.
- 6- Challa GER. 1993. *Polymer Chemistry an Introduction*. p30-40.
- 7- Lu S, Anseth KS. 1999. Photopolymerization of multilaminated poly(HEMA) hydrogels for controlled release. *J Control Release* 57: 291-300.
- 8- Elisseeff J, Anseth K, Sims D, McIntosh W, Randolph M, Langer R. 1999. Transdermal photopolymerization for minimally invasive implantation. *Proc Natl Acad Sci U.S.A* 96: 3104-3107.
- 9- Tripodo G, Pitarresi G, Palumbo FS, Craparo EF, Giammona G. 2005. UV-photocrosslinking of inulin derivatives to produce hydrogels for drug delivery application. *Macromol Biosci* 5: 1074-1084.
- 10- Quick DJ, Anseth KS. 2003. Gene delivery in tissue engineering: a photopolymer platform to coencapsulate cells and plasmid DNA. *Pharm Res* 20: 1730-1737.
- 11- Norman SA. 1985. Jan F. Rabek, *New Trends in the Photochemistry of Polymers*. P80-110.
- 12- John PF, David D, Paul SE, Antonios GM. 2001. Photoinitiated Polymerization of Biomaterials. *Annu Rev Mater Res* 31:171-181.
- 13- Fouassier JP. 1995. Photoinitiation, photopolymerisation and Photocuring: Fundamental and Applications, Hanser Publishers, Munich.
- 14- Allen NS. 1996. Photoinitiators for UV and visible curing of coatings: Mechanisms and properties *J. Photochem. Photobio. A: Chemistry*.100: 101-107.
- ~ 15- Li Q, Wang J, Shahani S, Sun DD, Sharma B, Elisseeff JH, Leong, K.W. 2006. Biodegradable and photocrosslinkable polyphosphoester hydrogel. *Biomaterials* 27: 1027-1034.
- 16- Kim MR, Park TG. 2002. Temperature-responsive and degradable hyaluronic acid/Phuronic composite hydrogels for controlled release of human growth hormone. *J Control Release* 80: 69-77.

- 17-Williams CG, Malik AN, Kim TK, Manson PN, Elisseeff JH. 2005. Variable cytocompatibility of six cell lines with photoinitiators used for polymerizing hydrogels and cell encapsulation. *Biomaterials* 26: 1211-1218.
- 18-Burkoth, AK, Anseth KS. 2000. A review of photocrosslinked polyanhydrides: *in situ* forming degradable networks. *Biomaterials* 21: 2395-404.
- 19-Hill-West JL, Chowdhury SM, Dunn RC, Hubbell JA. 1994. Efficacy of a resorbable hydrogel barrier, oxidized regenerated cellulose, and hyaluronic acid in the prevention of ovarian adhesions in a rabbit model. *Fertil Steril* 62: 630-634.
- 20-Hill-West JL, Chowdhury SM, Sawhney AS, Pathak CP, Dunn RC, Hubbell JA. 1994. Prevention of postoperative adhesions in the rat by *in situ* photopolymerization of bioresorbable hydrogel barriers. *Obstet Gynecol* 83: 59-64.
- 21-West JL, Hubbell JA. 1999. Polymeric biomaterials with degradation sites for proteases involved in cell migration. *Macromolecules* 32: 241-244.
- 22-Quick DJ, Anseth KS. 2006. Synthesis and characterization of hyperbranched polyglycerol hydrogels. *J Biomaterials* 27:5471-5479.
- 23-Davis KA, Burdick JA, Anseth KS. 2003. Photoinitiated crosslinked degradable copolymer networks for tissue engineering applications. *Biomaterials* 24: 2485-2495.
- 24-Poshusta AK, Anseth KS. 2001. Photopolymerized biomaterials for application in the temporomandibular joint. *Cells Tissues Organs* 169: 272-278.
- 25-Burdick JA, Mason MN, Anseth KS. 2001. *In situ* forming lactic acid based orthopaedic biomaterials: influence of oligomer chemistry on osteoblast attachment and function. *J Biomater Sci Polym Ed* 12: 1253-1265.
- 26-Chun KW, Lee JB, Kim SH, Park TG. 2005. Controlled release of plasmid DNA from photo-cross-linked pluronic hydrogels. *Biomaterials* 26: 3319-3326.
- 27-Elbert DL, Hubbell J A. 2001. Conjugate addition reactions combined with free-radical cross-linking for the design of materials for tissue engineering. *Biomacromolecules* 2: 430-441.
- 28-Cruise GM, Hegre OD, Scharp DS, Hubbell JA. 1998. A sensitivity study of the key parameters in the interfacial photopolymerization of poly(ethylene glycol) diacrylate upon porcine islets. *Biotechnol Bioeng* 57: 655-665.
- 29-Barbucci R. 2002. *Integrated Biomaterial Science*. p120-130.

- 30- Shin H, Quinten RP, Mikos AG, Jansen JA. 2003. *In vivo* bone and soft tissue response to injectable, biodegradable oligo(poly(ethylene glycol) fumarate) hydrogels. *Biomaterials* 24: 3201-3211.
- 31- Suggs LJ, Kao EY, Palombo LL, Krishnan RS, Widmer MS, Mikos AG. 1998. Preparation and characterization of poly(propylene fumarate-co-ethylene glycol) hydrogels. *J Biomater Sci Polym Ed* 9: 653-666.
- 32- Lin-Gibson S, Bencherif S, Cooper JA, Wetzel SJ, Antonucci JM, Vogel BM, Horkay F, Washburn NR. 2004. Synthesis and characterization of PEG dimethacrylates and their hydrogels. *Biomacromolecules*. 5: 1280-87.
- 33- Peppas NA, Scptt JE. 1992. Controlled release from poly(vinyl alcohol) gels prepared by freezing-thawing processes. *J Controlled Release* 18:95-100.
- 34- Fults KA, Johnston TP. 1990. Sustained-release of urease from a poloxamer gel matrix. *J Parenter Sci Technol* 44:58-65.
- 35- Korsmeyer RW, Gurny R, Doelker E, Biru P, Peppas NA. 1983. Mechanisms of solute release from porous hydrophilic polymers. *Int J Pharm* 15:25.
- 36- Tripodo G, Pitarresi G, Palumbo FS, Craparo EF, Giammona G. 2005. UV-photocrosslinking of inulin derivatives to produce hydrogels for drug delivery application. *Macromol Biosci* 5: 1074-1084.
- 37- Trudel J, Massia SP. 2002. Assessment of the cytotoxicity of photocrosslinked dextran and hyaluronan-based hydrogels to vascular smooth muscle cells. *Biomaterials* 23: 3299-3307.
- 38- Pitarresi G, Palumbo FS, Giammona G, Casadei MA, Micheletti MF. 2003. Biodegradable hydrogels obtained by photocrosslinking of dextran and polyaspartamide derivatives. *Biomaterials* 24: 4301-4313.
- 39- Kim IS, Jeong YI, Kim DH, Lee YH, Kim SH. 2001. Albumin release from biodegradable hydrogels composed of dextran and poly(ethylene glycol) macromer. *Arch Pharm Res* 24: 69-73.
- 40- Reynolds JEF, editor. 1993. Martindale, The extra pharmacopoeia, 30th ed. London: The Pharmaceutical Press p650-652.
- 41- Shalaby WS, Karen JLB. 2004. Absorbable and Biodegradable polymers. p143-159.
- 42- Dumitriu S. 2001. *Polymeric Biomaterials* (2nd Edition, Revised and Expanded) p334-350.

- 43- Nakayama Y, Miyamura M, Hirano Y, Goto K, Matsuda T. 1999. Preparation of poly(ethylene glycol)-polystyrene block copolymers using photochemistry of dithiocarbamate as a reduced cell-adhesive coating material. *Biomaterials* 20: 963-970.
- 44- Hubbell JA. 1996. Hydrogel systems for barriers and local drug delivery in the control of wound healing. *J Controlled Release* 39:305-313.
- 45- Hern DL, Hubbell JA. 1998. Incorporation of adhesion peptides into nonadhesive hydrogels useful for tissue resurfacing. *J Biomed Mater Res* 39: 266-76.
- 46- Barrera DA, Zylstra E, Lansbury Jr PT, Langer R. 1993. Synthesis and RGD peptide modification of a new biodegradable copolymer: poly(lactic acid-co-lysine). *J Am Chem Soc* 115:11010.
- 47- Malcolm NC, John PF, David D, Clare R, AntoniosGM. 2002. Use of Stereolithography to Manufacture Critical-Sized 3D Biodegradable Scaffolds for Bone Ingrowth. *J Biomed Mater Res Part B: Appl Biomater* 64: 65-69.
- 48- Poshusta AK, Anseth KS. 2001. Photopolymerized biomaterials for application in the temporomandibular joint. *Cells Tissues Organs* 169:272-278.
- 49- Anseth K, Newman S, Bowman C. 1995. Polymeric dental composites: properties and reaction behavior of multimethacrylate dental restorations. *Adv Polym Sci* 122: 177-217.
- 50- Khosroshahi ME, Atai M, Nourbakhsh MS. 2007. Photopolymerization of dental resin as restorative material using an argon laser. *Lasers Med Sci* 23:399-406
- 51- Cruise GM, Hegre OD, Lamberti FV, Hager SR, Hill R, Scharp DS, Hubbell JA. 1999. *In vitro* and *in vivo* performance of porcine islets encapsulated in interfacially photopolymerized poly(ethylene glycol) diacrylate membranes. *Cell Transplant* 8: 293-306.
- 52- Yu T, Chielini F, Schmal JD, Solaro R, Ober CK. 2000. Microfabrication of hydrogels as polymer scaffolds for tissue Engineering Applications. *Polymer Prepr* 41: 1699-1700.
- 53- Karp JM, Yeo Y, Geng W, Cannizarro C, Yan K, Kohane DS, Vunjak-Novakovic G, Langer RS, Radisic M. 2006. A photolithographic method to create cellular micropatterns. *Biomaterials* 27:4755-4764.
- 54- Burkoth AK, Anseth KS. 2000. A review of photocrosslinked polyanhydrides: *in situ* forming degradable networks. *Biomaterials* 21: 2395-2404.

- 55- Kohn D, Ducheyne P. 1992. In: R. Cahn, P. Haasen and E. Kramer, Editors, Medical and Dental Materials. Materials Science and Technology Vol. 14, VCH, New York p. 29-44.
- 56-Elisseeff J, McIntosh W, Anseth K, Riley S, Ragan P, Langer R. 2000. Photoencapsulation of chondrocytes in poly(ethylene oxide)-based semi-interpenetrating networks. *J Biomed Mater Res* 51: 164-171.
- 57-Bae KH, Yoon JJ, Park TG. 2006. Fabrication of hyaluronic acid hydrogel beads for cell encapsulation. *Biotechnol Prog* 22:297-302.
- 58-Nivasu, VM, Yarapathi VR, Tammishetti S. 2004. Synthesis, UV photopolymerization and degradation study of PEG containing polyester polyol acrylates. *Polym Adv Tech* 15:128-133.
- 59-Lawson MC, Bowman CN, Anseth KS. 2007. Vancomycin derivative photopolymerized to titanium kills *S. epidermidis*. *Clin Orthop Relat Res* 461: 96-105.
- 60-Quick DJ, Macdonald KK, Anseth KS. 2004. Delivering DNA from photocrosslinked, surface eroding polyanhydrides. *J Control Release* 97: 333-343.
- 61-Agis K. 1994. Treatise on Controlled Drug Delivery. p155-200.
- 62-Gu F, Younes HM, El-Kadi AO, Neufeld RJ, Amsden BG. 2005. Sustained interferon-gamma delivery from a photocrosslinked biodegradable elastomer. *J Control Release* 102: 607-617.
- 63-Burdick JA, Mason MN, Hinman AD, Thorne K, Anseth KS. 2002. Delivery of osteoinductive growth factors from degradable PEG hydrogels influences osteoblast differentiation and mineralization. *J Control Release* 83: 53-63.
- 64-Gu F, Neufeld R, Amsden B. 2006. Osmotic-driven release kinetics of bioactive therapeutic proteins from a biodegradable elastomer is linear, constant, similar, and adjustable. *Pharm Res* 23: 782-789.
- 65-Younes HM, Amsden BG. 2002. Interferon-gamma therapy: evaluation of routes of administration and delivery systems. *J Pharm Sci* 91: 2-17.
- 66-Quick DJ, Anseth KS. 2004. DNA delivery from photocrosslinked PEG hydrogels: encapsulation efficiency, release profiles, and DNA quality. *J Control Release* 96: 341-351.
- 67-Wieland JA, Houchin-Ray TL, Shea LD. 2007. Non-viral vector delivery from PEG-hyaluronic acid hydrogels. *J Control Release* 120:233-241.

- 68-Kim B, Peppas NA. 2003. *In vitro* release behavior and stability of insulin in complexation hydrogels as oral drug delivery carriers. *Int J Pharm* 266: 29-37.
- 69-Ramanan RM, Chellamuthu P, Tang L, Nguyen KT. 2006. Development of a temperature-sensitive composite hydrogel for drug delivery applications. *Biotechnol Prog* 22: 118-125.
- 70-Reynolds JEF, editor. 1993. *The extra pharmacopoeia*, 30th ed. London: The Pharmaceutical Press p 650-652.
- 71-Dumitriu S. 2001. *Polymeric Biomaterials* (2nd Edition, Revised and Expanded) p136-141.
- 72-Ward JH, Peppas NA. 2001. Preparation of controlled release systems by free-radical UV polymerizations in the presence of a drug. *J Control Release* 71: 183-192.
- 73-Shaker M, Younes HM. 2009. Interleukin-2: Evaluation of Routes of Administration and Current Delivery Systems in Cancer Therapy. *J Pharm Science* 98: 2268-2298.
- 74-Quick DJ, Macdonald KK, Anseth KS. 2004. Delivering DNA from photocrosslinked, surface eroding polyanhydrides. *J Control Release* 97: 333-343.
- 75-Jeong B, Bae YH, Lee DS, Kim SW. 1997. Biodegradable block copolymers as injectable drug-delivery systems. *Nature* 388: 860-862.
- 76-Drury JL, Mooney DJ. 2003. Hydrogels for tissue engineering: scaffold design variables and applications. *Biomaterials* 24: 4337-4351.
- 77-Jeong B, Kim SW, Bae YH. 2002. Thermosensitive sol-gel reversible hydrogels. *Adv Drug Deliv Rev* 54: 37-51.
- 78-Madsen S, Mooney DJ. 2000. Delivering DNA with polymer matrices: applications in tissue engineering and gene therapy. *Pharm Sci Technol Today* 3: 381-384.
- 79-Kim MR, Park TG. 1994. Temperature-responsive bioconjugates. 3. Antibody-poly(N-isopropylacrylamide) conjugates for temperature-modulated precipitations and affinity bioseparations. *Bioconjug.Chem.* 5: 577-582.
- 80-Serra L, Domenech J, Peppas NA. 2006. Design of poly(ethylene glycol)-tethered copolymers as novel mucoadhesive drug delivery systems. *Eur J Pharm Biopharm* 63: 11-18.
- 81-Christie RJ, Findley DJ, Dunfee M, Hansen RD, Olsen SC, Grainger DW. 2006. Photopolymerized hydrogel carriers for live vaccine ballistic delivery. *Vaccine* 24: 1462-1469.

- 82- Missirlis D, Kawamura R, Tirelli N, Hubbell JA. 2006. Doxorubicin encapsulation and diffusional release from stable, polymeric, hydrogel nanoparticles. *Eur J Pharm Sci* 29:120-129.
- 83- Guo K, Chu CC. 2007. Controlled release of paclitaxel from biodegradable unsaturated poly(ester amide)s/poly(ethylene glycol) diacrylate hydrogels. *J Biomater Sci Polym Ed* 18: 489-504.
- 84- Younes HM, Bravo-Grimaldo E, Amsden BG. 2004. Synthesis, characterization and *in vitro* degradation of a biodegradable elastomer. *Biomaterials* 25: 5261-5269.
- 85- Amsden B, Wang S, Wyss U. 2004. Synthesis and characterization of thermoset biodegradable elastomers based on star-poly(epsilon-caprolactone-co-D,L-lactide). *Biomacromolecules* 5: 1399-1404.
- 86- Amsden BG, Misra G, Gu F, Younes HM. 2004. Synthesis and characterization of a photo-cross-linked biodegradable elastomer. *Biomacromolecules*. 5: 2479-2486.
- 87- Korhonen H, Hakala RA, Helminen AO, Seppala JV. 2001. Synthesis and hydrolysis behaviour of poly(ester anhydrides) from polylactone precursors containing alkenyl moieties. *J V Polymer* 42: 3345-3353.
- 88- Aoyagi T, Miyata F, Nagase Y. 1994. Preparation of cross-linked aliphatic polyester and application to thermo-responsive material *J Control Rel* 32:87-96.
- 89- Matsuda T, Mizutani M, Arnold SC. 2000. Molecular Design of Photocurable Liquid Biodegradable Copolymers. 1. Synthesis and Photocuring Characteristics. *Macromolecules* 33:795-800.
- 90- Lang M, Chih-Chang C. 2002. Functionalized multiarm poly(epsilon-caprolactone)s: Synthesis, structure analysis, and network formation. *J Appl Polym Sci* 86: 2296-2306.
- 91- Nagata M, Sato Y. 2004. Biodegradable elastic photocured polyesters based on adipic acid, 4-hydroxycinnamic acid and poly(epsilon-caprolactone) diols. *Polymer* 45: 87-93.
- 92- Chapanian R, Amsden BG. 2010. Combined and sequential delivery of bioactive VEGF165 and HGF from poly(trimethylene carbonate) based photo-cross-linked elastomers. *J Control Release* 143: 53-63.
- 93- Shaker MA, Doré JE, Younes HM. 2010. Synthesis, characterization and cytocompatibility of poly(diols-tricarballoylate) visible light photocrosslinked biodegradable elastomer. *J. Biomater Sci Polym Ed* 21: 507-528.
- 94- Shaker M, Younes HM. 2010. Osmotic-Driven Release of Papaverine Hydrochloride from Novel Biodegradable Poly(Decane-co-tricarballoylate) Elastomeric Matrices. *Therapeutic Delivery* 1, 1, 37-50.

- 95-Shaker M, Daneshtalab N, Doré J, Younes HM. *In vitro* Cytotoxicity, *In vivo* Biocompatibility and Biodegradability of Photocrosslinked Poly(Decane-co-Tricarballylate) Elastomers. *J of bioactive and compatable polymers* accepted April 2011.

CHAPTER 3

Synthesis, Characterization and Cytocompatibility of Poly(diols-tricarballylate) Visible Light Photocrosslinked Biodegradable Elastomer

The content of this chapter was published in the Journal of Biomaterial Science 21, 4, 507-528 (2010).

Mohamed A. Shaker, Jules J.E. Doré and Husam M. Younes

ABSTRACT

The synthesis, characterization and *in vitro* cytocompatibility of a new family of photocrosslinked amorphous poly(diols-tricarballoylate) (PDT) biodegradable elastomeric polyesters are reported. The synthesis was based on the polycondensation reaction between tricarballoylic acid and alkylene diols, followed by acrylation. The formation of PDT and its acrylated derivatives (APDT) was characterized by means of FT-IR, ^1H -NMR, GPC and DSC. Liquid to solid photo-curing were carried out by exposing the APDT to visible light in the presence of camphorquinone as a photoinitiator. The thermal properties, mechanical characteristics, the sol content, long-term *in vitro* degradation and cytocompatibility of the prepared PDT elastomers were also reported. The mechanical and degradation properties of this new photocurable elastomer can be precisely controlled by varying the density of acrylate moieties in the matrix of the polymer, and through changes in the prepolymer chain length. The use of visible light crosslinking, possibility of solventless drug loading, the controllable mechanical properties and cytocompatibility of these new elastomers make them excellent candidates for use in controlled implantable drug delivery systems of protein drugs and other biomedical applications.

3.1. INTRODUCTION

In the past decade, biodegradable elastomeric polymers have gained considerable attention due to the renewed interest in their applications in the fields of biomedical tissue engineering¹⁻³ and implantable drug delivery systems.⁴⁻⁹ Elastomers can be regarded as one of the best biomaterials for such applications because their mechanical properties can be manipulated in a manner that makes them as soft as body tissues. They have the ability to recover and withstand the mechanical challenges upon implantation in a mobile part of the body and they are also proved to be well suited for drug controlled drug delivery applications.^{5,6}

Biodegradable elastomers reported in the literature have been synthesized as one of two types: thermoplastic¹⁰⁻¹² or thermoset elastomers.^{1,13,14} While thermoplastics offer the advantage of ease of fabrication, they degrade heterogeneously due to the mixture of crystalline and amorphous regions. This can lead to rapid loss of mechanical properties as well as large deformation as the material degrades. Conversely, although thermoset polymers are not easily fabricated by heat, they outperform thermoplastics in a number of areas, including uniform biodegradation, mechanical properties, and overall durability. This makes thermoset elastomers better suited for controlled drug delivery applications.

One of the common approaches reported earlier to prepare thermoset elastomers is to first prepare multi-arm star condensation polymers by subjecting biodegradable monomers to ring-opening polymerization in the presence of polyols as initiators.^{1,11,15-18} The prepared star-shaped condensation polymers are then crosslinked using thermal or non-thermal approaches. Some of the thermal crosslinking approaches reported involved the preparation of polyurethanes that contain the 4,4'-

methylphenidate diisocyanate which degrades to toxic and carcinogenic products and raises issues of biocompatibility.^{13,19} Other elastomers were prepared by thermal free-radical curing of terminal methacrylated oligomers which involved the use of incompatible catalysts and solvents.¹⁴ Some of the compatibility issues of crosslinkers used were overcome by using bis-lactone crosslinkers.²⁰ These crosslinking agents were previously reported in crosslinking lactides, ϵ -caprolactone and dioxepanone monomers²¹⁻²⁴ and lately in crosslinking star polymers made of ϵ -caprolactone and DL-lactide using glycerol as initiator.^{1,25} One of the disadvantages in the polymers prepared from ϵ -caprolactone and lactides is that they will only be composed of hydrophobic segments that contribute to their long and slow bioabsorption and decreased biocompatibility. This made such polymers more susceptible to protein adsorption²⁶⁻²⁸ and fibrous tissue formation around the implant which eventually result in device failure.²⁹⁻³⁰ On the other hand, the acrylated UV crosslinked version of the same thermally crosslinked polymers involved the use of organic solvents like tetrahydrofuran and dichloromethane to incorporate the drug into the pre-crosslinked mass. This raises issues with regard to compatibility and even stability of loaded bioactive agents.³¹ Finally, the preparation steps involved in preparing the above described elastomers required high temperatures (120-140 °C) and took at least 3 or more days to obtain the final preparations.^{1,4,32}

Another approach to prepare elastomeric polymers was also reported through polycondensation reactions between di- and tri-carboxylic acids and diols which were further subjected to thermal or photocrosslinking process. Elastomers based on tartaric acid, citric acid and sebacic acid monomers and their copolymers were reported earlier.³³⁻³⁷ Some of these reported elastomers either required long curing times ranging from a few days to weeks to prepare, or the elastomers prepared were tough and brittle with some inconsistency in their final physical properties. In addition, high crosslinking

temperatures were needed for their crosslinking which restricted their use in drug delivery of thermally sensitive therapeutic agents. Recently, UV photocured elastomer prepared from acrylated poly(glycerol sebacate) was reported.³⁸⁻³⁹ The elastomer's mechanical properties demonstrated dependence on the degree of acrylation and the percentage of PEG diacrylate added. Although this elastomer demonstrated to be promising, the nonacrylated prepolymers used in its photocrosslinking required almost two days to prepare. In addition, the prepolymers possessed a high polydispersity index (≈ 3.5), therefore, the elastomer may demonstrate non-linear degradation profiles once long term degradation studies are conducted. There remains a need for biodegradable and biocompatible elastomeric polymers that can circumvent some of those aforementioned limitations.

Herein, we demonstrate the ability to rapidly form elastomeric structures from acrylated poly(diols-tricarballoylate) (PDT) using visible light crosslinking under ambient and solventless conditions. We selected tricarballoylic acid and the alkylene diol as building blocks for the construction of the new elastomers since tricarballoylic acid (propane-1, 2, 3-tricarboxylic acid) is one of the simplest classes of aliphatic acids; it is abundantly present in food products and possesses structure similarity to several biological active compounds such as citric acid and amino acid.⁴⁰ On the other hand, aliphatic diols are biocompatible intermediate compounds used in the synthesis of polymeric systems including polyesters elastomers, coatings, adhesives and polymeric plasticizers. Diols add many high-performance characteristics to the final structure of the elastomer such as hydrolytic stability, increased flexibility, improved adhesion, and surface hardness. We also explored the visible light photocrosslinking in the presence of camphorquinone (CQ) as a photoinitiator. We selected camphorquinone because of its cytocompatibility and history in biomedical visible light photopolymerization.⁴¹

The main objective of this work is therefore, to report on the synthesis and characterization of PDT photo-cured biodegradable elastomers. In addition, we report on the effect of varying the density of acrylate moieties in the matrix of the polymer as well as varying the polymer chain length on the mechanical properties and degradation behavior of the newly prepared elastomers.

3.2. EXPERIMENTAL

3.2.1. Materials

Tricarballic acid, 1,6-hexanediol, 1,8-octanediol, 1,10-decanediol, 1,12-dodecanediol, stannous 2-ethylhexanoate, 4-dimethylamino pyridine, acryloyl chloride, triethyl amine, sodium sulphate, triethanol amine, and camphor-quinone were purchased from the Aldrich-Sigma chemical company. Acetone and chloroform were purchased from the Caledone chemical company. All chemicals were analytical grade and used as received without any further purification.

3.2.2. Synthesis of Poly(diols-tricarballic) Prepolymers

PDT prepolymers were prepared by solvent-free step growth polymerization.³³ A representative synthesis process of poly(1,8 octane diol-co- tricarballic) is described here. Into a three-neck 250 ml round-bottom flask equipped with a condenser, a nitrogen inlet and a magnetic stirrer, was added 9.504 g of 1,8 octane diol (0.065 mole), 7.05 g of tricarballic acid (0.04 mole) in the presence of stannous 2-ethylhexanoate as a catalyst (1×10^{-4} mol). The mixture was heated to 140 °C under continuous stirring for 20 minutes. After that, the reaction was continued for 10 more minutes under vacuum to remove the formed water. The prepared crude prepolymer was then purified by dissolving in acetone and

precipitation in cold anhydrous ethyl ether. The prepolymer formed was then dried under vacuum overnight. The following PDT prepolymers were synthesized: poly(hexane diol-co- tricarballoylate) (PHT), poly(octane diol-co- tricarballoylate) (POT), poly(decane diol-co- tricarballoylate) (PDET) and poly(dodecane diol-co- tricarballoylate) (PDDT).

3.2.3. Acrylation of Prepolymer

Acrylation of the prepared PDT prepolymers was carried out by reacting acryloyl chloride (ACRL) with the terminal hydroxyl groups of the prepolymers in the presence of triethylamine (TEA) and, 4-dimethylaminopyridine which acted as a catalyst. One mole of ACRL was used to react with every one mole of OH in the prepolymers identified based on end group analysis. The following procedure describes the methodology to acrylate POT. Figure 3.1 shows a schematic representation of the synthesis process. Into a 250 ml round-bottom flask equipped with a magnetic stirrer, 10 g of POT prepolymer was dissolved in 60 ml of acetone to which 10 mg of 4-dimethyl aminopyridine (DMAP) was added as a catalyst. The flask was sealed, flushed with argon and then immersed in a 0 °C ice bath. A stepwise addition of 2.37 ml of ACRL (2.92 mmole) with 4.05 ml of TEA (equimolar amounts) to the prepolymer solution was carried out over a period of 12 hrs. The equivalent molar amount of TEA was used to scavenge the hydrochloric acid formed during the reaction. The reaction was continued at room temperature for another 12 hrs. The final solution was filtered to remove triethylamine hydrochloride salt formed during the acrylation reaction. The acrylated prepolymer solution was then dried at 45 °C under vacuum using a rotary evaporator and then dissolved in chloroform. Further purification was carried out by washing this chloroformic solution several times with deionized water and then drying it

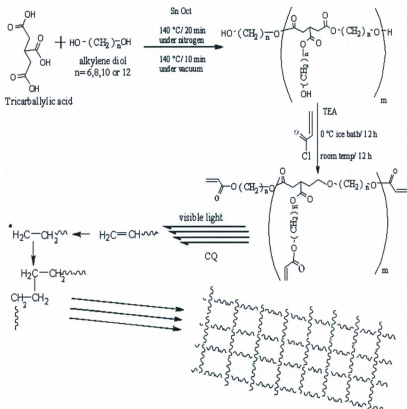


Figure 3.1. Schematic illustration of the synthesis, acrylation and photocuring of poly(diol-tricarballylate).

over anhydrous sodium sulphate. Chloroform was then evaporated at 45 °C under vacuum using a rotary evaporator and the acrylated prepolymer was left in the vacuum oven over night at room temperature for complete removal of solvents. The final purified product was then subjected to chemical and thermal analysis to confirm the chemical structure and the final product's purity and thermal properties. The acrylated PDDT prepolymers were prepared following the same procedure as described above but using varying reactant ratios that would achieve the preparation of prepolymers with 100%, 75% (PDDT_{0.75}) and 50% (PDDT_{0.5}) theoretical degrees of acrylation.

3.2.4. Photocuring of the Acrylated Prepolymers

The photocuring process was carried out in a dark fume hood equipped with a sodium lamp. On a watch glass, 5 µl of 10 % ethanolic solution of both camphorquinone and triethanolamine (equivalent to 0.01% (w/w) photoinitiator) was added to 5 grams of the acrylated prepolymer. The mixture was then left at 40 °C under vacuum for 4 hr to ensure complete removal of any traces of alcohol from the photoinitiator solutions. The dried mixture containing the acrylated prepolymer and the initiator was then poured into a Teflon mould using a spatula. The mould was then exposed to a visible light source (450-550 nm at a 40 mW/cm²) filtered from a 50 Watt tungsten-halogen lamp (Taewoo Co., Korea) for 10 minutes at a distance of 10 cm to form the elastomer which was then removed from the mould for further testing.

3.2.5. Chemical and Thermal Characterization

Fourier transform infrared (FT-IR) spectra of the prepared prepolymers, acrylated prepolymers and photocured elastomers were obtained at room temperature using a Bruker Tensor 27 infrared spectrometer equipped with a MIRacle attenuated total reflection accessory unit, over the wavelength range of 4000-400 cm^{-1} . The spectra were collected with a resolution of 4 cm^{-1} and a scan number of 32 using a mercury cadmium telluride (MCT) detector. Proton nuclear magnetic resonance ($^1\text{H-NMR}$) spectra for the octane tricarballlylate prepolymer and acrylated octane tricarballlylate prepolymer were recorded at room temperature on a Bruker Avance-500 MHz NMR spectrometer. The sample was dissolved in chloroform-*d* (CDCl_3 containing 0.1% (v/v) tetramethylsilane) in a 5 mm diameter NMR tubes. The chemical shifts in parts per million (ppm) for the $^1\text{H-NMR}$ spectra were referenced relative to tetramethylsilane (TMS, 0.00 PPM) as the internal reference. The signal intensity of the methylene groups of diols (1.3-1.7 ppm) and the acrylate groups' intensities (5.8-6.4 ppm) were used to calculate the degree of acrylation in the polymers. Molecular weights and molecular weight distributions were determined using a Waters gel permeation chromatography (GPC) system (Waters, Milford, CT) equipped with 410 Waters differential refractometer (RI Detector) and on-line multiangle laser light scattering (MALLS) detector (PD 2000 DLS, precision detectors, MA). The column configurations consisted of an HP guard column attached to a phenogel (2) linear 5μ column ($300 \times 7.8 \text{ mm}^2$). The mobile phase consisted of anhydrous tetrahydrofuran (THF) at a flow rate of 1 ml/min at 35 $^\circ\text{C}$. The sample concentration was 20 mg/ml and the injected volume was 75 μl . The absolute MWts determined by MALLS using a dn/dc value of 0.172 ml/g calculated from the RI detector response and assuming 100% mass recovery through the column. Data were collected and handled using Precision Acquire/Discovery software package. End group analysis was conducted to determine the hydroxyl

number of the prepared prepolymers by catalyzed acetylation.⁴² Briefly, in a 125 ml conical flask, 1 gram of the prepared prepolymer was dissolved in 1 ml acetone. Five milliliters of 2 % (w/v) 4-dimethylaminopyridine in pyridine followed by 2 ml of 25 % (v/v) acetic anhydride in pyridine, were transferred to the solution in the flask and mixed well. After 20 minutes, 25 ml of distilled water was added to the mixture followed by the addition of three drops of 1% phenolphthalein solution. The solution in the flask was then titrated against 0.5 N sodium hydroxide until the end point is reached indicated by pink color formation. A blank control experiment was also carried out following the exact procedure but without the addition of the prepolymers. The number of millimoles of hydroxyl group present in the prepolymer samples is given by $N(V_b - V_s)$, where V_b and V_s are the milliliters of sodium hydroxide solution of N normality required to titrate the blank and the prepolymer sample, respectively. The results of this end group analysis were compared with those estimated from weight average molecular weight analysis using GPC. The thermal properties of the polymers were characterized using Q200 differential scanning calorimeter (DSC) equipped with a liquid nitrogen cooling system. The measurements were carried out at a heating rate of 10 °C/ min. In order to provide the same thermal history, each sample was heated from room temperature to 150 °C and rapidly cooled down to -100 °C, then the DSC scan was recorded by heating from -100 to 150 °C.

3.2.6. Mechanical Properties and Sol Content Measurements

Tensile mechanical testing was conducted on an Instron model In-Spec 2200 tester with Merlin Data Management Software. The tensile tester was equipped with 500 N load cell. Dog-bone shaped samples of 30 mm in length, 3 mm in thickness, 5 mm in width at the narrow section and 15 mm in width at the gripping section were used for that purpose. The sample was pulled at a rate of 1.0 mm/sec and

elongated to failure. Five specimens of each elastomer were measured, and the mean and standard deviation were calculated. All specimens were tested at room temperature. Values were converted to stress-strain and plotted. Young's modulus was calculated from the initial slope of the stress-strain curve. The crosslink density (ρ_x) was calculated according to the theory of rubber elasticity following the equation: $\rho_x = E / 3RT$, where ρ_x represents the number of active network chain segments per unit volume (mole / m³), E represents Young's modulus in Pascal (Pa), R is the universal gas constant (8.3144 J/mol K) and T is the absolute temperature (K). Soxhlet extraction with dichloromethane as a solvent for 24 hours at 45 °C was used to determine the sol content of slab samples of the elastomers (20 x 20 x 3 mm³) with weight (W_1). Samples were then dried to constant weight in vacuum oven (W_2). These measurements were done in triplicate for each elastomer sample. The sol content was calculated from the equation: $S\% = [(W_1 - W_2) / W_1] \times 100$.

3.2.7. *In vitro* Degradation

Dog-bone-shaped samples of known weights (W_1), which were 30 mm in length, 3 mm in thickness and 5 mm and 15 mm in width at the narrow and gripping section, respectively, were placed in 40 ml vials each containing 35 ml of 0.1 M phosphate buffer saline (PBS) pH=7.4 and 0.01% of sodium azide. The vials were attached to a glass-coil's rugged culture rotator. The rotator was set at 20% rotation speed and placed in an oven at 37 °C for up to 12 weeks. The buffer was replaced daily to ensure a constant pH of 7.4. After 1, 2, 3, 4, 6, 8, 10 and 12 weeks, the swollen weight (W_2) and dried weight (W_3) were measured after wiping the surface water with filter paper and after vacuum-drying at 45 °C for 2 days, respectively. The water absorption & weight loss were calculated as follows:

$$\text{Weight loss \%} = [(W_1 - W_3) / W_1] \times 100.$$

$$\text{Water absorption \%} = [(W_2 - W_3) / W_3] \times 100.$$

The tensile properties of the degraded samples at these intervals were also measured. The results were reported as the mean and standard deviation of three measurements.

3.2.8. *In vitro* Cytocompatibility and Cell Proliferation

Murine fibroblast cell-line (AKR-2B) was grown in T-75 tissue culture treated flasks using Dulbecco's Modified Eagle Medium (DMEM; Invitrogen) supplemented with 10% (v/v) fetal bovine serum at 37 °C in a 5% CO₂/air atmosphere. Cells were plated in 24 well plates (Falcon), at a density of 40,000 cells/well, in 1 ml of medium and allowed to attach for 24 hours prior to the initiation of experiments. Photocured poly(diols-tricarballlylate) films were prepared by visible light polymerization on 22 mm cover-glasses. The film was then cut into pieces of approximately 100, 200 and 300 mg and sterilized by autoclaving. Film pieces of different mass were added directly into triplicate wells containing attached cells and incubated for 24 hrs at 37 °C. After 24 hrs phase contrast photomicrographs were taken using an inverted microscope (Diaphot, Nikon) equipped with digital camera (Coolpix4500, Nikon,). Cytotoxicity, expressed as relative cell density, was assessed spectrophotometrically using a modified neutral red dye staining assay.⁴³ Briefly, after 24 hrs incubation, elastomer pieces were removed and each well was washed twice with 500 µl of phosphate buffer saline (PBS). Following removal of wash buffer, 250 µl of 0.15 % (w/v) Neutral Red, in PBS, was added to each well and placed on an orbital bench top shaker for 30 min. Excess dye was removed with two washes of 500 µl PBS and cell associated dye solubilized with 250 µl of lysis buffer (50 % v/v ethanol in PBS) by shaking for 30 minutes. From each well 200 µl was transferred to a corresponding well of a 96-well plate and absorbance was read at $\lambda = 492$ nm in a Polarstar, Optima plate reader (BMG Scientific). The differences of cell density between the four different poly(diols-tricarballlylate) elastomeric films were compared to that of untreated cells. Results reported were the mean \pm SD from

three independent experiments each done in triplicate. Differences were evaluated with 2-way ANOVA using Graphpad Prism software.

3.3. RESULTS AND DISCUSSION

The goal of this research work was to prepare visible light photocrosslinked poly(diols-tricarballoylate) elastomers. As shown in Figure 1, the elastomers were prepared in three main steps. First, tricarballoylic acid was reacted with excess diol to produce low molecular weight prepolymers. To obtain low molecular weight prepolymers, the reaction was stopped after 30 minutes. The obtained prepolymers were colorless or clear light yellow viscous liquids. The second step involved the conversion of the terminal hydroxyl groups in the resulting prepolymer network into vinyl groups by an acrylation process. The obtained acrylated prepolymers were also colorless or clear light yellow viscous liquids. Both the acrylated and un-acrylated prepolymer did not dissolve in water but were soluble in most organic solvents. In the final stage, visible light photocrosslinking of the acrylated prepolymers was conducted which resulted in the formation of elastomeric crosslinked networks. The photocrosslinked elastomers were stretchable and rubbery and swelled but did not dissolve in organic solvents.

3.3.1. Chemical and Thermal Characterization

The molecular weights of the prepolymers as measured via GPC are listed in Table 3.1. As expected, the molecular weights of the prepared prepolymers increased upon increasing the number of methylene groups in the backbone of the used diol. The GPC analysis also showed that the prepared prepolymers demonstrated narrow distribution in molecular weights with polydispersity indices approaching unity

Table 3.1. Results of GPC and end group analysis of poly(diols-tricarballylate) prepolymers.

Pre-polymer	M_n (g/mol)	M_w (g/mol)	M_w/M_n	GPC estimated OH (mmol/g)	End group analysis OH (mmol/g)
PHT	667	694	1.04	2.89	2.70
POT	934	1131	1.21	2.67	2.90
PDET	1090	1366	1.25	2.80	2.90
PDDT	1332	1863	1.39	2.06	2.20

M_n : Number average molecular weight

M_w : weight average molecular weight.

(1.04-1.39). Also, the results of chemically determined millimoles of terminal hydroxyl groups which are listed in Table 3.1, were very close to those estimated from GPC analysis which indicated that the polymerization step proceeded as estimated. End group analysis for the prepared prepolymers was important to determine the number of hydroxyl groups available for further acrylation reaction (extent of acrylation) and to ensure that all the prepolymers reacted with the optimum amount of acryloyl chloride during the acrylation process. The POT purified prepolymer, acrylated prepolymer and elastomer were all characterized using FT-IR analysis. As shown in Figure 3.2, the IR spectrum of the purified POT prepolymer (Figure 3.2A) showed a broad absorption band at $3600\text{--}3400\text{ cm}^{-1}$ that was attributed to the hydroxyl stretching vibrations. The broadening in the band was attributed to the intermolecular hydrogen bond formation. The absorption bands at about 2930 cm^{-1} and 2857 cm^{-1} were attributed to C-H stretching vibrations of the methylene group. The carbonyl group of the formed ester appeared at about 1710 cm^{-1} . The bands from $1300\text{--}1000\text{ cm}^{-1}$ were attributed to C-O stretching vibrations. In the spectrum of the acrylated prepolymer (Figure 3.2 B), the disappearance of the broad OH band and the appearance of two new bands at around 1635 and 813 cm^{-1} was an evidence that the incorporation of the terminal acryloyl moieties was successfully achieved. The first band at 1635 cm^{-1} corresponds to the C=C bond stretching, while the band at 813 cm^{-1} corresponds to C=C bond twisting vibrations. These two bands are related only to the acrylated groups and known not to be present in the FT-IR of acryloyl chloride. The same two bands at 1635 and 813 cm^{-1} completely disappeared after photopolymerization took place (Figure 2 C). This was attributed to the crosslinking process which consumed the C=C terminal bonds in the free radical initiated reaction. As illustrated in Figure 3.1, a free radical was formed by the decomposition or oxidation of the photoinitiator in the presence of light. This free radical initiated abstraction of one hydrogen atom of the double bond -CH=CH_2 of the acryloyl moiety. The acrylated free radical then attacked a double bond in an adjacent polymer chain. Figures 3.3a and 3b

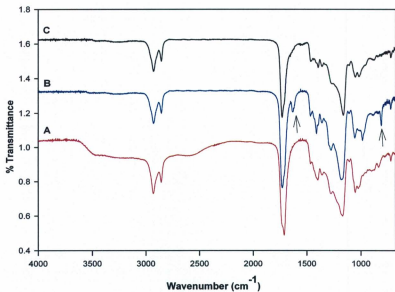


Figure 3.2. FTIR analysis of POT , A: before acrylation, B: after acrylation and C: after photocuring.



121

show the $^1\text{H-NMR}$ spectra of POT and the acrylated POT prepolymers respectively. The incorporation of the terminal acrylated groups was confirmed by the appearance of three peaks at 5.8, 6.1 and 6.4 ppm, which were attributed to the presence of vinyl group. The decrease in the integration of the overlapped peaks, which appeared at about 3.63 ppm, was due to the disappearance of the terminal OH proton.

The thermal behavior of the prepolymers, acrylated prepolymers and photocured elastomers are shown in Figure 3.4 and summarized in Table 3.2. The thermal analysis of the prepolymers showed that PHT and POT were both amorphous while PDET and PDDT were both crystalline. The reported crystallinity of the PDET and PDDT were calculated from the heat of fusion assuming proportionality to the experimental enthalpy. The reported enthalpy of fusion of 1,10 decanediol (249.6 J/g)⁴⁴ and 1.12 dodecanediol (234.8 J/g)⁴⁵ were respectively used as references for 100% crystalline PDET and PDDT. Following acrylation the T_g of PHT and POT increased. PDET became amorphous while the T_m and ΔH of PDDT decreased to 0 °C and 31 J/g, respectively. After photopolymerization all the crosslinked elastomers were amorphous with T_g 's below 37 °C which indicated that all elastomers were in a well rubbery state at body temperature. The thermal behavior of the prepolymers, acrylated prepolymers and photocured elastomers can be explained as follows: First, as the number of methylene groups in the polymer chain increased, the molecular weight also increased resulting in an increase in both the T_g and the degree of the polymer crystallinity. This is consistent with the fact that T_g and crystallinity for an aliphatic polyester increases with an increase in the number of methylene groups in their chain length.⁴⁶ Second, the incorporation of acryloyl group at the terminals of the prepolymers led to an increase in the T_g as well as a decrease in the crystallinity compared to those of the unacrylated prepolymers. This behavior has previously been observed for some polyester elastomeric networks.^{4,47} This change in T_g ranged from 11 to 6 °C for PHT and POT, respectively. It was also noted that the acrylation process

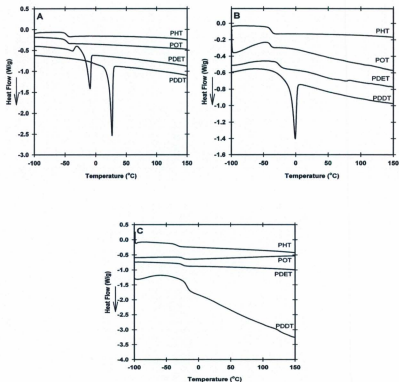


Figure 3.4. Differential Scanning Calorimetry thermograms of poly(diols-tricarballylate) (A) prepolymers, (B) acrylated prepolymers and (C) elastomers.

Table 3.2. Thermal properties of poly(diols-tricarballoylate) prepolymers, acrylated prepolymer and elastomers.

	Prepolymer				Acrylated prepolymer				Elastomer
	T _g (°C)	T _m (°C)	ΔH (J/g)	* % Crystal.	T _g (°C)	T _m (°C)	ΔH (J/g)	* % Crystal.	T _g (°C)
PHT	-49	-----	-----	-----	-38	-----	-----	-----	-32
POT	-46	-----	-----	-----	-40	-----	-----	-----	-25
PDET	-36	-9	32	12.8	-26	-----	-----	-----	-24
PDDT	-----	26	55	23.4	-----	0	31	13.2	-19

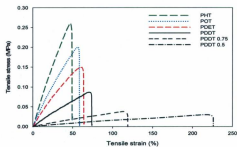
*Degree of crystallinity was calculated from the equation, $\Delta H/\Delta H^\circ \times 100$, where ΔH is the enthalpy change of the each compound and ΔH° is that of a single crystal of corresponding diol.

diminished the crystallinity of PDET and PDDT due to the fact that the acrylated domain's rigidity disrupted the regularity of the prepolymers and decreased the ability of the crystal lattice in the polymer from regularly arrange. Third, crosslinking resulted in additional increase in T_g and decrease in the crystallinity compared to those of the uncrosslinked acrylated prepolymers. In particular, crystal formation of acrylated PDDT was remarkably diminished by the photocrosslinking reaction, thus the PDDT networks became completely amorphous. This is also explained by the fact that crosslinking suppressed the mobility of molecular chain and prevented chain rearrangement as a result of which an obstruction of crystal formation took place.⁴⁸

3.3.2. Mechanical Properties and Sol Content Measurements

To determine the effect of chain length of the diol monomer and the degree of acrylation (DA) on the mechanical properties of the crosslinked elastomers, polymers listed in Table 3.3 were subjected to tensile testing. Figure 3.5a shows that tensile testing of the photocrosslinked PDT elastomers produced representative uniaxial tensile stress-strain curves which are characteristics of typical elastomeric materials. Average values for Young's modulus (E), ultimate tensile stress (σ), cross-linking density (ρ_x), and maximum strain (ϵ) are summarized in Table 3.3. The mechanical properties spanned from elastic to brittle depending on the diol used and the degree of elastomer acrylation. No permanent deformation was observed during the mechanical testing (Figure 3.5 b). The value of σ was as high as 0.25 MPa while the value of ϵ was as high as 238.28 %, under the synthesis condition. As reported in Table 3.3, PHT elastomer has the highest σ and E values. This was attributed to the fact that PHT possessed the lowest number of methylene groups in the chain of the diol used in the prepared prepolymers. As the diol chain length of the prepolymers decreased, the ρ_x of the polymer increased

a



b



Figure 3.5. (a) stress-strain curves of poly(diol-tricarballylate) elastomers. (b) POT elastomer shows 100% recovery after being stretched to break.

Table 3.3. Mechanical properties and sol content of poly(diols-tricarballoylate) elastomers.

Elastomer	σ (MPa)	ϵ (%)	E (MPa)	ρ_x (mole / m ³)	S (%)	DA* (%)	Description
PHT	0.25 ± 0.03	47.36 ± 1.39	0.65 ± 0.05	87.44 ± 6.72	9.36 ± 2.96	0.87	Hard, Brittle
POT	0.18 ± 0.02	53.30 ± 3.6	0.44 ± 0.025	59.19 ± 3.36	8.02 ± 3.11	0.86	Hard, Brittle
PDET	0.14 ± 0.02	61.23 ± 5.83	0.33 ± 0.023	44.39 ± 3.09	11.95 ± 5.69	0.91	Tough, Brittle
PDDT	0.072 ± 0.012	72.35 ± 6.4	0.11 ± 0.016	14.79 ± 2.15	10.42 ± 3.80	0.89	Tough, Elastic
PDDT _{0.75}	0.036 ± 0.002	121.2 ± 2.14	0.029 ± 0.001	3.9 ± 0.13	34.25 ± 9.17	0.59	Weak, Elastic
PDDT _{0.5}	0.029 ± 0.002	238.2 ± 6.11	0.012 ± 0.002	1.6 ± 0.26	59.06 ± 11.03	0.38	Very weak, Elastic

*estimated by NMR

which resulted in the formation of a crosslinked elastomer that is stiffer and less extensible. On the other hand, increase in the alkylene diol chain length decreased ρ_x and therefore, increased ε of the elastomer. Finally, it was also noted that the decrease in DA of PDDT prepolymer resulted in a decrease in the ρ_x which increased the elastomer stretchability and elasticity (Figure 3.5a). The sol content for the different PDT elastomers did not change appreciably as a function of the chain length of the prepolymers; however, it was affected by varying the DA. The sol content represents the mass difference after removal of the uncrosslinked prepolymer which is soluble in dichloromethane. As such, the decrease in the number of terminal acrylated groups in the prepolymers decreased the crosslinking during photocuring and increased the sol content in the prepared elastomer. Therefore, PDDT_{0.5} elastomer, with the lowest calculated degree of acrylation (0.38), possessed the highest sol content among all the prepared elastomers. Although stretchability will strongly improve as a result of increasing the sol content of PDDT elastomer, the relatively low sol content will help in maintaining the mechanical properties after implantation.

3.3.3. *In vitro* Degradation

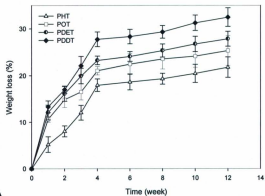
3.3.3.1. *Influence of chain length on in vitro degradation*

In order to examine the influence of chain length on the degradation rate and the changes in the mechanical properties of the elastomer during the *in vitro* degradation, four different PDT elastomers, based on varying chain lengths of alkylene diol were prepared and tested. Figure 3.6 shows the weight loss and water absorption data for the four prepared PDT elastomers. As can be seen, the water absorption and weight loss of the elastomers were directly proportional to the chain length of the

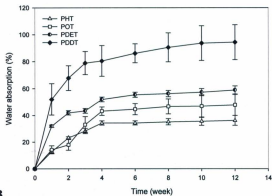
alkylene diol used and inversely proportional to the elastomers' ρ_x (Table 3.3). For example, at the end of the 12 weeks period, PHT elastomer, which had the lowest number of methylene groups in its chain and the highest ρ_x , demonstrated the lowest weight loss with minimal water uptake rate. Such findings were consistent with our previously reported results regarding the diffusion of water into the bulk of elastomeric polyesters at temperatures above their glass transition.¹ Also, the results are in accordance with the fact that water diffusion and mass loss are inversely proportional to the polymer's ρ_x .⁴⁹⁻⁵⁰

3.3.3.2. Degradation behavior

It is well known that surface erosion occurs when the elastomer's degradation rate is faster than the rate of water diffusion into the elastomer.^{51,52} Conversely, bulk erosion occurs if degradation and weight loss are correlated with the rate of water penetration into the bulk of the elastomers.^{51,52} As shown in Figure 3.6, all the elastomers exhibited a two-stage water absorption and weight loss behavior. In the first stage, which lasted up to 4 weeks, the water absorption and weight loss proceeded rapidly which resulted in the changes in elastomer's morphology (Figure 3.7). However, in the second stage, the water absorption and weight loss took place in a slower rate and exhibited little observable changes in the dimensions of the prepared elastomer (Figure 3.7 d). The degradation of PDT elastomers proceeded as follows: after the immersion of the elastomers in the phosphate buffers saline, water diffusion and absorption into the elastomer mass took place and resulted in the hydrolysis of the polymer chains. This process was not limited to the surface but mainly took place in the bulk of the elastomer. The first stage



A



B

Figure 3.6. Degradation results of poly(diols-tricarballoylate) elastomers in PBS at 37 °C. (a) percentage weight loss versus time. (b) percentage water absorption versus time. Error bars represent the standard deviation of the mean of measurements from three samples.

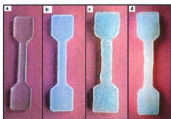


Figure 3.7. Images of the PDDT elastomers during *in vitro* degradation after: (a) 0, (b) 1, (c) 4, and (d) 12 weeks.

of degradation was also accelerated by the diffuse out of the hydrolysis products from the sol phase of the polymer which further contributed in the formation of oligo carboxylic acids within the polymer mass which auto-catalyzed the degradation rate further and increased the hydrophilic character of the polymer due to the formation of free -COOH and -OH moieties within the elastomer bulk. As such, the elastomers became more susceptible to water absorption and therefore swelling in the matrix and changes in elastomers from flat shape to a bloated convex shape occurred. In addition, the surface became smooth and translucent (Figure 3.7c) and further mass loss took place with water absorption. At the end of the first 4 weeks period, the rate of production of short chain fragments decreased significantly which resulted in a much lower internal pressure or driving force that enables those fragments to diffuse into the surrounding medium. As a result of that, the weight loss in the tested samples proceeded in a much slower fashion after the initial 4 weeks period. The above degradation behavior confirms that all matrices underwent bulk erosion similar to other previously reported polyesters.^{1,49,51}

3.3.3.3. Changes in the mechanical properties during *in vitro* degradation

Figure 3.8 shows the changes in the mechanical properties of the elastomers with respect to time during the *in vitro* hydrolytic degradation study. Although the elastomers showed a decrease in their mechanical strength with time, they maintained their shape and extensibility over the testing period. Both E and σ decreased in a linear fashion with time as indicative of zero-order degradation mechanism. This linear decrease was observed regardless of the network composition, the crosslinking density and the initial E and σ of the elastomers. Figure 3.8 C shows that the change in ϵ was less sensitive to the degradation of those elastomers. No significant change in ϵ was found up to 12 weeks of the *in vitro*

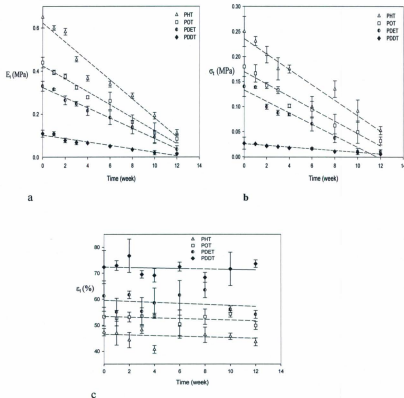


Figure 3.8. Change in tensile properties of the elastomers during degradation in PBS at 37°C. (a) Young's modulus, (b) ultimate stress and (c) ultimate strain, lines are fitted curves to equation (1) and (2). Error bars represent the standard deviation of the mean of measurements from three samples.

degradation time. These results confirmed that the hydrolytic degradation of these elastomers followed a bulk erosion mechanism, resembling the behavior of biodegradable polyesters reported previously.⁴⁹ It is only with surface erosion degradation pattern that the elastomers can maintain their mechanical properties unchanged⁵³. Additionally, Figures 8a and b, show that E and σ for all the elastomers linearly decreased with time.

Through a linear regression of the zero-order degradation kinetics of the data in Figure 3.8 a and b using equations (1) & (2), the rate constants were calculated and are listed in Table 3.4.

$$E_t = E_0 - K_E t. \quad (1)$$

$$\sigma_t = \sigma_0 - K_\sigma t. \quad (2)$$

In equations 1 and 2, t denoted the immersion time (in weeks) in PBS. The values of E_0 and σ_0 corresponded to the intercepts obtained from extrapolating the zero-order fitted line. K_E and K_σ represented the zero-order degradation constants for Young's modulus and the ultimate tensile stress, respectively. The decrease in the alkylene diol chain length in the elastomer was accompanied by an increase in K_E and K_σ . As seen, the K_E and K_σ for PHT were 0.0441 and 0.0154 MPa/week, respectively, while K_E and K_σ for PDDT were 0.0080 and 0.0018 MPa/week, respectively. We previously reported that Young's modulus of the elastomers depended mainly on the crosslinking density and the ultimate tensile stress depended on the distribution of end to end distances between crosslink points within the matrix.^{1,49} As well, it is well known that degradation occurred by the hydrolysis of the ester bond in the end to end distance between crosslinks. As such, lower molecular weight PDT elastomers demonstrated faster decline in their mechanical strength compared to higher molecular weight PDT elastomers. Furthermore, it was previously reported that the mechanical parameters decrease in a much faster rate as the molecular weight between cross-links decreases.⁴⁹ By the end of the 12 weeks study period in PBS,

Table 3.4. The linear regression coefficients values for PDT elastomers during *in vitro* degradation in PBS (pH 7.4).

Elastomer	E_0 (MPa)	K_E (MPa/week)	σ_0 (MPa)	K_σ (MPa/week)
PHT	0.6237	0.0441	0.2359	0.0154
POT	0.4244	0.0301	0.1697	0.0124
PDET	0.3239	0.0237	0.1331	0.0114
PDDT	0.1026	0.0080	0.0261	0.0018

the degradation study was stopped. At that stage, the elastomers maintained their original shape and did not degrade completely.

3.3.4. *In vitro* Cytocompatibility with Fibroblast Cell

In order to determine if there was a dose dependant effect of the elastomer on cytotoxicity we treated fibroblasts were treated with three different masses of PDT elastomers (100, 200 and 300 mg), for 24 hrs. After 24 hrs of culturing, all wells incubated with elastomer were examined and results indicated growth and morphology as an objective measure of cytotoxicity of each formulation of PDT elastomer. The density of treated cells was measured and compared to that of control cells, arbitrarily set at 100% (Figure 3.10). The relative cell density/well of 100 mg was found to range from 101 % \pm 7% (PHT) to 97 % \pm 5% (PDDT), demonstrating 100 mg of all elastomer formulations is biocompatible and exhibited no adverse effect on cell viability. The elastomer pieces weighing greater than 100 mg exhibited only slightly lower cell densities, with 200 mg and 300 mg samples of the four different elastomers on fibroblast cell viability. The relative densities shown with 200 mg ranged from 95 % \pm 4% (PHT) to 91.4 % \pm 4% (PDDT). For 300 mg, the same trend in cell density was found ranging from 97.6 % \pm 4% (PHT) to 91.4 % \pm 8% (PDDT). However, there was no statistical significance found between the cell densities of control or any of the elastomer treatments independent of the mass of elastomer used. The small differences in cell density between samples of different mass may be related to the fact that a larger piece of elastomer was placed in each well potentially scraping different amount of cells from the well as it settled to the bottom. In all, these results show that PDT is cytocompatible and could function as biomaterial for controlled drug delivery and for tissue engineering applications without causing adverse cellular effects.



(A) POT



(B) Polystyrene plate (control).

Figure 3.9. Phase contrast images of human fibroblasts cells with POT elastomeric films and polystyrene plate control after 24 hr of culturing.

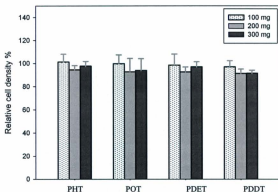


Figure 3.10. Human fibroblasts cell density after 24 hr incubation with different weight of different PDT elastomeric films, relative to control polystyrene plate.

The PDT elastomers studied were found to possess a few advantages which possibly make them good candidates for controlled drug delivery applications. First, the polymers are degradable by bulk hydrolysis of the ester bonds and none of their building blocks are toxic. Second, altering the chain length of the alkylenediol can vary the hydrophilic and hydrophobic properties of the elastomers. Thus, the elastomers can be tailored to satisfy a particular purpose. Additionally, all the prepared elastomers were amorphous with glass transition temperatures below physiological body temperature, so they are suitable as elastomeric implants *in vivo*. Moreover, PDT elastomers used visible light in their crosslinking, avoiding some of the drawbacks associated with using UV photocuring.⁵⁴ The polymerization conditions were also sufficiently mild to be carried out in the presence of other biological materials. (e.g., for encapsulation of cells and proteins, in drug screening, or in biosensing applications). Additionally, visible light penetrates deeper through tissues than UV light (less scattering and less absorption). This property may limit the need for invasive surgical procedures by allowing trans-tissue polymerizations, whereby the material is injected subcutaneously or even subdermally and irradiated through the skin to polymerize the material *in situ*.

3.4. CONCLUSIONS

This study demonstrated the preparation of a new family of elastomeric thermoset biomaterials which are crosslinked at room temperature using visible light photopolymerization technique. It was also shown that the physical properties of these elastomers can be controlled through manipulations of the chain length of the used diol and the degree of polymer acrylation. All the obtained elastomers were rubbery and their mechanical properties ranged from hard brittle to very weak and elastic and their Young's modulus, the ultimate tensile strength and % strain depended on the degree of acrylation and the length of the diol chain used. As well, the sol content of the prepared elastomers significantly

depended on the degree of acrylation. Additionally, the *in vitro* degradation of poly(diols-tricarballoylate) elastomers was determined. All the elastomers underwent bulk erosion similar to that of the previously investigated biodegradable polyester elastomers. A linear decrease was observed in the Young's modulus and the ultimate stress with time that was also accompanied with an increase in water absorption and weight loss. The PDT networks degraded relatively slowly after a period of 12 weeks with no appreciable dimension changes. The exploration of visible light crosslinking, the solventless preparation process, and the controllable mechanical properties of these biodegradable polymers make them excellent candidates for use in controlled drug delivery, particularly for thermosensitive therapeutic proteins and peptides. Solid particles of such drugs can be mixed with the pure acrylated prepolymers which are then rapidly crosslinked using visible light at room temperature to be formulated as drug delivery systems (implants or microspheres) that will undergo biodegradation in the body.

3.5. REFERENCES

- 1- Younes HM, Bravo-Grimaldo E, Amsden BG. 2004. Synthesis, characterization and *in vitro* degradation of a biodegradable elastomer. *Biomaterials* 25: 5261-5269.
- 2- Yang J, Webb AR, Pickerill SJ, Hageman G, Ameer GA. 2006. Synthesis and evaluation of poly(diols citrate) biodegradable elastomers. *Biomaterials* 27:1889-1898.
- 3- Guan J, Stankus JJ, Wagner WR. 2007. Biodegradable elastomeric scaffolds with basic fibroblast growth factor release. *J Control Release* 120:70-78.
- 4- Amsden BG, Misra G, Gu F, Younes HM. 2004. Synthesis and characterization of a photocross-linked biodegradable elastomer. *Biomacromolecules* 5:2479-2486.
- 5- Gu F, Younes HM, El-Kadi AO, Neufeld RJ, Amsden BG. 2005. Sustained interferon-gamma delivery from a photocrosslinked biodegradable elastomer. *J Control Release* 102:607-617.
- 6- Gu F, Neufeld R, Amsden B. 2007. Sustained release of bioactive therapeutic proteins from a biodegradable elastomeric device. *J Control Release* 117:80-89.
- 7- Folkman J, Long DM. 1964. The use of silicone rubber as a carrier for prolonged drug therapy. *J Surg Res* 4:139-142.

- 8- Pitt CG, Gratzl MM, Jeffcoat AR, Zweidinger R, Schindler A. 1979. Sustained drug delivery systems II: Factors affecting release rates from poly(epsilon-caprolactone) and related biodegradable polyesters. *J Pharm Sci* 68:1534-1538.
- 9- Wada R, Hyon SH, Nakamura T, Ikada Y. 1991. *In vitro* evaluation of sustained drug release from biodegradable elastomer. *Pharm Res* 8:1292-1296.
- 10- Hiljanen-Vainio M, Karjalainen T, Seppala J. 1996. *In vitro* evaluation of sustained drug release from biodegradable elastomer. *J Appl Polym Sci* 59:1281-1288.
- 11- Schindler A, Hibionada YM, Pitt CG. 1982. Aliphatic Polyesters. III. Molecular Weight and Molecular Weight Distribution in Alcohol-Initiated Polymerizations of epsilon-Caprolactone. *J Polym Sci Part A: Polym Chem* 20: 319-326.
- 12- Nijenhuis AJ, Grijpma DW, Pennings A. 1996. Crosslinked poly(L-lactide) and poly(epsilon-caprolactone). *J Polymer* 37: 2783-2791.
- 13- Storey RF, Hickey TP. 1994. Degradable polyurethane networks based on D,L-lactide, glycolide, epsilon -caprolactone, and trimethylene carbonate homopolyester and copolyester triols. *Polymer* 35: 830-838.
- 14- Storey RF, Warren SC, Allison CJ, Puckett AD. 1997. Methacrylate-encapped poly(d,l-lactide-co-trimethylene carbonate) oligomers. Network formation by thermal free-radical curing. *Polymer* 38: 6295-6301.
- 15- Hiljanen-Vainio MP, Orava PA, Seppala JV. 1997. Properties of epsilon-caprolactone/DL-lactide (epsilon-CL/DL-LA) copolymers with a minor epsilon-CL content. *J Biomed Mater Res* 34: 39-46.
- 16- Joziasse CAP, Veenstra H, Top MDC, Grijpma DW, Pennings AJ. 1998. Rubber toughened linear and star-shaped poly(d,l-lactide-co-glycolide): Synthesis, properties and *in vitro* degradation. *Polymer* 39:467-473.
- 17- Kim SH, Han YK, Kim YH, Hong SI. 1992. Multifunctional initiation of lactide polymerization by stannous octoate/pentaerythritol. *Macromol Chem Phys* 193: 1623-1631.
- 18- Lang M, Wong RP, Chu CC. 2002. Synthesis and structural analysis of functionalized poly(epsilon-caprolactone)-based three-arm star polymers. *J Polym Sci Part A: Polym Chem* 40: 1127-1141.
- 19- Bruin P, Veenstra GJ, Nijenhuis AJ, Pennings AJ. 1988. Design and synthesis of biodegradable poly(ester-urethane) elastomer networks composed of non-toxic building blocks. *Macromol Chem Rapid Commun* 9: 589-594.

- 20- Starcher PS. 1963. Bis-epsilon-caprolactone. US Patent 3,072,680.
- 21- Andronova N, Srivastava RK, Albertsson AC. 2005. Potential tissue implants from the networks based on 1,5-dioxepan-2-one and epsilon-caprolactone. *Polymer* 46: 6746-6755.
- 22- Pitt CG, Schindler A. 1983. Biodegradable polymers of lactones. US Patent 4379138.
- 23- Schindler A, Pitt CG. 1982. Biodegradable Elastomeric Polyesters. *Polym Prepr (Am Chem Soc Div Polym Chem)* 23:111-112.
- 24- Palmgren R, Karlsson S, Albertsson AC. 1997. Synthesis of degradable crosslinked polymers based on 1,5-dioxepan-2-one and crosslinker of bis-epsilon-caprolactone type. *J Polym Sci Part A: Polym Chem* 35: 1635-1649.
- 25- Amsden BG. 2006. Biodegradable elastomers and methods of preparing same. US Patent 20030105245.
- 26- Jonsson M, Johansson HO. 2004. Effect of surface grafted polymers on the adsorption of different model proteins. *Colloids Surf B: Biointerfaces* 37: 71-81.
- 27- Leiva A, Gargallo L, Radic D. 2004. Interfacial properties of poly(caprolactone) and derivatives. *J Macromol Sc Part A: Pure Appl Chem* 41: 577-583.
- 28- Satulovsky J, Carignano MA, Szeleifer I. 2000. Kinetic and thermodynamic control of protein adsorption. *Proc Natl Acad Sci USA* 97: 9037-9041.
- 29- Wildemore JK, Jones DH. 2006. Persistent Granulomatous Inflammatory Response Induced by Injectable Poly-L-lactic Acid for HIV Lipatrophy. *Dermatol Surg* 32: 1407-1409.
- 30- Zegzula HD, Buck DC, Brekke J, Wozney JM, Hollinger JO. 1997. Bone formation with use of rhBMP-2 (recombinant human bone morphogenetic protein-2). *J Bone Joint Surg Am* 79: 1778-1790.
- 31- Younes HM. 2003. New biodegradable elastomers for interferon-gamma delivery. University of Alberta. Doctorate Thesis.
- 32- Takao A, Fusae M, Yu N. Preparation of cross-linked aliphatic polyester and application to thermo-responsive material. *J Control Release* 1994;32:87-96.
- 33- Borzacchiello A, Ambrosio L, Nicolais L, Huang SJ. 2000. Synthesis and characterization of saturated and unsaturated poly(alkylene tartrate)s and further cross-linking. *J Bioact Compat Pol* 15: 60-71.
- 34- Wang Y, Ameer GA, Sheppard BJ, Langer R. 2002. A tough biodegradable elastomer. *Nat Biotechnol* 20: 602-606.

- 35- Yang J, Webb A, Ameer GA. 2004. Novel Citric Acid-Based Biodegradable Elastomers for Tissue Engineering. *Adv Mater* 16: 511-516.
- 36- Lei L, Ding T, Shi R, Liu Q, Zhang L, Chen D, Tian W. 2007. Synthesis, characterization and *in vitro* degradation of a novel degradable poly((1,2-propanediol-sebacate)-citrate) bioelastomer. *Polym Degr and Stab* 92: 389-396.
- 37- Bruggeman JP, de Bruin BJ, Bettinger CJ, Langer R. 2008. Biodegradable Poly(polyol sebacate) Polymers. *Biomaterials* 29: 4726-4725.
- 38- Nijst CL, Bruggeman JP, Karp JM, Ferreira L, Zumbuehl A, Bettinger CJ, Langer R. 2007. Development of Multifunctional Photocurable Degradable Elastomers *Biomacromolecules* 8: 3067-3073.
- 39- J. L. Ifkovits, R. F. Padera and J. A. Burdick, 2008. Biodegradable and radically polymerized elastomers with enhanced processing capabilities. *Biomed Mater* 3:034104.
- 40- Abdel-Sattar S, Elgazwy H. 2004. The chemistry of tricarballic acid. *Current organic chemistry* 8: 1405-1423.
- 41- Bryant SJ, Nuttelman CR, Anseth KS. 2000. Cytocompatibility of UV and visible light photoinitiating systems on cultured NIH/3T3 fibroblasts *in vitro*. *J Biomater Sci Polym Ed* 11: 439-457.
- 42- Connors KA, Albert KS. 1973. Determination of hydroxy compounds by 4-dimethylaminopyridine-catalyzed acetylation. *J Pharm Sci* 62: 845-846.
- 43- Borenfreund E, Puerner JA. 1984. A simple quantitative procedure using monolayer culture for toxicity assays. *J Tissue Cult Method* 9: 7-9.
- 44- Li L, Zhi-cheng T, Shuang-He M, Yong-Ji S. 1999. A thermochemical Study of 1,10-decanediol. *Thermochimica Acta* 342: 53-57.
- 45- Van Krevelen DW. 1990. Properties of polymers, 3rd ed. Amsterdam: Elsevier Academic press, p118.
- 46- Hill R, Walker EE. 1948. Polymer constitution and fiber properties. *J Polym Sci* 3: 609-630.
- 47- Aoyagi T, Miyata F, Nagase Y. 1994. Preparation of cross-linked aliphatic polyester and application in thermo-responsive material. *J Control Release* 32: 87-96.
- 48- Miyasako H, Yamamoto K, Nakao A, Aoyagi T. 2007. Preparation of cross-linked poly[(epsilon-caprolactone)-co-lactide] and biocompatibility studies for tissue engineering materials. *Macromol Biosci* 7: 76-83.

- 49- Shen JY, Pan XY, Lim CH, Chan-Park MB, Zhu X, Beuerman RW. 2007. Synthesis, characterization, and *in vitro* degradation of a biodegradable photo-cross-linked film from liquid poly(epsilon-caprolactone-co-lactide-co-glycolide) diacrylate. *Biomacromolecules* 8: 376-385.
- 50- Nijst CL, Bruggeman JP, Karp JM, Ferreira L, Zumbuehl A, Bettinger CJ, Langer R. 2007. Synthesis and characterization of photocurable elastomers from poly(glycerol-co-sebacate). *Biomacromolecules* 8: 3067-3073.
- 51- Tamada JA, Langer R. 1993 Erosion kinetics of hydrolytically degradable polymers. *Proc Natl Acad Sci USA* 90: 552-556.
- 52- Von BF, Schedl L, Gopferich A. 2002. Why degradable polymers undergo surface erosion or bulk erosion. *Biomaterials* 23: 4221-4231.
- 53- Burdick JA, Philpott LM, Anseth KS. 2001. Synthesis and characterization of tetrafunctional lactic acid oligomers: A potential *in situ* forming degradable orthopaedic biomaterial. *J Polym Sci Part A: Polym Chem* 39: 683-692.
- 54- Vile GF, Tyrrell RM. 1995. UVA radiation-induced oxidative damage to lipids and proteins *in vitro* and in human skin fibroblasts is dependent on iron and singlet oxygen. *Free Radic Biol Med* 18: 721-730.

CHAPTER 4

Osmotic-Driven Release of Papaverine Hydrochloride from Novel Biodegradable Poly(decane-co-tricarballylate) Elastomeric Matrices

The content of this chapter was published in the Journal of Therapeutic Delivery 1, 1, 37-50 (2010).

Mohamed A. Shaker and Husam M. Younes

ABSTRACT

We have recently reported on the synthesis, characterization and biocompatibility of a novel family of visible-light photocrosslinked poly(diols-co-tricarballate) elastomers intended for use in drug delivery and tissue engineering applications. In this work, the osmotic-driven-controlled release of the water soluble drug, papaverine hydrochloride, from poly(decane-co-tricarballate) elastomeric cylindrical monoliths is reported. We also examined the influence of various parameters such as the degree of prepolymer acrylation, crosslinking density, and the incorporation of osmotic excipients like trehalose on the release kinetics of the drug. The release rate of papaverine hydrochloride was found to decrease in dissolution media of higher osmotic activity as an indication of the predominant involvement of the osmotic-driven release mechanism from the elastomeric devices. The drug release rate was also found to be dependent on the degree of macromer acrylation. Furthermore, it was found that co-formulating papaverine hydrochloride with trehalose increases the release rate without altering the linear nature of the drug release kinetics. A new delivery vehicle composed of biodegradable poly(decane-co-tricarballate) elastomers demonstrated to be a promising and effective matrix for linear, constant and controllable osmotic-driven release of drugs.

4.1. INTRODUCTION

The development and use of biodegradable polymers with elastomeric properties in tissue engineering¹⁻³ and implantable drug delivery⁴⁻⁶ have recently gained considerable attention in the biomedical and pharmaceutical fields. Elastomers can be regarded as one of the best biomaterials for such applications as they can offer many advantages over the other fabricated tough materials. Their mechanical properties can be manipulated in a manner that makes them as soft as body tissues. They have the ability to recover and withstand the mechanical challenges upon implantation in a mobile part of the body,⁷ and they are also proven to be well suited for controlled drug delivery applications.^{4,5} Therapeutically, elastomers utilized in controlled delivery of drugs such as paclitaxel,⁸ dexamethasone,⁹ levonorgestrel¹⁰ and colindine hydrochloride¹¹ have been extensively investigated for use in many clinical applications which include but are not restricted to cancer therapy, hormonal contraception and inflammation therapy.⁸⁻¹¹

One strategy of controlling the release of water soluble drugs and therapeutic proteins (e.g., interferons, interleukins and growth factors) from implantable elastomeric monoliths is achieved by dispersing the active drug mixed with osmotic excipients and relying on the osmotic rupture as the predominant mechanism for achieving constant zero-order release.⁴ Osmotically-driven delivery of water soluble drugs from elastomeric polymers has been the focus of many previous studies.¹²⁻¹⁸ Several reports have investigated the different drug and elastomer physicochemical and mechanical factors that affect the rate and mode of release from those systems.¹²⁻¹⁵ Others have focused on the development of different mathematical models that describe the release profiles from such systems.^{16,17}

The generally accepted view of drug release from an elastomeric monolith is as follows: When the volumetric loadings of the drug are below a critical volume fraction called the percolation threshold (30-35 % v/v), the drug particles will not be appreciably interconnected to each other. The drug particles located on the surface dissolve and produce an initial burst effect, accounting for 5 to 15% of the initially loaded drug, followed by a slow release period. This slow release depends on the rate of degradation of the polymer when the polymer is degradable and/or the rate of formation of cracks and interconnected pores resulting from water imbibition into the polymer. The rate of this water imbibition is proportional to the porosity of the polymer and the osmotic activity of the loaded drug.¹⁹ When the elastomer degradation rate is slow enough to maintain the implant's geometry and mechanical properties (extension ratio) during the release period, the osmotic-driven mechanism will dominate the linear controlled-release and polymer degradation will play only a minor role in the overall release pattern.⁴

A description for the release of drugs via an osmotic mechanism is illustrated in Figure 4.1. As shown in the figure, the drug release by osmotic rupture starts by the diffusion of water vapor through the polymer to the first layer of drug particles. The saturated drug solution formed creates an osmotic gradient that drags more water into the drug compartment, exerting a pressure which acts radially outward causing it to swell. If the generated osmotic pressure was high enough to exceed the inward resisting pressure caused by the polymer elasticity, the drug compartment will rupture, releasing its contents upon relaxation of the elastomer to the outside medium through the generated microcracks. The same process is repeated for the following layers of dispersed drug particles (i.e., in a serial fashion) towards the center of the device, creating a network of microcracks that leads to the external medium.

Traditionally, osmotic-driven controlled release offer distinct and practical advantages over other means of delivery. First, the drug release is essentially constant as long as the osmotic gradient remains

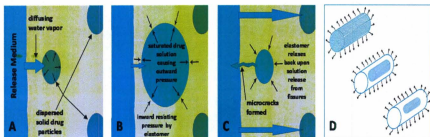


Figure 4.1. Schematic representation of osmotic swelling, rupture and release mechanism. **(A)** Water vapor diffuses to the inside of the elastomer. **(B)** The water dissolves the solid drug and exert osmotic pressure on the inside wall. **(C)** The pressure causes micro-cracks in the elastomer and the drug content is then released upon polymer relaxation. **(D)** The process occurs in a serial fashion towards the center of the cylinder as each cross-sectional layer of compartments rupture.

constant, and typically gives a zero-order release profile with a high degree of *in vitro* and *in vivo* correlation.^{12,15} Second, the release pattern is well characterized and understood and may be delayed or pulsed if desired.¹³ Finally, the rationale for this approach is that the presence of water in the external release environment is relatively constant, at least in terms of the amount required for initiation and controlling osmotically base theory.

In our recent study on the preparation of a polymeric carrier for proteins and peptides, we succeeded in preparing and characterizing a novel family of visible light photocrosslinked poly(diols-co-tricarbalylate) elastomers.^{20,21} These newly synthesized elastomers offer many advantages over other previously reported polymers. First, they are amorphous thermoset polymers that degrade by bulk and surface erosion, which often results in the retention of their three dimensional structure throughout the hydrolytic period. Second, altering the chain length of the alkylene diol used in their preparation can vary the hydrophilic and hydrophobic properties of the elastomers. Thus, these elastomers can be tailored to satisfy a particular application and need. Third, drugs can be dispersed into the prepolymer in a solventless manner and further photocrosslinked using visible light at temperatures near the physiological range. Thus, it would avoid many of the drawbacks associated with using organic solvents and UV photocrosslinking upon dealing with biologically thermo-sensitive therapeutics like proteins and other heat-sensitive drugs.^{20,21} Finally, the curing process proceeds rapidly, on the order of minutes.

The purpose of the present study, therefore, is to demonstrate the osmotic-driven release from these newly synthesized photo-cured biodegradable elastomers. Poly(decane-co-tricarbalylate) (PDET) was used as a representative for this new family of biodegradable elastomers. We also chose papaverine hydrochloride (PH) as a model for a drug with a reasonably moderate osmotic activity, reasonable water solubility (1g in 30 ml), and good candidacy for extended-release delivery. PH is a pharmacologically

potent vasodilating agent that is used for the treatment and prevention of symptomatic cerebral vasospasm after hemorrhage caused by aneurysm rupture.²² Since PH therapeutic effects are very short-lived, it is typically administered by continuous systemic or localized infusion (intra-arterial, intravenous, intrathecal or intracisternal). This delivery mode has its inherent technical problems, involves risks of infection and usually results in severe PH side effects and toxicity.²³ As such, developing a prolonged-release elastomeric device that can be implanted intracranially at the time of surgery for aneurysm clipping is expected to prevent vasospasm significantly, while maintaining an appropriate safe and effective concentration of papaverine in the cistern.²⁴

4.2. EXPERIMENTAL

4.2.1. Materials

Tricarballic acid, 1,10-decanediol, stannous 2-ethylhexanoate, 4-dimethylamino pyridine, acryloyl chloride, triethyl amine, sodium sulphate, amaranth trisodium, triethanol amine, champhore-quinone, and papaverine HCl were purchased from Aldrich-Sigma chemical company (Canada). Acetone and chloroform were purchased from Caledone chemical company (Canada). The osmolality standards of 100, 290 and 1000 mmol/kg were all purchased from Wescor Company. All chemicals were used as received without any further purification.

4.2.2. Synthesis and Characterization of Acrylated Poly(decane-co-tricarballylate) Prepolymer

Acrylated PDET was synthesized according to the previously described method in chapter 3 (section 3.2.2.) which is illustrated in Figure 4.2 A.²¹

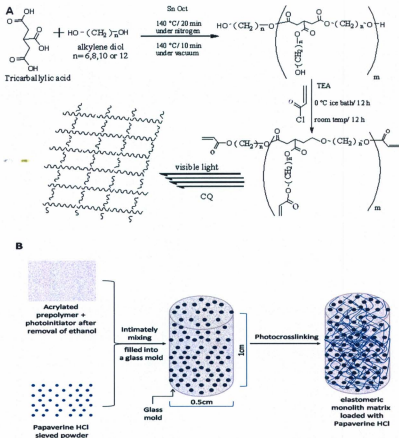


Figure 4.2. Schematic illustration of the synthesis, acrylation and photocuring of poly(decane-tricarballylate). (A) The step-reaction polymerization of tricarballic acid and decane diol was catalyzed by stannous 2-ethylhexanoate. The acrylation was carried out using acryloyl chloride in the presence of triethylamine. To photo-crosslink, acrylated prepolymer was mixed with camphorquinone (the photoinitiator) and crosslinked under visible light (40mW/cm²). (B) Schematic representation of the method of preparing PH loaded elastomeric cylindrical monoliths.

The final purified product was characterized using proton nuclear magnetic resonance ($^1\text{H-NMR}$) to confirm the final product's purity. The signal intensity of the methylene groups of diol (1.3-1.7 ppm) and the acrylate groups' intensities (5.8-6.4 ppm) were used to calculate the degree of acrylation in the prepolymers.²¹

4.2.3. Elastomeric Matrices Preparation and Characterization

The photocuring process was carried out in a dark fume hood equipped with a sodium lamp. On a watch glass, 5 μl of 10 % ethanolic solution of both camphorquinone and triethanolamine (equivalent to 0.01% (w/w)) photoinitiator was added to 5 grams of the acrylated prepolymer. The mix was then left at 40 °C under vacuum for 1 hr to ensure complete removal of any traces of alcohol from the photoinitiator solutions. The mix was then poured into the bottom of a sealed cylindrical silanized glass mould of 1 cm in length and 0.5 cm in diameter. The mould was then exposed to a visible-light source (450-550 nm at a 40 mW/cm^2) filtered from a 50 Watt tungsten-halogen lamp (Taewoo Co., Korea) for 10 minutes at a distance of 10 cm to form the elastomer which was then removed from the mould for further testing. The tensile mechanical properties of elastomeric cylinders (1.5 cm in length and 0.5 cm in diameter) were tested using an Instron model In-Spec 2200 tester equipped with 500 N load cells and run by Merlin Data Management Software. The sample was pulled at a rate of 1.0 mm/sec and elongated to failure. Values were converted to stress-strain and plotted. Young's modulus was calculated from the initial slope of the stress-strain curve. Finally, the obtained elastomers were subjected to solid-state carbon 13 nuclear magnetic resonance ($^{13}\text{C-NMR}$) to confirm full crosslinking of the acrylated moieties and complete consumption of the C=C terminal bonds in the free radical photoinitiated reaction.

4.2.4. Fabrication of PH loaded Elastomeric Cylinders

As illustrated in Figure 4.2 B, PH was first ground into fine powder using a glass mortar and a pestle and then sieved through a 45 μm mesh using CSC sieve shaker. The sieved powder was then intimately mixed with the acrylated PDET prepolymer to achieve a total of 10% v/v loading of the drug. The resulting mixture was photocrosslinked in a cylindrical glass mould of 1 cm in length and 0.5 cm in diameter under the procedure described above. Each prepared drug-loaded cylinder was weighed and the amount of PH in each was calculated. The final loading of PH in each cylinder was found to be equivalent to 14.5 ± 0.5 mg.

When a mixture of PH and TH was used to load the cylinder, both were co-lyophilized to obtain an intimately mixed powder which was further passed through a 45 μm mesh size sieve to obtain the final micronized mixture. A 10% v/v volumetric loading of the lyophilized mixture was also used in all of the prepared cylinders. The total loaded amount of PH was equivalent to 6.5 ± 0.1 mg and 4.5 ± 0.2 mg in the 1:1 and 1:2 PH to TH weight ratio loaded cylinders, respectively.

A similar procedure was followed in loading PDET₁₀₀ elastomeric cylinders with 10% v/v amaranth trisodium (AT) powder. A mixture of AT and TH (weight ratio 1:2 AT/TH) was co-lyophilized and further passed through a 45 μm mesh size sieve to obtain the final micronized mixture.

4.2.5. Osmotic Activity Measurements

The osmolality of 10 μ l of triplicate samples of saturated solutions of PH, TH, distilled water, 3% w/v NaCl and PBS of pH 7.4 was measured using a Wescor vapour pressure osmometer which was previously calibrated using 100, 290 and 1000 mmol/kg (NaCl) standards at 37°C.

4.2.6. *In vitro* Release Studies

The prepared monolithic cylinders were subjected to *in vitro* release studies using distilled water (DW), phosphate buffer saline (PBS) of pH 7.4 and 3% w/v NaCl as release media. Four samples of each cylinder were put into 40 ml scintillation vials and filled with 30 ml of release medium. The vials were attached to a Glas-Col rugged culture rotator. The rotator was set at 20% rotation speed and placed in an oven at 37 \pm 0.5 °C. To ensure sink conditions and constant osmotic pressure driving force, the receptor release medium was replaced with fresh medium over the release period or until 100 % cumulative release was achieved. Solutions withdrawn were filtered and PH concentrations were determined using a Beckman Du-70 UV/VIS scanning spectrophotometer at 245 nm.²⁵ Results reported were the mean \pm standard deviation from three independent experiments. Similar procedure was followed upon testing the release of AT from PDET₁₀₀ elastomeric cylinders in PBS over a period of 3 months.

4.2.7. *In vitro* Degradation Study

PDET cylinders, with different degrees of acrylation (50, 70 and 100%), of initial known weights ($W1$) were subjected to a degradation study in PBS at 37°C. Conditions were similar to those applied in the release study. The buffer was replaced daily to ensure a constant pH of 7.4. At different time intervals, the swollen weight ($W2$) and dried weight ($W3$) were measured after wiping the surface water with filter paper and after vacuum-drying at 45°C for 2 days, respectively.

The water absorption and weight loss of cylinders were calculated as follows:

$$\text{Water absorption \%} = [(W2 - W3) / W3] \times 100.$$

$$\text{Weight loss \%} = [(W1 - W3) / W1] \times 100.$$

The results were reported as the mean of three measurements.

4.2.8. Scanning Electron Microscopy

Scanning electron microscope (SEM) was utilized to investigate the changes in the surface and the interior of the PDET₁₀₀ elastomer after PH release in terms of surface pores and micro-crack formation. PH/TH (weight ratio 1:2) loaded matrices of both newly fabricated and after complete release, were vacuum dried for 24 hours. The cylinders were mounted on a conductive carbon adhesive, attached to aluminum stubs and then sputter-coated with gold palladium. Gold was evaporated onto the specimen to a thickness of approximately 15 nm. Samples were examined using a Hitachi model S-570 scanning electron microscope. The microscope was interfaced with electron backscatter diffraction (EBD) system and an energy dispersive X-ray (EDX) analytical system from Tracor Northern. The electron gun was a

tungsten hairpin type filament and the sample images were digitally captured using a digital imaging system.

4.3. RESULTS AND DISCUSSION

In the following discussion, the abbreviated PDET refers to poly(1,10 decane-co-tricarballoylate) while the subscripted number following this abbreviation refers to its theoretical degree of acrylation.

4.3.1. Elastomer Preparation and Characterization

As shown in Figures 4.3 A and 4.3 B, $^1\text{H-NMR}$ analysis confirmed the purity and the chemical structure of the PDET prepolymer and also confirmed the formation of acryloyl moieties following the acrylation at the terminals of the formed chains. The calculated degree of prepolymer acrylation as estimated via $^1\text{H-NMR}$ (Figure 4.3 B) are listed in Table 4.1. The full interpretation of each individual peak of the two $^1\text{H-NMR}$ spectra is reported on the figures. Figure 4.3 C which reports the solid-state $^{13}\text{C-NMR}$ spectrum of the elastomer, shows peaks at 25, 60 and 170 ppm which are attributed to $-\text{CH}_2-$, $\text{O}-\text{CH}_2-$ and $-\text{C}=\text{O}$ groups, respectively. The spectrum also confirmed that there are no peaks corresponding to $-\text{CH}=\text{CH}_2$ terminal groups in the prepared elastomer. These observations form constituted evidence that the acrylated groups were fully consumed during the photopolymerization process.

The obtained photocrosslinked PDET elastomers were stretchable and rubbery and swelled but did not dissolve in most of organic solvents. The mechanical properties spanned from tough to elastic depending on the degree of acrylation. Figure 4.4 shows that tensile testing of the photocrosslinked

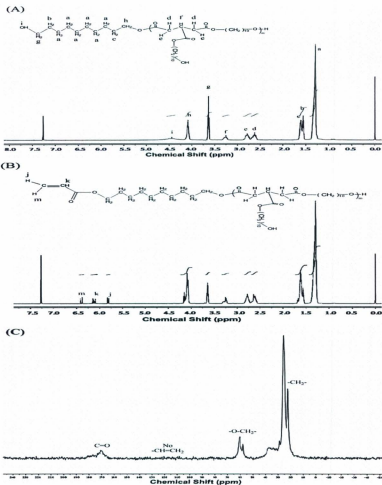


Figure 4.3. NMR spectra of PDET (A) ^1H -NMR of PDET prepolymer before acrylation (B) ^1H -NMR of PDET prepolymer after acrylation. (C) Solid-state ^{13}C -NMR spectrum of PDET100 elastomer.

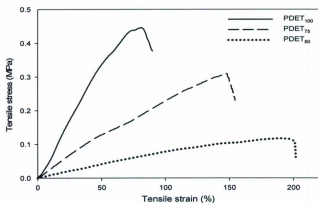


Figure 4.4. Stress-strain curves of PDET elastomers of different degrees of acrylation.

Table 4.1. Mechanical properties and sol content of poly(decane-co-tricarballoylate) elastomers.

Elastomer	σ (MPa)	ϵ (%)	E (MPa)	ρ_x (mole/m ³)	S (%)	DA*
PDET ₁₀₀	0.45 \pm 0.06	80.9 \pm 6.2	0.54 \pm 0.031	72.65 \pm 4.17	9.63 \pm 2.38	0.83
PDET ₇₅	0.31 \pm 0.09	148.3 \pm 7.8	0.18 \pm 0.005	24.22 \pm 0.67	32.19 \pm 8.75	0.69
PDET ₅₀	0.12 \pm 0.03	200.8 \pm 12.8	0.06 \pm 0.002	8.07 \pm 0.27	59.11 \pm 9.03	0.47

*Degree of acrylation estimated by NMR.

PDET elastomers produced representative uniaxial tensile stress-strain curves which are characteristics of typical elastomeric materials. No permanent deformation was observed during the mechanical testing. Average values for Young's modulus (E), ultimate tensile stress (σ), cross-linking density (ρ_x), and maximum strain (ϵ) are summarized in Table 4.1. The elastomers exhibited controllable mechanical properties. The value of σ was as high as 0.45 MPa while the value of ϵ was as high as 200 %, under the synthesis condition. Young's modulus values ranged between 0.54 and 0.06 MPa.

The crosslink density (ρ_x) was calculated according to the theory of rubber elasticity following the equation: $\rho_x = E/3RT$, where ρ_x represents the number of active network chain segments per unit volume (mole / m³), E represents Young's modulus in Pascal (Pa), R is the universal gas constant (8.3144 J/mol K) and T is the absolute temperature (K). The crosslinking density changes appreciably as a function of the degree of acrylation. As such, the decrease in the number of terminal acrylated groups in the prepolymers resulted in a decrease in the linking anchors between the polymer chains during photocuring which resulted in an increase in the elastomers' stretchability and elasticity.

Manipulation of elastomers' sol content was also found to depend mainly on the degree of acrylation. The sol content represents the mass difference after removal of the un-crosslinked prepolymer which is soluble in dichloromethane. Therefore, PDET₅₀ elastomer, with the lowest calculated degree of acrylation (0.47), possessed the highest sol content among all the prepared elastomers (59%). Although stretchability will strongly improve as a result of increasing the sol content of elastomer, the relatively low sol content will help in maintaining the mechanical properties after implantation.

Table 4.2. Osmotic activity of saturated solutions of papaverine hydrochloride, trehalose and used release media.

Solution	Osmolality (mmol/kg)*
Saturated papaverine HCl solution	105 ± 13
Distilled water	20 ± 6
Phosphate buffer saline of pH 7.4	280 ± 21
3% NaCl	918 ± 32
Trehalose	1620 ± 35

*Average of three readings. Values are mean ± standard deviation.

4.3.2. *In vitro* Release and Degradation Studies

In an attempt to demonstrate the osmotic-driven release of water soluble agents from this newly synthesized photoset biodegradable elastomer, PH was used as a model compound because of its moderate osmotic activity (Table 4.2) and the ease of determining its concentration in the release media using a validated spectrophotometric method of analysis.²⁵ The stability of PH in the release media was tested by monitoring the changes in the concentration of PH in prepared stock solutions (n=5) over a period of one week. The study showed that there was no statistical significant difference ($P>0.01$) in PH from its initial concentration in each medium over the tested period. Also, the UV spectra of PH in the stock solution coincided with those of the freshly prepared PH solution.

The release of the PH from PDET₁₀₀ elastomer in different dissolution media is illustrated in Figure 4.5. In all cases, the cumulative release profile showed an initial rapid release period which extended up to almost 3 weeks followed by a slower linear release phase that extended up to 33 weeks. Generally, the release pattern of PH can be described as follows: After the immersion of the PH loaded cylinders in the release media, water started to diffuse into the matrix mass and typical osmotic-driven release started. The dumpiness in the release which occurred at the beginning can be explained by the combination of osmosis mechanism in the outside layers of the cylindrical matrix as well as emancipation of those particles located on the surface of the cylinder and those incorporated in the un-crosslinked part (sol content) of the outer most layer of the cylinder. This initial high release period was then followed by a period of constant but slow release. This slower release rate can be attributed to the fact that the initial polymer swelling and gelling which took place in the outermost layer of the elastomeric cylinder resulted in the formation of a boundary layer that slowed down further penetration of water into the

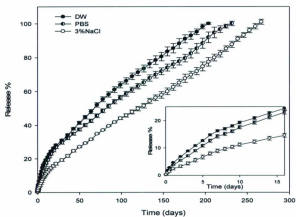


Figure 4.5. Cumulative percent of PH released from PDET₁₀₀ elastomers in different release media. Error bars represent the standard deviation of the mean of measurements from four samples.

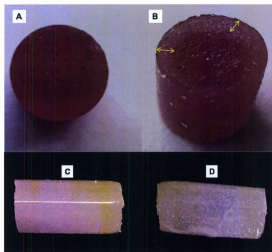


Figure 4.6. Release of amaranth trisodium dye from PDET₁₀₀ elastomeric cylinders and the change in the cylinders geometry in PBS release medium. (A) A representative image of amaranth trisodium loaded elastomeric cylinders before the start of the release study. (B) A representative image of amaranth trisodium loaded cylinders after 3 months of the start of the release study. (C) A representative image of a blank elastomeric cylinder before the start of the degradation study. (D) The image of the same cylinder at the conclusion of the release study.

subsequent matrix layers with subsequent delay in drug dissolution. In such circumstances, it is expected that the deport of the solid drug particles from the successional layer to the adjacent outer layers and then to the surface of the matrix is also retarded. To demonstrate the formation of such a boundary layer, the release of amaranth trisodium dye from cylinders over a period of 3 months was examined (Figure 4.6). As shown in Figure 4.6B, the arrows point to the limits of the formed boundary gel layer which also confirms that osmotic-driven release mechanism is taking place in a serial fashion towards the center of the device as has been also reported in Figure 4.1D.

4.3.2.1. Impact of polymer degradation on drug release

A detailed long-term degradation study using dog-bone-shaped elastomeric samples in PBS was carried out previously.²¹ In that study, it was demonstrated that the degradation rate, water absorption and weight loss of the elastomers were directly proportional to the chain length of the alkylene diol and inversely proportional to the elastomers' ρ_x . The elastomers were also found to follow slow zero-order degradation rate kinetics and exhibited the ability to maintain their shape and extensibility over the studied period.

Water absorption and change in weight of blank elastomeric cylinders over the drug release period was further investigated in this study to assess the exact possible contribution of degradation on the device geometry and the overall drug release mechanism. As seen in Figure 4.7, by the end of the 100% release period, the average cumulative water absorption was equivalent to 67%, 56% and 48% in the PDET₅₀, PDET₇₅, and PDET₁₀₀ respectively. Such findings were consistent with our previously reported results regarding the diffusion of water into the bulk of elastomeric polyesters at temperatures above

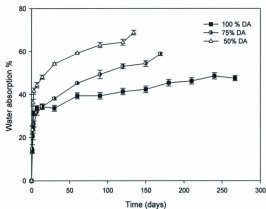


Figure 4.7. Percentage water absorption versus time of PDET elastomeric cylinders of different degrees of acrylation in PBS at 37°C. Error bars represent the standard deviation of the mean of measurements from three samples.

their glass transition.¹ Also, the results are in accordance with the fact that water diffusion and mass loss are inversely proportional to the polymer's ρ_2 . In addition, it is clear from Figure 4.7 that all the cylinders exhibited a two-stage water absorption behavior. In the first stage, which lasted up to 2-3 weeks, the water absorption preceded rapidly in a manner that matches the observations reported in the release study. However, in the second stage, the water absorption took place in a much slower rate and resulted in almost no changes in the dimensions of the prepared cylinders (Figure 4.6 C & 4.6 D). This is also consistent with our previous findings with dog-boned-shaped elastomers.²¹ On the other hand, the mean weight loss of the tested cylinders at the end of the release period was found to be equivalent to 28%, 21% and 16% in cylinders made using PDET₃₀, PDET₇₅, and PDET₁₀₀ respectively. The above data confirm that degradation played only a limited role in the overall release of the PH from the cylindrical devices. In addition, since PH is a weak basic drug ($pK_a = 5.9$), it could have also contributed in the reduction of the autocatalytic hydrolysis of the polymer chains which might have lead to a further decrease in the rate of elastomer degradation. It is also obvious that none of the reported drug release profiles exhibited a distinct release phase that can be clearly attributed to the polymer degradation. Finally, there was no evidence of major degradation or loss in the geometry of the cylinders at the end of the release studies (Figure 4.6 D) which is important in having the osmotic-driven mechanism predominate the overall drug release profile.

4.3.2.2. Impact of the osmolality of the release media

In order to assess the role of the osmotic-driven mechanism, the effect of osmolality of the release medium on the rate and extent of PH release was examined. The release of PH from a 10 % v/v loaded PDET₁₀₀ elastomeric cylinders in three release media (DW, PBS and 3% NaCl) of different osmotic

activities was investigated. Figure 4.5 shows the release kinetics of the PH as influenced by the difference in the osmolalities of the release media. It is shown that the relative PH release rate significantly decreased upon increasing the osmolality of the release medium. However, the same pattern of release has taken place irrespective of the release medium used.¹⁸ The above observations can be attributed mainly to the decrease in the water penetration rate into the matrix upon decreasing the difference in the osmotic gradient (i.e. between PH inside the capsule formed in the matrix and the outside release medium) which lead to delayed drug dissolution, less micro-cracks formation and subsequently, less drug forcing out of the cylinder.

To elucidate on the constant release profile through the PDET₁₀₀ elastomer, a linear regression of the release data after the first 3 weeks until the completion of release was carried out. As shown in Figure 4.8, the linear release over this period resulting from the osmotic-driven delivery mechanism can be described as zero-order release kinetics with constant daily release.¹⁵ The linear regression correlation coefficient was found to be equal to 0.999 for the release of PH in phosphate buffer and 3% NaCl. On the other hand, it was equal to 0.996 for the release in distilled water. In addition, the linear controlled release of PH in PBS was maintained over a period of 232 days with an average daily release of 0.35 % per day.

4.3.2.3. Effect of degree of prepolymer acrylation

In order to investigate the effect of manipulating the elastomers' physicochemical properties on drug release rate, we examined the effect of varying the prepolymer degree of acrylation on the release kinetics of PH from these elastomeric matrices. PH loaded cylinders using prepolymers of different

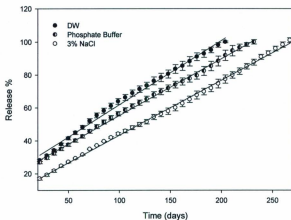


Figure 4.8. Linear regression of release data of PH from PDET₁₀₀ elastomeric cylinders in different release media. Error bars represent the standard deviation of the mean of measurements from four samples.

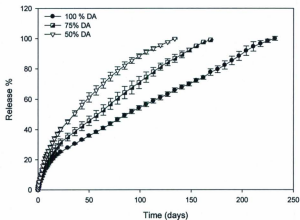


Figure 4.9. Cumulative percent of PH released in phosphate saline buffer from PDET cylinders with different degrees of acrylation (DA). Error bars represent the standard deviation of the mean from four measurements. Where error bars are not shown when the standard deviation is smaller than the symbol.

degrees of acrylation (100, 75 and 50%), were prepared and the release of PH from these cylinders was examined. Figure 4.9 shows the release of PH from the prepared cylinders in PBS at pH 7.4. The resulting release data showed a significant dependence of the drug release on the prepolymer degree of acrylation and the corresponding crosslinking density as reported in Table 4.1. It is also apparent that the same release pattern was followed in all cases with the highest release rate achieved from the elastomer of the least crosslinking density as a result of its lowest degree of acrylation. The release of PH from PDET₅₀ and PDET₇₅ 10% v/v loaded cylinders was completed within 13 and 24 weeks, respectively. On the other hand, the release of PH from PDET₁₀₀ cylinders reached 100% only after 33 weeks. This expected release behavior can be explained by the fact that water diffusion is inversely proportional to the degree of prepolymer acrylation.^{1,20} This observation is consistent with our previously reported results regarding the effect of degree of acrylation on the diffusion of water into the elastomeric matrices at temperatures above their glass transition temperatures.¹ In addition, the decrease in the crosslinking density would result in increasing the void volumes between each crosslink in the elastomer which increase the possibility of formation of inter-connected networks and channels between the encapsulated drug particles.²¹ The above results demonstrated the ability to control the drug release rate by changing the structure nature of the PDET matrix which confirms its potential use in controlled drug delivery.

4.3.2.4. Effect of osmotic excipient

One goal of the development of this system was the delivery of therapeutic protein drugs such as Interleukin-2 and Endostatin for cancer immunotherapy. Since most proteins cannot be loaded at high volume fractions, pore-forming agents of high osmotic activity have been used in many cases when the protein does not have enough osmotic activity to elicit the required capsule fracture or when a complete

release of the loaded fraction was needed. In addition, in order to be incorporated as solid particles, most proteins need to be lyophilized with cryoprotectants and other stabilizing agents like sugars (e.g., mannitol, trehalose) which also possess high osmotic activity. As such, and to better understand the impact of intimately mixing such agents with the drug on the osmotic-driven release rate, we examined the effect of loading the elastomeric cylinders with a co-crystallized mixture composed of different weight ratios of TH: PH while maintaining the 10% w/v overall particles loading in the device. Figure 4.10 shows the release kinetics of PH in PBS using different drug to TH intimately mixed ratios loaded into PDET₁₀₀ elastomeric cylinders. As shown, when no TH was incorporated, PH was released in a tardy declining manner, at an average rate of 1.1 %/day during the first phase (22 days) and later dropped to 0.35%/day during the second phase of release. On the other hand, the cylinders which contained a 1:1 PH/ trehalose ratio released the drug at a rate of 0.6 %/day ($r^2=0.9957$) over a period of 20 weeks while when trehalose concentration was increased to two third of the particles content (PH/ trehalose 1:2), the release rate was increased to 0.8 %/day ($r^2=0.9891$) over a period of 13 weeks. It is evident that the high loading of trehalose has accelerated the uptake of water into the elastomer matrix and generated a greater solution osmotic activity and subsequently increased the release rate.^{12,15} The results also confirm that the mechanism of PH release from the PDET elastomer can be also controlled by varying in the mixture the weight ratio of osmotic excipient to the drug while maintaining the same overall volumetric loading of the incorporated mixture in the device.

Although the release of PH from loaded elastomeric cylinders with different ratios of TH might serve as a reasonable estimate for assessing the release behavior of protein drugs, it cannot be overlooked that the aberrant geometrical and physicochemical properties of peptides (three dimensional

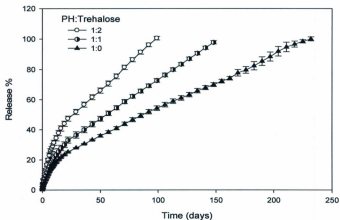


Figure 4.10. Effect of incorporating different weight ratios of trehalose to papaverine hydrochloride on the osmotic-driven release rate from PDET₁₀₀ elastomeric cylinders. Error bars represent the standard deviation of the mean from four measurements. Where error bars are not shown when the standard deviation is smaller than the symbol.

structure nature, relative large molecular weight and isoelectric point) might affect the release rate from the PDET matrices. From a practical standpoint, the obtained results in this study is useful in terms of suggesting that the mechanism of protein release from such similar elastomeric cylinders would be controlled mainly by the amount of TH incorporated with the loaded drug.

4.3.3 Scanning electron microscopy

In order to further investigate and demonstrate the proposed theory of the osmotic-driven release mechanism, the changes in the surface and interior architecture of the loaded cylinders before and after the release was examined. Figure 4.11 shows the SEM images of the PH/trehalose (molar ratio 1:2) loaded PDET₁₀₀ cylinder before and after the conduction of release studies. As shown, the cylinders before the conduction of release showed a smooth surface without any channels. However, after the osmotic drug release, the surface and cross-section images showed cracks and pores corresponding to the routes which the drug took for release in concordance with the proposed osmotic-driven drug released mechanism.

4.4. CONCLUSIONS

The osmotic-driven release mechanism of PH of 10% v/v loadings from monolithic cylinders of newly synthesized elastomer was demonstrated. The results revealed that the drug release profiles possessed linear zero-order release and were influenced by the osmolality of the release medium. It has also been shown that the rate of PH release can be controlled through manipulations in the elastomer's degree of acrylation and co-formulation with osmotic diluents like trehalose. In all situations, osmotic-

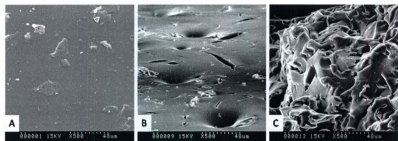


Figure 4.11. Scanning electron microscopy photographs of PH/TH (weight ratio 1:2) loaded PDET₁₀₀ cylinders. (A) Surface image before the start of the release study. (B) Surface image after the conclusion of the release study. (C) Cross-sectional view of the cylinder at the conclusion of the release study.

driven release mechanism was the dominant mechanism that contributed to that enhancement in the drug release. These novel photocrosslinked elastomeric matrices constitute a promising delivery system for water soluble proteins and peptides. In particular, their planned use in long-term implantable cytokines delivery for treatment of a variety of solid tumors. The incorporation of therapeutic proteins with osmotic pharmaceutical excipients as well as the selection of the proper prepolymer degree of acrylation can be efficiently used to achieve desired release rates. Finally, as they are degradable, once introduced to the diseased lesions into the body they require no retrieval or further manipulation and are degraded into soluble, non toxic by-products.²¹

4.5. REFERENCES

- 1- Younes H M, Bravo-Grimaldo E, Amsden B G. 2004. Synthesis, characterization and *in vitro* degradation of a biodegradable elastomer. *Biomaterials* 25: 5261-5269.
- 2- Amsden B G, Misra G, Gu F, Younes H M. 2004. Synthesis and characterization of a photo-cross-linked biodegradable elastomer. *Biomacromolecules* 5: 2479-2486.
- 3- Ilagan B G, Amsden B G. 2009. Surface modifications of photocrosslinked biodegradable elastomers and their influence on smooth muscle cell adhesion and proliferation. *Acta Biomater.* 5: 2429-2440.
- 4- Gu F, Younes H M, El-Kadi A O, Neufeld R J, Amsden B G. 2005. Sustained interferon-gamma delivery from a photocrosslinked biodegradable elastomer. *J Control. Release* 102: 607-617.
- 5- Yan X, Zheng R, Guan S, Yi B. 2009. Application of thermoplastic elastomer in hot-melt pressure sensitive adhesives for transternal drug delivery. *Zhongguo Zhong. Yao Za Zhi.* 34: 1612-1614.
- 6- Guan J, Stankus J J, Wagner W R. 2007. Biodegradable elastomeric scaffolds with basic fibroblast growth factor release. *J Control. Release* 120: 70-78.
- 7- Younes H M, Ellaboudy H, Shaker M A. 2008. WO 2008144881 A1.
- 8- Richard R, Schwarz M, Chan K, Teigen N, Boden M. 2009. Controlled delivery of paclitaxel from stent coatings using novel styrene maleic anhydride copolymer formulations. *J. Biomed. Mater. Res. A* 90: 522-532.

- 9- Simmons A, Padsalgikar A D, Ferris L M, Poole-Warren L A. 2008. Biostability and biological performance of a PDMS-based polyurethane for controlled drug release. *Biomaterials* 29: 2987-2995.
- 10- Pasquale S A, Brandeis V, Cruz R I, Kelly S, Sweeney M. 1987. Norplant contraceptive implants: rods versus capsules. *Contraception* 36: 305-316.
- 11- Carelli V, Di Colo G, Nannipieri E. 1987. Factors in zero order release of colonidine hydrochloride from monolithic polydimethylsiloxane matrices. *Int J Pharm* 35: 21-28.
- 12- Di Colo G, Campigli V, Carelli V, Nannipieri E, Serafini M F, Vitale D. 1984. Release of osmotically active drugs from silicone rubber matrixes. *Farmaco Prat.* 39: 310-319.
- 13- Sheppard N F, Madrid M Y, Langer R. 1992. Polymer matrix controlled release systems: influence of polymer carrier and temperature on water uptake and protein release. *J Applied Polymer Science* 64: 19-26.
- 14- Scherrier R, Thepine P. 1992. Water absorption, swelling rupture and salt release in salt silicone rubber compounds. *J Material science* 27: 3424-3434.
- 15- Carelli V, Di Colo G, Nannipieri E. 1988. Zero-order drug release from monolithic polydimethylsiloxane matrices through controlled polymer cracking. *Farmaco Prat.* 43: 121-135.
- 16- Wright J, Chandrasekaran SK, Gale R, Swanson D. 1981. A model for the release of osmotically active agents from monolithic polymeric matrices. *AIChE Symp. Ser.* 77: 62-68.
- 17- Amsden B G. 2003A model for osmotic pressure driven release from cylindrical rubbery polymer matrices. *J Control Release* 93: 249-258.
- 18- Micheals A S, Guilloid S. 1979. US 4177256.
- 19- Younes H M: 2003. New biodegradable elastomers for interferon-gamma delivery, PhD Thesis, Faculty of Pharmacy, University of Alberta, Edmonton, AB.
- 20- Shaker M A, Younes H M. 2008. Synthesis and Characterization of Poly(diols-tricarballlylate) Photocrosslinked Biodegradable Elastomers. *Am. J. Pharm. Ed.* 72, 118.
- 21- Shaker M A, Doré J E, Younes H M. 2010. Synthesis, Characterization and Cytocompatibility of Poly(diols-tricarballlylate) Visible Light Photo-crosslinked Biodegradable Elastomer. *J Biomaterials Science* 21: 507-520.
- 22- Liu J K, Couldwell W T. 2005. Intra-arterial papaverine infusions for the treatment of cerebral vasospasm induced by aneurysmal subarachnoid hemorrhage. *Neurocritical Care* 2: 124-132.
- 23- Rath P., Mukta, Prabhakar H, Dash H H, Suri A. 2006Haemodynamic changes after intracisternal papaverine instillation during intracranial aneurysmal surgery. *Br. J. Anaesth.* 97: 848-850.

- 24-Shiokawa K, Kasuya H, Miyajima M, Izawa M, Takakura K. 1998. Prophylactic effect of papaverine prolonged-release pellets on cerebral vasospasm in dogs. *Neurosurgery* 42: 109-116.
- 25-Yeow Y L, Azali S, Ow S Y, Wong M C, Leong Y K. 2005. Evaluating the third and fourth derivatives of spectral data. *Talanta* 68: 156-164.

CHAPTER 5

Biocompatibility and Biodegradability of Implantable Drug Delivery Matrices Based on Novel Poly(decane-co-tricarballylate) Photocured Elastomers

The content of this chapter is submitted to the Journal of Bioactive and Compatible Polymers.

Mohamed A. Shaker, Noriko Daneshtalab, Jules J.E. Doré and Husam M. Younes

ABSTRACT

Visible-light photocrosslinked biodegradable amorphous elastomers based on poly(decane-co-tricarallylate) [PDET] of varying crosslinking densities were synthesized and their cytotoxicity, biocompatibility and biodegradability were reported. Cytotoxicity of PDET extracts of the elastomers were assessed for mitochondrial succinate dehydrogenase activity by 3-(4,5-dimethylthiazol-2-yl)-2,5-diphenyltetrazolium bromide (MTT assay) and inhibition of [3 H]thymidine incorporation into DNA of epithelial cells. To assess *in vivo* biocompatibility and biodegradability, subcutaneous implantation of PDET micro-cylinders was undertaken in twenty five male Sprague-Dawley rats over a period of 12 weeks. Biodegradable poly(lactic-co-glycolic acid) sutures served as controls. The *in vivo* changes in physical and mechanical parameters of implants were compared to those observed *in vitro*. The treated epithelial cells revealed no signs of cytotoxicity and the elastomers degradation products caused a slight stimulation to both mitochondrial activity and DNA replication. The implantation results showed that no macroscopic signs of inflammation or adverse tissue reactions were observed at implant retrieval sites. Moreover, the retrieved implanted micro-cylinders were found to maintain their original geometry and extensibility in a manner similar to those observed *in vitro*. The findings confirmed that these new elastomers have good biocompatibility and are expected to be useful as biodegradable and biocompatible biomaterials for controlled drug delivery and tissue engineering applications.

5.1. INTRODUCTION

Biodegradable polymers with elastomeric properties have lately attracted special attention for their uses in controlled-drug delivery systems¹⁻⁶ and tissue engineering.⁷⁻¹⁶ Elastomers can be regarded as one of the best biomaterials for such applications as they can offer many advantages over the other fabricated tough materials. Their mechanical properties can be manipulated in a manner that makes them as soft as body tissues. They have the ability to recover and withstand the mechanical challenges upon implantation in a mobile part of the body,¹⁵ and they are also proven to be well suited for controlled-drug release applications.^{6,17}

— —

Biodegradable elastomers reported in the literature have been synthesized as one of two types: thermoplastic^{8,9,12} or thermoset elastomers.^{1,7,10} While thermoplastics offer the advantage of ease of fabrication, they degrade heterogeneously due to their semi-crystalline nature. This leads to rapid non-linear loss of mechanical properties as well as large deformations as the material degrades. Conversely, although thermoset polymers are not easily fabricated, they outperform thermoplastics in a number of areas, including uniform biodegradation, better mechanical properties, and overall increased durability. This makes thermoset elastomers better suited for most biomedical applications.

As one of the techniques utilized in preparing such elastomeric polymers, the use of light-activated curing approaches in preparing photosest elastomers have recently gained considerable attention as it would offer a number of advantages over the conventional thermal or solution crosslinking techniques in preparing biodegradable thermoset elastomers.¹⁵ First, the process excludes the use of thermal energy, in other words, the polymers can be formulated at temperatures near physiological range even once

loaded with biologically thermo-sensitive therapeutics like proteins and other heat-sensitive drugs. Second, the process proceeds rapidly, on the order of minutes. Third, the process can be carried out *in situ*. Finally the degree of crosslinking and mechanical properties of the photocured elastomer can be tailored by changing the density of photosensitive termini in the prepolymer.¹⁶

We have recently reported on the synthesis, characterization and cytocompatibility of a novel family of amorphous photose poly(diols-co-tricarballate) elastomers^{15,16} and their use in controlled-release of small-molecule pharmaceuticals and protein drugs.^{6,15,17} These newly synthesized elastomers utilized a preparation process which involved using visible light photoinitiated polymerization and a solventless strategy of drug loading.^{6,17} The elastomers were optically transparent, exhibited controllable mechanical properties and proven to be amorphous with glass transition temperatures below physiological body temperature, which make them suitable as elastomeric implants *in vivo*. It was also illustrated that altering the chain length of the alkylene diol can vary the hydrophilic and hydrophobic properties of the elastomers that can be tailored to satisfy a particular purpose.¹⁶

The newly prepared elastomers also demonstrated to be a promising biomaterial for protein drug delivery and other tissue engineering applications. Specifically, the use of visible light crosslinking helped in eliminating many of the drawbacks associated with using UV photocuring by making the polymerization conditions sufficiently mild to be carried out in the presence of other biological materials *i.e.* for encapsulation of viable cells, in drug screening, or in biosensing applications.¹⁸ Additionally, visible light was able to penetrate deeper through tissues than UV light (less scattering and less absorption). This property may limit the need for invasive surgical procedures by allowing trans-tissue polymerizations, whereby the material is injected subcutaneously or even subdermally and irradiated

through the skin to polymerize the material *in situ*. In the most recent study conducted in our lab, we have demonstrated that therapeutic proteins such as Interleukin-2 (IL-2) have retained almost 100% of their stability during drug loading and after its release from the elastomers. The cell based bioactivity studies on the released IL-2 showed that more than 94% of its original activity was retained over a 28 days release period.¹⁷ In addition, it was shown that osmotic-driven controlled release of drugs from these new elastomeric matrices is linear, constant and controllable.⁶

In this study, we have focused on determining the *in vitro* cytotoxicity of these biodegradable elastomers and evaluating their biological performance after long term contact with soft tissue *in vivo*. We have also examined the *in vivo* changes in the physical and mechanical properties of these elastomers and the influence of changing the polymer crosslinking density on those properties. Furthermore, we have attempted to compare the *in vivo* degradation changes to those observed *in vitro* as a mean of establishing an *in vitro/in vivo* comparison for the changes in elastomers' physical and mechanical properties during the degradation.

5.2. EXPERIMENTAL

5.2.1. Materials

The chemicals used for the preparation of elastomers were tricarballic acid (99%), 1,10-decanediol (98%), stannous 2-ethylhexanoate (95%), 4-dimethylamino pyridine (99%), acryloyl chloride (96%), triethylamine (TEA; 99.5%), sodium sulphate (99%), triethanolamine (99%), and camphorquinone (96%) and were purchased from the Aldrich-Sigma chemical company. Acetone (99%) and chloroform

(99%) were purchased from the Caledon chemical company. All chemicals were used as received without any further purification.

5.2.2. Preparation of Prepolymers and Elastomers

The detailed method of preparation was described in chapter 3 (section 3.2.2.),¹⁶ outlined in Figure 5.1 and summarized herein. First, PDET prepolymer was prepared by solvent-free step growth polymerization. Briefly, 11.33 g of 1,10-decane diol (0.065 mole) and 7.05 g of tricarballic acid (0.04 mole) was added into a three-neck flask in the presence of stannous 2-ethylhexanoate as a catalyst. The mixture was heated to 140 °C under nitrogen with continuous stirring for 20 minutes and for an extra 10 minutes under vacuum. Molecular weights and molecular weight distributions of the resulting prepolymer were determined using a Waters GPC system (Waters, Milford, CT) equipped with 410 Waters differential refractometer and an on-line multi-angle laser light scattering (MALLS) detector (PD 2000 DLS, precision detectors, MA). The column configurations consisted of an HP guard column attached to a phenogel (2) linear 5 μ m column (300 \times 7.8 mm²). The mobile phase consisted of anhydrous tetrahydrofuran at a flow rate of 1 ml/min at 35 °C. The sample concentration was 20 mg/ml and the injected volume was 75 μ l. The absolute MWs were determined by MALLS using a dn/dc value of 0.172 ml/g. Data were collected and handled using Precision Acquire/Discovery software package.

A 100% acrylation of the prepared prepolymers (PDET₁₀₀) was carried out by reacting acryloyl chloride (ACRL) with the terminal hydroxyl groups of the prepolymers. Into a flask, 10 g of the prepared prepolymer was dissolved with 60 ml of acetone, to which 10 mg of 4-dimethyl aminopyridine was added as a catalyst. The flask was sealed, flushed with argon and then immersed in a 0 °C ice bath. A stepwise addition of 2.35 ml of ACRL (29 mmol) with 4.02 ml of TEA (equimolar amounts) to the

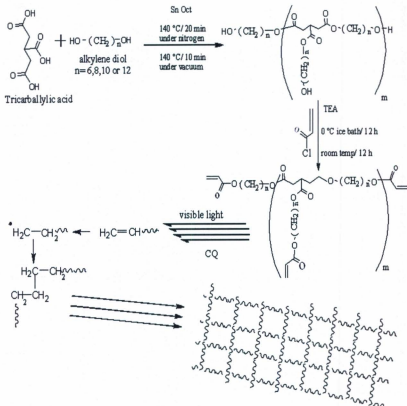


Figure 5.1. A schematic illustration of the synthesis, acrylation and photocuring of poly(diols-tricarballic) elastomers. The step growth polymerization of tricarballic acid and alkylene diol was catalyzed by stannous-2-ethylhexanoate. The acrylation was carried out using acryloyl chloride in the presence of triethylamine. To photo-crosslink, the acrylated prepolymer was mixed with the photoinitiator, camphorquinone and triethanolamine and crosslinked under visible light.

prepolymer solution was carried out over a period of 12 h. The reaction was later continued at room temperature for another 12 hrs. The 75 % and 50 % acrylated PDET prepolymers (PDET₇₅ and PDET₅₀ respectively) were prepared by following the same procedure as described above but using 75 % and 50 % of ACRL and TEA molar amounts. The final product's purity was confirmed by a proton nuclear magnetic resonance (¹H-NMR) spectroscopic analysis in chloroform-*d* using a Bruker Avance-500 MHz NMR spectrometer. The signal intensity of the methylene groups of diol (1.3-1.7 ppm) and the acrylate groups' intensities (5.8-6.4 ppm) were then used to calculate the degree of acrylation in the prepolymers.

16

The following describes the procedure followed in preparing the final elastomers. Briefly, in a dark fume hood equipped with a sodium lamp, 5 μ l of 10 % ethanolic solution of both camphorquinone and triethanolamine [equivalent to 0.01% (w/w) photoinitiator] were added to 5 grams of the acrylated prepolymer. The mixture was then left under vacuum for 4 hrs at 40 °C to ensure complete removal of any traces of alcohol from the photoinitiator solutions. The dried sample of the prepolymer that was mixed with the initiator was then poured into the glass mould using a spatula. The mould was exposed to a visible light source (450-550 nm at a 40 mW/cm²) filtered from a 50 Watt tungsten-halogen lamp (Taewoo Co., Korea) for 10 minutes at a distance of 10 cm to form the microcylinder specimens which were removed from the mould by breaking and peeling the glass. The thermal properties of the PDET₁₀₀ elastomer were characterized using Q200 DSC at a heating rate of 10 °C/ min. The samples were heated from room temperature to 150 °C and rapidly cooled down to -100 °C. The DSC scan was recorded as the sample was being reheated from -100 to 150 °C.

5.2.3. *In vitro* Cytotoxicity and Proliferation Assays

5.2.3.1. *Preparation of degradation aliquots*

The PDET elastomers were subjected to degradation in sterile phosphate buffered saline (PBS) of pH=7.4 to test the cytotoxicity of the degradation products. Photocured PDET films, with different degrees of acrylation (50, 75 and 100%), were prepared by visible light polymerization on 22 mm cover-glasses. Three different preparations of each elastomer were used. The elastomer films were cut into pieces of approximately 300 mg and sterilized by autoclaving. The degradation media were prepared by incubating these pieces in 600 μ l of PBS for 1, 7, 14 and 28 days at 37 °C, in sealed sterile plastic endpordorf tubes. Samples were done in triplicate from each elastomer preparation. PBS incubated under the same conditions but without the addition of the elastomer was used as a negative control. Aliquots from each elastomer degradation buffer solution were added directly to the cell culture medium, to test for cytotoxic effects.

5.2.3.2. *Cell culture*

Mink lung epithelial cell line (Mv1Lu, American Type Culture Collection, Manassas, VA, USA) was used for *in vitro* toxicity assessment. The cells were grown in Delbecco's Modified Eagle Medium (DMEM; Invitrogen, Carlsbad, CA) supplemented with 10% (v/v) fetal bovine serum (Growth Medium; PAA Laboratories, Etobicoke, ON), at 37°C in an atmosphere of 5% CO₂/air and 100% relative humidity. For assays, cells were trypsinized to remove them from the T-75 flasks they were grown in and re-suspended in growth medium. Cell density was determined by manual counting using a hemocytometer. Cells were then diluted in growth medium to the appropriate density and plated as described for the specific assay.

5.2.3.3. *The MTT 3-(4,5-dimethylthiazol-2-yl)-2,5-diphenyltetrazolium bromide assay*

Mv1Lu cells were seeded in 96-well plates (Falcon) at a density of 5×10^4 cells/well in a volume of 200 μ l culture media, and incubated in a humidified atmosphere (5% CO₂/air), at 37 °C. After 24 hrs, 20 μ l/well of each sterile degradation sample or the appropriate PBS control was added into duplicate of three wells. This resulted in a dilution of elastomer degradation supernatant equivalent to 45 mg elastomer/ml. After another 24 hrs, 20 μ l of MTT labeling reagent (final concentration 0.5 mg/ml) was added to each well and incubated for 4 hrs in humidified atmosphere at 37 °C. Unreacted dye was then removed by aspiration and the insoluble formazan crystals were dissolved in 200 μ l/well solubilization buffer (10% sodium dodecyl sulphate in 0.01M HCl) and incubated over night and then measured spectrophotometrically at $\lambda = 580$ nm, using a Polarstar, Optima plate reader (BMG Lab technologies, Durham, NC USA). Results were recorded as percentage absorbance relative to untreated control cells. The cytotoxicity assay results were used to calculate cell viability after incubation with elastomer as follows:

$$\text{Cell viability (\%)} = [A] / [A]_C \times 100$$

Where [A] is the absorbance in a well containing the elastomer degradation sample and [A]_C is the mean absorbance for untreated control cells. Results reported as the mean \pm SD from three different elastomer preparations of each degree of acrylation.

5.2.3.4. *³H-Thymidine incorporation assay for DNA synthesis*

Mv1Lu cells were plated in 24-well plates (Falcon) at a density of 40,000 cells/well in 1 ml of growth medium and allowed to attach in a humidified atmosphere (5% CO₂/air), at 37 °C for 24 hours prior to the initiation of experiment. One hundred μ l of each elastomer degradation sample (45 mg

elastomer/ml equivalent), or time-matched PBS, was added to duplicate wells and incubated for 18 hrs. As a positive control, transforming growth factor β (2ng/ml) was added to duplicate wells to demonstrate responsiveness to growth inhibitors, and sterile saline treated wells served as a negative control. After the incubation period, 1 μCi ^3H -thymidine was added to each well and incubated for 1 hr. Media was aspirated and the radioactivity incorporated into macromolecules was precipitated by washing each well twice with 1 ml of 10% ice cold trichloroacetic acid solution added to each well for 10 min at room temperature. The solution was aspirated and the precipitated radioactivity was then dissolved in 0.25 ml of solubilization buffer (0.2M NaOH, 0.25mg/ml sheared DNA) by shaking for 30 minutes at room temperature. Solubilized radioactivity was added to 5 ml of scintillation cocktail and the amount of radioactivity determined using a 6500LS liquid scintillation counter (Beckman Coulter Inc., Brea, CA, USA). The incorporated radioactivity results were used to calculate percentage of DNA synthesis after incubation as follows:

$$\text{DNA synthesis (\%)} = [R] / [R]_c \times 100$$

Where [R] is the measured radioactivity in a well containing the elastomer degradation sample and $[R]_c$ is the mean measured radioactivity for untreated control cells. Results reported are the mean \pm SD from three independent elastomer preparations.

5.2.4. *In vivo* Biocompatibility and Degradation Studies

5.2.4.1. *Animal preparation and subcutaneous implantation*

The study was carried out following the guidelines set by the Canadian Council on Animal Care, outlining the code of ethics governing animal experimentation and with approval of the protocol by the Memorial University Animal Care and Use Committee. Twenty five adult male Sprague-Dawley rats,

16-20 weeks of age and 200–250 g in weight, obtained from the Vivarium at Memorial University Health Sciences Center (St John's, NL, Canada) were utilized for this research. The rats were housed in Macrolon IV polycarbonate cages in a thermostatically controlled room, and were given normal tap water and regular Purina rodent diet (Prolab RMH 3000, PMI Mills Inc, Brentwood, MO, USA). To allow acclimatization of the animals to the lab environment and to minimize stress prior to experimental procedures, all animals were housed for at least 24 hrs prior to surgery under 12/12 h light/dark cycles with free access to regular purina chow and water.

The implantation surgery was carried out under aseptic conditions and performed under general anesthesia of 2.5% isoflurane (PPC Richmond Hill, ON, Canada) and 70% O₂. At the surgical anesthesia level (indicated by the lack of tail and corneal reflexes), the hair was shaved from the dorsal nape and back region (around the implantation sites) and disinfected by brushing with iodine solution. This area was chosen so as to minimize the possibility of rats chewing on the implant site postoperatively, hence, minimizing loss of sample and the risk of infections (Figure 5.2). On each side of the vertebral column, two paravertebral incisions of approximately 10 mm were made. Lateral to these incisions, small subcutaneous pockets were created by blunt hemostats to allow the subcutaneous implantation. A "sham" surgery was used to examine the prejudicial scar tissue formation due to the surgical procedure itself.

The rats were divided into five groups with each group containing five randomly chosen rats ($n=5/\text{group}$). From each of the five groups of animals, two rats were implanted with two samples each of PDET₁₀₀ and PDET₅₀ autoclaved microcylinder specimens (1 cm in length and 2 mm in diameter), $n=2$ of specimen/rat. The third rat, again from each of the five groups was implanted with two PDET₁₀₀ and one PDET₅₀ microcylinder and one PLGA suture of 1 cm length and 0.3 mm diameter (2-0 CL-811 3 Metric Polysorb®, Covidien Syneture, Norwalk, CT, USA). The fourth one was fixed with one PDET₁₀₀

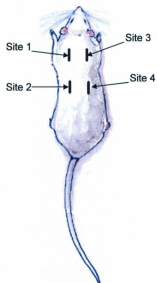


Figure 5.2. A diagrammatic illustration of the implantation sites for the specimens in each rat.

and two PDET₅₀ microcylinders and one PLGA suture. The fifth rat was implanted with one PLGA suture, one PDET₁₀₀ and one PDET₅₀ samples in addition to the sham surgery. Hence, a total of 95 implants consisting of 15 PLGA sutures, 40 PDET₁₀₀, and 40 PDET₅₀ were inserted subcutaneously. After the insertion of the implants, the surgical cuts were closed using skin staples (Agravas®; InstruVet C.V., Cuijk, the Netherlands) as well as 50,000 IU of Duplicillin (Intervet Canada Ltd.-Whitby, ON, Canada) was injected in the hind leg to minimize risk of infection. Following implantation, each group of rats was selected randomly at weeks 1, 2, 4, 8, and 12 and the rats were euthanized using intra-peritoneal injection of 32.5 mg Phenobarbital (Somnotol®, MTC pharmaceuticals, Cambridge, ON, Canada). The implants were dissected along with soft tissue and skin around the sample.

5.2.4.2. Implant retrieval and histological preparations.

For each of the above implantation periods, a total of five PDET₁₀₀ and PDET₅₀ tissue-covered implants from different rats were retrieved. As well, three of PLGA suture and one sham specimen were recovered. The tissue specimens were fixed in 10% buffered formalin for at least 24 hrs. Subsequently, the specimens were routinely processed and embed into methyl methacrylate embedding. The block was then cut precisely perpendicular to the longitudinal axis of the implant site using Leica RM 2165 rotary microtome (Meyer Instruments, Inc. Houston, TX, USA). Several 4- μ m sections were cut from each sample block perpendicular to the long axis of the tissue at the midsagittal site of the implant. The sections were stained with hematoxylin/eosin for cellular identification and routine histological examination to observe the interface between implant and surrounding tissue. In addition, Van Gieson's stain was used for differential staining of collagen and connective tissue.

5.2.4.3. Macroscopic and histological evaluation.

For each implantation period, the tissue samples were visually checked for any abnormalities such as discoloration or marks of macroscopic corrosion. General morphologic and histological observations of stained sections were performed and digital phase contrast photomicrographs were captured using Olympus FV 300 microscope (Olympus Canada, Inc., Markham, ON, Canada) coupled with SPOT R/T slider camera (Diagnostic Instruments, Inc., Sterling Heights, MI, USA) with complete image analysis software (Image Pro Plus, version 4.1, Media Cybernetics, Inc., Bethesda, MD, USA). Special attention was given to examining the connection of the implant to the surrounding tissue. Each tissue sample received a score by the histopathologist, based on graded scales to assess the cellular response and determine tissue reaction to implant. All samples were compared to tissue which was obtained by sham surgery. An inflammatory cell infiltrate score for each implant was determined using a grading scale. The scale was graded as follows: 0 = no difference from normal control tissue, no presence of macrophages, giant cells, lymphocytes, eosinophils, or neutrophils at or around implant site; 1 = presence of a few lymphocytes or macrophages, no presence of giant cells, eosinophil, or neutrophils; 2 = presence of several lymphocytes, macrophages, with a few giant cells and a small foci of neutrophils; 3 = presence of large numbers of lymphocytes, macrophages, and giant cells, with notable presence of eosinophils and neutrophils; 4 = severe cellular infiltrate response to implant followed by tissue necrosis at or around the implant site. Each cell type was identified separately using an arbitrary scale of + to +++, denoting the range from few cells to dense infiltrate, respectively, with - denoting no observed cells. In addition, the fibrous capsule membrane thickness around each implant was measured and expressed as the mean value of four readings per slide out of five slides at each time point. All histological preparations were assessed by the pathologist (P.W), who was blinded to the identity of each slide.

5.2.4.4. Physical characterization of excised cylinders

Three of the PDET₁₀₀ and PDET₅₀ cylinders shaped samples, each of known weight (*W1*), were retrieved from different rats after each implantation period for physical and mechanical measurements. Immediately after excision to remove attached tissue, the elastomer cylinders were weighed after wiping the surface with filter paper to determine the swollen weight (*W2*). The mechanical properties of the freshly excised elastomers were measured by uniaxial tension using an Instron model In-Spec 2200 tester with Marlin PDA Data Management Software (Instron Corporation, Norwood, MA, USA). At room temperature, each sample was pulled longitudinally at a rate of 1.0 mm/sec and elongated to failure. Values were converted to stress-strain and Young's modulus was calculated from the initial slope of the stress-strain curve. The results reported are the mean \pm SD of four measurements. The crosslink density (ρ_x) was calculated according to the theory of rubber elasticity following the equation: $\rho_x = E/3RT$, where ρ_x represents the number of active network chain segments per unit volume (mol/m^3), E represents Young's modulus in Pascal (Pa), R is the universal gas constant (8.3144 J/mol K) and T is the absolute temperature (K). The samples from the tensile measurement were collected and dried under vacuum at room temperature in the presence of a desiccant for 48 hrs, the dried mass (*W3*) was then measured. The weight loss was calculated as follows:

$$\text{Weight loss \%} = [(W1 - W3) / W1] \times 100.$$

5.2.4.5. *In vitro* degradation.

Fifteen of known weight (*W1*) PDET₁₀₀ and PDET₅₀ autoclaved cylinder-shaped samples, were placed in 20 ml scintillation vials containing 15 ml PBS (pH=7.4) and 0.01% of sodium azide. The vials were placed in an oven at 37 °C for up to 12 weeks. The buffer was replaced daily to ensure a constant

pH of 7.4. After 1, 2, 4, 8 and 12 weeks, the cylinders were removed, blotted dry, weighed after wiping the surface water with filter paper to determine the swollen weight (W_2). The samples were then subjected to a uniaxial tensile measurement while hydrated. The samples from the tensile measurement were dried as above and the dried mass (W_3) was then measured. The weight loss was calculated as above.

5.2.5. Statistical analysis.

Statistical analyses of data were performed using Graphpad Prism software (version 5.02) by using 2-way ANOVA followed by the Bonferroni post-tests. Data reported as means \pm standard deviation (SD). Statistical differences between the groups were considered significant if the p value was < 0.05 unless otherwise reported.

5.3. RESULTS

The PDET prepolymer molecular weight and polydispersity index were measured to be 1366 Da and 1.25, respectively. There was no ^1H -NMR evidence of unreacted monomers in the prepolymer analysis and the incorporation of the terminal acrylated groups in the prepolymer was confirmed by the appearance of three peaks at 5.8, 6.1 and 6.4 ppm. Table 5.1 provides a short summary of the mechanical properties of the prepared elastomers, their crosslink densities and the corresponding estimated degrees of prepolymer acrylation based on NMR analysis. The PDET₁₀₀ elastomer was amorphous and exhibited only one glass transition temperature, at -24°C , with no melting point.

5.3.1. *In vitro* Cytotoxicity

This study evaluated the cytotoxicity of PDET elastomers *in vitro* using MTT test and ^3H -Thymidine incorporation assay. Both methods are considered a sensitive index to evaluate the cytotoxicity of these

Table 5.1. Mechanical properties and sol content of PDET prepared elastomers.

Elastomer	σ (MPa)	E_0 (MPa)	ϵ (%)	ρ_x (mol/m ³)	S (%)	DA*
PDET ₁₀₀	0.457 ± 0.03	2.140 ± 0.36	61.23 ± 5.83	288 ± 48.4	11.95 ± 5.69	0.91
PDET ₇₅	0.297 ± 0.05	1.270 ± 0.08	98.45 ± 4.03	171 ± 10.7	35.56 ± 7.35	0.63
PDET ₅₀	0.180 ± 0.02	0.394 ± 0.01	115.3 ± 3.60	53.0 ± 0.40	58.05 ± 8.98	0.46

* Estimated by NMR

biomaterials with each test reflecting not only cell number but also cellular metabolic status (MTT) and replication (thymidine incorporation).

5.3.1.1. MTT assay

The MTT assay measures mitochondrial dehydrogenase activity and thus indicates cell viability and metabolic function. The results of the assay on the PDET elastomers with different degrees of acrylation (50, 75 and 100 %) are shown in Figure 5.3. The differences in mitochondrial function associated with each PDET elastomer were expressed as a percentage relative to that from control PBS treated cells (arbitrarily set at 100%), where higher absorbance values indicate increased metabolic activity of viable cells. Exposure of epithelial cells to the PDET elastomer degradation products with different degrees of acrylation resulted in a maintenance of high metabolic rate independent of degradation period or degree of acrylation. This assay therefore provides confirmation of the biocompatible nature of these elastomers.

5.3.1.2. ^3H -Thymidine incorporation assay

The ^3H -thymidine incorporation assay was used to measure DNA synthesis of cells as a second measure of cell viability and function. The relative degree of thymidine incorporation into cells, after incubation with different elastomer degradation aliquots is shown in Figure 5.4. These results are calculated as a percentage of incorporation of ^3H -thymidine, relative to the incorporation rate of the appropriate time related PBS treated cells, using the positive and negative controls to define limits of replication effects. No statistical significant difference was seen in incorporation of ^3H -thymidine into replicating DNA for PDET degradation aliquot treated cells, regardless of elastomer's degree of acrylation or time of degradation.

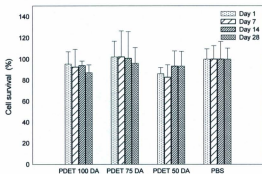


Figure 5.3. The effect of PDET elastomers of different degrees of acrylation on the Mv1Lu epithelial cell viability estimated by MTT assay after 1, 7, 14 and 28 days of elastomer degradation. Results are expressed as the percentage of viable cells compared with phosphate buffer saline (PBS) treated controls (mean \pm SD, $n = 6$). The significance of the results was determined by comparison with control value using 2-way ANOVA; * $p < 0.05$.

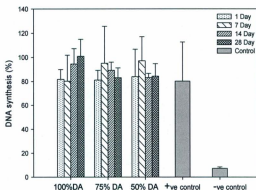


Figure 5.4. The effect of PDET elastomers of different degrees of acrylation on Mv1Lu epithelial cells proliferation and DNA synthesis using ^3H -thymidine incorporation assay after 1, 7, 14 and 28 days of elastomer degradation in comparison to control. Results are expressed as the percentage of ^3H -thymidine incorporation relative to that of PBS-treated controls (mean \pm SD, $n = 6$). Transforming growth factor β (2ng/ml) was used as a positive control (+ve control) and sterile saline treated wells served as a negative control (-ve control). The significance of the results was determined by comparison with control value using 2-way ANOVA; * $P < 0.05$.

5.3.2. *In vivo* Biocompatibility

Evaluation of the local pathological effects was carried out at both the gross level and the microscopic level. Gross evaluations of the rats were conducted daily for 12 weeks. These evaluations showed no exudative inflammatory reaction on the dermis, even though the implants could be palpated. The rats were recorded as being healthy and active throughout the study, with no abnormal behavior noted in any of the animals. Daily weights did not reveal any abnormalities in food consumption. There was no abnormal swelling, skin irritation/infection or discoloration of the tissue around the implant, as shown in Figure 5.5.

5.3.2.1. *Biological responses and histology*

Practically, our fundamental aspects of the tissue response in this study included inflammatory and foreign body reactions as well as ultimately fibrous encapsulation. Therefore, two different crosslinked densities of the elastomer (PDET₁₀₀ and PDET₅₀) were implanted to assess the *in vivo* biocompatibility and to investigate the influence of the degradation rate on the magnitude of the biological reaction. Table 5.2 provides an overview of the nature and extent of observed tissue reactions after each implantation period. Based on the histological evaluation, the various cellular responses were rated as shown in the table. The sections were also examined for the presence of fibrin, the induction of vascularization, and the formation of a fibrous capsule around the implant.

As shown in Figure 5.6 (B, E, H) and Table 5.2, up to the second week of implantation, high concentrations of macrophages surrounded the implants and were clearly seen at 20x magnification and their amount was relatively high compared to that of sham surgery. As well, no significant difference in

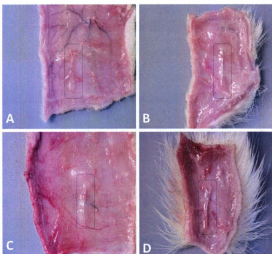


Figure 5.5. Elastomer implants as dissected along with soft tissue and skin around them. Images (A) and (B) show representative PDET₁₀₀ implants at 4 and 12 weeks respectively. Images (C) and (D) show representative PDET₅₀ implants at 4 and 12 weeks respectively. No necrosis, granulomas, or sign of dystrophic soft tissue calcification can be seen around any of the implants.

Table 5.2. Tissue reactions to PDET implanted samples of different degrees of acrylation and PLGA sutures.

Sample	Time (Week)	Macro-phages	Lympho-cytes	Eosino-phils	Neutro-phils	Giant cells	[†] Inflammatory cell score	[*] Fibrous Capsule Thickness (μm)
PDET ₁₀₀	1	+++	+	+	++	++	2.5	40 \pm 2.5
	2	+++	+	+	++	+	2.0	35 \pm 2.5
	4	++	++	-	+	+	1.0	30 \pm 2.5
	8	+	+	-	-	-	1.0	25 \pm 5.0
	12	+	+	-	-	-	0.5	25 \pm 5.0
PDET ₅₀	1	+++	+	-	+++	-	3.0	50 \pm 2.5
	2	+++	++	+	++	++	2.5	50 \pm 5.0
	4	+++	+++	-	+	+	1.5	35 \pm 5.0
	8	+++	++	-	+	+	1.5	35 \pm 5.0
	12	++	+	-	-	-	0.75	30 \pm 5.0
PLGA Suture	1	+++	++	+	+	+++	3.0	50 \pm 5.0
	2	+++	++	+	+	+++	2.5	45 \pm 2.5
	4	+++	++	+	-	+++	2.0	45 \pm 5.5
	8	+++	++	+	-	+++	2.0	45 \pm 2.5
	12	+++	+	-	-	++	1.0	20 \pm 2.5
Sham Surgery	1	+	+	+	+	+	1.0	-
	2	++	+	+	+	++	2.0	-
	4	+	-	+	-	++	1.0	-
	8	+	-	+	-	+	1.0	-
	12	-	-	-	-	+	1.0	-

[†] Scale for inflammatory cell infiltrate = 0-4.

- Not present; + to ++++ = sporadic to severe.

^{*} Fibrous capsule thickness was measured in the thickest part as the thickness around the implant was not uniform. The measurements represent mean \pm standard deviation (n=5 for both PDET₅₀ & PDET₁₀₀ and =3 for PLGA suture).

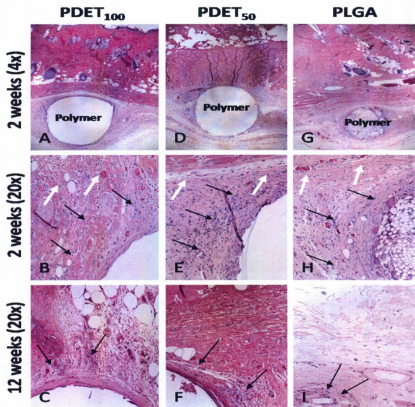


Figure 5.6. Representative histological images of the tissue surrounding cylindrical PDET elastomeric implants and PLGA sutures (control) showing macrophages (black arrows) and fibrin layer (white arrows) at the implantation site. PDET₁₀₀ implants after (A) 2 weeks at 4x magnification (B) 2 weeks at 20 x magnification and (C) 12 weeks at 20x magnification. PDET₅₀ implants after (D) 2 weeks at 4x magnification (E) 2 weeks at 20 x magnification and (F) 12 weeks at 20x magnification. PLGA implants after (G) 2 weeks at 4x magnification (H) 2 weeks at 20 x magnification and (I) 12 weeks at 20x magnification.

the number of macrophages could be found between the various implants. In the surrounding tissue of all implants, leukocytes such as eosinophils, neutrophils and lymphocytes were also detected in comparable levels to sham surgery, but the neutrophils were higher in the PDET implants than the PLGA samples. Basically, the presence of high concentration of leukocytes (predominantly neutrophils) indicates the presence of an acute inflammatory response to the tissues injury occurred during the surgical process of implantation. Neutrophils were chemotaxically emigrated or moved from the blood vessels to the perivascular tissues and the injury (implant) site, depending on the extent of injury and the size of implanted material. Thus, more neutrophils in the PDET than the PLGA might be attributed to the foreign material response as the major role of the neutrophils in acute inflammation is to phagocytose foreign materials. This is considered the normal wound healing response to implanted biomaterials. The acute inflammation was of relatively short duration and started to resolve after 2 weeks, as neutrophils have short lifetimes (hours to days) and disappear rapidly.

Following the localization of leukocytes at the implant site, in particular neutrophils, phagocytosis and the release of leukocyte enzymes started to occur in an attempt to phagocytose foreign materials. Although implants were not generally phagocytosed by neutrophils or macrophages because of the size disparity (i.e. the surface of the implant is greater than the size of the cell), frustrated phagocytosis might have occurred. This process did not involve engulfment of the implants but caused the increase of lymphocytes and macrophages as well as the extracellular release of leukocyte products in an attempt to degrade the implant. The accumulation of macrophages was the most important feature for foreign body giant cell formation. These giant cells most likely originated from fused macrophages and were an indication of normal foreign body reaction (Table 5.2).

At weeks 4 and 8, macrophages still surrounded all of the implants, however, the density of the macrophages started to diminish with PDET₁₀₀ samples showing lower macrophage density when compared with PDET₅₀ and PLGA. This relatively high number of macrophages seen in PDET₅₀ was not likely due to leachable products from the elastomers since their aliquots did not show any inhibition of cellular functions *in vitro* (Figures 5.3 and 5.4). A possible explanation might be the relative faster rate of PDET₅₀ degradation when compared to PDET₁₀₀, keeping high numbers of macrophages around the implant site in an attempt to phagocytose the degradation products. Neutrophils and eosinophils started to disappear which were mostly replaced by monocytes that differentiate into macrophages. The giant cells also started to decrease in number with the implanted elastomers at week 4 and reached to the same density or below that of sham surgery, nonetheless, in case of implanted PLGA sutures they continued to stay at high levels. By week 8 and 12, the giant cells had virtually disappeared around PDET₅₀ and PDET₁₀₀ implants, respectively.

By 12 weeks (Figure 6 C, F, I), the PLGA suture was completely absorbed and couldn't be detected, nonetheless, macrophages and giant cells were present in the area where originally the PLGA suture had been implanted. All of the PDET implants were still surrounded by macrophages compared to sham surgery but less than the PLGA suture implant site. All implanted samples showed considerably lower leukocytes density at week 12 compared to 1 or 2 weeks post implantation, although, there was no considerable number of eosinophils or neutrophils observed in all implants. There were very few numbers of lymphocytes, compared to 4 weeks, in the vicinity of implanted elastomer specimens, an amount which is quite similar to that of the PLGA suture. These remaining lymphocytes and macrophages were an indicator of chronic inflammatory or immune response due to persistent inflammatory stimuli confined to the implant site.

Within one week following implantation, the healing response, initiated by the action of macrophages, was followed by proliferation of fibroblasts and vascular endothelial cells at the implant site. Mature fibroblasts were found to form similar distinct fibrous capsules (vascular collagen layer) around both PDET elastomers and the PLGA suture within the first week. As the capsule thickness was unequal around the implant, measurements were taken at the thickest part of the capsule. Actually, the foreign body reaction with granulation tissue development is considered the normal wound healing response to implanted biomaterials (i.e. the normal foreign body reaction).

5.3.5. *In vitro* and *In vivo* Degradation

The *in vitro* and *in vivo* percentage weight loss of the elastomers versus degradation time is shown in Figure 5.7. As can be seen, the percentage weight loss of the elastomers reported both *in vitro* and *in vivo* was inversely proportional to the crosslink density of the prepared elastomers (Table 5.1).¹⁶

The PDET₅₀ elastomers underwent weight loss at a faster rate (3.20 %/day and 2.47%/day *in vivo* and *in vitro*, respectively) than the PDET₁₀₀ elastomers (1.85%/day and 1.22%/day *in vivo* and *in vitro*, respectively), indicating that the crosslink density of the elastomer contributes to its degradation rate and behavior. For both crosslink densities, a significant increase in the degradation rate was found to take place *in vivo* when compared to that observed *in vitro*. By 12 weeks, the *in vivo* experiments showed that mass loss was approximately 38.4±3.9 % and 22.1±3.6 % for PDET₅₀ and PDET₁₀₀, respectively. However in the *in vitro* system, elastomer degradation appeared to be slower, having only lost 29.6±0.8 % and 14.6±0.6 % of their initial mass for PDET₅₀ and PDET₁₀₀, respectively.

To determine the kinetics of the changes in the mechanical properties of the elastomers (Young's modulus, *E*, tensile stress at break, σ , and strain at break, ϵ), the *in vitro* and *in vivo* degradations of the PDET elastomers were investigated (Figure 5.8 and Table 5.3). The results revealed that for both *in vitro*

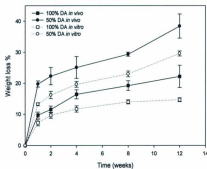


Figure 5.7. Degradation studies of PDET elastomers of different degrees of acrylation. (A) *In vitro* and *in vivo* percentage weight loss versus time. (B) *In vitro* and *in vivo* percentage water absorption versus time. Each point represents mean \pm SD ($n = 3$).

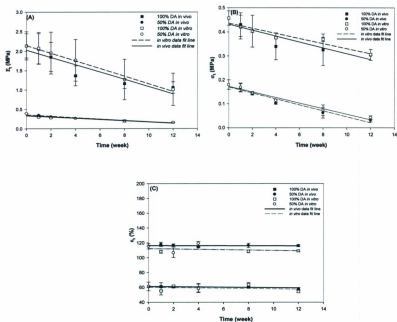


Figure 5.8. Changes in mechanical properties of PDET₁₀₀ and PDET₅₀ elastomers during *in vivo* and *in vitro* degradation. (A) Young's modulus at time t , E_t (B) Ultimate tensile stress at time t , σ_t (C) Ultimate tensile strain at time t , ϵ_t . Lines on the figures are fitted curves to zero-order degradation kinetics equation. Each point represents mean \pm SD ($n = 3$). Kinetics parameters and linear regression coefficients are reported in table 2.

Table 5.3. Zero-order kinetic parameters and linear regression coefficients of the changes in the mechanical data for PDET elastomers during *in vitro* and *in vivo* degradation studies.

	Elastomer	E_s (MPa)	K_E (MPa/Week)	R^2	σ_0 (MPa)	K_σ (MPa/Week)	R^2
<i>in vivo</i>	PDET ₁₀₀	2.031	0.0942	0.981	0.432	0.0122	0.969
	PDET ₅₀	0.339	0.0162	0.978	0.173	0.0117	0.979
<i>in vitro</i>	PDET ₁₀₀	2.149	0.0989	0.966	0.436	0.0106	0.933
	PDET ₅₀	0.362	0.0185	0.989	0.170	0.0125	0.972

and *in vivo* degradation, the changes in the mechanical properties with respect to time followed the same pattern of degradation and were significantly dependent ($p < 0.001$) on the degree of acrylation of the PDET elastomer. Although the elastomers showed a decrease in their mechanical strength with time, they maintained their original shape and extensibility over the testing period, *in vivo* as well as *in vitro*.

In both *in vivo* and *in vitro* studies, the measured values of E (Figure 5.8A) as well as σ (Figure 5.8 B) decreased with time in a linear fashion as an indicative of a zero-order degradation mechanism. This linear decrease was observed regardless of the network composition, the crosslinking density and the initial E and σ of the elastomers. On the other hand, the change in ϵ was less sensitive to the degradation of those elastomers and no significant changes in ϵ values during the *in vivo* and *in vitro* degradation period were observed (Figure 5.8 C). These results confirmed that the *in vivo* hydrolytic degradation of these elastomers followed a bulk erosion mechanism resembling the *in vitro* behavior, as we reported previously.¹⁶ It is only with a surface erosion degradation pattern that the elastomers can maintain their mechanical properties unchanged.¹⁶

Through a linear regression of the zero-order degradation kinetics of the data in Fig. 5.8 A & 5.8 B using equations (1) & (2), the rate constants were calculated and are listed in Table 5.3.

$$E_t = E_0 - K_E t \quad (1)$$

$$\sigma_t = \sigma_0 - K_\sigma t \quad (2)$$

In equations 1 & 2, t denoted the degradation time (in weeks). The values of E_0 and σ_0 corresponded to the intercepts obtained from extrapolating the zero-order fitted line. K_σ and K_E represented the zero-order degradation constants for Young's modulus and the ultimate tensile stress, respectively.

For the *in vivo* degradation of PDET₁₀₀, E as well as σ decreased linearly with time (correlation coefficient, R^2 , of 0.981 and 0.969, respectively). The rate constants for the decrease in E (K_E) and σ

(K_σ) were 0.0942 and 0.0122 MPa/Week, respectively. PDET₅₀ *in vivo* degradation also exhibited a linear decrease in E and σ with time ($R^2 = 0.978$ and 0.979 , respectively). The rate constants for the decrease in σ was nearly the same as PDET₁₀₀ ($K_\sigma = 0.0117$ MPa/Week), while the decrease rate constants in E was slower than that of PDET₁₀₀ ($K_E = 0.0162$ MPa/Week).

5.4. DISCUSSION

We have previously conducted a preliminary cytocompatibility study by incubating intact elastomers with fibroblast cells for 24 hrs and examined cell morphology and density for any signs of cytotoxicity.¹⁶ Those results showed that PDT elastomers could function without causing adverse cellular effects, but those results only indicated cytocompatibility with a cell line after short term contact time. Therefore, one of the objectives of this study was to assess the effects on cell viability and proliferation ability in the presence of elastomer degradation products, to further investigate the *in vitro* cytotoxicity profile of the PDET elastomers.

While the choice of the cell line used for cytotoxicity testing remains controversial and a vast number of cell lines have been used, we chose a phenotypically normal cell line, Mv1Lu, because of its high sensitivity to replication inhibitors and stimulators¹⁹ and its relevance as a non-transformed epithelial cell, thereby serving as a useful model system for the study of cytotoxicity on cell proliferation.²⁰ The MTT assay was chosen because it measures the metabolic activity of cells, although it has been extrapolated for use as a measure of cellular proliferation. This assay has also been recently developed as an effective method for preliminary screening of *in vitro* cytotoxicity of polymeric biomaterials.²¹ To measure effects on DNA replication of cells after exposure to polymer degradation products, we chose to use ³H-thymidine incorporation assay, one of the most common methods to determine cell viability or cytotoxicity. The method is as sensitive as the 5-bromo-2-deoxyuridine

(BrdU) incorporation assay and traditionally used as a sensitive screening for *in vitro* toxicity of new biomaterials.²² As the results clearly illustrate (Figures 5.3 and 5.4), the response of epithelial cells treated with the degradation product of PDET elastomers, with different degrees of acrylation, demonstrate the ability of the cells to interact favorably with this new biomaterial as verified by maintenance of metabolic activity and proliferation when compared to control cells.

From a practical perspective, the *in vivo* assessment of tissue compatibility is carried out to investigate the possible biological and/or immunological events, indicating an adverse tissue response to the presence of the implant, that could accompany the *in vivo* application and result in implant failure. Elastomer microcylinders were implanted subcutaneously into rats, with the main intent to identify any local responses of the living tissue to these implants, as well as the response of the implants to the living system by evaluations under conditions simulating clinical use. In this study, biodegradable PLGA (poly L-lactide-co- 30% glycolide) was chosen as a control biomaterial for *in vivo* biocompatibility because of its ubiquitous uses in a variety of Food and Drug Administration (FDA) approved therapeutic devices and due to its well reported biocompatibility.

As shown in Figure 5.5, the mild local tissue responses were confirmed by the lack of necrosis, granulomas, or signs of dystrophic soft tissue calcification around any of the investigated specimens when observed daily throughout the study. A mild to moderate inflammatory response characterized by an initial increase of leukocytes was localized to the vicinity of the implants, a response that is expected and consistent with the introduction of a foreign material into the body. Usually, the normal foreign body reaction is consisting mainly of macrophages and/or foreign body giant cells that may persist at the tissue-implant interface for the lifetime of the implant. Therefore, leukocytes (predominantly

macrophages, neutrophils, lymphocytes and giant cells) were the predominant inflammatory cell type present as an indicative marker of acute inflammatory response. They were found to be very close to all of the implant-tissue interfaces and were most notable during the first 1-4 weeks post-implantation and remained up to week 12 of the study. However, their densities were reduced considerably for PDET₁₀₀ by 4 weeks, while for PDET₅₀, the macrophage density had diminished by 8 weeks compared to the PLGA implant.

This above discussion indicates that implantation of PDET elastomers was associated with an acute inflammatory response as shown by the high amount of leukocytes followed by a chronic inflammation as indicated by the remaining cells through the 12 weeks of the test.^{23,24} Our observations are similar to the immune reactions seen with other absorbable materials, such as crosslinked dermal sheep collagen²⁵, tyrosine-derived polymers²⁶ and matrices of polylactic acid and polyglycolic acid. In those models, the severity of inflammation decreased upon decreasing degradation rate.²⁷

It is known that the formation of the multinucleated giant cells occurs as a common response towards a biodegradable material as these cells participate in the overall biodegradation process and often contained fragments of the degradation products. Although the nature of the initial tissue response for the PDET elastomers and that of the PLGA control was quite similar, the giant cells were considerably less around PDET elastomer implants during the 2nd to 8th week of implantation. This observation can be attributed to the fact that PDET elastomers appeared to remain stable *in vivo* for a much longer time than the PLGA suture which was found to be completely absorbed by the week 12 of the implantation period. At 12 week post-implantation, giant cells had disappeared from all implants but

not from control samples (PLGA suture), even though a complete absorption of the PLGA suture had occurred. Such a response was also observed previously with polylactic and polyglycolic acid matrices.²⁷

In part, the body reaction to PDET elastomers and PLGA produced thin vascularized fibrous capsules within the first week of implantation. The overall thickness of these capsules appeared to become thinner over time as reported in Table 5.2. This is similar to the response observed with other polymeric absorbable materials upon implantation.²⁵⁻²⁷ Some newly formed blood vessels and capillaries were seen located between the capsule layer and soft tissue, regardless of the implant type. The number of these blood capillaries as well as the leukocyte number diminished over the implantation time. There was, however, a significant decrease in thickness with PLGA suture at 12 weeks as the suture was completely absorbed. Therefore, it is expected that the complete disappearance of collagen layer at the implant site would restore its histological architecture after complete absorption of PDET elastomers implant, as a classical end-stage of fibrous capsules.²⁸ All of these observed tissue responses indicated that the PDET elastomers are able to coexist with subcutaneous tissues without causing harm, regardless of the time period of implantation and therefore can be considered biocompatible. In addition, there were not any qualitative differences in histology between PDET₁₀₀ and PDET₅₀ specimens that could be detected under the light microscope and differential staining methods.

The examined *in vivo* and *in vitro* changes in the physical and mechanical properties of the PDET have revealed the following. First, a marked increase in the *in vivo* degradation rate has been noticed when compared to that observed *in vitro* over the twelve week of implantation. This is likely due to the acute-inflammatory response *in vivo* and reasonably to a greater degree of solubility of the degradation products present at the surface in the *in vivo* aqueous environment.²⁴ Second, the elastomers did not

absorb as much water during the *in vivo* degradation period as in the *in vitro* period, but rather shrunk slightly or remained at their nearly initial weight and volume. This observed behavior was independent of the crosslink density used. This is a useful finding as it indicates that the elastomers maintained their geometry and stability *in vivo* during the degradation period, a factor which is important for their use in drug delivery and mechanically challenged implantable devices. Third, although the implants were encapsulated by fibrous tissue *in vivo*, the pattern of the changes in the mechanical properties with time was essentially the same *in vivo* as *in vitro*. These results were consistent with what has been reported earlier for uncrosslinked²⁹ and crosslinked³⁰ aliphatic polyesters. The mechanical properties of the elastomers decreased at the same rate and to the same extent *in vivo* as was observed *in vitro*, and were mainly dependent on the crosslink density of the elastomer (Figure 5.8 and Table 5.3). We have previously reported that Young's modulus of the elastomers depended mainly on the crosslinking density while the ultimate tensile stress depended on the distribution of end to end distances between crosslink points within the matrix.¹⁶ As well, it is well known that biodegradation (either *in vivo* or *in vitro*) occurred by the hydrolysis of the ester bond in the end to end distance between crosslinks. As such, PDET₁₀₀ with higher crosslinking density demonstrated faster decline in the Young's modulus compared to PDET₅₀ with lower crosslinking density, while, the ultimate tensile stress for both decline at the same rate.

Finally, it cannot be overlooked that neither the *in vitro* nor the *in vivo* degradation conditions in this study represent a perfect sink for dissolving or absorbing the elastomer degradation products and removing them from the site of degradation. As well, the structure and nature of the degradation products are likely to be different between *in vivo* and *in vitro* as well as for each degree of acrylation as a result of their different crosslinking density. However, from a practical standpoint, this close

correlation between *in vitro* and *in vivo* degradation is useful in terms of designing long-term resorbable matrices using these elastomers, for controlled drug delivery and tissue engineering applications.

5.6. CONCLUSIONS

In this study, we reported on the results of the cytotoxicity, biocompatibility and biodegradability of PDET elastomers, one of our previously developed and characterized novel biodegradable polyesters, as determined in an *in vitro* and *in vivo* system. We have demonstrated that PDET elastomers, with different degrees of acrylation, showed promising cytotoxicity results with Mv1Lu cells and received reasonably consistent results between the two common cell viability assays (MTT and thymidine incorporation). We also have shown *in vivo* justification to confirm the potential of these elastomers as soft-tissue friendly materials as well as the candidacy of these elastomers as biodegradable biomaterials on long run. We have also demonstrated that PDET elastomers, with different degrees of acrylation degrade at different rates within the body and therefore elastomer selection can be tailored to achieve the desired implantation period and release rates. All the collected data are enabling properties for PDET elastomers, which make them potentially suitable as a developed resorbable matrix for medical devices use in long-term pharmaceutical delivery. Promising results regarding osmotic-driven controlled release and stability of papaverine hydrochloride from PDET matrices have already been achieved.⁶

5.7. REFERENCES

- 1- Amsden BG, Misra G, Gu F, Younes HM. 2004. Synthesis and characterization of a photocross-linked biodegradable elastomer. *Biomacromolecules* 5:2479-2486.
- 2- Gu F, Younes HM, El-Kadi AO, Neufeld RJ, Amsden BG. 2005. Sustained interferon-gamma delivery from a photocrosslinked biodegradable elastomer. *J Control Release* 102: 607-617.

- 3- Wada R, Hyon SH, Nakamura T, Ikada Y. 1991. *In vitro* evaluation of sustained drug release from biodegradable elastomer. *Pharm Res* 8: 1292-1296.
- 4- Guan J, Stankus JJ, Wagner WR. 2007. Biodegradable elastomeric scaffolds with basic fibroblast growth factor release. *J Control Release* 120: 70-78.
- 5- Jeong SI, Kim BS, Kang SW, Kwon JH, Lee YM, Kim SH, Kim YH. 2004. *In vivo* biocompatibility and degradation behavior of elastic poly(L-lactide-co-epsilon-caprolactone) scaffolds. *Biomaterials* 25: 5939-5946.
- 6- Shaker MA, Younes HM. 2010. Osmotic-Driven Release of Papaverine Hydrochloride from Novel Biodegradable Poly(Decane-co-tricarballylate) Elastomeric Matrices. *Therapeutic Delivery* 1: 37-50.
- 7- Younes HM, Bravo-Grimaldo E, Amsden BG. 2004. Synthesis, characterization and *in vitro* degradation of a biodegradable elastomer. *Biomaterials* 25: 5261-5269.
- 8- Borzacchiello A, Ambrosio L, Nicolais L, Huang SJ. 2000. Synthesis and characterization of saturated and unsaturated poly(alkylene tartrate)s and further cross-linking. *J Bioact Compat Pol* 15:60-71.
- 9- Wang Y, Ameer GA, Sheppard BJ, Langer R. 2002. A tough biodegradable elastomer. *Nat Biotechnol* 20:602-606.
- 10- Yang J, Motlagh D, Webb AR, Ameer GA. 2005. Novel biphasic elastomeric scaffold for small-diameter blood vessel tissue engineering. *Tissue Eng* 11: 1876-86.
- 11- Lijuan L, Tao D, Rui S, Quanyong L, Liqun Z, Dafu C, Wei T. 2007. Synthesis, characterization and *in vitro* degradation of a novel degradable poly((1,2-propanediol-sebacate)-citrate) bioelastomer. *Polymer Degradation and Stability* 92: 389-96.
- 12- Bruggeman JP, De Bruin BJ, Bettinger CJ, Langer R. 2008. Biodegradable poly(polyol sebacate) polymers. *Biomaterials* 29: 4726-4735.
- 13- Bettinger J, Bruggeman JP, Borenstein JT, Langer RS. 2008. Amino alcohol-based degradable poly(ester amide) elastomers. *Biomaterials* 29: 2315-2325.
- 14- Ifkovits JL, Padera RF, Burdick JA. 2008. Biodegradable and radically polymerized elastomers with enhanced processing capabilities. *Biomed Mater* 3:034104.
- 15- Younes H M, Ellaboudy H, Shaker M A. 2008. Biodegradable elastomers prepared by the condensation of an organic di-, tri- or tetra-carboxylic acid and an organic diol. *International Patent No. 144881 A1*.

- 16-Shaker MA, Doré JE, Younes HM. 2010. Synthesis, characterization and cytocompatibility of poly(diol-tricarballoylate) visible light photo-crosslinked biodegradable elastomer. *J Biomater Sci* 21:507-28.
- 17- Shaker MA, Younes HM. Sustained interleukin-2 delivery from photocrosslinked biodegradable poly(decane-co-tricarballoylate) elastomer. Submitted to *J Controlled Release*.
- 18- Vile GF, Tyrrell RM. 1995. UVA radiation-induced oxidative damage to lipids and proteins *in vitro* and in human skin fibroblasts is dependent on iron and singlet oxygen. *Free Radic Biol Med* 18: 721-730.
- 19-Kim MS, Ahn SM, Moon A. 2002. *In vitro* bioassay for transforming growth factor-beta using XTT method. *Arch Pharm Res* 25:903-909.
- 20-Serini S, Trombino S, Oliva F, Piccioni E, Monego G, Resci F, Boninsegna A, Picci N, Ranelletti FO, Calviello G. 2008. Docosahexaenoic acid induces apoptosis in lung cancer cells by increasing MKP-1 and down-regulating p-ERK1/2 and p-p38 expression. *Apoptosis* 13: 1172-1183.
- 21-Ciapetti G, Cenni E, Pratelli L, Pizzoferrato A. 1993. *In vitro* evaluation of cell/biomaterial interaction by MTT assay. *Biomaterials* 14: 359-364.
- 22- Mansurva LA, Skorniakova AB, Kazimirovskaja VB, Trofimov VV, Slutskii LI, Voronkov MG. 1996. Biocompatible properties of implantable polymeric materials *Dokl Akad Nauk* 350: 408-410.
- 23-Osborn JF. 1979. Biomaterials and their application to implantation. *SSO Schweiz Monatsschr Zahnheilkd* 89: 1138-9.
- 24-Suggs LJ, Shive MS, Garcia CA, Anderson JM, Miko AG. 1999. *In vitro* cytotoxicity and *in vivo* biocompatibility of poly(propylene fumarate-co-ethylene glycol) hydrogels. *J Biomed Mater Res* 46: 22-32.
- 25-van Wachem PB, van Luyn MJ, Olde Damink LH, Dijkstra PJ, Feijen J, Nieuwenhuis P. 1994. Biocompatibility and tissue regenerating capacity of crosslinked dermal sheep collagen. *J Biomed Mater Res* 28: 353-363.
- 26-Hooper KA, Macon ND, Kohn J. 1998. Comparative histological evaluation of new tyrosine-derived polymers and poly(L-lactic acid) as a function of polymer degradation 1. *J Biomed Mater Res* 41: 443-454.
- 27-Holder WD, Gruber HE, Moore AL, Culberson CR, Anderson W, Burg KJ, Mooney DJ. 1998. Cellular ingrowth and thickness changes in poly-L-lactide and polyglycolide matrices implanted subcutaneously in the rat. *J Biomed Mater Res* 41: 412-421.

- 28- Dee KC, Puleo DA, Bizios R. Wound healing. 2002. In: An introduction to tissue-biomaterial interactions. New Jersey: John Wiley & Sons Inc.p165-214.
- 29- Weir NA, Buchanan FJ, Orr JF, Dickson GR. 2004. Degradation of poly-L-lactide. Part 1: *in vitro* and *in vivo* physiological temperature degradation. Proc Inst Mech Eng H 218: 307-319.
- 30- Woodward SC, Brewer PS, Moatamed F, Schindler A, Pitt CG. 1985. The intracellular degradation of poly(epsilon-caprolactone). J Biomed Mater Res19:437-444.

CHAPTER 6

Sustained Interleukin-2 Delivery from Photocrosslinked Biodegradable Poly(decane-co- tricarballylate) Elastomer

The content of this chapter is to be submitted to the Journal of Controlled Release

Mohamed A. Shaker and Husam M. Younes

ABSTRACT

One of the main challenges in interleukin-2 (IL-2) cancer immunotherapy is achieving localized and efficient delivery over a sustained period of time with proper maintenance of its stability and bioactivity. In the present study, new biodegradable elastomeric poly(decane-co-tricarballoylate) [PDET] matrices which utilize the osmotic-driven-controlled release mechanism were designed in an attempt to overcome these stability and bioactivity challenges facing IL-2 delivery. Elastomer synthesis was achieved by polycondensation reaction between tricarballoylic acid and alkylene diols, followed by acrylation and photo-curing. IL-2 loaded micro-cylinder and disk-shaped elastomers were prepared by intimately mixing lyophilized IL-2 powder with the acrylated prepolymer prior to photocrosslinking. IL-2 release was analyzed using IL-2 enzyme-linked immunosorbent assay method and the *in vitro* bioactivity of released IL-2 was assessed using C57BL/6 mouse cytotoxic T lymphocyte. The influence of various parameters such as the elastomer crosslinking density, the volumetric loading percentage and the incorporation of osmotic excipients like trehalose on the release kinetics of the drug was also examined. The disk-shaped specimens showed faster controlled IL-2 release profiles than microcylinders, with drug release proceeding via typical zero-order release kinetics. The increase in the device's surface area and the incorporation of trehalose in the loaded lyophilized mix increased the IL-2 release rate. As well, it was shown that the decrease in the degree of prepolymer acrylation of the prepared devices increased the IL-2 release rate. Cell based bioactivity assay for IL-2 over a release period of 28 days showed that the released IL-2 retained more than 94% of its initial activity. The new PDET elastomers demonstrated to be promising as a protein drug delivery vehicle for localized and sustained IL-2 immunotherapy.

6.1. INTRODUCTION

Interleukin-2 (IL-2) is a cytokine messenger protein that plays an important role in the activation of cell-mediated immunotherapy against cancer.^{1,2} IL-2 is currently indicated for systemic administration via multiple injection regimens to treat a number of different types of cancer diseases such as metastatic melanoma,³ kidney carcinoma,⁴ as well as surgical minimal residual tumor disease after cancer resection surgery,⁵ or the use of chemotherapy.⁶ Systemic IL-2 therapy has always been associated with rapid clearance and life-threatening toxicities that restrict its full clinical relevance.⁷ Loco-regional IL-2 delivery, however, is used to localize IL-2 actions and activities into the vicinity of tumors and can result in an improved therapeutic outcome with much less side effects or toxicity.⁸ Although, the effectiveness of local IL-2 delivery system has been extensively investigated and approved for the use in the treatment of a broad range of solid tumors,^{8,9} IL-2 still possesses many stability problems that challenge its bioactivity with the formulation approaches. Firstly, IL-2 molecule is sensitive to acidic conditions ($\text{pH} \leq 2.1$) as it contains one intramolecular critical disulphide bridge linkage between cysteine amino acid at positions 58 and 105, that is essential for maintaining the stability of the tertiary structure and subsequently the biological activity.^{10,11} Secondly, as with many other therapeutic proteins, IL-2 is heat sensitive and undergoes irreversible thermal denaturation and aggregation in solution at temperature exceeding 44°C.¹² Furthermore, IL-2 is subject to unfolding and formation of compact denaturated hydrophobic clusters (aggregation) with subsequent loss of activity when present for a relatively long time and in high concentrations in aqueous solution.¹¹

In spite of the aforementioned challenges, extensive research has focused on the development of drug delivery systems capable of achieving sustained and localized delivery of IL-2. Such delivery systems include but are not restricted to the use of liposomes,¹³ hydrogels,¹⁴ polymeric

microspheres/nanospheres,^{15,16} thermo responsive synthetic polymers (ReGel®),¹⁷ and injectable polymeric controlled release systems (Medusa II®).¹⁸ An extensive evaluation of the different routes of administration and formulation approaches utilized for the delivery of IL-2 has recently been reviewed and the reader is strongly advised to refer to that review for detailed discussion related to advantages and limitations of each of those IL-2 delivery systems.¹⁹ One of the most recently used strategies for localized therapeutic protein delivery was achieved by dispersing the protein mixed with osmotic excipients inside implantable biodegradable polymers and relying on the osmotic-rupture mechanism as the predominant mechanism for achieving constant zero-order release.²⁰⁻²² These polymeric devices were prepared by UV photo-crosslinking of an acrylated star-poly(ϵ -caprolactone-co-D,L-lactide) prepolymers,²⁰ acrylated poly(octane- tartarate)²³ or trimethylene carbonate copolymerized with D,L-lactide and ϵ -caprolactone based elastomer.²⁴ Although the mechanism of osmotic-driven release offered distinct and practical advantages over other means of delivery, there were a number of issues which have an impact on the stability and activity profiles of loaded proteins. Mainly, the use of organic solvent during the formulation may change the protein conformation.^{25,26} In addition, the use of ultra-violet radiation during the photocuring was reported to denature proteins and consequently result in loss of their biological activity.²⁵

We have recently reported on the synthesis, characterization, biodegradation and biocompatibility of a novel family of amorphous photocurable poly(diols-co-tricarballoylate) elastomers²⁶ and their use in the controlled-release of small molecule drugs.²⁷ These newly synthesized elastomers also exhibited many characteristics which make them a promising matrix to overcome the aforementioned stability and activity challenges facing the delivery of therapeutic proteins.^{26,27} Firstly, protein drug loading was achieved in a solventless manner which helped in preventing possible drug denaturation and precipitation due to its exposure to organic solvents and disruption of protein hydrophobic interactions.²⁶

Secondly, the use of visible-light crosslinking helped in eliminating many of the drawbacks associated with using UV photocuring by making the polymerization conditions sufficiently mild to be carried out in the presence of sensitive biological materials like proteins.^{25,26} Additionally, visible light was able to penetrate deeper through tissues than UV light (less scattering and less absorption). This property may limit the need for invasive surgical procedures by allowing trans-tissue polymerizations, whereby the material is injected subcutaneously or even subdermally and irradiated through the skin to polymerize the material *in situ*.²⁶ Thirdly, it was shown that osmotic-driven controlled release of drugs from these new elastomeric matrices is linear, constant and controllable.²⁷ Finally, the use of a slowly hydrolysable copolymer such as poly(decane-co-tricarbalylate) [PDET] would reduce or eliminate the production of acidic monomers/oligomers within the elastomers until the vast majority of the loaded protein is released, via the osmotic-rupture mechanism, before any significant reduction in the mechanical properties of the elastomer occurs due to its hydrolysis.^{26,28} A description for the proposed controlled release of IL-2 via the osmotic-rupture mechanism is illustrated in Figure 6.1 and described as follows: The drug particles located on the surface dissolve and produce an initial burst effect, accounting for up to 15% of the initially loaded drug, followed by a slow release period, predominant osmotic driven mechanism. This slow release depends on the rate of degradation of the polymer when the polymer is degradable and/or the rate of formation of cracks and interconnected pores resulting from water imbibition into the polymer.^{22,27} When the elastomer degradation rate is slow enough to maintain the implant's geometry and mechanical properties (extension ratio) during the release period, the osmotic-driven mechanism will dominate the linear controlled-release and polymer degradation will play only a minor role in the overall release pattern.^{21,27}

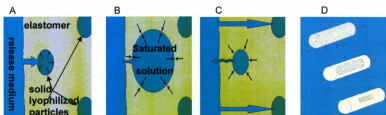


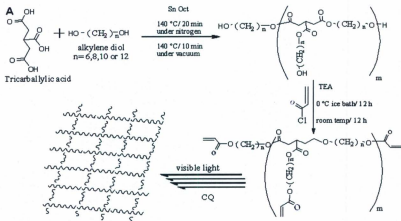
Figure 6.1. Schematic representation of osmotic swelling, rupture and release mechanism A) water diffusion through the elastomer reach to the first layer of encapsulated drug particles. B) the imbibed water dissolves the solid drug at solid polymer interface, creating a saturated solution surrounding elastomer, causes it to swell and exert pressure on the inside wall. C) the pressure causes micro-cracks to form in the elastomer and the dissolved protein/excipients content is then released. The process is repeated with the subsequent layer of particle which leads to interconnected network formation. D) the osmotic release from a cylinder shape elastomer.

The purpose of the present study, therefore, is to further investigate the use of this new family of synthesized photo-cured PDET biodegradable elastomers as controlled release matrices for therapeutic proteins and their ability to maintain the stability and bioactivity of loaded IL-2 during loading and preparation stages and after drug release.

6.2. EXPERIMENTAL

6.2.1. Materials

Chemicals used in elastomer synthesis and purification include tricarballic acid (99%), 1,10-decanediol (98%), stannous 2-ethylhexanoate (95%), 4-dimethylamino pyridine (99%), acryloyl chloride (96%), triethyl amine (99%), sodium sulphate ($\geq 99\%$) and champhore-quinone(97%) were purchased from Aldrich-Sigma chemical company, Canada. Solvents used in the purification of the synthesized prepolymers and acrylated prepolymers include ethyl ether (99%) acetone (99%) and chloroform (99%) were purchased from Caledone chemical company, Canada. For the release study, recombinant murine interleukin 2 (rmIL-2) and rmIL-2 ELISA kit were purchased from Peprotech Inc., Canada. Trehalose dihydrate, bovine serum albumin and ABTs liquid substrate system for ELISA were obtained from Sigma, Canada. Chemicals used in calorimetric assays include phenol (99%), sulfuric acid (95-98%) obtained from Fischer, Canada, and Pierce BCA protein assay kit was obtained from thermo scientific, Canada. For the bioactivity assay, Dulbecco's phosphate buffer saline, GIBCO® RPMI medium 1640, penicillin and streptomycin were obtained from Invetrogen, Canada and Rat T-STIM with Concanavalin A was purchase from BD biosciences, Canada. MTT cell Proliferation Kit was purchased from Roche, Canada. All chemicals were used as received without any further purification.



B

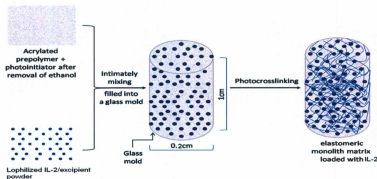


Figure 6.2. Schematic illustration of the synthesis, acrylation and photocuring of poly(decane-tricarballylate). The step-reaction polymerization of tricarballic acid and decane diol was catalyzed by stannous 2-ethylhexanoate. The acrylation was done by reacting with acryloyl chloride in the presence of triethylamine. To photo-crosslink, acrylated prepolymer was mixed with the photoinitiator, poured into a sealed glass mold and crosslinked under visible light (40mW/cm²).

6.2.2. Synthesis and Characterization of Acrylated Poly(decane-co-tricarallylate) Prepolymer

Acrylated PDET was synthesized according to the previously described method in chapter 3 (section 3.2.2.) which is illustrated in Figure 6.2.²⁶ The final purified product was characterized using proton nuclear magnetic resonance (¹H-NMR) to confirm the final product's purity and the signal intensity of the methylene groups of diol (1.3-1.7 ppm) and the acrylate group' intensities (5.8-6.4 ppm) were used to calculate the degree of acrylation in the prepolymers.²⁶

6.2.3. Elastomeric Matrices Preparation and Characterization

The photocuring process was carried out in a dark fume hood equipped with sodium lamp. On a watch glass, 5 µl of 10 % ethanolic solution of both camphorquinone and triethanolamine (equivalent to 0.01% (w/w)) photoinitiator was added to 5 grams of the acrylated prepolymer. The mix was then left at 40 °C under vacuum for 1 hr to ensure complete removal of any traces of alcohol from the photoinitiator solutions. The mix was then poured into the bottom of a sealed cylindrical silanized glass mould of 1 cm in length and 2 mm in diameter. The mould was then exposed to a visible light source (450-550 nm at a 40 mW/cm²) filtered from a 50 Watt tungsten-halogen lamp (Taewoo Co., Korea) for 10 minutes at a distance of 10 cm to form the elastomer which was then removed from the mould for further testing. The tensile mechanical properties of elastomeric cylinders (1.5 cm in length and 2 mm in diameter) were tested using an Instron model In-Spec 2200 tester equipped with 500 N load cells and run by Merlin Data Management Software. The sample was pulled at a rate of 1.0 mm/sec and elongated to failure. Values were converted to stress-strain and plotted. Young's modulus was calculated from the initial slope of the stress-strain curve.

For *in vitro* degradation, PDET₁₀₀ and PDET₅₀ cylinder-shaped samples (1 cm in length and 2 mm in diameter) of known weight (*W1*) were placed in 20 ml scintillation vials containing 15 ml PBS (pH=7.4) and 0.01% of sodium azide. The vials were placed in an oven at 37 °C for up to 12 weeks. The buffer was replaced daily to ensure a constant pH of 7.4. After 1, 2, 4 and 8 weeks, the cylinders were removed, blotted dry, weighed after wiping the surface water with filter paper to determine the swollen weight (*W2*). The samples were dried at room temperature for a week and the dried mass (*W3*) was then measured. The water absorption & weight loss were calculated as follows:

$$\text{Weight loss \%} = [(W1 - W3) / W1] \times 100.$$

$$\text{Water absorption \%} = [(W2 - W3) / W3] \times 100.$$

6.2.4. Preparation of IL-2 Loaded Elastomeric Delivery Systems

Recombinant murine IL-2 (rmIL-2) was first co-lyophilized with different ratios of trehalose (TH) and bovine serum albumin (BSA) in 10 mM sodium citrate, pH=4. Various amounts of rmIL-2, trehalose and BSA were used, while keeping the ratio of rmIL-2 to the total of TH and BSA 1:10, unless otherwise stated. The formulation solution was lyophilized and the obtained solid was ground into fine powder using a glass mortar and a pestle and then sieved through a 45 µm mesh using CSC sieve shaker. The sieved protein particles were intimately mixed with the acrylated PDET prepolymer by gently vortexing and photocrosslinked as per the procedure described above. For the micro-cylinder samples, the photocrosslinking was carried out in a cylindrical glass mould of 1 cm in length and 2 mm in diameter. On the other hand, disk sample photocrosslinking was carried out in disk shape teflon moulds of 1 cm in diameter and 1 mm in the thickness. Each prepared IL-2 loaded cylinder was weighed and the amount of IL-2, albumin and trehalose in each were calculated. Cylindrical devices had an average

weight of 20 ± 1.2 mg, while the disk-shaped devices had an average weight of 40.0 ± 2.7 mg. The volumetric loading of the lyophilized protein/excipient was 2, 10 and 20% of the elastomer volume to ensure that the drug loading was below the percolation threshold.

6.2.5. Effect of Formulation Conditions on the IL-2 Bioactivity

To determine whether IL-2 maintained its bioactivity during the formulation and analysis condition, in triplicate, known amount of IL-2 solid particles with different TH/BSA mass ratio were dissolved in PBS and the solutions of each TH/BSA mass ratio were divided into three equal aliquots. To examine the photocuring effect, in the first part 10 % ethanolic solution of both camphorquinone and triethanolamine (equivalent to 0.01% (w/v)) was added and the solution exposed to a visible light source (450-550 nm at a 40 mW/cm^2) at a distance of 10 cm for 10 minutes. To see the lyophilization effect, the second part was lyophilized and the obtained solid re-dissolved in sterile water. To assess the freezing and thawing cycles on protein stability, the third aliquot was frozen at -85°C for subsequent 24 hr and then thawed at room temperature. These solutions were then added to a CTLL-2 cell culture to assess the bioactivity of IL-2. CTLL-2 cell are T cell lymphocyte obtained from C57BL/6 mouse and can proliferate only in the presence of bioactive IL-2.

6.2.6. *In vitro* Release Studies

The prepared monolithic micro-cylinders and disks loaded with lyophilized IL-2 were subjected to *in vitro* release studies using phosphate buffer saline (PBS) of pH 7.4 as a release medium. Each of the triplicate micro-cylinder samples was put into 200 μl microcentrifuge vials filled with 100 μl of release

medium. As well, each of the disk samples was put into 2 ml microcentrifuge vials filled with 200 μ l of release medium. The vials were attached to a Glas-Col rugged culture rotator. The rotator was set at 20% rotation speed and placed in an oven at 37 ± 0.5 °C. To ensure sink conditions and constant osmotic pressure driving force, the receptor release medium was replaced with fresh medium over the release period. Solutions collected were divided into aliquots, frozen at -85 °C for subsequent IL-2, albumin and trehalose concentration analysis as well as IL-2 bioactivity assay using cytotoxic T-cell.

IL-2 concentration was analyzed using rmlIL-2 enzyme-linked immunosorbent assay (ELISA) assay system. A 100 μ l of capture antibody solution (2 μ g/ml) was added to each well immediately after dilution in Dulbecco's PBS. The plate was sealed and incubated overnight at room temperature. The wells were then aspirated and washed 4 times using 300 μ l of wash buffer (0.05% Tween 20 in Dulbecco's PBS), after the last wash, the plate was inverted to remove residual buffer and blotted on paper towel. A 300 μ l of block buffer (1% bovine serum albumin in Dulbecco's PBS) was then added to each well and incubated for 1 hr at room temperature, then aspirated and washed 4 times. A 10 μ l of the released samples was added to each well in duplicate followed by 90 μ l of PBS and incubated at room temperature for another 2 hr. The wells were aspirated and washed 4 times and 100 μ l of detection antibody (0.25 μ g/ml) was added to each well after dilution in diluent (0.05% Tween 20 and 0.1% bovine serum albumin in Dulbecco's PBS) and incubated at room temperature for 2 hr. The plate was then aspirated and washed 4 times and 100 μ l of avidin-HRP conjugate (1:2000 in diluent) was added in each well and incubated for 30 minutes at room temperature. The plate was aspirated and washed 4 times and 100 μ l of ABTS liquid substrate was added to each well and incubated at room temperature for color development. The developed color was measured at 405 nm with wave-length correction set at 650 nm using Polarstar, Optima ELISA plate reader (BMG Scientific). The obtained optical densities were used

to determine the amount of IL-2 released using a calibration curve constructed with different concentrations of IL-2 standard (0-3ng/ml) run at each measurement.

Total protein concentrations were detected using Pierce® BCA protein assay kit. A 5 µl of the released samples was added in duplicate into a microplate well and 200 µl of BCA working reagent [mixture of 50 parts of BCA reagent A (bicinchonic acid, Na_2CO_3 , NaHCO_3 and sodium tartrate in 0.1 M NaOH) and 1 part of BCA reagent B (4% cupper sulphate)] was added to each well and mixed thoroughly on plate shaker for 30 second. The plate was covered and incubated at 37 °C for 30 minutes and then left to cool to room temperature. The absorbance of each well was measured at 560 nm using Polarstar, Optima ELISA plate reader and the amount of albumin in each sample was calculated using a calibration curve constructed with different concentrations of albumin standard (20-2000 µg/ml) run at each measurement.

TH concentrations were analyzed by phenol-sulfuric acid method for carbohydrate assay.²⁹ A 5 µl of the released samples was added in duplicate into a microplate well and 150 µl of concentrated sulfuric acid and 30 µl of 5% phenol were added to each well. The plate was heated for 5 minutes at 90 °C in a water bath and then brought to room temperature for 5 min. It was then wiped dry and the absorbance was measured at 492 nm using Polarstar, Optima plate reader.

6.2.7. Cell Line Culture and IL-2 Bioactivity Assay

The bioactivity of the released IL-2 was assessed through its ability to stimulate the proliferation of the C57BL/6 mouse cytotoxic T lymphocyte (CTL-2).³⁰ Proliferation of the CTL-2 was measured

using the MTT cell proliferation assay. Using sterile cell culture flasks, the cells were cultured in GIBCO® RPMI-1640 medium supplemented with 2 mM/L glutamine, 1mM sodium pyruvate, 10% fetal bovine serum and 10% rat T-STIM with Concanavalin A in a humidified incubator in 5% CO₂ at 37 °C. The cells were sub-cultured twice per week, before they have reached a cell density of 2×10^5 cells/ml, to avoid the loss of cell viability. Before culturing into 96-well sterile culture plate, the cell was centrifuged and re-suspended in GIBCO® RPMI-1640 medium supplemented with 2 mM/L glutamine, 1mM sodium pyruvate, 10% fetal bovine serum, 2.5 µg/ml amphotericin B, and 50 gentamycin to a cell density of 1×10^6 cells/ml. From this stock cell suspension, 100 µl was transferred into each well, then, 5-20 µl of the standard or released IL-2 samples were added to each well in duplicate and incubated in a humidified incubator in 5% CO₂ at 37 °C. After 48 hrs incubation, 10 µl of MTT labeling reagent was added to each well and incubated for 4 hrs in humidified atmosphere at 37°C. The formed insoluble formazan crystals were dissolved in 100 µl/well solubilization buffer (10% sodium dodecyl sulphate in 0.01M HCl) and incubated over night and then measured spectrophotometrically at $\lambda = 544$ nm with wave length correction set at 650 nm using Polarstar, Optima ELISA plate reader.

IL-2 bioactivity results of released samples were recorded as percentage absorbance relative to absorbance of IL-2 standard as follows:

$$\text{IL-2 bioactivity (\%)} = [A] / [A]_S \times 100$$

Where [A] is the absorbance difference (at 544 nm and 650 nm) for cells incubated with released IL-2 sample and [A]_S is the absorbance difference for cells incubated with equivalent IL-2 standard.

6.2.8. Scanning Electron Microscopy

Scanning electron microscope (SEM) was utilized to investigate the change in the surface of the PDET₁₀₀ elastomer after IL-2 release in terms of surface pores and micro-crack formation. Micro-cylinder loaded matrices of both newly fabricated and after complete release, were vacuum dried for 24 hours. The cylinders were mounted on a conductive carbon adhesive attached to aluminum stubs and then sputter-coated with gold palladium. Gold was evaporated onto the specimen to a thickness of approximately 15 nm. Samples were examined on a Hitachi model S-570 scanning electron microscope. The microscope was interfaced with an electron backscatter diffraction (EBD) system and energy dispersive X-ray (EDX) analytical system from Tracor Northern. The electron gun was a tungsten hairpin type filament and the sample images were digitally captured using a digital imaging system.

6.2.9. Statistics Analysis

Statistical analyses of data were performed using Graphpad Prism software (version 5.02) by using 2-way ANOVA followed by the Bonferroni post-tests. Unless otherwise stated, data reported as the mean, and the error bars in the figures represent the standard deviation (SD) about the mean, of triplicate samples. Statistical differences between the groups were considered significant if the *p* value was < 0.05 unless otherwise reported.

6.3. RESULTS AND DISCUSSION

In the following discussion, the abbreviated PDET will refer to poly(decane-co-tricarballoylate) while the subscripted number following this abbreviation refers to its theoretical degree of acrylation.

6.3.1. Elastomer Preparation and Characterization

^1H -NMR analysis confirmed the purity and the chemical structure of the PDET prepolymer and also confirmed the formation of acryloyl moieties following the acrylation at the terminals of the formed chains. The calculated degree of prepolymer acrylation as estimated via ^1H -NMR are listed in Table 6.1. The charts and the full interpretation of each individual peak of the two ^1H -NMR spectra was reported previously.²⁶ Solid-state ^{13}C -NMR spectrum of the elastomer confirmed that there is no peaks corresponding to $-\text{CH}=\text{CH}_2$ terminal groups in the prepared elastomer, reported previously.²⁷ These observations form constituted evidence that the acrylated groups were fully consumed during the photopolymerization process.

The obtained photocrosslinked PDET elastomers were stretchable and rubbery and swelled but did not dissolve in most of organic solvents. The mechanical properties spanned from tough to elastic depending on the degree of acrylation. Figure 6.3 shows that tensile testing of the photocrosslinked PDET microcylinders produced representative uniaxial tensile stress-strain curves which are characteristic of typical elastomeric materials. No permanent deformation was observed during the mechanical testing. Average values for Young's modulus (E), ultimate tensile stress (σ), cross-linking density (ρ_x), and maximum strain (ϵ) are summarized in Table 6.1. The elastomers exhibited controllable mechanical properties. The value of σ was as high as 0.44 MPa while the value of ϵ was as high as 120.4 %, under the synthesis condition. Young's modulus values ranged between 0.73 and 0.19 MPa.

Table 6.1. Mechanical properties and sol content of poly(decane-co-tricarballate) elastomers.

Elastomer	σ (MPa)	ϵ (%)	E (MPa)	ρ_s (mole / m ³)	S (%)	DA*
PDET ₁₀₀	0.44 ± 0.06	60.2 ± 6.1	2.140 ± 0.036	288 ± 48	9.63 ± 2.38	0.83
PDET ₇₅	0.34 ± 0.11	94.8 ± 6.3	1.27 ± 0.08	171 ± 10.7	32.19 ± 8.75	0.69
PDET ₅₀	0.24 ± 0.05	120.4 ± 9.8	0.39 ± 0.01	53.0 ± 0.4	59.11 ± 9.03	0.47

**Degree of acrylation estimated by NMR*

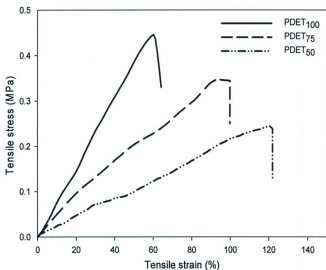


Figure 6.3. Stress-strain curves of different PDET elastomeric micro-cylinders

The crosslink density (ρ_x) was calculated according to the theory of rubber elasticity following the equation: $\rho_x = E/3RT$, where ρ_x represents the number of active network chain segments per unit volume (mole / m³), E represents Young's modulus in Pascal (Pa), R is the universal gas constant (8.3144 J/mol K) and T is the absolute temperature (K). The crosslinking density changes appreciably as a function of the degree of acrylation. As such, the decrease in the number of terminal acrylated groups in the prepolymers resulted in a decrease in the linking anchors between the polymer chains during photocuring which resulted in an increase in the elastomers' stretchability and elasticity.

Manipulation of elastomers' sol content was also found to depend mainly on the degree of acrylation. The sol content represents the mass difference after removal of the un-crosslinked prepolymer which is soluble in dichloromethane. Therefore, PDET₅₀ elastomer, with the lowest calculated degree of acrylation (0.47), possessed the highest sol content among all the prepared elastomers (59%). Although stretchability will strongly improve as a result of increasing the sol content of the elastomer, the relatively low sol content will help in maintaining the mechanical properties after implantation.

For the different formulation parameters effect on the IL-2 bioactivity, the relative bioactivity results showed that there was no statistical significant difference ($P < 0.05$) in the obtained IL-2 bioactivity from its incipient bioactivity in each of the formulation and analysis condition tested, over the different TH/BSA mass ratio.

6.3.2. *In vitro* Release Studies

Our main aspect of the development of this biodegradable implantable system was to provide an extended release of an active IL-2 for an established period of time that can be easily and fittingly controlled. IL-2 as with most pharmaceutical proteins is usually co-lyophilized with cryoprotectants in order to be incorporated as solid particles in the PDET elastomer. For this reason, TH was used as a cryoprotectant for maintaining IL-2 native structure during freezing and frozen storage. TH demonstrated to be an excellent stabilizer for various recombinant protein pharmaceuticals.³¹ On the other hand, since most of therapeutic proteins do not have enough osmotic activity to elicit the required osmotic mechanistic action, pore-forming agents of high osmotic activity like TH have to be used in order to load IL-2 at high volume fraction and to ensure the complete release of the loaded protein fraction. We also selected BSA to protect IL-2 molecules from freezing damage due to its known effect in preventing the drop in the pH that occurs during the lyophilization in buffer as well as its role in preventing the protein adsorption to the surface.³¹ Consequently, to get IL-2 loaded networks conducted in the study, TH/BSA was first co-lyophilized with IL-2 and the obtained solid particles were dispersed in the acrylated macromer preceding photo-crosslinking. Different geometries of these elastomeric networks were made from three different degrees of acrylated macromers, as well; different loading percentage ratios and different TH/BSA were also prepared. The release kinetics was performed in PBS (pH 7.4) at 37 °C for 60 days and the results as well as the impact of different variables used on the release, as depicted in Figures 6.4-6.8, are discussed in the following sections.

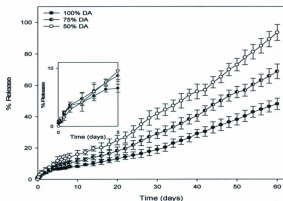
6.3.2.1. *Effect of degree of prepolymer acrylation*

In order to investigate the effect of manipulating the elastomer's physicochemical properties on the IL-2 release profile, we examined the effect of varying the prepolymer degree of acrylation on the

release kinetics from these elastomeric matrices. Based on the chemical structure of the PDET elastomer, it is assumed that changing the elastomer's crosslinking density would change the void volumes between each crosslink in the elastomer and consequently alters the network's water permeability during the release process. In order to test this, prepolymers with three different degrees of acylation were prepared (PDET₁₀₀, PDET₇₅ and PDET₅₀) and loaded with the same volumetric loading of IL-2/BSA/TH particles during photocuring.

Figure 6.4A shows that in the three networks prepared, an initial small burst release, which corresponds to approximately 6-7% of the loaded IL-2 content, was observed within the first 4 days of IL-2 release. This burst release was followed by a phase of linear and sustained release which steadfastly continued until the release of the loaded protein was completed. This release pattern of IL-2 can be described typically as follows: After the immersion of the loaded devices in the release medium, water started to diffuse into the matrix mass and subsequent osmotic-driven release started. The occurred celerity in the release in the first 4 days can be explained by the combination of osmotic mechanism in the outside layers of the matrix as well as emancipation of those particles located on the surface of the device and those incorporated in the un-crosslinked part (sol content) of the outer most layer of the device. This initial high release period was then followed by a period of constant but slow release. This slow release rate can be attributed to the fact that the initial polymer swelling and gelling which took place in the outermost layer of the elastomeric cylinder resulted in the formation of a boundary layer that slowed down further penetration of water into the subsequent matrix layers with subsequent delay in protein dissolution. In such circumstances, it is expected that deport of the solid IL-2 particles from the successional layer to the adjacent outer layers and then to the surface of the matrix is also retarded. The formation of such a boundary layer and the demonstration that osmotic-driven release mechanism to

A



B

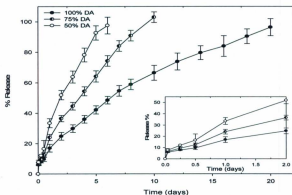


Figure 6.4. Cumulative percent of IL-2 released in phosphate saline buffer from 10% v/v Loaded PDET micro-cylinders (A) disks (B) shape specimens, with different degrees of acrylation (DA). Each point represents the mean of triplicate experiments, and the error bars represent one standard deviation about the mean. Error bars are not shown when the standard deviation is smaller than the symbol.

place in a serial fashion towards the center of the device have been reported in our latest study on the release of amaranth trisodium dye from PDET elastomers.²⁷

Figure 6.4A also shows that for the microcylinders, the same release pattern was followed in all matrices with the highest release rate achieved from the elastomer of lowest degree of acrylation. In the first four days, the release behavior from the networks of different degrees of acrylation was comparable. Following that period, the release from the elastomers of less degree of acrylation was faster in comparison to the release from the networks with high degree of acrylation. The cumulative release data showed a significant dependence of the release on the prepolymer degree of acrylation and the corresponding crosslinking density as reported in table 6.1. The release of IL-2 from PDET₃₀ was approximately completed within 60 days of the release study. While the release from PDET₇₅ and PDET₁₀₀ cylinders reached 69% and 48% of the loaded IL-2, respectively. In the same manner, Figure 6.4B shows that IL-2 is released faster from the less densely crosslinked disk-shaped networks and this is in agreement with the release pattern obtained from micro-cylinders presented in figure 6.4A. Loaded protein was released within 6 days from PDET₃₀ networks, while the PDET₇₅ and PDET₁₀₀ networks released its content within approximately 10 and 20 days, respectively.

The aforementioned discrepancy in the release rate may be attributed to the fact that water diffusion is inversely proportional to the degree of prepolymer acrylation^{26,27} and this is in agreement with the water-uptake values presented in the degradation study. Decrease in the crosslinking density would result in increasing the void volumes in the elastomer which increase the possibility of faster water diffusion through the matrix. This observation is consistent with our previously reported results regarding the effect of degree of acrylation on the diffusion of water into the elastomeric matrices at

temperatures above their glass transition temperatures.²⁶ From these results, it can be revealed that IL-2 release can be tuned by adjusting the crosslinking density by changing the chemical structure nature of these networks.

To elucidate on the constant release profile, a linear regression of the release data from the microcylinders after the first 4 days until the 60 days of release and from the disks during the 60 days of release were carried out. The linear release over this period resulting from the osmotic-driven delivery mechanism can be described as zero-order release kinetics with nearly constant daily release. The linear regression correlation coefficient was found to be equal to 0.993, 0.990 and 0.987 for the release from PDET₅₀, PDET₇₅, and PDET₁₀₀, respectively (Table 6.2).

6.3.2.2. Effect of the device shape on the release

Micro-cylindrical and disk-shaped specimens were used to study the influence of device shape and geometry on the release of entrapped IL-2. As shown in Figure 6.5, IL-2 loaded into PDET₁₀₀ disk samples exhibited a rapid release of approximately 97 % within 20 days while approximately only 48 % of loaded protein was released in 60 days from the microcylinder samples with the same degree of acrylation. On the other hand, IL-2 loaded into PDET₅₀ disk samples exhibit a faster release pattern in the first six days with approximately 97 % of the IL-2 released, showing an extremely rapid release, while the microcylinder samples followed a typical sustained release pattern for approximately 94 % of the IL-2 over a period of 60 days.

This disparity in the release rate was in agreement with the osmotic release theory in that the release rate depends on the device geometry including its surface area and thickness (the length of its

Table 6.2. The regression values of IL-2 released from PDET micro-cylinders and disks shape specimens, with different degrees of acrylation (DA).

	Cylinders (release data 4-60 days)				Disks (release data 0-60 days)			
	R value for Linear regression		R value for square root time regression		R value for Linear regression		R value for square root time regression	
	R ²	R	R ²	R	R ²	R	R ²	R
50% DA	0.9855	0.9927	0.9330	0.9659	0.9670	0.9833	0.9865	0.9932
75% DA	0.9814	0.9906	0.9225	0.9604	0.9779	0.9889	0.9833	0.99162
100% DA	0.9746	0.9872	0.9112	0.9546	0.9519	0.9756	0.9933	0.9916

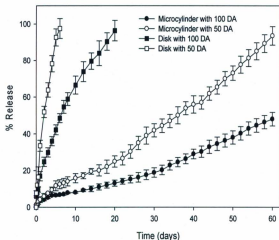


Figure 6.5. Cumulative percent of IL-2 released from 10% v/v Loaded PDET elastomers with different degree of acrylation (DA) and different device shape. Each point represents the mean of triplicate experiments. The error bars represent the standard deviation about the mean. Error bars are not shown when the standard deviation is smaller than the symbol.

smallest dimension). Device's surface area represents the outer boundary of the device with the release medium, and thereby affecting the rate and extent of the water penetration into the elastomer. Having said that, initiating the osmotic driven release is a matter of water diffusion into the system followed by the formation of aqueous microcapsules from the dissolved embedded IL-2 particles. The larger the surface area of the device, the more space/surface area through which water can diffuse, the higher the rate and extent of water imbibitions into the device. In addition, the device's thickness represents the length of the distance required to transport by the IL-2 molecules to release from the device. The shorter the length of this distances, the faster the release of the dissolved protein. Consequently, IL-2 release through a 1 mm thick disk film with a surface area of 188.5 mm² was sufficiently faster to enable complete release within 6 and 20 days with half and full acrylated samples, respectively. While the release from 2 mm diameter microcylinders, with a surface area of 69.1 mm², was much slower.

The results of this release experiment demonstrated that controlled delivery for IL-2 can be constructed from this bio-resorbable elastomer at a rate manipulated by the device shape and geometry and determined by the body needs over a specific period of time. The IL-2 release rate could be easily tuned as needed; for example, increase the release rate by increasing the geometrical surface area of the prepared device, or extend the required treatment period by increasing the thickness of the device.

6.3.2.3. Effect of loading percentage

To assess the effect of IL-2 loading percentage used on the release properties, IL-2 was copolyphylized with BSA and TH and loaded with a 2, 10 and 20 volumetric loading percentage. These loading percentages were chosen to ensure that the total loading was well below the particle percolation threshold so that osmotic pressure would remain the dominant mechanism of release throughout the

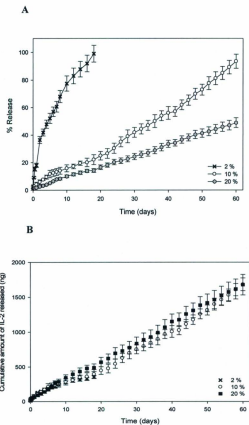


Figure 6.6. Release data of IL-2 from different loaded percentage PDET micro-cylinders with 50% degree of acrylation, (A) represent the percentage released and (B) represent the cumulative amount of IL-2 release. Each point represents the mean of triplicate experiments. The error bars represent standard deviation about the mean. Error bars are not shown when the standard deviation is smaller than the symbol.

study. While three different loading percentage microcylinders were prepared, the amount of TH/BSA co-lyophilized with IL-2 was fixed during the formulation. Figure 6.6A shows the released IL-2 versus time profiles from PDET₅₀ micro-cylinder samples. As shown, when IL-2/excepiant was incorporated at 2 % loading, IL-2 was completely released over a period of 18 days while samples loaded with 10 % and 20 % showed a release of 93 % and 49 % of the loaded IL-2, respectively, after 60 days. On the other hand the cumulative amount of the IL-2 released, from these different loaded samples is illustrated in Figure 6.6 B. The Figure shows that there are no distinct differences in the amount of IL-2 released per day among all the different loading percentage, in the first 10 days of the release study. It was interesting to note that although there was a slight difference in the release rate between the 2 % and 20 % volumetric loadings, after the first ten days, this difference was not significant. It seems likely that the zero-order release rate is nearly kept constant and was not affected by the volumetric loading percentage of the IL-2. These results show that the difference in volumetric loading does not affect the effluent rate of IL-2 from the PDET elastomer once it is below the percolation threshold.

6.3.2.4. Effect of BSA/TH mass ratio on IL-2 release

Albumin and trehalose are extremely different in their osmotic activities; the osmolarity of saturated BSA and trehalose solution in water at 37°C is 142 and 1620 mmol/kg, respectively, as measured using vapour pressure osmometer.²⁷ Therefore, the BSA/TH ratio in the loaded elastomer might considerably affects the exerted osmotic pressure property and protein release rate from the matrix. In this study, elastomers with different BSA/TH mass ratios were prepared by keeping IL-2 mass ratio constant. The cumulative IL-2 release profiles are shown in Figure 6.7. When BSA was used alone without trehalose in the particles, only 19% of the IL-2 incorporated in the 100% acrylated micro-cylinders was released during the 60 days of release at an average rate of 6.4 ng/day, and approximately 33 % of the

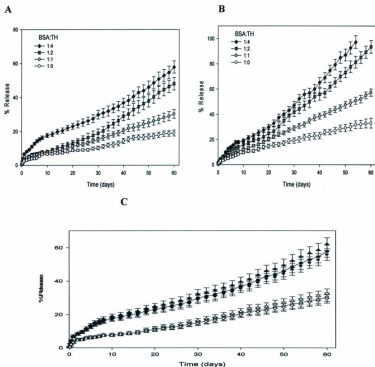


Figure 6.7. (A) and (B) are cumulative percent of IL-2 released from PDET micro-cylinders with 100% and 50% degree of acrylation, respectively, in existence of different molar ratio of bovine serum albumin (BSA) and trehalose (TH). (C) The release kinetic of TH (triangles), BSA (circles) and IL-2 (squares) from PDET micro-cylinders with 100% degree of acrylation. The solid symbols are for 50% degree of acrylation, the hollow symbols are for 100% degree of acrylation and the lines correspond to the IL-2 release.

Each point represents the mean of triplicate experiments, and the error bars represent one standard deviation about the mean. Where error bars are not shown when the standard deviation is smaller than the symbol.

incorporated IL-2 was released from the 50% acrylated samples at an average rate of 11 ng/day. However, the IL-2 release rate significantly increased by the combination of TH to the BSA in all the prepared samples regardless of their degree of acrylation. The total mass fraction of IL-2 released over the time frame observed increased as the trehalose content on the co-lyophilized particles increased; for example, complete release occurred after 54 days for IL-2 containing BSA/TH (1:4 weight ratio) from micro-cylinders prepared with PDET₅₀. Most importantly, the release profiles of BSA and TH were superimposed on the IL-2 release data. Figure 6.7 C shows the release profiles of BSA, IL-2 and TH from the PDET₁₀₀ microcylinders containing 1:1 and 1:4 BSA/TH weight ratios. The data for 1:0 and 1:2 ratios are omitted for clarity. Within the 60 days of the study, the BSA and trehalose release rate were absolutely equivalent to the rate of IL-2 release.

These results demonstrate that the mechanism of protein release from the PDET elastomer matrices is controlled by the amount of TH loaded. It is evident that the high loading of trehalose has accelerated the uptake of water into the elastomer matrix and generated a greater solution osmotic activity and subsequently increased the release rate.^{7,10} The results also reveal that the mechanism of IL-2 release from the PDET elastomer can be also controlled by varying the volumetric loading of the incorporated osmotic excipients.

6.3.2.5. Impact of elastomer degradation on IL-2 release

We have previously reported on the long-term degradation of the studies elastomers using dog-bone-shaped elastomeric samples in PBS.²⁶ In that study, the elastomers were found to follow slow zero-order degradation rate kinetics and exhibited the ability to maintain their shape and extensibility over the studied period. Water absorption and change in weight of blank PDET₅₀ and PDET₁₀₀ microcylinders over a 12 week period was further investigated in this study to assess the exact possible contribution of

degradation on the device geometry and the overall drug release mechanism. As seen in Figure 6.8, the samples exhibited a two-stage of water absorption and weight loss behavior. In the first stage (4 weeks) the water absorption and weight loss proceeded rapidly due to the diffuse out of the sol phase from the samples. However, in the second stage, the water absorption and weight loss took place in a slow rate. By the end of the study period, the average cumulative water absorption was equivalent to 68 % and 45 % in the PDET₅₀ and PDET₁₀₀ respectively. In addition, the mean weight loss at the end of the 12 weeks was found to be equivalent to 29 % and 14 % in micro-cylinders in the PDET₅₀ and PDET₁₀₀ respectively. Such results confirms that matrices underwent bulk erosion, similar to what we report previously, and the obtained data are in accordance with the fact that water diffusion and mass loss are inversely proportional to the polymer's crosslinking density.²⁶

The data above revealed that degradation played only a limited role in the overall release of the IL-2 from the cylindrical devices. In addition, it is also obvious that none of the reported IL-2 release profiles exhibited a distinct release phase that can be clearly attributed to the polymer degradation. Finally, the structure integrity of the matrices were maintained and there was no evidence of major degradation or loss in the geometry of the cylinders at the end of the release and degradation studies (Figure 6.9) which is important in having the osmotic-driven mechanism predominate the overall drug release profile. When the elastomer degradation rate is slow enough to maintain the implant's geometry and mechanical properties (extension ratio) during the release period, the osmotic-driven mechanism will dominate the linear controlled-release and polymer degradation will play only a minor role in the overall release pattern.^{21,27}

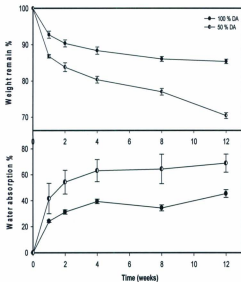


Figure 6.8. Percentage water absorption and weight remain versus time of PDET elastomeric microcylinders of different degrees of acrylation (DA) in PBS at 37°C. Error bars represent the standard deviation of the mean of measurements from three samples.

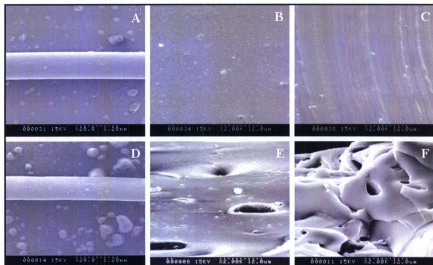


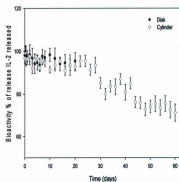
Figure 6.9. A, B and C are scanning electron photomicrographs of blank PDET₁₀₀ microcylinders at the end of 12 week degradation. D, E and F are scanning electron photomicrographs of IL-2 loaded (with BSA:TH ratio 1:4). PDET₁₀₀ microcylinders at the end of 60 days release study. A and D are microcylinders images at 20X magnification. B and E are surface images at 2000X magnification. C and F Cross-sectional view of the microcylinders at 2000X magnification.

6.3.3. Bioactivity of the Released IL-2

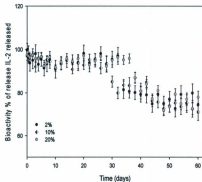
To characterize the bioactivity of the released IL-2, the released supernatant was collected, frozen and stored at -85°C until thawing immediately prior to the bioactivity assay. The percentage of IL-2 bioactivity was calculated by dividing the CCTL cellular proliferation response to the bioactive protein in the release medium and by the maximum cellular response of an equivalent concentration of freshly reconstituted IL-2. The bioactivity of the recovered IL-2 in the release media are shown in Figure 6.10. Despite achieving a zero-order release, the released IL-2 shown, for each formula, over 94% of the IL-2 released in the first 28 days remained biologically active and as the release continued, the fraction of bioactive IL-2 started to drop in the subsequent days. As shown in Figure 6.10A, for the IL-2 embedded in the PDET₁₀₀ formulation, the decrease of bioactivity indicated that nearly all the IL-2 released from loaded disk-shaped specimens was kept bioactive during the first 20 days of the release period. On the other hand, IL-2 released from the micro cylinders specimens started to lose fraction of its bioactivity after the first 28 days of the release. As such, there was no major influence for PDET matrices device shape and degree of acrylation as well as IL-2 loading concentration and BSA/TH ratio on the bioactivities of IL-2 recovered in the release media. Although IL-2 release from PDET₅₀ showed more decrease in its bioactivity compared to that released from PDET₇₅ and PDET₁₀₀ devices, nonetheless, this difference was not statistically significant.

Keeping the native bioactivity of the released IL-2 is considered the main key for the success of its delivery system for potential therapeutic application. Having said that, a numerous approaches have gone into the achievements of that but most of them have been associated with limited success in keeping it bioactive enough for the clinical setting. Despite the observed reduction in the IL-2 bioactivity after the first month of the release from our elastomeric matrices, these bioactivity results

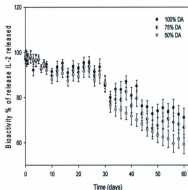
(A)



(C)



(B)



(D)

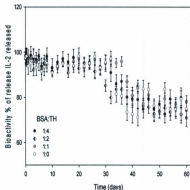


Figure 6.10. Bioactivity profiles of IL-2 released from PDET with Different, (A) shape of releasing device (B) degree of acrylation (c) loading % (D) different weight ratio of BSA and TH. Each point represents the mean of triplicate experiments. The error bars represent the slandered deviation about the mean.

represent an improvement over the previously published results provided with a quantitative analysis of the actual percentage of bioactive IL-2 released during the study. Using a prepared poly(lactic acid) (PLA) nanospheres, *Sharma et al.*, was able to control the release of IL-2 for 30 days with only maintaining 40% of the post-release bioactivity.³² In a similar approach, *Egilmez et al.*, also loaded IL-2 into PLA nanospheres that showed total IL-2 release process lasted for 7 days and the composite bioactivity of all IL-2 released was approximately 50%.³³ *Thomas et al.*, using a prepared poly(lactide-co-glycolide) [PLG](50/50) by the double emulsion (DE) and single emulsion (SE) methods demonstrated the IL-2 sustained release ability over a period of almost 30 days. The bioactivity of IL-2 released from microspheres prepared by DE was around 80% for the first 5 days, and then rapidly dropped to less than 40% by day 10. On the other hand, the bioactivity of IL-2 released from microspheres prepared by SE was around 85% for the first 4 days, and then rapidly dropped to less than 50% by day 7.³⁴ *Rhines et al.*, encapsulated IL-2 in gelatin-chondroitin-6-sulphate based microspheres. The study revealed that the release profile was characterized with a rapid release rate (almost 80%) within the first 7 days followed by a very slower release over a total period of approximately 52 days.³⁵ The *in vitro* bioassay studies conducted by the same team in a previous study using the same formulation approach demonstrated that IL-2 retained only a total of approximately 50% of its original bioactivity over a total release period of 2 weeks.³⁶ In our elastomers, IL-2 bioactivity was greatly maintained by the using the solventless formulation strategy and visible light photocuring which are protein and peptide friendly condition. In addition to using the osmotic pressure driven release which allow for IL-2 release before significant PDET elastomer bulk hydrolytic degradation occurred.

6.3.4. Scanning Electron Microscopy

In order to further investigate and demonstrate the proposed theory of the osmotic-driven release mechanism, the changes in the surface architecture of the loaded cylinder before and after the release was examined. Figure 9 (A, B and C) shows the SEM micrographs of the PDET₁₀₀ micro-cylinder, taken after the conductance of the 12 weeks degradation study in PBS. It can be seen that, in the dry state, the integrity of the microcylinder was maintained. In addition, it exhibited a quite uniform surface and a nonporous smooth crosssection view that revealed absence of any visible pore throughout the matrix, when 2000 x magnification was used. Figure 10 (D, E and F), on the other hand, shows the SEM micrographs of the IL-2 with BSA/TH (weight ratio 1:2) loaded PDET₁₀₀ microcylinder, taken after the conduction of release studies. As shown, after the 60 days release study, the images showed evident cracks and pores in the range of 1 to 15 μm on the surface corresponding to the routes the IL-2 took for release. In the same manner, the cross section photomicrograph showed a formed channel owing to the release process in concordance with the proposed osmotic-driven released mechanism.

6.4. CONCLUSIONS

This study explored the potential of monolithic, photocrosslinked PDET matrices as implantable delivery system for protein and peptide based drug. An IL-2 loading up to 20% was incorporated in the matrix with the utilization of visible light crosslinking and without using additional organic solvent. IL-2 release results shown that the release can be controlled through osmotic pressure of the core by adjusting the TH mass incorporated, shape of the formulated device, and degree of PDET prepolymer acrylation. At the same time the release was at a rate to be fairly independent of loaded IL-2 percentage. These

matrices can release slow, steady dose of IL-2 over extended period with keeping the native bioactivity after the release, that represent an improvement over the previously published study from any type of formulation. The control release, biocompatibility and slow degradation properties of these elastomers combine to make it an attractive candidate for use in the preparation of implantable devices to provide delivery of a biological cargo for therapeutic protein with different molecular weights and physical properties and/or temporary mechanical support for tissue regeneration without the need for surgical removing procedures.

6.5. REFERENCES

- 1- Morgan DA, Ruscetti FW, Gallo R. 1976. Selective *in vitro* growth of T lymphocytes from normal human bone marrows. *Science* 193: 1007-1008.
- 2- Smith KA. 1988. Interleukin-2: inception, impact, and implications. *Science* 240: 1169-1176.
- 3- Radny P, Caroli UM, Bauer J, Paul T, Schlegel C, Eigentler TK, Weide B, Schwartz M, Garbe C. 2003. Phase II trial of Intralesional therapy with interleukin-2 in soft tissue melanoma metastases. *Br J Cancer* 89: 1620-1626.
- 4- Sosman JA, Kohler PC, and Hank J, Moore KH, Bechhofer R, Storer B, Sondel PM. 1988. Repetitive weekly cycles of recombinant human interleukin- 2: Responses of renal carcinoma with acceptable toxicity. *J Natl Cancer Inst* 80: 60-63.
- 5- Bubenik J, Mikyskova R, Vonka V, Mendoza L, Simova J, Smahel M, Indrova M. 2003. Interleukin-2 and dendritic cells as adjuvants for surgical therapy of tumours associated with human papillomavirus type 16. *Vaccine* 21: 891-896.
- 6- Mikyskova R, Indrova M, Simova J, Jandlova T, Bieblova J, Jinoch P, Bubenik J, Vonka V. 2004. Treatment of minimal residual disease after surgery or chemotherapy in mice carrying HPV16-associated tumours: Cytokine and gene therapy with IL-2 and GM-CSF. *Int J Oncol* 24: 161-167.
- 7- Lotze MT, Matory YL, Rayner AA, Ettinghausen SE, Vetto JT, Seipp CA, Rosenberg SA. 1986. Clinical effects and toxicity of interleukin-2 in patients with cancer. *Cancer* 58: 2764-2772.

- 8- Den Otter W, Jacobs JJ, Battermann JJ, Hordijk GJ, Krastev Z, Moiseeva EV, Stewart RJ, Ziekman PG, Koten JW. 2008. Local therapy of cancer with free IL-2. *Cancer Immunol Immunother* 57:931-50.
- 9- Thatcher N, Dazzi H, Johnson RJ, Russell S, Ghosh AK, Moore M, Chadwick G, Craig RD. 1989. Recombinant interleukin-2 (rIL-2) given intrasplenically and intravenously for advanced malignant melanoma. A phase I and II study. *Br J Cancer* 60: 770-774.
- 10- Robb RJ, Kutny RM, Panico M, Morris HR, and Chowdhry V. 1984. Amino acid sequence and post-translational modification of human interleukin 2. *Proc Natl Acad Sci USA* 81: 6486-6490.
- 11- Liang SM, Thatcher DR, Liang CM, Allet B. 1986. Studies of Structure-Activity Relationships of Human Interleukin-2. *J Biol Chem* 261: 334-337.
- 12- Gounili P. 1999. PhD Thesis: The effect of pH and temperature on the conformational stability of recombinant human interleukin-2. University of Connecticut, USA.
- 13- Johnston D, Reynolds SR, Bystry J. 2006. Interleukin-2/liposomes potentiate immune responses to a soluble protein cancer vaccine in mice. *Cancer Immunol Immunother* 55: 412-419.
- 14- Qiao M, Chen D, Hao T, Zhao X, Hu H, Ma X. 2008. Injectable thermosensitive PLGA-PEG-PLGA triblock copolymers-based hydrogels as carriers for interleukin-2. *Pharmazie* 63: 27-30.
- 15- Rhines LD, Sampath P, Di-Meco F, Lawson HC, Tyler BM, Hanes J, Olivi A, Brem H. 2003. Local immunotherapy with interleukin-2 delivered from biodegradable polymer microspheres combined with interstitial chemotherapy: a novel treatment for experimental malignant glioma. *Neurosurgery* 52: 872-879.
- 16- Hsu W, Lesniak MS, Tyler B, Brem H. 2005. Local delivery of interleukin-2 and adriamycin is synergistic in the treatment of experimental malignant glioma. *J Neurooncol* 74: 135-140.
- 17- Samlowski WE, McGregor JR, Jurek M, Baudys M, Zentner GM, Fowers KD. 2006. ReGel polymer-based delivery of interleukin-2 as a cancer treatment. *J Immunother* 29: 524-535.
- 18- Chan YP, Meyrueix R, Kravtsoff R, Nicolas F, Lundstrom K. 2007. Review on Medusa: a polymer-based sustained release technology for protein and peptide drugs. *Expert Opin Drug Deliv* 4: 441-451.
- 19- Shaker M, Younes HM. 2009. Interleukin-2: Evaluation of Routes of Administration and Current Delivery Systems in Cancer Therapy. *J Pharm Science* 98: 2268-2298.

- 20- Gu F, Younes HM, El-Kadi AO, Neufeld RJ, Amsden BG. 2005. Sustained interferon-gamma delivery from a photocrosslinked biodegradable elastomer. *J Control Rel* 102: 607-617.
- 21- Gu F, Neufeld R, Amsden B. 2007. Sustained release of bioactive therapeutic proteins from a biodegradable elastomeric device. *J Control Release* 117: 80-89.
- 22- Younes H M: 2003. New biodegradable elastomers for interferon-gamma delivery, PhD Thesis, Faculty of Pharmacy, University of Alberta, Edmonton, AB.
- 23- Younes H M, Ellaboudy H, Shaker M A. Biodegradable elastomers prepared by the condensation of an organic di-, tri- or tetra-carboxylic acid and an organic diol. International Patent No. 144881 A1, 2008
- 24- Chapanian R, Amsden BG. 2010. Combined and sequential delivery of bioactive VEGF165 and HGF from poly(trimethylene carbonate) based photo-cross-linked elastomers. *J Control Release* 143: 53-63.
- 25- Glenn FV, Rex MT. 1995. UVA radiation-induced oxidative damage to lipids and proteins *in vitro* and in human skin fibroblasts is dependent on iron and singlet oxygen. *Free Radic Biol Med* 18: 721-730.
- 26- Shaker MA, Doré JE, Younes HM. 2010. Synthesis, characterization and cytocompatibility of poly(diols-tricarballlylate) visible light photocrosslinked biodegradable elastomer. *J. Biomater Sci Polym Ed* 21: 507-528.
- 27- Shaker M, Younes HM. 2010. Osmotic-Driven Release of Papaverine Hydrochloride from Novel Biodegradable Poly(Decane-co-tricarballlylate) Elastomeric Matrices. *Therapeutic Delivery* 1: 37-50.
- 28- Shaker M, Daneshtalab N, Doré J, Younes HM. *In vitro* Cytotoxicity, *In vivo* Biocompatibility and Biodegradability of Photocrosslinked Poly(Decane-co-Tricarballlylate) Elastomers. *Journal of Bioactive and Compatible Polymers* (accepted April 2011).
- 29- Masuko T, Minami A, Iwasaki N, Majima T, Nishimura S, Lee YC. 2005. Carbohydrate analysis by a phenol-sulfuric acid method in microplate format. *Analytical Biochemistry* 339: 69-72.
- 30- Lyanne Weston, Andrew Geczy and Caroline Farrell. 1998. A convenient and reliable IL-2 bioassay using frozen CTLL-2 to improve the detection of helper T lymphocyte precursors. *Immunology and Cell Biology* 76: 190-192.
- 31- Wei Wang. 2000. Lyophilization and development of solid protein pharmaceuticals *International Journal of Pharmaceutics* 203: 1-60.

- 32-Sharma A, Harper CM, Hammer L, Nair RE, Mathiowitz E, Egilmez NK. 2004. Characterization of cytokine encapsulated controlled-release microsphere adjuvants. *Cancer Biother Radiol* 19: 764-769.
- 33-Egilmez NK , Jong YS , Iwanuma Y , Jacob JS , Santos CA , Chen FA, Mathiowitz E, Bankert RB. 1998. Cytokine immunotherapy of cancer with controlled release biodegradable microspheres in a human tumor xenograft/SCID mouse model. *Cancer Immunol Immunother* 46: 21-24.
- 34-Thomas TT, Kohane DS, Wang A, Langer R. 2004. Microparticulate formulations for the controlled release of interleukin-2. *J Pharm Sci* 93: 1100-1109.
- 35-Rhines LD, Sampath P, Di-Meco F, Lawson HC, Tyler BM, Hanes J, Olivi A, Brem H. 2003. Local immunotherapy with interleukin-2 delivered from biodegradable polymer microspheres combined with interstitial chemotherapy: a novel treatment for experimental malignant glioma. *Neurosurgery* 52: 872-879.
- 36-Hanes J, Sills A, Zhao Z, Suh KW, Tyler B, DiMeco F, Brat DJ, Choti MA, Leong KW, Pardoll DM, Brem H. 2001. Controlled local delivery of interleukin-2 by biodegradable polymers protects animals from experimental brain tumors and liver tumors. *Pharm Res* 18: 899-906.

CHAPTER 7

General Discussion and Conclusions

In the past years as the number of people who diagnosed with cancer increased, with the understanding of cytokines as a cancer immunotherapy, an extensive research has focused on the development of drug delivery systems capable of achieving sustained and localized delivery of IL-2. Therefore, Chapter 1 of the thesis introduces the current status of interleukine-2 therapy with more evaluation of the different routes of administration and formulation approaches utilized for the delivery from two perspectives. The first included an assessment of the most efficient strategies used to deliver IL-2 in a non-toxic, efficient, stable and safe manner. The second introduce the advantages and the limitation of each of the current used delivery systems for this cytokines. It was shown, in chapter 1, that in most of the cancer immunotherapy cases it is desirable to have a site specific and continuous delivery of IL-2 in the vicinity of the tumour site is a desirable mode of delivery as it closely reflects the cytokine natural release pattern and results in a more effective treatment with fewer side effects. It is also indicted that long-acting formulations such as PEGylation and protein fusion techniques, prolongs IL-2 action but do not adapt with IL-2 localization concept.

Although an extensive research has been focused on the development of drug delivery systems capable of achieving sustained and localized delivery of IL-2, keeping the native bioactivity is considered the main key for the success of its delivery system for potential therapeutic application. Such delivery systems include but not restricted to the use of liposomes, hydrogels, polymeric microspheres/nanospheres, thermo responsive synthetic polymers (ReGel®), and injectable polymeric controlled release systems (Medusa II®). Of the examined release strategies, biodegradable polymeric vehicles would be able to circumvent the problems associated with short-term stability of liposomes and other similar delivery systems. However the use of conventional degradable polymer such as

poly(lactide-co-glycolide), have been demonstrated to change the tertiary structure and subsequently the biological activity of protein drugs before they are released from the delivery systems. Controlling the microclimate pH of the delivery system and avoiding the use of organic solvents in the preparation and drug loading steps are among the biggest challenges that are faced to stabilize IL-2 in any biodegradable polymeric carrier. Therefore, an area of future investigation is the investigation of novel biomaterials, able to keep the stability and bioactivity of therapeutic proteins by utilizing solvent-free drug loading and more protein friendly crosslinking techniques to overcome the limitations associated with the preparation and use of UV photo-crosslinking in the star-poly(ϵ -caprolactone co D,L-lactide).

Basically, biomaterials are synthetic substances contained in therapeutic or medical devices that are in contact with biological tissue or fluids. Typically these materials involve the use of synthetic polymers, at least in part. Biodegradable polyesters have significant potential for biomedical applications including tissue engineering, drug delivery, and biosensors. The most commonly used materials for these applications have been polylactic acid, polyglycolic acid, poly- ϵ -caprolactone and their copolymers. Many medical devices are implanted in dynamic environment of the body, which require elastomeric materials that will respond to these stresses. The material must be soft and resilient to minimize irritation of surrounding tissue, and have mechanical properties similar to the surrounding tissue. Furthermore, biodegradable materials can be especially advantageous when only temporary mechanical support is needed with the controlled released purpose. Photopolymerization techniques, which have been used to prepare biodegradable drug delivery carriers for various biomedical applications such as hydrogels, have been also utilized recently to prepare photoset elastomers. This approach involved the preparation of prepolymers with various photosensitive termini which in the presences of the proper photoinitiator can undergo free radical polymerization once exposed to a suitable light source. This photopolymerization approach would offer a number of advantages over the

conventional techniques in preparing biomaterials. Firstly, the spatial and temporal control is easily achieved during the photopolymerization process. Through controlling the exposure area and the time of light incidence, precise control of polymerization can be achieved. Secondly, photopolymerization can take place very rapidly at room temperature, in a matter of few seconds to minutes. Thirdly, the process can be conducted at a temperature and pH that resemble the physiological ranges during fabrication which allows easy and rapid production of complex matrix devices. In addition to the above, the biomaterials can be created *in situ* in a minimally invasive manner. Fabrication of polymers *in situ* is attractive for a variety of biomedical applications because it allows one to form complex shapes that adhere and conform to tissue structures. Consequently, the utilization of photopolymerized polymer networks has been suggested in drug delivery system and other biomedical application.

Chapter 3 reported on the synthesis, characterization and *in vitro* cytocompatibility of a new family of photocrosslinked amorphous poly(diols-tricarballoylate) (PDT) biodegradable elastomeric polyesters. In these elastomeric biomaterials, we demonstrated the preparation of a new family of polymers which are crosslinked at room temperature using visible light photopolymerization technique. The synthesis was based on the polycondensation reaction between tricarballoylic acid and alkylene diols, followed by acrylation. The prepared and acrylated poly(diols-tricarballoylate) (APDT) was characterized by means of FT-IR, ^1H -NMR, GPC and DSC. Liquid to solid photo-curing were carried out by exposing the APDT to visible light in the presence of camphorquinone as a photoinitiator. The thermal properties, mechanical characteristics, the sol content, long-term *in vitro* degradation and cytocompatibility of the prepared PDT elastomers were also reported. The results have shown that the physical properties of these elastomers can be controlled through manipulations of the chain length of the used diol and the degree of polymer acrylation. All the obtained elastomers were rubbery and their mechanical properties ranged from hard brittle to very weak and elastic and their Young's modulus, the ultimate tensile

strength and % strain, depended on the degree of acrylation and the length of the diol chain used. As well, the sol content of the prepared elastomers significantly depended on the degree of acrylation. The mechanical and degradation properties of this new photocurable elastomer can be precisely controlled by varying the density of acrylate moieties in the matrix of the polymer, and through changes in the prepolymer chain length. Additionally, we demonstrated the *in vitro* degradation of poly(dioltetricarballylate) elastomers. All the elastomers underwent bulk erosion similar to that of the previously investigated biodegradable polyester elastomers. A linear decrease was observed in the Young's modulus and the ultimate stress with time that was also accompanied with an increase in water absorption and weight loss. The PDT networks degraded relatively slowly after a period of 12 weeks with no appreciable dimension changes.

The use of visible light crosslinking, possibility of solvent free drug loading, the controllable mechanical properties and cytocompatibility of these new elastomers make them excellent candidates for use in controlled implantable drug delivery systems of protein drugs and other biomedical applications. Solid particles of such drugs can be mixed with the pure acrylated prepolymers which are then rapidly crosslinked using visible light at room temperature to be formulated as drug delivery systems (implants or microspheres) that will undergo biodegradation in the body.

In chapter 4, the osmotic-driven-controlled release of the water soluble drug, papaverine hydrochloride (PH), from poly(decane-co-tricarballlylate) elastomeric cylindrical monoliths is reported. A 10% v/v PH loaded cylinder-shaped matrices were prepared by visible-light photocrosslinking of the intimately mixed PH micronized powder and acrylated PDET macromers of varying degrees of acrylation (100%, 75% and 50%). We also examined the influence of various parameters such as the crosslinking density and the incorporation of osmotic excipients like trehalose on the release kinetics of the drug. To assess

the contribution of the osmotic-driven release mechanism, the loaded elastomeric devices were subjected to long term release studies using vials filled with release media of different osmotic activities. The release rate of papaverine hydrochloride was found to decrease in dissolution media of higher osmotic activity as an indication of the predominant involvement of the osmotic-driven release mechanism from the elastomeric devices. The PH release rate was also found to be dependent on the degree of PDET macromers acrylation. Decreasing the degree of acrylation of the prepolymers resulted in reduction in the crosslinking density of the formed elastomeric matrices which was associated with and increase in the void volumes between crosslinks in the elastomer. This has possibly resulted in an increase in the polymer pores size and also increased the inter-connected networks and channels between the encapsulated drug particles in the elastomer. Furthermore, it was found that co-formulating papaverine hydrochloride with trehalose increases the release rate without altering the linear nature of the drug release kinetics. These results indicated the great potential of using these elastomers for controlled drug release, through changing the structure nature of the matrix as well as increase the osmotic activity of the loaded drug.

In chapter 5, we reported on the results of the cytotoxicity, biocompatibility and biodegradability of PDET elastomers, of varying crosslinking densities were synthesized and cytotoxicity of PDET extracts of the elastomers were assessed for mitochondrial succinate dehydrogenase activity by 3-(4,5-dimethylthiazol-2-yl)-2,5-diphenyltetrazolium bromide (MTT assay) and inhibition of [3 H]thymidine incorporation into DNA of epithelial cells. We have demonstrated that PDET elastomers, with different degrees of acrylation, showed promising cytotoxicity results with Mv1Lu cells and received reasonably consistent results between the two common cell viability assays (MTT and thymidine incorporation). The treated epithelial cells revealed no signs of cytotoxicity and the elastomers degradation products

caused a slight stimulation to both mitochondrial activity and DNA replication. To assess *in vivo* biocompatibility and biodegradability, subcutaneous implantation of PDET micro-cylinders was undertaken in twenty five male Sprague-Dawley rats over a period of 12 weeks. Biodegradable poly(lactic-co-glycolic acid) sutures served as controls. The *in vivo* changes in physical and mechanical parameters of implants were compared to those observed *in vitro*. The implantation results showed that no macroscopic signs of inflammation or adverse tissue reactions were observed at implant retrieval sites. We have shown *in vivo* justification to confirm the potential of these elastomers as soft-tissue friendly materials as well as the candidacy of these elastomers as biodegradable biomaterials on long run. We have also demonstrated that PDET elastomers, with different degrees of acrylation degrade at different rates within the body and therefore elastomer selection can be tailored to achieve the desired implantation period and release rates. Moreover, the retrieved implanted micro-cylinders were found to maintain their original geometry and extensibility in a manner similar to those observed *in vitro*. All the collected data are enabling properties for PDET elastomers, which make them potentially suitable as a developed resorbable matrix for medical devices use in long-term pharmaceuticals delivery. The findings confirmed that these new elastomers have good biocompatibility and are expected to be useful as biodegradable and biocompatible biomaterials for controlled drug delivery and tissue engineering applications.

In chapter 6, poly(decane-co-tricarballoylate) (PDET) matrices which utilize the osmotic-driven-controlled release mechanism were designed in an attempt to overcome these stability and bioactivity challenges facing IL-2 delivery. IL-2 loaded micro-cylinder and disk-shaped elastomers were prepared by intimately mixing lyophilized IL-2 powder with the acrylated prepolymer prior to photocrosslinking. IL-2 release was analyzed using IL-2 enzyme-linked immunosorbent assay method and the *in vitro*

bioactivity of released IL-2 was assessed using C57BL/6 mouse cytotoxic T lymphocyte. The influence of various parameters such as the elastomer crosslinking density, the volumetric loading percentage and the incorporation of osmotic excipients like trehalose on the release kinetics of the drug was also examined. The disk-shaped specimens showed faster controlled IL-2 release profiles than microcylinders, with drug release proceeding via typical zero-order release kinetics. The increase in the device's surface area and the incorporation of trehalose in the loaded lyophilized mix increased the IL-2 release rate. As well, it was shown that the decrease in the degree of prepolymer acrylation of the prepared devices increased the IL-2 release rate. Cell based bioactivity assay for IL-2 over a release period of 28 days showed that the released IL-2 retained more than 94% of its initial activity.

Promising results regarding osmotic-driven controlled IL-2 release have been demonstrated using novel PDET biodegradable elastomers. An area of future investigation is the use of these elastomers to formulate and deliver other therapeutic protein drugs (ex. Endostatin) in a stable, efficient and active manner benefiting from the protein friendly preparation and crosslinking environment that would avoid the drawbacks of using harsh preparation and crosslinking conditions like organic solvents or UV photopolymerization.

As mentioned before, the reported biodegradable elastomers in the literature have been synthesized as either thermoplastic¹⁻³ or thermoset elastomers^{4,6}. The undesirable heterogeneous degradation of thermoplastics restricted their uses for biomedical purposes particularly in the drug delivery applications. One of the common approaches reported earlier to prepare thermoset elastomers is to first prepare multi-arm star condensation polymers by subjecting biodegradable monomers to ring opening polymerization in the presence of polyols as initiators. Some of the most common biodegradable monomers used in that approach included lactides, ϵ -caprolactone, glycolides, δ -valerolactone, urethane,

para-dioxanone, dioxepanone and trimethylene carbonate. The most commonly used polyol initiators included glycerol, lauryl alcohol, pentaerythritol, and inositol.^{2,6-10} The prepared star shaped condensation polymers were then crosslinked using thermal or non-thermal approaches.^{4,11}

Although the elastomers made of ϵ -caprolactone and dl-lactide polymers can be described as absorbable, they have hydrophobic character that contributes to their long and slow bioabsorption and decreased biocompatibility. It is known that highly hydrophobic polymer surfaces have very high contact angles with water and are more susceptible to protein adsorption.¹²⁻¹⁴ On the other hand the acrylated UV crosslinked version of the same reported polymers involved the use of organic solvents like tetrahydrofuran and dichloromethane to incorporate the drug into the precrosslinked mass. This issue raises the concern with regard to compatibility and even stability of loaded bioactive agents.¹⁵ Finally, the steps involved in preparing the above elastomers require higher heat and takes at least 3 days to obtain the final preparation.^{6,16}

Another approach to prepare elastomeric polymers was also reported through polycondensation reactions between di- and tricarboxylic acids and diols which were further subjected to thermal crosslinking. Elastomers based on citric acid, tartaric acid, and sebacic acid monomers were reported earlier.¹⁷⁻²¹ These elastomers either required long curing times ranging from a few days to weeks with inconsistency in the final physical and mechanical properties or the elastomers prepared were tough and brittle. In addition, high crosslinking temperatures were needed for their crosslinking which restricted their use in drug delivery of thermally sensitive therapeutic agents and other heat sensitive drugs. There remains a need for bioabsorbable and biocompatible elastomeric polymers. Accordingly, the reported PDT elastomers possessed few advantages over the reported biodegradable elastomers in the literature, which possibly make them good candidates for controlled drug and therapeutic protein delivery

applications. First, the polymers are degradable by bulk hydrolysis of the ester bonds and none of their building blocks are toxic. Second, altering the chain length of the alkylenediol can vary the hydrophilic and hydrophobic properties of the elastomers. Different degrees of acrylation degrade at different rates within the body and release the loaded drug at different rate, thus, the elastomers can be tailored to satisfy a particular purpose. Third, bioactivity of the loaded IL-2 was greatly maintained by using solvent-free formulation strategy and protein and peptide friendly photocuring condition. In addition to using the osmotic pressure driven release which allows for IL-2 release before significant PDET elastomer bulk hydrolytic degradation occurred.

Moreover, we put also more emphasis here on the usage of visible light photopolymerization rather than UV photocuring. Visible light is much less destructive to the protein drugs and other material compared to UV. The polymerization conditions are also sufficiently mild to be carried out in the presence of other biological materials. (e.g., for encapsulation of cells and proteins, in drug screening, or in biosensing applications). Visible light penetrates deeper through tissues than UV light (less scattering and less absorption). This property may limit the need for invasive surgical procedures by allowing trans-tissue polymerizations, whereby the material is injected subcutaneously or even subdermally and irradiated through the skin to polymerize the material *in situ*. Much efficient photocrosslinking is achieved upon using visible light. Most polymeric materials absorb the UV light, which hampers the penetration of UV light into the deeper surface region or often results in no bonding between photocured polymers and the surface if the coated layer is thick. In addition, a procedure involving UV light irradiation through the external side of the prepared device is not applicable because UV light is completely adsorbed by the external surface before it reaches the internal surface to be modified. In other words, visible light can pass through even thick transparent polymeric material. Finally, UV has a strong chemical action against the human body and causes danger at work. In addition, UV ray

apparatus must have facilities such as a specialized power supply and exhausting duct. This will require much cost and make the scale of the facilities bigger and high cost of production. Visible light photopolymerization is safer and uses simpler light source (easier to use).

In addition, the bioactivity results obtained from PDET elastmer represent an improvement over the previously published polymers provided with a quantitative analysis of the actual percentage of bioactive IL-2 released during the study. Using a prepared poly(lactic acid) (PLA) nanospheres resulted in controlling the release of IL-2 for 30 days with maintaining only 40% of the post-release bioactivity.²² In a similar approach, loaded IL-2 into PLA nanospheres that showed total IL-2 release process lasted for 7 days and the composite bioactivity of the released IL-2 was approximately 50%.²³ Using a prepared PLG (50/50) by DE and SE methods demonstrated the IL-2 sustained release ability over a period of almost 30 days. The bioactivity of IL-2 released from microspheres prepared by DE was around 80% for the first 5 days, and then rapidly dropped to less than 40% by day 10. On the other hand, the bioactivity of IL-2 released from microspheres prepared by SE was around 85% for the first 4 days, and then rapidly dropped to less than 50% by day 7.²⁴ Another research group encapsulated IL-2 in gelatin-chondroitin-6-sulphate based microspheres. The study revealed that the release profile was characterized with a rapid release rate (almost 80%) within the first 7 days followed by a very slower release over a total period of approximately 52 days.²⁵ The *in vitro* bioassay studies conducted by the same team in a previous study using the same formulation approach demonstrated that IL-2 retained only a total of approximately 50% of its original bioactivity over a total release period of 2 weeks.²⁶

Another promising perspective for these elastomers is their use as a new carrier to deliver DNA/siRNA into targeted cells in therapy of cancer or genetic diseases. The DNA can be incorporated with a chemically surface modified acrylated prepolymer which possess a targeting moiety and

photocured to form nanospheres that can effectively target and enter the cell and degrade via hydrolytic cleavage of the back bone ester group. Nonetheless, the proposed application requires efficient and reliable *in vitro* testing of DNA activity and binding ability, nanospheres intracellular uptake and finally, the *in vivo* protein expression for examining the transfer of genes to target cell or tumor model. These elastomer-based new vectors can offer a new incitation to gene therapy because they are less toxic than viral vectors and possess many previously discussed advantages (no endogenous recombination, fewer or no immunological reactions, easy production, and delivery of large-sized plasmid).

REFERENCES

- 1- Hiljanen-Vainio M, Karjalainen T, Seppala J. 1996. Biodegradable lactone copolymers. I. Characterization and mechanical behavior of ϵ -caprolactone and lactide copolymers. *J Appl Polym Sci* v 59: 1281-1288.
- 2- Schindler A, Hibionada YM, Pitt CG. 1982. Aliphatic Polyesters. III. Molecular Weight and Molecular Weight Distribution in Alcohol-Initiated Polymerizations of epsilon-Caprolactone. *Journal of Polymer Science: Polymer Chemistry Edition* 20: 319-326.
- 3- Nijenhuis AJ, Grijpma DW, Pennings AJ. 1996. Crosslinked poly(L-lactide) and poly(ϵ -caprolactone). *Polymer* 37: 2783-2791.
- 4- Storey RF, Hickey TP. 1994. Degradable polyurethane networks based on D,L-lactide, glycolide, epsilon -caprolactone, and trimethylene carbonate homopolyester and copolyester triols. *Polymer* v 35: 830-838.
- 5- Storey RF, Warren SC, Allison CJ, Puckett AD. 1997. Methacrylate-encapped poly(d,l-lactide-co-trimethylene carbonate) oligomers. Network formation by thermal free-radical curing. *Polymer* 38: 6295-6301.
- 6- Younes HM, Bravo-Grimaldo E, Amsden BG. 2004. Synthesis, characterization and *in vitro* degradation of a biodegradable elastomer. *Biomaterials* 25: 5261-5269.
- 7- Hiljanen-Vainio MP, Orava PA, Seppala JV. 1997. Properties of epsilon-caprolactone/DL-lactide (epsilon-CL/DL-LA) copolymers with a minor epsilon-CL content. *Journal of Biomedical Materials Research* 34: 39-46.

- 8- Joziase CAP, Veenstra H, Top MDC, Grijpma DW, Pennings AJ. 1998. Rubber toughened linear and star-shaped poly(d,l-lactide-co-glycolide): Synthesis, properties and in vitro degradation. *Polymer* 39: 467-473.
- 9- Kim SH, Han Y-K, Kim YH, Hong SI. 1992. Multifunctional initiation of lactide polymerization by stannous octoate/pentaerythritol. *Makromol Chem* 193: 1623-1631.
- 10- Lang M, Wong RP, Chu C C. 2002. Synthesis and structural analysis of functionalized poly (ϵ -caprolactone)-based three-arm star polymers. *J Polym Sci Part A: Polym Chem* 40: 1127-1141.
- 11- Bruin P, Veenstra GJ, Nijenhuis AJ, Pennings AJ. 1988. Design and synthesis of biodegradable poly(ester-urethane) elastomer networks composed of non-toxic building blocks. *Makromol Chem , Rapid Commun* v 9: 589-594.
- 12- Jonsson M, Johansson HO. 2004. Effect of surface grafted polymers on the adsorption of different model proteins. *Colloids Surf B Biointerfaces* 37: 71-81.
- 13- Leiva A, Gargallo L, Radic D. 2004. Interfacial properties of poly(caprolactone) and derivatives. *Journal of Macromolecular Science - Pure and Applied Chemistry* 41 A: 577-583.
- 14- Satulovsky J, Carignano MA, Szleifer I. 2000. Kinetic and thermodynamic control of protein adsorption. *Proc Natl Acad Sci USA* 97: 9037-9041.
- 15- Younes, H. M. 2003. New biodegradable elastomers for interferon-gamma delivery. University of Alberta. Doctorate Thesis.
- 16- Amsden BG, Misra G, Gu F, Younes HM. 2004. Synthesis and characterization of a photo-cross-linked biodegradable elastomer. *Biomacromolecules* 5: 2479-2486.
- 17- Borzacchiello A, Ambrosio L, Nicolais L, Huang SJ. 2000. Synthesis and characterization of saturated and unsaturated poly(alkylene tartrate)s and further cross-linking. *Journal of Bioactive and Compatible Polymers* 15: 60-71.
- 18- Huang, S. J., Edelman, P. G., and Cameron, J. A. Crosslinkable polyesters for biomedical composites. *Polymeric Materials Science and Engineering, Proceedings of the ACS Division of Polymeric Materials: Science and Engineering, Volume 53, Fall Meeting 1985.* 53, 515-519. 1985. Chicago, IL, USA, ACS, Washington, DC, USA. *Polymeric Materials Science and Engineering, Proceedings of the ACS Division of Polymeric Material.*
- 19- Webb, A., Yang, J., and Ameer, G. A novel elastomer for small diameter blood vessel tissue engineering. *Transactions - 7th World Biomaterials Congress, May 17-21 2004.* 1674. 2004. Sydney, Australia, *Biomaterials 2004 Congress Managers, Sydney, NSW 2001, Australia. Transactions - 7th World Biomaterials Congress.*

- 20- Wang Y, Ameer GA, Sheppard BJ, Langer R. 2002. A tough biodegradable elastomer. *Nat Biotechnol* 20: 602-606.
- 21- Ameer, A., Yang, J., and Webb, A. 2005. Novel biodegradable elastomeric scaffold for tissue engineering and light scattering fingerprinting methods for testing the same. US Patent 10/945354.
- 22- Sharma A, Harper CM, Hammer L, Nair RE, Mathiowitz E, Egilmez NK. 2004. Characterization of cytokine encapsulated controlled-release microsphere adjuvants. *Cancer Biother Radiol* 19: 764-769.
- 23- Egilmez NK, Jong YS, Iwanuma Y, Jacob JS, Santos CA, Chen FA, Mathiowitz E, Bankert RB. 1998. Cytokine immunotherapy of cancer with controlled release biodegradable microspheres in a human tumor xenograft/SCID mouse model. *Cancer Immunol Immunother* 46: 21-24.
- 24- Thomas TT, Kohane DS, Wang A, Langer R. 2004. Microparticulate formulations for the controlled release of interleukin-2. *J Pharm Sci* 93: 1100-1109.
- 25- Rhines LD, Sampath P, Di-Meco F, Lawson HC, Tyler BM, Hanes J, Olivi A, Brem H. 2003. Local immunotherapy with interleukin-2 delivered from biodegradable polymer microspheres combined with interstitial chemotherapy: a novel treatment for experimental malignant glioma. *Neurosurgery* 52: 872-879.
- 26- Hanes J, Sills A, Zhao Z, Suh KW, Tyler B, DiMeco F, Brat DJ, Choti MA, Leong KW, Pardoll DM, Brem H. 2001. Controlled local delivery of interleukin-2 by biodegradable polymers protects animals from experimental brain tumors and liver tumors. *Pharm Res* 18: 899-906.



